Luiz Leal

IRSN/PSN-EXP/SNC/LNR
Institut de radioprotection et de sûreté nucléaire

Mémoire d'Habilitation à Diriger des Recherches
Présenté à l'Université Paris-Sud

Sujet : **Role of Nuclear Data in Response to Practical Applications**

Soutenue le 13 Juillet 2016 devant la commission d'examen

Réza Ansari	Président
Gerald Rimpault	Rapporteur
Philippe Dessagne	Rapporteur
Elsa Merle-Lucotte	Rapporteur
Frank Gunsing	Examinateur
Laurent Tassan-Got	Examinateur

Acknowledgments

I want to take the opportunity to recognize several people that directly or indirectly assisted me in completing this work. My colleagues at the Institut de Radioprotection et de Sûreté Nucléaire, Sophie Pignet for her encouragement, support and assistance throughout the work, Raphaelle Ichou for converting the English summary into a French résumé, Wim Haeck and Julien Taforeau for their help with computer issues, and Eric Dumonteil for his careful reading of the manuscript. Notably, I would like to express my sincere gratitude to Eric Létang and Stephane Evo for their support.

I want to acknowledge my colleagues Gilles Noguere and Olivier Bouland from CEA/Cadarache for the indications on how to proceed with an HDR and for our friendship throughout all these years.

I want to give a special thanks to Professor Réza Ansari for taking the time to guide me through the HDR procedures. His highly professional manners and patience are very much appreciated.

I would like to thank the committee members Professor Elsa Merle-Lucotte, Professor Philippe Dessagne, Dr. Gerald Rimpault, Dr. Frank Gunsing, and Dr. Laurent Tassan-Got for their advice and recommendations.

I want to thank past and present students, in particular Andrew Holcomb for reading the manuscript and providing me with some suggestions.

Lastly I want to thank my lovely wife Tuca Leal for her friendship, caring, support and unique sense of humor that provided me with the grounds for completing this work.

Contents

Résumé

L'encadrement des étudiants est un sujet complexe et difficile, qui exige non seulement des compétences de management d'un point de vue scientifique, mais aussi une compréhension fine de la capacité des étudiants à mener des recherches. Il s'agit d'un engagement qui exige un dialogue riche et entretenu entre l'étudiant et son encadrant, de façon à aboutir à des résultats fructueux. Ce dialogue vise à maintenir un bon équilibre entre soutien, exigences et autonomie.

L'aboutissement positif du travail d'un étudiant est généralement mesuré en fin de période, lors de la soutenance, en présence d'un jury. En conséquence, la relation étudiant-encadrant et leur bonne entente tout le long de la thèse détermineront le résultat final, qui sera de la responsabilité des deux partis. Dans tous les cas, l'encadrement d'étudiants est une expérience magnifiquement enrichissante.

Dans le cadre de la demande d'obtention de l' «Habilitation à diriger des recherches» (HDR), le présent document a été rédigé afin de fournir une indication de la capacité de l'auteur à mener des recherches, ainsi qu'à encadrer des étudiants. Il comprend une sélection de plusieurs sujets utilisés pour les travaux d'étudiants. Il contient également un rapport des contributions apportées dans le domaine des données nucléaires et décrit l'impact des travaux de recherche dans des domaines tels que la physique des réacteurs nucléaires, la sûreté-criticité, etc. Les activités décrites ici sont le résultat de nombreuses années de travail de recherche aux États-Unis (US) dans des laboratoires nationaux, ainsi que de présentations lors de conférences dans des universités aux États-Unis et dans des instances internationales.

Le présent document ne vise pas à traiter les sujets qui sont déjà décrits dans la littérature, souvent abordés de façon déjà très détaillée. Au contraire, il est destiné à fournir un aperçu général et à mettre en évidence les informations pertinentes à l'appui de la demande de l'auteur d'obtenir une accréditation à encadrer et mener des recherches.

La première partie de ce document présente un résumé des travaux de recherche de l'auteur au fil des ans incluant l'encadrement d'étudiants. La deuxième partie présente un panorama exhaustif du rôle des données nucléaires et de leur importance au niveau applicatif, ainsi qu'une approche théorique pour le traitement de l'effet de la température sur les sections efficaces. La troisième partie décrit une évaluation de donnée nucléaire, ainsi que son impact direct au niveau applicatif. Enfin, l'auteur dressé une liste non exhaustive des matières qu'il a enseignées dans des universités aux États-Unis. En annexe, une sélection de publications importantes de l'auteur en relation avec les sujets traités dans ce mémoire est fournie.

Summary

Student supervision is a complex and challenging subject that requires not only supervisor skills in the scientific field of supervision but also a conscientious understanding of the student capability to conduct research. It is a commitment that demands a consonance between student and supervisor for completion of a successful work. The notion whether a positive accomplishment for a supervised work has been achieved is in general measured during the progress of the dissertation culminating with a defense in the presence of a selected examination committee. As a result, the student-supervisor relationship, friendship through the work development will dictate the final outcome that both are responsible for. Student supervision is a rewarding experience for both student and supervisor.

As part of the requirement to obtain the "Habilitation `a Diriger des Recherches" (HDR), the present document was written in order to provide indication that the author is capable of conducting research as well as supervising students. It includes some selected topics that have been used for students' developments and in addition, it also contains a report of contributions made to the nuclear data field and the impact of the research in areas such as nuclear reactor physics, criticality safety and others. The activities depicted are the result of several years of work at United States (US) national laboratories as well as lectures presented at universities in the US and around the world.

The present document is not intended to replicate topics that are already described in text books or published in the open literature, which are often described in great detail. It is intended to provide a general overview and highlight relevant information in support of the author's request for an accreditation to supervise and conduct research.

The first part of this document provides a synopsis of the author's activities over the years, including research developments and student supervision. Following, an overview on the role of nuclear data and its importance in practical applications is given, including a complete example that is provided in accompanying published paper listed in appendices. A detailed development of a theoretical approach for the treatment of temperature on cross sections is presented. A description of an evaluation with direct impact in practical application is presented. Lastly, a short listing of material taught at universities in the US is given.

1. General Information

Prior to working in the US, the author worked as an assistant professor at the Federal University of Paraiba and was an employee of the National Research Council of Brazil working on reactor physics for reactor analysis and design. Around 1985 the author was awarded a fellowship from the International Atomic Energy Agency (IAEA) to work on a job training assignment at the US Argonne National Laboratory (ANL) specifically in the nuclear data field. It was at that time that the author had his first interaction with the nuclear data field. The author found the subject to be very fascinating and extremely challenging, and ever since the author has continuously been studying and improving his knowledge on activities related to nuclear data including analysis, data evaluation and applications to the nuclear field. The ANL assignment was a remarkable opportunity of working with one of the greatest nuclear data theorists. It was at that time that a new methodology for temperature dependence of the cross section, the Doppler broadening of the cross section, was developed. This approach has been named Leal-Hwang Doppler broadening technique[1] and it has received a great deal of attention. It has been implemented in cross-section evaluation computer codes, such as the computer code SAMMY.[2] Recently, the approach was adopted in the SCALE code system[3] and the MAcCARD code,[4] a Monte Carlo code developed at the Seoul National University, South Korea, for calculating temperature effects of the cross section on the fly for reactor applications as part of a PhD dissertation.[5] After completion of the activities at ANL the author was invited to work for a short period of time at the US Oak Ridge National Laboratory (ORNL) on nuclear data measurements and evaluation. The work included data measurements of the uranium isotopes, in particular, transmission measurements for ^{235}U at the Oak Ridge Electron Accelerator (ORELA).[6] At the time there was an ongoing interest on having new evaluations for the uranium isotopes for applications in a current program called Integral Fast Reactor Program (IFR).[7] In addition to the ^{235}U data measurements the author got involved in the resonance analysis and evaluation of this isotope. The resonance evaluation of the ^{235}U was part of a PhD dissertation at the University of Tennessee (UT). The evaluation was proposed for inclusion in the US Evaluated Nuclear Data File (ENDF).[8]

After the ORNL and UT appointment the author was hired as an employee by ANL to work on the IFR project and a project named Reduced Enrichment for Research and Test Reactors (RERTR).[9] The ANL tenure lasted about 4 years and afterward the author returned to ORNL as a permanent employee. The author worked at ORNL for about 22 years serving in several capacities. The work performed at ORNL consisted of nuclear data evaluation for applications in reactor and criticality safety. Additionally, the author has also worked on computer code developments, working on methods for data processing in the unresolved resonance region[10, 11] and data handling for isotopic depletion calculations and decay analysis.[12] Several evaluations performed at ORNL have been accepted for inclusion in major data libraries in the US and in data libraries around the world. As an example, the ^{235}U

evaluation has been adopted as part of the Evaluated Nuclear Data Files (ENDF/B), the Joint Evaluated Fission and Fusion (JEFF), the Japanese Evaluated Nuclear Data Libraries (JENDL), Chinese Evaluated Nuclear Data Libraries (CENDL), and the Russian Evaluated Nuclear Data Libraries (BROND).

While developing research activities at ORNL the author has also lectured at universities in the US and abroad,[13] held position as Researcher Affiliate at the Massachusetts Institute of Technology (MIT) and mentored PhD students.[14] The author has also mentored a PhD student from the University of Texas working on the issue of nuclear data covariance for molybdenum isotopes for fuel fabrication research for reactor applications[15] and a student from the Georgia Institute of Technology.[16] Selected publications related to PhD developments are listed in Appendix A.

Currently the author is an employee at the Institut de Radioprotection et de Sûreté Nucléaire (IRSN). The author's recent research activities include low-energy neutron interaction with molecules for determination of double differential cross-sections and resonance evaluation of neutron cross-section. These two working activities are in response to reactor and criticality safety applications. The former is the subject of an ongoing PhD work under the author's supervision at IRSN.

2. Nuclear Data and Applications

2.1 General Description of Nuclear Data Role

The first step in the design and calculation of a nuclear system consists of generating cross-section libraries in the multi-group or continuous-energy form that is suitable for use in reactor physics computer codes. These working libraries are derived from general purpose libraries, named evaluated nuclear data libraries that are constructed based on data evaluations using physical models and theories. Presently, the most common used evaluated nuclear data libraries are the ENDF/B, JEFF, JENDL, CENDL, and BROND. These libraries are referred to as general purpose nuclear data libraries are the backbone of any design involving neutron-target interactions.

The data for neutron interaction in these libraries spans from fractions of electron-volts (eV), that is 10^{-5} eV, up to millions of electron-volts (MeV), that is 20 MeV or even higher energies. For the last 10 years a great deal of effort has been devoted to making nuclear data uncertainties available in these libraries.

It is a common practice to split the neutron interaction energy into four regions: the thermal scattering region, resolved and unresolved resonance range, and high-

energy region. While the physics concepts remain the same for each of the energy regions, the treatment of the neutron interaction is distinct. A synopsis of the characteristics of each energy region is as follows:

1. Thermal Scattering Region: neutron incident energy is comparable to the chemical binding energy in the molecules. It extends to few electron-volts (eV), say ~5 eV. The detail of the neutron elastic and inelastic scattering cross section shape is demanded for a comprehensive analysis and design of thermal reactors. This is a subject of a PhD dissertation presently developed under the author's supervision.

2. Resolved Resonance Region: experimental resolution is smaller than the width of the resonances and the individual resonances can be distinguished. The cross section representation can be made by resonance parameters using the general R-matrix formalisms or derived formalisms. The extent of this energy region varies with the nature of the nuclide and changes as a function of the experimental energy resolution achieved by the experimental measurements facilities. The knowledge of the resolved energy region is essential for the prediction of reactor properties such as resonance absorption, resonance scape probability, and resonance self-shielding.

3. Unresolved Resonance Region: cross section fluctuations still exist, but the experimental resolution is not enough to distinguish individual resonances. The cross-section representation is made by average resonance parameters. This region goes from a few kilo-electron-volts (keV) up to the million-electron-volts (MeV) region. This is the region of relevance to fast reactor physics and design. In addition to the self-shielding effects properties such as the Doppler effects and sodium void reactivity coefficients need a detailed representation of the neutron cross section.

4. High Energy Region: no cross section fluctuations exist and the cross sections are represented by smooth curves. This is the energy region pertinent to fast reactor and shielding applications.

The author has developed research activities in the first three energy regions including data evaluation and uncertainty determination through covariance generation. An example of a complete evaluation is in Appendix B, which includes work done in energy regions 2 and 3. It is the result of an evaluation carried out for ^{233}U isotope in the resonance region that is the resolved and unresolved resonance regions, including covariance data generation and application to benchmark calculation. This document demonstrates the paths needed to develop a nuclear data evaluation from the point of view of differential data, the data test of the evaluation including benchmark system sensitive to the evaluated isotope, and nuclear data uncertainty generation. While the work is described for the ^{233}U the procedure can be applied to generating evaluation to any other isotope.

2.2 Nuclear Data Treatment for Applications

Ever-increasing computational capabilities coupled with refined techniques, stochastic, deterministic or combination of both, allow an accurate solution of the transport equation for determining the neutron population in a nuclear system. The uncertainties in connection with the modeling of the problem at hand are very small if not negligible. However, the solution of the transport equation requires the knowledge of nuclear constants, known as the neutron interaction cross-sections that give the probability of a neutron-nucleus interaction leading to neutron scattering (elastic, inelastic), neutron being absorbed, neutron causing fission, etc. Therefore, the effectiveness in the prediction of the neutron population is intimately related to the knowledge of the nuclear constants, that is, how well the neutron cross sections as well as their uncertainties are known.

The description of the neutron-nucleus interaction with the underlying nuclear theory is a subject which deserves much attention due to the complex mechanism in representing the neutron cross section for practical application. An illustrative example of the complexity of the energy dependent cross-section is shown in Fig. 1. It represents the capture cross-section data for ^{238}U in the energy 0.001eV to 1 keV.

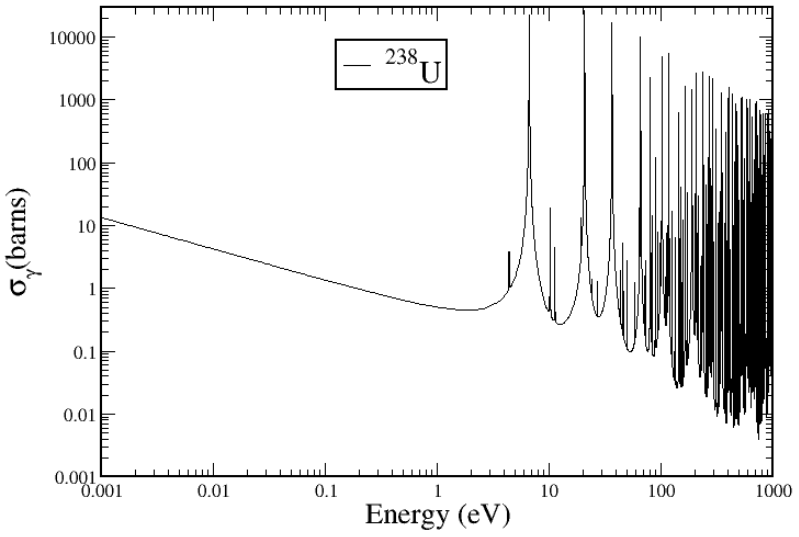

Fig 1 ^{238}U capture cross-section in the energy range 0.001 eV to 1 keV.

Quite often questions arise as to whether one should devote much time and attention on measuring, evaluating, and validating nuclear data. Indeed queries such as: why do you keep reanalyzing and changing the nuclear data? Why don't you do it right in the first time? It is not uncommon to hear statements such as "if I requested

a nuclear reactor code the nuclear data would expect to be included with the code package without any cost". There are several misconceptions regarding nuclear data that has to be addressed. For so it is worthwhile to illustrate the efforts and procedures used for getting the nuclear data ready for use in practical applications.

Nuclear cross-section data measurements, often referred to as the differential data, are carried out at experimental facilities throughout the world and are collected for inclusion in nuclear data repositories such as the EXFOR experimental database.[17] Time-of-flight (TOF) machines using linear accelerators as pulsed neutron sources such as for instance the Gaerttner[18] Linear Accelerator located at the Rensselaer Polytechnic Institute (RPI) in the US, the Geel Electron Linear Accelerator (GELINA)[19] located in Belgium, or the n_TOF machine[20] at the European Organization for Nuclear Research (CERN) in Geneva, Switzerland are examples of sources of nuclear cross-section measurements facilities. In addition to the energy-dependent experimental cross-section the conditions how the experiments were carried out are needed. The required information is, for instance, the TOF resolution, normalization, self-shielding, multiple scattering, etc. For a reaction x, the experimental effective cross section, namely, $< \sigma_x(E) >$, which relates to the true cross-section $\sigma_x(E)$, is given as

$$< \boldsymbol{\sigma_x(E)} > = \int \boldsymbol{f(E', E)}\, \boldsymbol{\sigma_x(E')}\, \boldsymbol{dE'}, \qquad (1)$$

where the function $f(E', E)$ describes the experimental conditions as for instance the TOF resolution. Therefore, besides reporting the energy-dependent cross-section experimentalists must also provide, as much as possible, information on the condition for which the experiments were performed. The information will be used by evaluators to build the function $f(E', E)$ to perform data evaluation to determine the true cross-section$\sigma_x(E)$. Since the experimental conditions are very distinct from every experimental facility, that is $f(E', E)$ is very different from machine-to-machine, clearly the measured experimental cross-section data cannot be used directly in practical applications, i.e., an evaluation process is needed.

The data evaluation process is generally based on the analysis and evaluation of total, capture, fission, and elastic and inelastic energy- and angle-differential scattering data performed at TOF facilities. Sophisticated computer codes are used in the evaluation procedure to determine the best fit of the calculated cross section in comparison with the experimental data. As an example, in the resolved and unresolved energy regions the computer code SAMMY[2] is used to fit the cross-section data through a resonance parameter evaluation whereas the EMPIRE[21] code is used in the high-energy range. The use of the code SAMMY in the fitting process is illustrated in Fig. 2. It represents a comparison of the ^{235}U fission cross-section in the energy region 2 eV to 30 eV for which the solid line is the theoretical prediction of the experimental data and dots are the experimental data.

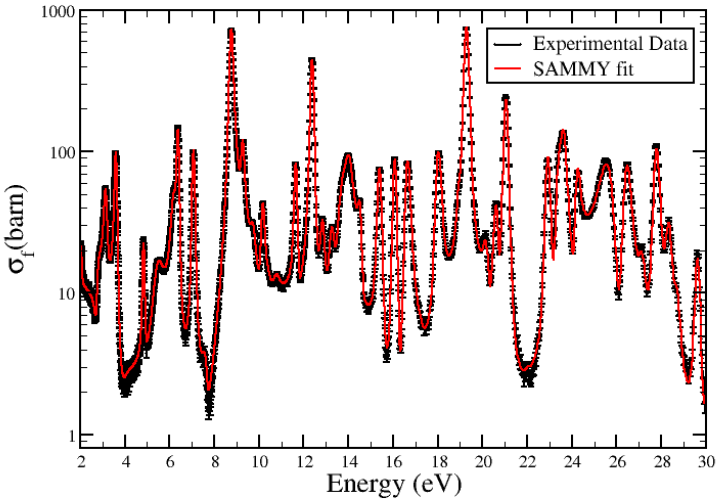

Fig. 2 Comparison of the SAMMY fit of the ^{235}U fission cross-section.

Another issue that has gained much attention over the last 15 years is the evaluation of experimental data uncertainties and their use in practical applications. The data uncertainty in a TOF measurement is described by the experimental conditions. It is not an easy task for the evaluator to fully understand the experimental conditions of a particular experiment. It is a hard undertaking if not impossible. To name a few, the source of uncertainties can be credited to data normalization, uncertainty related to the TOF length, detectors efficiency, etc. The evaluated nuclear data uncertainties are translated into evaluated covariance data. The ultimate goal is to propagate the evaluated nuclear data uncertainty in the nuclear system calculations. Figure 3 shows the uncertainty and covariance for the ^{235}U evaluated fission cross section in the energy region from 10^{-5} eV to 20 MeV. As can be seen from Fig. 3 the uncertainty around 1000 eV is about 8 %. This information can be used in actual analysis and design of nuclear systems. For instance, in nuclear criticality safety calculations in connection to material outside reactors the nuclear data play a very important role. The safety margin regarding the design of a spent fuel storage cask will greatly rely on how well the evaluated nuclear data and their uncertainties are known and their effect on the neutron multiplication factor (also known as k_{eff}).

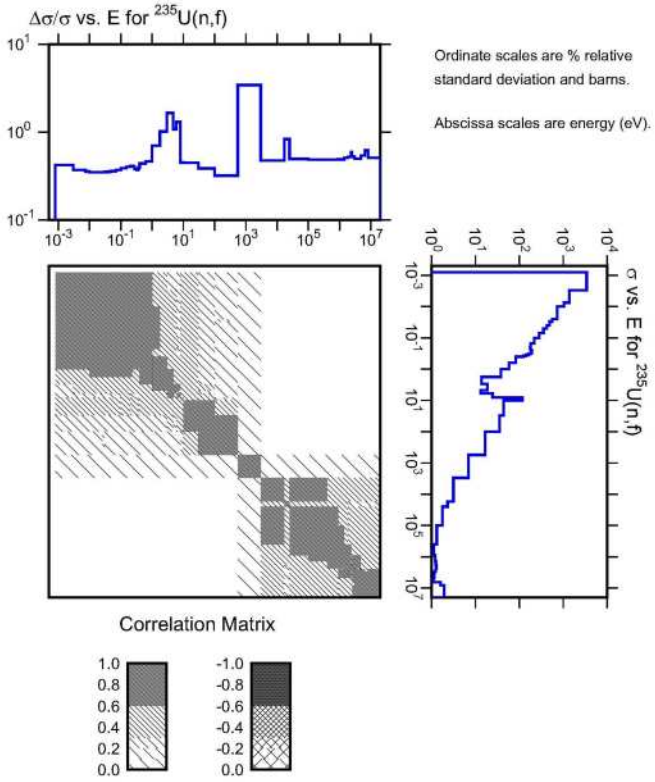

Fig. 3 Uncertainty and covariance for the ^{235}U fission cross-section in the energy range 10^{-5} eV to 20 MeV.

A complete example of data and uncertainty evaluation is reported in the Appendix B. In particular the error propagation to benchmark calculations is shown in the section entitled 'BENCHMARK CALCULATIONS AND DATA UNCERTAINTY.' The work developed in Appendix B is in response to a request of the US Department of Energy to improve the ^{233}U cross-section and uncertainties for criticality safety applications.

Prior proposing an evaluation for inclusion in the nuclear data library one additional step is needed which consists of performing integral testing to verify the effectiveness of the evaluated data in predicting reactor parameters such as k_{eff}. For that purpose, there are available integral experiments for criticality safety application such as the International Criticality Safety Benchmark Experiments (ICSBEP)[22] or the International Reactor Physics Experiment Evaluation (IRPhE)[23] aimed at reactor applications. The result of the integral benchmark testing may indicate whether the differential data evaluation at issue needs to be revised to

improve reactor prediction. Generally an integral benchmark system includes several isotopes and hence provides the grounds to test the contribution of a number of reaction cross sections and their impact on the k_{eff} estimation.

Each nuclear data project in the world, ENDF, JEFF, JENDL, etc., has their own committees devoted to differential and integral data testing prior accepting the evaluated data for inclusion in the nuclear data library. For instance, the Cross Section Evaluation Working Group (CSEWG)[24] is the ENDF body responsible for inspecting the proposed evaluated nuclear data. After the evaluated data have passed all the scrutiny they become available in the nuclear data libraries.

2.3 Novel Approach for Doppler Broadening

There have been ongoing efforts to develop multiphysics computer codes to address complex nuclear reactor problems. One challenging issue concerns the coupling of neutronics and thermal hydraulics computer codes for the understanding and better prediction of Doppler reactivity coefficients and other quantities. In reactor applications the required temperature-dependent cross sections can vary from different regions such as fuel, coolant, moderator, etc. Even within each of these regions the temperature is not constant. Presently, the common practices consist of taking an average temperature or performing interpolations based on series of predetermined stored cross-section libraries and subsequently calculating the reactor constants. One major issue, regardless of whether the treatment is performed with either deterministic or Monte Carlo computer codes, is the temperature update of the nuclear data used in the calculations. While the methodologies for dealing with the temperature effects in the cross section have been around for a long time their direct application to the multiphysics computer codes might not be adequate. The purpose here is to present a methodology that can be used to account for the temperature effects in the cross section in a suitable manner for practical applications. The approach has received much attention lately but has not been fully described. The intent here is to describe the steps used in the methodology development.

The effect of the material temperature on the cross section, known as the Doppler Effect, is characterized by a convolution of the energy (incoming particle velocity) dependent cross-section with a Maxwell velocity distribution of the target nucleus. Indeed the Doppler Effect appears due to the relative velocity of the incident particle and the target nucleus. A very commonly used form of the temperature dependent cross section is that known as the Solbrig's Kernel[25] which is given as

$$\boldsymbol{u^2\bar{\sigma}(E)} = \frac{\mathbf{1}}{\mathbf{2\sqrt{\pi\theta}}}\int_{\mathbf{0}}^{\infty} \boldsymbol{\sigma(u')\, u'^2}\left[\boldsymbol{exp}\left(-\frac{\boldsymbol{(u-u')^2}}{\boldsymbol{4\theta}}\right) - \boldsymbol{exp}\left(-\frac{\boldsymbol{(u+u')^2}}{\boldsymbol{4\theta}}\right)\right]\boldsymbol{du'} \qquad (2)$$

with $\boldsymbol{u} = \sqrt{\boldsymbol{E}}$, $\boldsymbol{\theta} = \frac{\boldsymbol{kT}}{\boldsymbol{2A}}$, $\boldsymbol{A} = \frac{\boldsymbol{M}}{\boldsymbol{m}}$, where m is the neutron mass, M is the target mass and k is the Boltzmann constant. The observation made here is that Eq. 2 is the

result of a convolution of a kernel, which is the Maxwell distribution of velocities, with the cross section. Hence Eq. 2 must be a solution of a differential equation. Undoubtedly, this is the case if one defines a function $\boldsymbol{F}(\boldsymbol{u},\boldsymbol{\theta}) = \boldsymbol{u}^{\boldsymbol{2}}\overline{\boldsymbol{\sigma}}(\boldsymbol{E})$ and $\boldsymbol{\vartheta} = \boldsymbol{2\theta}$ which leads to a simple second-order differential equation in the variables u and ϑ as

$$\frac{\boldsymbol{\partial^2 F}}{\boldsymbol{\partial u^2}} = \frac{\boldsymbol{\partial F}}{\boldsymbol{\partial \vartheta}} \tag{3}$$

The initial condition $\boldsymbol{F}(\boldsymbol{u},\boldsymbol{0})$ for $-\infty < \boldsymbol{u} < +\infty$ and the boundary conditions $\boldsymbol{F}(\infty,\boldsymbol{\vartheta}) = \boldsymbol{F}(\infty,\boldsymbol{0})$ and $\boldsymbol{F}(-\infty,\boldsymbol{\vartheta}) = \boldsymbol{F}(-\infty,\boldsymbol{0})$ afford a solution of Eq. 2 using the finite difference method.

The strategy pursued for solving Eq. 2 using the explicit finite difference method includes the following features:

1. Use a constant mesh in the variable u, that is a $\boldsymbol{h} = \Delta\boldsymbol{u} =$ constant ;
2. Use a constant mesh in the variable ϑ, that is a $\boldsymbol{\gamma} = \Delta\boldsymbol{\vartheta} =$ constant;
3. Minimize the error by relating h and γ.

In the finite difference approach the operators in Eq. 3 can be approximated, for a constant mesh, as

$$\frac{\boldsymbol{\partial^2 F_i^j}}{\boldsymbol{\partial u^2}} = \frac{\boldsymbol{F_{i+1}^j - 2F_i^j + F_{i-1}^j}}{\boldsymbol{h^2}} \tag{4}$$

and

$$\frac{\boldsymbol{\partial F_i^{j+1}}}{\boldsymbol{\partial \vartheta}} = \frac{\boldsymbol{F_i^{j+1} - F_i^j}}{\boldsymbol{\gamma}} \tag{5}$$

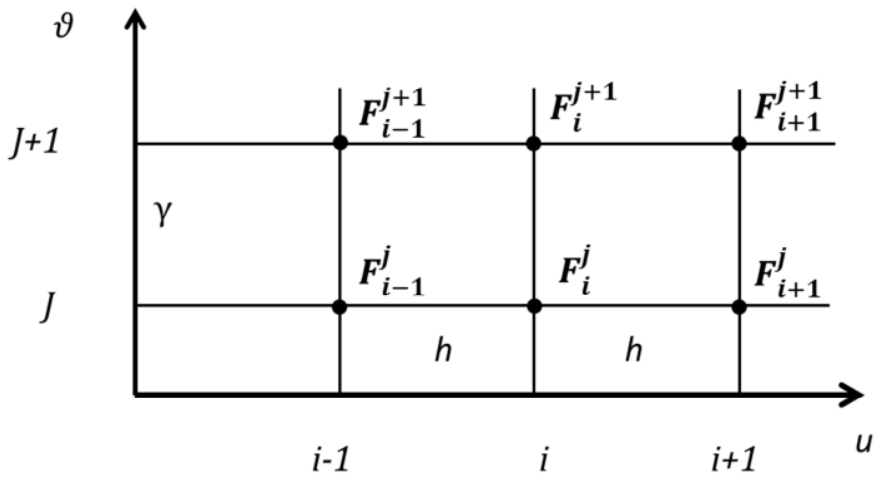

Fig. 4 *u* and ϑ variables for discretization

From this point we will seek to infer and characterize the error associated with the approximations based on the finite difference method for solving Eq. 2.

a) In the *u* space a Taylor expansion around *i* can be written as

$$F_{i+1}^{j} = F_i^{j} + h\frac{\partial F_i^{j}}{\partial u} + \frac{h^2}{2}\frac{\partial^2 F_i^{j}}{\partial u^2} + \frac{h^3}{6}\frac{\partial^3 F_i^{j}}{\partial u^3} + \frac{h^4}{24}\frac{\partial^4 F_i^{j}}{\partial u^4} + \frac{h^5}{120}\frac{\partial^5 F_i^{j}}{\partial u^5} + \frac{h^6}{720}\frac{\partial^6 F_i^{j}}{\partial u^6} + \ldots. \quad (6)$$

Likewise,

$$F_{i-1}^{j} = F_i^{j} - h\frac{\partial F_i^{j}}{\partial u} + \frac{h^2}{2}\frac{\partial^2 F_i^{j}}{\partial u^2} - \frac{h^3}{6}\frac{\partial^3 F_i^{j}}{\partial u^3} + \frac{h^4}{24}\frac{\partial^4 F_i^{j}}{\partial u^4} - \frac{h^5}{120}\frac{\partial^5 F_i^{j}}{\partial u^5} + \frac{h^6}{720}\frac{\partial^6 F_i^{j}}{\partial u^6} + \ldots \quad (7)$$

Combination of Eq. 6 and Eq. 7 leads to

$$\frac{F_{i+1}^{j} - 2F_i^{j} + F_{i-1}^{j}}{h^2} = \frac{\partial^2 F_i^{j}}{\partial u^2} + \frac{h^2}{12}\frac{\partial^4 F_i^{j}}{\partial u^4} + \frac{h^4}{360}\frac{\partial^6 F_i^{j}}{\partial u^6} + \ldots \quad (8)$$

b) Similar to the u space we can derive an expression for the ϑ space with a Taylor expansion around *j* as

$$\frac{F_i^{j+1} - F_i^{j}}{\gamma} = \frac{\partial F_i^{j}}{\partial \vartheta} + \frac{\gamma}{2}\frac{\partial^2 F_i^{j}}{\partial \vartheta^2} + \frac{\gamma^2}{6}\frac{\partial^3 F_i^{j}}{\partial \vartheta^3} + \ldots \quad (9)$$

One observes that from Eq. 3 the following three equations hold:

$$\frac{\partial^4 F}{\partial u^4} = \frac{\partial^3 F}{\partial u^2 \partial \vartheta} \tag{10}$$

and

$$\frac{\partial^3 F}{\partial u^2 \partial \vartheta} = \frac{\partial^2 F}{\partial \vartheta^2} \tag{11}$$

Hence

$$\frac{F_{i+1}^j - 2F_i^j + F_{i-1}^j}{h^2} - \frac{F_i^{j+1} - F_i^j}{\gamma} = \frac{h^2}{2}\frac{\partial^4 F_i^j}{\partial u^4}\left(\frac{1}{6} - \frac{\gamma}{h^2}\right) + O(h^4, \gamma^2)\left\{\frac{\partial^6 F_i^j}{\partial u^6}, \frac{\partial^3 F_i^j}{\partial \vartheta^3}\right\} \tag{12}$$

An obvious choice is to make $\frac{\gamma}{h^2} = \frac{1}{6}$ whereby the error becomes on the order of $\frac{h^4}{360}\frac{\partial^6 F}{\partial u^6} - \frac{\gamma^2}{6}\frac{\partial^3 F}{\partial \vartheta^3}$. Hence the explicit finite difference equation becomes

$$F_i^{j+1} = \frac{\gamma}{h^2}F_{i+1}^j + \left(1 - \frac{2\gamma}{h^2}\right)F_i^j + \frac{\gamma}{h^2}F_{i-1}^j \tag{13}$$

Or writing $s = \frac{\gamma}{h^2}$ and $a = \frac{(1-2s)}{s}$ then

$$F_i^{j+1} = s(F_{i+1}^j + aF_i^j + F_{i-1}^j) \tag{14}$$

The stability condition requires that $s < \frac{1}{2}$ which is granted since $s = \frac{1}{6}$.

It is observed that successive substitution, starting from ***j=0***, in Eq. 14 leads to a series of coefficients the follow an interesting pattern as shown bellow

$$j = 0$$
$$F_i^1 = s^1(F_{i+1}^0 + aF_i^0 + F_{i-1}^0) \tag{15}$$

$$j = 1$$
$$F_i^2 = s^2\left(F_{i+2}^0 + 2aF_{i+1}^0 + (a^2+2)F_i^0 + 2aF_{i-1}^0\right) + F_{i-2}^0) \tag{16}$$

$$j = 2$$
$$F_i^3 = s^3\left(F_{i+3}^0 + 3aF_{i+2}^0 + (3a^2+3)F_{i+1}^0 + (a^3+6a)F_i^0\right) + (3a^2+3)F_{i-1}^0)3aF_{i-2}^0 + F_{i-3}^0 \tag{17}$$

The coefficients display a Pascal triangle-like structure as shown in Table 1 as follows

			1			
		1	a	1		
	1	$2a$	a^2	$2a$	1	
1	$3a$	$3a^2+3$	a^3+6a	$3a^2+3$	$3a$	1

Table 1. Pascal triangle-like structure of coefficients

Similar to a Newton binomial expansion these coefficients can be determined through a generating function of the form $(1 + ax + x^2)^N$ multiplied by s^N. Hence a general solution of Eq. 14 ca be accomplished as

$$F_i^N = \sum_{k=0}^{2N} C_{Nk}\, F_{i+N-k}^0 \tag{18}$$

with

$$C_{Nk} = s^N \sum_{i=(k+1)/2}^{\min(N,k)} \frac{N!}{(N-i)!\,(k-i)!\,(2i-k)!}\, a^{2i-k} \tag{19}$$

The advantage of using this approach as opposed to using Eq. 2 directly is that there is no need to perform an integral over the whole energy region for determining the temperature-dependent cross-section at one single-energy point. Also, since the coefficients C_{Nk} are determined for fixed values of $s = 1/6$ and $a = 4$, they can be pre-calculated, stored and used as needed. The time the methodology was developed[1] it did not receive much attention since it made use of computer resources (storage, CPU speed) beyond the limits available.

The methodology has been applied to computer codes used for data evaluation[2] and also to reactor physics codes, including the MAcCARD code,[4] to account for the temperature effects in actual reactor core calculations. See also the paper listed in Appendix C. Comparison of the Doppler broadened cross section calculated using the code SAMMY based on Eq. 2, the Solbrig's approach for 300 K, and using the methodology presented here is displayed in Fig. 5. It is applied to the total cross section of ^{16}O in the energy range of 0.0001 eV to 6 MeV. The relative differences between the two calculations done with the code SAMMY are in the range of -0.002 and 0.002 with a comparable amount of CPU time to perform both calculations. The choice for testing the method for ^{16}O is because of the huge dip in the cross section around 2.3 MeV which provides an excellent ground for testing the Doppler broadening effects.

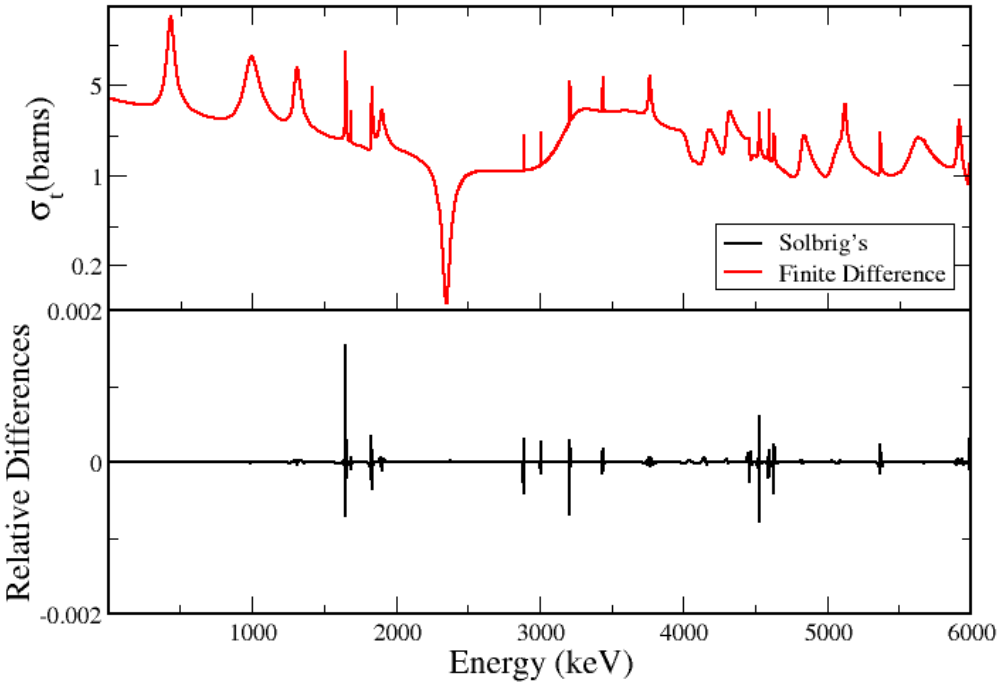

Fig. 5 Solbrig's kernel and the finite difference Doppler broadening method for ^{16}O at the temperature 300 K.

3. Resonance Evaluation: Combining Integral and Differential Data

The intent of this section is to demonstrate the use of differential and integral data for solving issues in connection with nuclear data evaluation.

3.1 New ^{239}Pu Evaluation in the Energy Range 10^{-5} eV to 2.5 keV

In the 1980s and early 1990s, Derrien et al.[26] performed a ^{239}Pu evaluation in a collaborative work, including CEA and ORNL. At that time, due to computer limitations for data storage and processing, a decision was made to split the resonance region into three parts, namely, 10^{-5} eV to 1 keV, 1 keV to 2 keV, and 2 keV to 2.5 keV. The evaluation was accepted for inclusion in the ENDF and JEFF nuclear data libraries and is still included in the latest releases of ENDF, the ENDF/B-VII.1, and the JEFF-3.1 libraries. While the evaluation was performed based on high resolution data, mainly transmission data[6] measurements taken at the Oak Ridge Electron Linear Accelerator (ORELA) at ORNL, no benchmark testing was done at the time the evaluation was released. Later, benchmark calculations indicated deficiencies in the ^{239}Pu evaluation in reproducing integral results. Additional issues with the previous evaluation can be attributed to the use of three distinct sets of resonance parameters. Specifically, the cross sections calculated at the energy boundary of two consecutive, disjoint resonance parameter sets could be different, leading to a discontinuity. Another concern relates to data uncertainty assessments using resonance parameter covariance data. For data uncertainty analyses, the use of a single resonance parameter set covering the entire energy region is preferable because the disjoint set of resonance parameters does not permit the determination of uncertainty correlations in the entire energy region. Hence, the decision was made to combine the three sets of resonance parameters and redo the evaluation. The task of generating a single resolved resonance region evaluation was achieved because computer resources have improved substantially since the previous ^{239}Pu evaluation effort. As a result, a resonance parameter evaluation was completed at ORNL in 2008 by Derrien, and this ^{239}Pu evaluation covers the energy range 10^{-5} eV to 2.5 keV;[27] however, the evaluation was unable to improve benchmark results and was not proposed for inclusion in either the ENDF or JEFF project. At about the same time as the work was being performed at ORNL, Bernard et al.[28] at CEA/Cadarache performed a reevaluation of the ^{239}Pu resonance parameters and nubar ($\bar{\nu}$). Since the resonance evaluation for the whole energy region was not available, the work performed by Bernard was based on the JEFF-3.1 evaluation (i.e., with the three disjoint sets of resonance parameters). Bernard's ^{239}Pu evaluation improved the results of benchmark calculations; however, the evaluation did not provide resonance parameter covariance data. By building upon the previous ^{239}Pu evaluation work efforts, a new ^{239}Pu evaluation that provides

improved benchmark performance for thermal plutonium solution systems has been produced.

3.2 Resonance Parameter Evaluation Procedure

With the set of resonance parameters covering the entire energy region up to 2.5 keV, a good set of external resonance parameters were determined. The technique used for deriving the external levels is that described in Ref. 29. Six resonance levels with negative energies and nine levels above 2.5 keV were enough to represent the external resonances' interference effect in the energy region 10^{-5} eV to 2.5 keV. The first negative level (close to zero) has a very small neutron width. It does not contribute much to the interference effect in the resonance region. However, it is used to influence the shape of eta (η) that bends down at very low energy.[30] Figure 6 shows the cross section shape in the resonance region due only to the external energy resonance levels. It should be noted that the cross section value converges to 11.13 barns, which represents the potential cross section for ^{239}Pu determined with an effective scattering radius of 9.41 fm. This feature indicates that the external levels' contribution to the cross section in the energy range 10^{-5} eV to 2.5 keV is appropriate. The experimental database used in the new evaluation is essentially the same as that listed in Reference 27. However, information derived from the knowledge of benchmark calculation results was also included in the SAMMY analysis together with the fitting of the differential data. Two quantities were essential in determining the best set of resonance parameters that fitted the experimental differential data and improved the benchmark results. The two quantities are eta (η) and the effective K1. These quantities are defined as follows:

a) Eta (η)

$$\eta = \frac{\bar{\nu}\,\sigma_f}{\sigma_a} = \frac{\bar{\nu}}{1+\alpha} \tag{20}$$

Where α is defined as $\alpha = {}^{\sigma_\gamma}/_{\sigma_f}$

b) K1

$$K1 = \bar{\nu}\,\sigma_{0f} g_f - \sigma_{0a} g_a \tag{21}$$

The cross-sections σ_{0f} and σ_{0a} are, respectively, the fission and absorption cross sections at the thermal energy (0.0253 eV), whereas g_f and g_a are the Westcott g-factors. The value used in calculating the efective K1 from Eq. 20 is taken at thermal energy. It was noted that the benchmark results were very sensitive to η and K1. The benchmark results indicated that in some cases the sensitivity to K1 was more

significant than on η. The K1 value for ^{239}Pu is higher than that of other major isotopes. For instance, the ^{235}U K1 value is around 722 barns, whereas for ^{239}Pu it is 1160 barns. An example of the SAMMY fit of the experimental differential data is displayed in Fig. 7 for the total cross-section of Bollinger,[31] fission cross-section of Wagemans,[32] and capture cross-section of Gwin[33] in the energy region from 0.01 eV to 7 eV. Values of the cross section at thermal (0.0253 eV), fission Westcott factors, thermal $\overline{\nu}$, resonance integrals, and K1 value are shown in Table 2. The unit for cross sections, K1, and resonance integral is barns, whereas the Westcott factor is dimensionless. Also, shown in Table 2 are the values listed in the Atlas of Neutron Resonance (ANR),[34] ENDF/B-VII.1, and the values calculated using Bernard's evaluation that is included in JEFF3.1.1. The thermal cross-section values listed in the ANR were used in the SAMMY evaluation. The values listed in Table 2 were calculated with the SAMMY code.

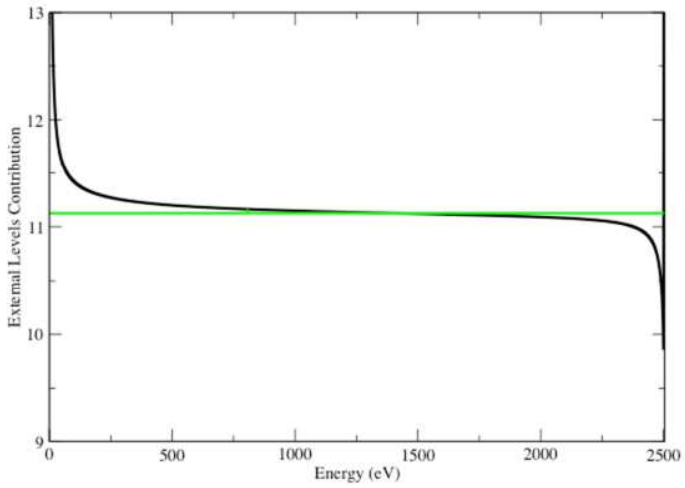

Fig. 6 Contribution of the external levels in the resonance region to the scattering cross section.

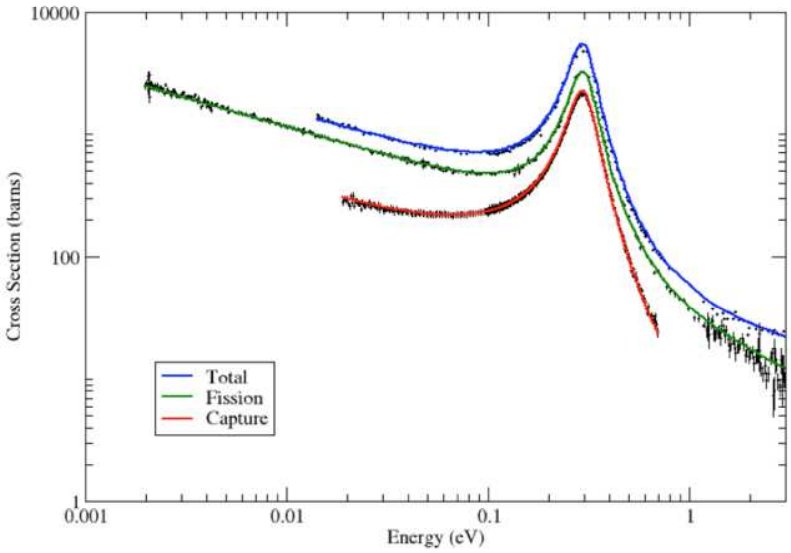

Fig. 7 Results of SAMMY fit of the total, fission, and capture cross-section data.

Quantity	ANR[34]	ENDF/B-VII.1	JEFF3.1.1	New Evaluation
σ_γ	269.3 ± 2.9	270.64	272.61	270.06
σ_f	748.1 ± 2.0	747.65	747.08	747.19
g_f	1.0553 ± 0.0013	1.0544	1.0495	1.0516
g_a	1.0770 ± 0.0030	1.0784	1.0750	1.0771
$\overline{\nu}$	2.879 ± 0.006	2.873	2.873	2.873
I_γ	180 ± 20	181.44	181.50	180.09
I_f	303 ± 10	302.60	303.58	309.09
K1	1177.25	1166.62	1156.35	1161.30

Table 2. Thermal values and integral quantities calculated with SAMMY

3.3 Benchmark Results

To verify the performance of the ^{239}Pu evaluation in benchmark calculations, seven critical experiments were chosen from the International Criticality Safety Benchmark Evaluation Project (ICSBEP) in the International Handbook of Evaluated Criticality Safety Benchmark Experiments.[27] These benchmark experiments consist of light water reflected spheres of plutonium nitrate solutions. The benchmarks, listed in Table II, have the average of neutron lethargy causing fission (EALF) spanning the energy range of 0.04 eV to 3 eV. It should be noted that the uncertainty in these benchmarks is around 500 PCM.

Several resonance parameters were derived from the SAMMY fitting of the experimental differential data. Each time a resonance parameter was obtained with a satisfactory fitting of the differential data (a good χ^2), the SAMMY resonance parameters were converted in the ENDF format (MT2 MF151) and combined with the JEFF3.1.1 by replacing the existing resonance parameters. The cross section library created was then processed for use in Monte Carlo calculations using the MCNP code. The MCNP libraries were generated with the NJOY code.[36] All the cross-section data for the remaining isotopes present in the benchmark experiments were taken from the ENDF/B-VII.0. The process from the SAMMY fitting of the experimental data to the MCNP calculation was automated, validated, and tested. Various k_{eff} results were obtained for the seven benchmarks listed in Table III. The impact of the cross section change in the k_{eff} values was analyzed, and it was noted that a very minor change in the thermal cross section and in the first resonance around 0.2956 eV would significantly change the k_{eff} value of the thermal benchmark listed in Table 3. In addition results of sensitivity calculations, using the TSUNAMI sequence of the SCALE code,[37] indicated that in order to achieve a reasonable k_{eff} result, a combined change on $\overline{\nu}$ and on the fission and capture cross-sections values was needed as opposed to a simple change in one of these quantities alone. The very first attempt made was to focus on η (or α) since it involves these three quantities, as indicated in Eq. 20. However, further investigations indicated that the k_{eff} was also very sensitive to K1. No experimental measurement of K1 was found in the literature for ^{239}Pu. Nevertheless, integral experiments performed at the CEA/Cadarache MINERVE facility could be used to infer the value of K1 that provided the best results for reactivity changes. A K1 value of around 1161 barns indicated that a reasonable k_{eff} could be achieved for the seven benchmarks listed in Table 3. Hence, in addition to fitting the experimental differential data, SAMMY also fitted K1. The calculated results for the seven benchmarks displayed in Table 3 are shown in Fig. 8. The new ^{239}Pu evaluation provides consistent C/E results for benchmark systems with plutonium aging leading to discrepancies of less than +200 PCM on the average.

Benchmark	Experimental k_{eff}	EALF (eV)	Contents
PST12.13	1.0000±0.0050	0.04282	19.5 % ^{240}Pu
PST4.1	1.0000±0.0047	0.0531	0.5 % ^{240}Pu
PST12.10	1.0000±0.0033	0.0535	25 % ^{240}Pu
PST18.6	1.0000±0.0047	0.0761	43 % ^{240}Pu
PST1.4	1.0000±0.0047	0.154	5 % ^{240}Pu
PST34.4	1.0000±0.0047	0.231	116g % pu/L 1.42 Gd/L
PST34.15	1.0000±0.0047	2.730	363g Pu/L, 20.25 Gd/L

Table 3. ICSBEP ^{239}Pu thermal benchmark

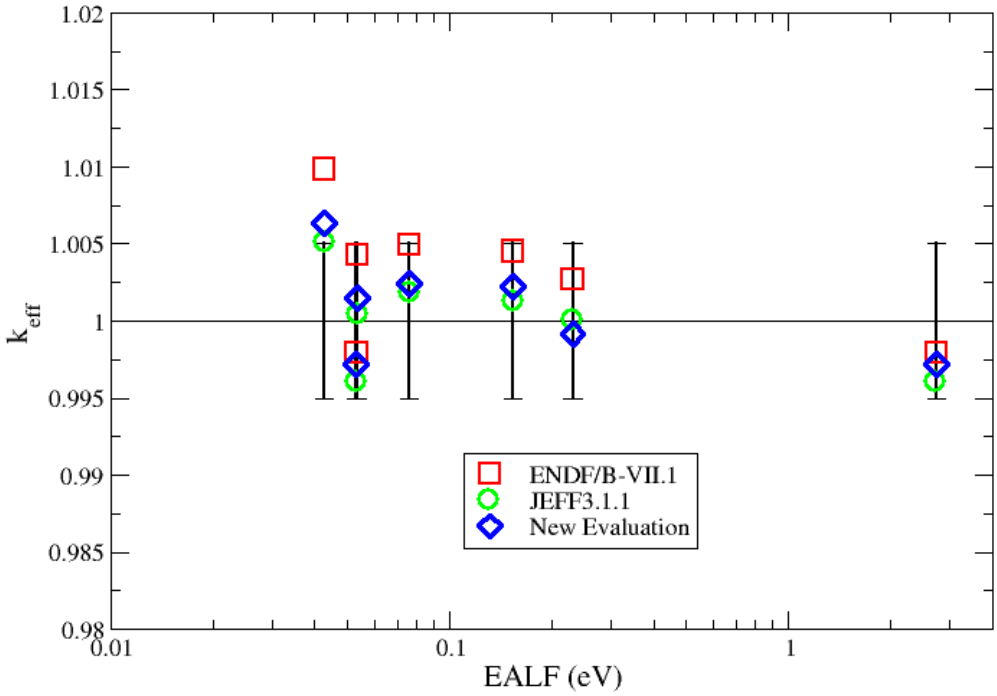

Fig. 8 MCNP benchmark results.

4. Lecture at US universities

Teaching endeavors at universities have always been part of the author's career. It all started at the Federal University of Paraiba, Brazil. At the time, the teaching activities consisted of teaching courses at undergraduate levels. Working at ORNL in the US has given the author the opportunity to not only teach at university but also supervise students and Post-doctoral researchers. Since a long time ago ORNL has established partnership with US universities providing an excellent opportunity to its employees to become assistant professors, adjunct professors, etc. at the partner universities. The major benefit to ORNL has been the identification of students with potential researcher skills that could be brought to the laboratory.

The teaching activities at universities consisted of lecturing on the neutron interaction theory tailored to practical applications in fission and fusion reactors, criticality safety of material outside reactors, etc. Each nuclear data field has its own needs for data applications. For instance, in fusion reactor devices one is interested in shielding, heating production by neutron interactions, neutron damages, etc. For fission reactor applications the interest is on the neutron flux population and how to control it so as to keep the nuclear system critical position producing enough thermal energy and consequently electrical energy for consumption. In criticality safety applications for material outside reactors the main concern is whether the nuclear material can be safely handled without the risk of achieving a criticality condition. An example of this risk is the shipping of spent nuclear fuel to a repository. The latter can be regarded as one very important issue that requires not only a good knowledge of nuclear data but also their uncertainties. In all the aforementioned situations the knowledge of nuclear data and its uncertainty are fundamental. A great deal of the teaching activities encompasses the theoretical developments pertinent to the nuclear data treatment. However the implication and the importance of the nuclear data in practical application have always been emphasized.

An example of a teaching module of the R-matrix theory is listed in Appendix D.

Conclusions

The role of nuclear data in practical applications such as the design and analysis of a nuclear system device has been discussed in this document. Various nuclear data projects, namely nuclear data libraries, exist to assist the nuclear engineering practitioners to perform their duties in a reliable and efficient manner. The nuclear data analysts, nuclear data experimentalist, nuclear data evaluators, etc. have the responsibility to assure whether the final product has the quality assurance required for practical application. This document has provided, to a certain extent, a view on the procedures used for constructing a nuclear data evaluation. The author of this document hopes that it contains enough information to the understanding of what nuclear data are used for and how important they are in practical applications.

The ability to conduct research and perform student supervision has been demonstrated with descriptive examples in attached documents provided in the Appendices whereby topics related to research toward PhD developments are shown.

References

1. L. C. Leal and R. N. Hwang, "A Finite Difference Method for Treating the Doppler Broadening of Neutron Cross Sections," American Nuclear Society, Los Angeles, CA, Nov 1987.
2. N. M. Larson, *Updated Users' Guide for SAMMY: Multi-level R-Matrix Fits to Neutron Data Using Bayes's Equations*, ENDF-364/R2, Oak Ridge National Laboratory USA (2008). Available at Radiation Safety Information Computational Center (RSICC) as PSR-158.
3. *Scale: A Comprehensive Modeling and Simulation Suite for Nuclear Safety Analysis and Design*, ORNL/TM-2005/39, Version 6.1, Oak Ridge National Laboratory, Oak Ridge, Tennessee, June 2011. Available from Radiation Safety Information Computational Center at Oak Ridge National Laboratory as CCC-785.
4. Soo Min Kang, Hyung Jin Shim, Luiz C. Leal, "Development of an On-The-Fly Doppler Broadening Module in McCARD," Transaction of the Korean Nuclear Society Spring Meeting, Jeju, Korea, May 29-30, 2014.
5. Shane William Daniel Hart, "Automated Doppler Broadening of Cross Section for Neutron Transport Applications," PhD Dissertation Presented at the University of Tennessee, December 2014.
6. J. A. Harvey, N. W. Hill, F. G. Perey, G. L. Tweed and L. C. Leal, "High-Resolution Neutron Transmission Measurements on ^{235}U, ^{239}Pu, and ^{238}U," in *Proceedings of the International Conference on Nuclear Data for Science and Technology*, Mito, Japan, May 1988.
7. "Plentiful Energy: The Story of the Integral Fast Reactor," by Charles E. Till and Yoon Chang, December 2011. Book available on Amazon.com
8. L. C. Leal, G. de Saussure, and R. B. Perez," An R-Matrix Analysis of the ^{235}U Neutron-Induced Cross Section up to 500 eV," *Nuc. Sci. Eng.* **109**, 1-17 (1991).
9. L. C. Leal, G. de Saussure, and R. B. Perez, "URR Computer Code: A Code to Calculate Resonance Neutron Cross-Section Probability Tables, Bondarenko Self-Shielding Factors and Self-Indication Ratios for Fissile and Fertile Nuclides," ORNL/TM-11297, Oak Ridge National Laboratory, August 1989.
10. A. Travelli, "Status and Progress of the RERTR Program," 1993 International Meeting on Reduced Enrichment for Research and Test Reactor, October 3-7, 1993, Oarai, Ibaraki, Japan.
11. M. E. Dunn and L. C. Leal, "Calculating Probability Tables for the Unresolved-Resonance Region Using Monte Carlo Methods," *Nuc. Sci. Eng.*, **148**, 30-42 (2004).
12. Luiz C. Leal, Otto W. Hermann, Stephen M. Bowman, and Cecil V. Parks, "Automatic Rapid Process for the Generation of Problem-Dependent SAS2H/ORIGEN-S Cross-Section Libraries," *Nuc. Tech.* **127**, July 1999.
13. The Abdus Salam International Centre for Theoretical Physics, ICTP Lecture Notes, Nuclear Reaction Data and Nuclear Reactors 2001, Volume 1, pp. 1-496, Trieste, Italy.

14. Vladimir Sobes, "Coupled Differential and Integral Data Analysis for Improved Uncertainty Qualification of the ^{63,65}Cu Cross-Section Evaluations," PhD Thesis presented at the MIT Nuclear Engineering Department, February 2014.
15. C. van der Hoeven, E. Schneider, and L. Leal, "Generation of Improved Isotopic Molybdenum Covariances from Elemental Cross-Section Data Using SAMMY," *Nucl. Sci. Eng.* **179**, 1-21, (2015).
16. A. Holcomb, "A New Unresolved Resonance Region Methodology," PhD dissertation presented at the Georgia Institute of Technology, November 2016.
17. (EXFOR) V. Semkova, N. Otuka, S.P. Simakov, V. Zerkin, Experimental Nuclear Reaction Data Collection EXFOR, 2nd International Conference on Advancements in Nuclear Instrumentation, Measurement Methods and their Applications (ANIMMA 2011), June 6-9, 2011, Ghent, Belgium, IEEE Conference Proceedings CFP1124I-CDR.
18. (Gaertner) Y. Danon, R. M. Bahran, E. J. Blain, A. M. Daskalakis, B. J. McDermott, D. G. Williams, D. P. Barry, G. Leinweber, M. J. Rapp, and R. C. Block, "Nuclear Data for Criticality Safety and Reactor Applications at the Gaerttner LINAC Center," *Trans. Am. Nucl. Soc.*, San Diego, November 11–15, Vol. 107, pp. 690–693, (2012).
19. (GELINA) W. Mondelaers and P. Schillebeeckx, Notizario Neutroni e Luce di Sincrotrone 11 (2), 19 (2006).
20. (n_TOF) C. Guerrero et al., 'Performance of the neutron time-of-flight facility n_TOF at CERN,' February 2013.
21. (EMPIRE) Herman, M.; Capote, R.; Carlson, B. V.; Obložinský, P.; Sin, M.; Trkov, A.; Wienke, H.; Zerkin, V., 'EMPIRE: Nuclear Reaction Model Code System for Data Evaluation,' Nuclear Data Sheets, Volume 108, Issue 12, p. 2655-2715, December 2007.
22. (ICSBEP) International Handbook of Evaluated Criticality Safety Benchmark Experiments, NEA/NSC/DOC(95)/01/1-IX, Organization for Economics Co-operation and Development, Nuclear Energy Agency (OECD-NEA), September 21013.
23. (IRPhE) International Handbook of Evaluated Reactor Physics Benchmark Experiments, NEA/NSC/DOC(2006), Organization for Economics Co-operation and Development, Nuclear Energy Agency (OECD-NEA), March 21013.
24. (CSEWG) Cross Section Evaluation Working Group, "A CSEWG Retrospective," National Nuclear Data Center, Brookhaven National Laboratory, November 5, 2001.
25. A. W. Solbrig, Jr. *Nucl. Sci. Eng.* **10** (1961) 167.
26. H. Derrien et al., Nucl. Sci. Eng. 106, 434, (1990); also H. Derrien, J. Nucl. Sci. Technol. 30, 845, (1993).
27. H. Derrien, L. C. Leal, and N. M. Larson, "^{239}Pu Neutron Resonance Parameters Revisited and the Covariance Matrix in the Neutron Energy Range Thermal to 2.5 keV," in *Proceedings of International Conference on Nuclear Data for Science and Technology (ND-2007)*, Nice, France, April 22-27, 2007.
28. D. Bernard it et al., Proc. International Conference on Nuclear Data for Science and Technololgy, Nice, France April 2227, 2007.

29. L. C. Leal *et al.*, *Nucl. Sci. Eng.* **131**, 230 (1999).
30. L. Erradi *et al.*, *Nucl. Sci. Eng.* 144, 47 (2003).
31. L. M. Bolinger et al., Bul. Am. Phys. Soc. 1, 187 (K5)(1956).
32. C. Wagemans et al., Proc. Int. Conf. Nuclear Data for Science and Technology, Mito, Japan May 30-June 3, 1988.
33. R. Gwin et al., Nucl. Sci. Eng. 45, 25 (1971).
34. S. F. Mughabghab, Atlas of Neutron Resonances, Resonance Parameters and Neutron Cross Sections Z = 1-100, Elsevier (2006).
35. ICSBEP, NEA/NSC/DOC(95)03, OECD Nuclear Energy Agency (Rev. September 2007).
36. R. E. MacFarlane and A. C. Kahler, Nuclear Data Sheets 110, 2739-2890 (2010).
37. SCALE Version 6.1, ORNL/TM{2005/39 (2004).

Appendix A: Selected Publications Related to PhD Developments

NUCLEAR SCIENCE AND ENGINEERING: **179**, 1–21 (2015)

Generation of Improved Isotopic Molybdenum Covariances from Elemental Cross-Section Data Using SAMMY

C. van der Hoeven* and E. Schneider

University of Texas at Austin, Nuclear Engineering Teaching Laboratory
Pickle Research Campus, R-9000, Austin, Texas 78712

and

L. Leal

Oak Ridge National Laboratory
P.O. Box 2008, Building 5700, Oak Ridge, Tennessee 37831-6170

Received September 25, 2013
Accepted February 15, 2014
http://dx.doi.org/10.13182/NSE13-78

Abstract—*There is a need for improved molybdenum isotope covariance data for use in modeling a new uranium-molybdenum fuel form to be produced at the Y-12 National Security Complex (Y-12). Covariance data correlate the uncertainty in an isotopic cross section at a particular energy to uncertainties at other energies. While high-fidelity covariance data exist for key isotopes, the low-fidelity covariance data available for most isotopes, including the natural molybdenum isotopes considered in this work, are derived from integral measurements without meaningful correlation between energy regions. This paper provides a framework for using the Bayesian R-matrix code SAMMY to derive improved isotopic resonance region covariance data from elemental experimental cross-section data. These resonance-wise covariance data were combined with integral uncertainty data from the Atlas of Neutron Resonances, uncertainty data generated via a dispersion method, and high-energy uncertainty data previously generated with the Empire-KALMAN code to produce an improved set of covariance data for the natural molybdenum isotopes. The improved covariance data sets, along with the associated resonance parameters, were inserted into JENDL4.0 data files for the molybdenum isotopes for use in data processing and modeling codes. Additionally, a series of critical experiments featuring the new U(19.5%)-10Mo fuel form produced at Y-12 was designed. Along with existing molybdenum sensitive critical experiments, these were used to compare the performance of the new molybdenum covariance data against the existing low-fidelity evaluation. The new covariance data were found to result in reduced overall bias, reduced bias due to the molybdenum isotopes, and improved goodness of fit of computational to experimental results.*

I. INTRODUCTION

The use of accurate cross-section data is critical to modeling nuclear systems. Cross-section data are typically derived from a combination of experimental measurements and particle interaction models. Both of these sources inevitably give rise to uncertainty. Uncertainty in experimental data arises from statistical and systematic errors or biases as well as variables in the experimental systems that are difficult or impossible for the experimenter to control.[1] Uncertainty in interaction models derives from the differences between the model's approximations and the physical reality of the particle interaction. Neglecting this "model defect" can result in unrealistically small uncertainties being assigned to nuclear cross-section data.[2]

*E-mail: cvanderh@gmail.com

To be taken into account, these uncertainty data must be assessed and compiled in evaluated nuclear data files in a format that can be used in analysis code packages. These data include both the energy-dependent uncertainty in the cross section and the correlation between uncertainties at other energies. So-called covariance data of this type have been included in the last two generations of the Evaluated Nuclear Data Files[3,4] (ENDF). High-fidelity covariance data have been produced for key isotopes such as ^{235}U; ^{238}U; ^{239}Pu; and ^{1}H, ^{2}H, and ^{3}H (Refs. 5 and 6). However, the majority of fission product isotopes and isotopes found in structural reactor components either lack covariance data entirely or have only low-fidelity data.[7] This can be problematic when isotopes lacking high-fidelity covariance data comprise significant fractions of fuel material, such as is the case for the intermediate enrichment U-10Mo fuel form developed at the Y-12 National Security Complex[8] (Y-12).

A key goal of this paper is to provide a new set of improved covariance data for the naturally occurring molybdenum isotopes utilizing a newly completed experimental evaluation of molybdenum cross-section data by Rensselaer Polytechnic Institute (RPI) and the retroactive approach of the SAMMY code package.[9] These experimental data are for an elemental molybdenum sample, and isotopic covariance data will be generated from it. Derivation of isotopic covariance data from an elemental sample has not previously been attempted with SAMMY, so this work illustrates a novel capability of the SAMMY code package. The improved covariance data will make possible more accurate modeling of nuclear systems containing molybdenum. However, in order to use the newly generated covariance data in modeling codes, they must first be inserted into a complete nuclear data file. The improved molybdenum covariance data will therefore be inserted into ENDF/B-VII.1, JEFF3.1, and JENDL4.0 data files, and the best library will be selected based on a goodness-of-fit test of the calculated results for selected critical experiment benchmarks versus the reported experimental results.

Table I details isotopic abundances for natural molybdenum, as well as the resonance region boundaries currently used in ENDF/B-VII.1.

The remainder of this paper is organized as follows. Section II reviews methods for assembling covariance data. Section III briefly describes existing molybdenum sensitive critical experiments and a set of proposed benchmark critical experiments to utilize the U(19.5%)-10Mo fuel. Section IV details the method used to generate improved fidelity covariance data for the molybdenum isotopes and compares uncertainty analyses using the existing low-fidelity molybdenum covariance data and the newly generated improved data. Section V provides conclusions of the work.

II. BACKGROUND AND THEORY

Cross-section covariance data are intrinsically tied to the formalism used to generate the cross-section data it describes. This section reviews the cross-section formalism utilized most commonly in the resolved energy region, namely, R-matrix theory, as well as the generation of covariance data tied to this formalism. Additionally, the use of covariance data in sensitivity and uncertainty analysis codes of experimental system models will also be covered.

II.A. Cross-Section Data

R-matrix theory was developed to address the need for a compact and accurate means of describing the resolved resonance region.[10] R-matrix theory describes the cross section in the resolved resonance region in terms of parameters E_λ(eV) and $\gamma_{\lambda l}$(eV), the resonance energy and width, and resonance spin, which can be evaluated by fitting the experimental cross-section data. The SAMMY R-matrix code is used to fit measured interaction data, such as neutron transmission or capture, to E_λ and $\gamma_{\lambda l}$ values utilizing a generalized least-squares approach. These resonance parameter values will have some

TABLE I

Molybdenum Isotope Abundances and ENDF/B-VII.1 Resonance Region Boundaries

	Molybdenum Isotope Abundances	ENDF/B Resolved Resonance Boundaries	ENDF/B Unresolved Resonance Boundaries
^{92}Mo	14.84%	10^{-5} eV to 40 keV	40 to 100 keV
^{94}Mo	9.25%	10^{-5} eV to 20 keV	20 to 100 keV
^{95}Mo	15.92%	10^{-5} eV to 2.1412 keV	2.1412 to 206.2685 keV
^{96}Mo	16.68%	10^{-5} eV to 19 keV	19 to 100 keV
^{97}Mo	9.55%	10^{-5} eV to 2 keV	2 to 100 keV
^{98}Mo	24.13%	10^{-5} eV to 32 keV	32 to 100 keV
^{100}Mo	9.63%	10^{-5} eV to 26 keV	26 to 100 keV

associated uncertainties. The work flow described below derives covariance data for the resolved resonance region from those uncertainties.

II.B. Cross-Section Covariance Data

For the molybdenum isotopes, ENDF/B cross-section data in the resolved resonance region are stored as R-matrix parameters using ENDF File 2 conventions. Cross-section processing codes such as NJOY or AMPX can process the stored parameters into usable working libraries of interaction cross sections.[11,12] In order to produce those parameters, evaluation codes such as SAMMY are used to fit experimental data to a chosen R-matrix formalism. Such an evaluation must also take into account sources of uncertainty in the experimental data.

As stated previously, SAMMY utilizes a generalized least-squares method to fit its parameter set and covariance matrix to experimental data. This Bayesian method for fitting the resonance parameters results in an updated resonance parameter set P', which consists of the E_λ and $\gamma_{\lambda l}$ values introduced previously, as

$$P' = P_0 + M' Y , \tag{1}$$

where M' is the associated resonance parameter covariance matrix,

$$M' = \left(M_0^{-1} + W\right)^{-1} , \tag{2}$$

W is defined as

$$W = G^t V^{-1} G , \tag{3}$$

and Y is defined as an auxiliary matrix given by

$$Y = G^t V^{-1} (D - T) , \tag{4}$$

where

- P_0 = initial parameter set "guess" with associated resonance parameter covariance matrix M, which is unknown initially and therefore frequently is assumed to be diagonal and infinite, meaning $M^{-1} = 0$ (Ref. 13)
- V = data covariance matrix
- T = theoretical value corresponding to the experimental data D
- G = sensitivity matrix of the theoretical values with respect to the parameters given by

$$G = \frac{\partial T}{\partial P} . \tag{5}$$

SAMMY should utilize all available experimental data of all types in the fitting procedure, as well as the full covariance matrix for each data set. Integral constraints such as resonance integrals and thermal cross sections can also be included. Upon completion, the final parameter set P can be written in the ENDF File 2 format for inclusion in evaluated nuclear data files, while the covariance matrix M can be stored in ENDF File 32 format.

II.C. Current Molybdenum Cross-Section and Covariance Data

As an initial investigation of the molybdenum cross-section uncertainty, existing cross-section data from three general-purpose libraries were compared: ENDF/B, maintained by Brookhaven National Laboratory (BNL) in the United States; JEFF, maintained by the Organisation for Economic Co-operation and Development/Nuclear Energy Agency; and JENDL, maintained by the Japan Atomic Energy Agency.[14–16] Significant differences among these libraries were evident, particularly in the resolved resonance and high-energy regions, including differences in the number of resonances tracked by each library, how those resonances were organized by quantum numbers, and values for the resonance parameters describing each resonance.

Currently, only the ENDF/B-VII.1 cross-section library includes covariance data for the molybdenum isotopes. However, these covariance data are low fidelity. They were generated as part of the Low Fidelity Covariance Project, described in Ref. 8, a joint undertaking among Oak Ridge National Laboratory (ORNL), BNL, and Los Alamos National Laboratory. The goal of that project was to quickly and transparently produce modeling usable uncertainty estimates for all isotopes in ENDF. In order to accomplish this, the process for producing covariance data had to be extremely streamlined. For structural materials and fission products, integral uncertainty measurements (thermal capture, resonance integral) were assigned as the uncertainty values for whole energy regions (thermal, resonance) and were coupled with high-energy covariance data generated at BNL. Complete correlation was assigned throughout the energy domain.

As an example, Fig. 1 shows the current low-fidelity capture covariance data for ^{97}Mo as is available in ENDF/B-VII.1. As a comparison, Fig. 2 shows high-fidelity capture covariance data for ^{235}U. Figures 1 and 2 were generated using the processing code NJOY. The top image in each figure gives the groupwise interaction cross section for the reaction of interest. The image to the left gives the groupwise uncertainty in that cross section. Finally, the central image is a visual representation of the correlation matrix relating the uncertainty at a particular energy to the uncertainty at all other energies. All diagonal values in the correlation matrix are by definition 1; all off-diagonal values can vary between -1 and 1. Figures 1 and 2 are plotted using a 33-group energy structure detailed in Ref. 17.

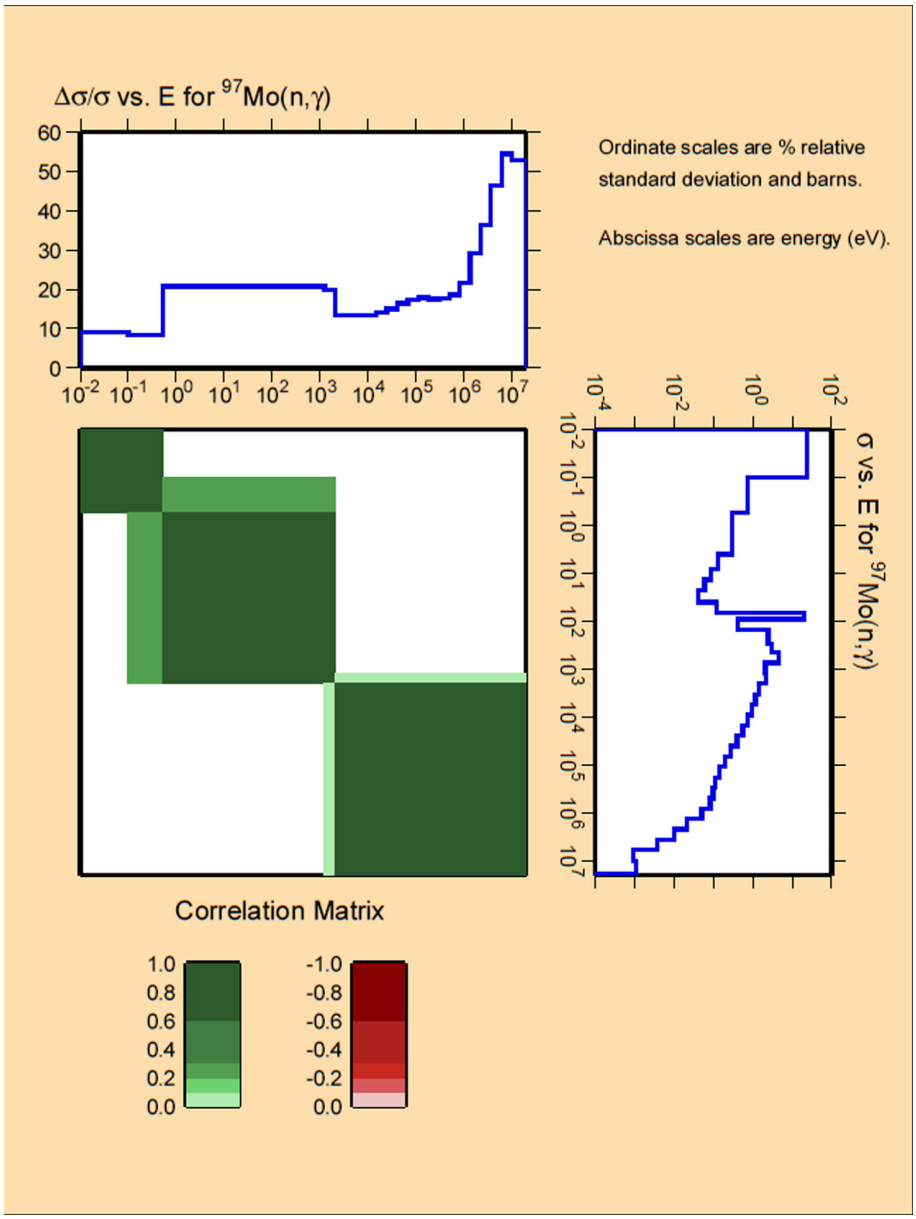

Fig. 1. Molybdenum-97 low-fidelity capture covariance data.

The correlation matrix for uranium shows significant structure, whereas the low-fidelity molybdenum data assign full correlation within all energy regions.

II.D. Sensitivity and Uncertainty Analysis

Covariance data such as shown above can be used with purpose-made codes for sensitivity and uncertainty analysis. One such code package is SCALE, a modular general-purpose nuclear analysis code maintained at ORNL (Ref. 18). Several modules of SCALE have been developed for sensitivity and uncertainty analysis tasks, two of which will be used for this project: Tools for Sensitivity and Uncertainty Analysis Methodology Implementation (TSUNAMI) and Tool for Sensitivity/Uncertainty Analysis of Response Functionals Using Experimental Results (TSURFER).

TSUNAMI is a SCALE control module for the application of sensitivity and uncertainty theory to criticality safety analysis.[19] TSUNAMI computes the sensitivity of the system multiplication factor to the evaluated nuclear cross-section data used to model the system. These sensitivity data are coupled with cross-section covariance data to produce an uncertainty in the multiplication factor due to the underlying cross-section data uncertainty. TSUNAMI is a multigroup code, and the groupwise sensitivity data it

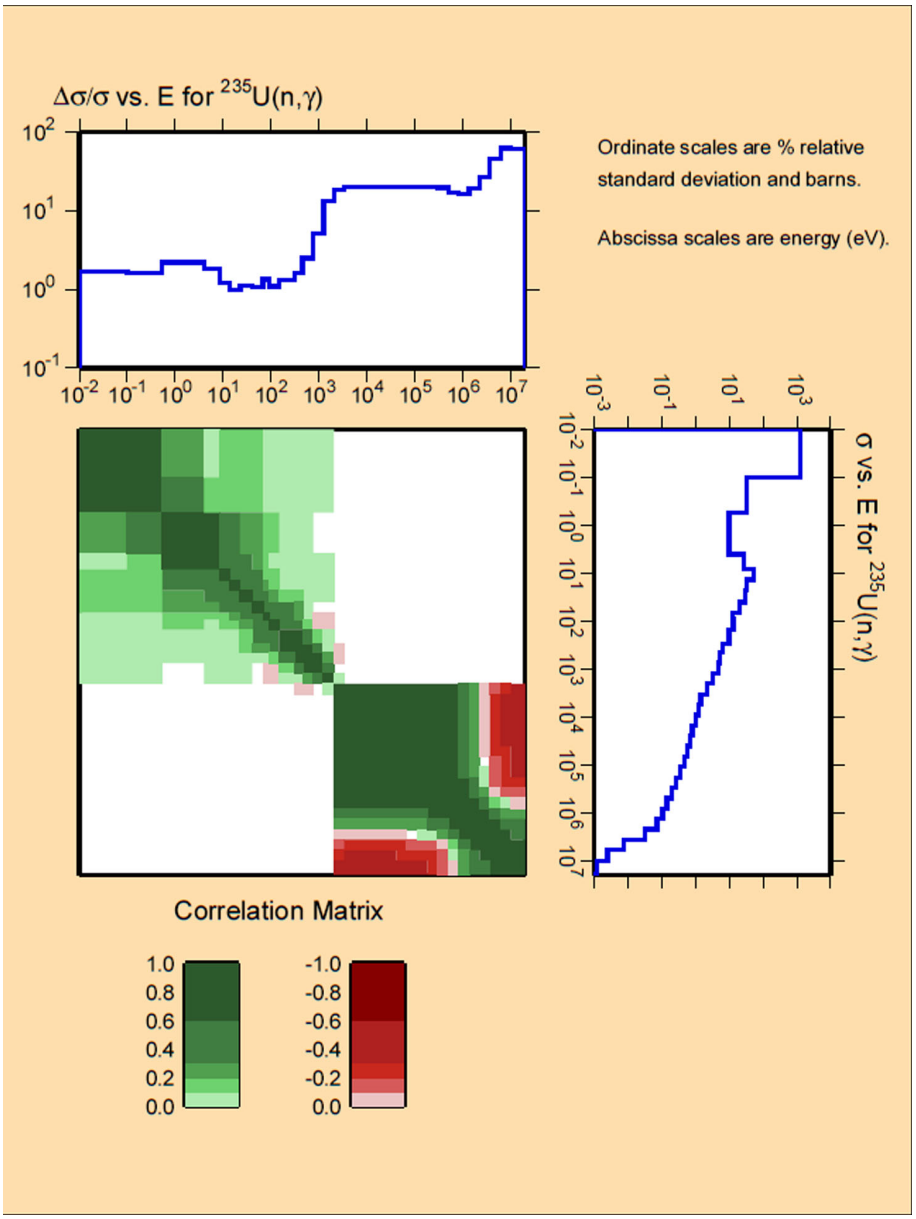

Fig. 2. Uranium-235 high-fidelity capture covariance data.

generates are stored in sensitivity data files for use with other SCALE sensitivity and uncertainty modules.

TSURFER is a module of SCALE responsible for computing uncertainties in integral system parameters, primarily multiplication factor, due to uncertainties in the cross-section data used to model the system.[20] By applying a generalized linear least-squares (GLLS) methodology to the sensitivity profiles generated by TSUNAMI, TSURFER can be used to reduce discrepancies between experimentally measured integral system parameters and calculated system parameters by adjusting the nuclear cross-section data such that the overall consistency is maximized. Finally, TSURFER can analyze measured responses from benchmark experiments and establish bias and associated uncertainty in calculated application responses. The results of TSURFER for application responses can be affected by cross-correlations between the experimental response integral benchmarks selected. Information detailing possible cross-correlation between the integral benchmarks utilized for this work was not available, so these impacts were not considered.

TSURFER defines two types of responses: experiment responses and application responses. An experiment response has both a calculated and measured integral value associated with it. An example would be a critical experiment with a reported experimental multiplication

factor, as well as a calculated multiplication factor from a modeling simulation. An application response has only a calculated integral value. Applications typically correspond to hypothetical or proposed systems considered in the context of a design study for which the computational bias and uncertainty associated with cross-section uncertainty are desired. If the application response shares nuclear cross-section data sensitivities with the experimental responses, it will be affected by the same data adjustments that impact the experiment responses. This provides a systematic, well-defined method for utilizing benchmark measurements to establish bias and uncertainty estimates arising from nuclear data uncertainty in the calculation of system parameters in proposed nuclear system designs. Typically, an additional figure of merit for sensitivity and uncertainty studies is the "representativity" of the experimental responses utilized to the application response selected. Representativity is defined as

$$r_{AE} = \frac{S_A^t U S_E}{\sqrt{\left(S_A^t U S_A\right)\left(S_E^t U S_E\right)}} , \qquad (6)$$

where

S_A = sensitivity vector of the application response to the nuclear data

S_E = sensitivity vector of the experimental response to the nuclear data

U = covariance matrix for the nuclear data.[21]

Representativity is a measure of the degree to which the selected experimental responses represent the proposed application responses.

A high representativity value helps to ensure maximum reduction in calculation uncertainty due to nuclear data uncertainty.[22] For this study a measure of representativity was not available through TSURFER. However, all molybdenum sensitive integral benchmarks available were utilized for the GLLS fitting; therefore, the maximum of representativity with respect to the application responses was achieved, given the molybdenum sensitive benchmarks that were available.

II.E. Existing Molybdenum Sensitive Critical Experiments

In order to utilize TSUNAMI and TSURFER as outlined above, appropriate experimental responses are required. Published critical benchmark experiments provide the necessary experimental responses. There are few critical experiments that exhibit high sensitivity to the molybdenum isotopes. Most of the critical benchmark experiments cataloged by the International Criticality Safety Benchmark Evaluation Project (ICSBEP) Handbook that include molybdenum isotopes feature them as a minor structural material with minimal neutronic effect, as molybdenum is used in some alloys of stainless steel, or as reflectors.[23]

However, a series of critical experiments was completed in the early 1960s relating to the ORNL Fast Burst Reactor (FBR), later renamed the Health Physics Research Reactor.[24,25] In these experiments a series of five critical assemblies featuring cylindrical or annular geometries, both bare and reflected, were studied.

The fuel for the FBR critical experiments was 93% enriched uranium metal, alloyed with 10 wt% natural molybdenum. While this fuel is of significantly higher enrichment than the U(19.5%)-10Mo fuel foils to be produced by Y-12, these critical experiments offer the only set of experimental data for systems in which molybdenum makes up a key component of the fuel itself.

The molybdenum sensitive critical experiments in the ICSBEP Handbook, along with the ORNL FBR critical experiments, comprise the set of critical experiment sensitivity responses that will be utilized in the sensitivity and uncertainty analysis for this work using the SCALE modules TSUNAMI and TSURFER. Table II describes the selected benchmark experiments. Further detail can be found in the ICSBEP Handbook.[23]

III. CRITICAL EXPERIMENT DESIGNS

This section presents two fast spectrum and two thermal spectrum experiment concepts designed in accordance with standards set by the National Criticality Experiments Research Center.[26] The two fast spectrum experiment designs are referred to as the Fast Bare critical experiment and the Fast Reflected critical experiment, while the two thermal spectrum experiment designs are referred to as the Thermal critical experiment and the Thermal Maximum critical experiment. These designs are intended for use with one of the vertical lift tables available at the National Criticality Experiments Research Center: In each design two subcritical systems would be brought together to a calculated critical configuration using the vertically movable platen of a lift table machine. These proposed critical experiments are also necessary since they will be used as "applications" for TSURFER, providing a means of comparing the performance of the new molybdenum covariance data to the existing low-fidelity covariance data.

III.A. Fast Spectrum Critical Experiment Designs

The U(19.5%)-10Mo fuel form is designed for use in a thermalized spectrum, complicating attempts to use the fuel in a fast neutron spectrum critical experiment. In the first TSURFER application design, to overcome the relatively low enrichment of the uranium-molybdenum–alloy foils, two layers of highly enriched uranium (HEU) were added to the system, equal in length and width to the central layer of uranium-molybdenum. To ensure the

TABLE II

Molybdenum Sensitive Critical Experiments

ICSBEP Identifier	Title	Location of Molybdenum
N/A[a]	"Oak Ridge National Laboratory Fast Burst Reactor: Critical Experiments and Calculations"	U-Mo Fuel
HEU-MET-FAST-005-001 through HEU-MET-FAST-005-006	"Beryllium and Molybdenum Reflected Cylinders of Highly Enriched Uranium"	Reflector
HEU-SOL-THERM-001-001 through HEU-SOL-THERM-001-002	"Minimally Reflected Cylinders of Highly Enriched Solutions of Uranyl Nitrate"	Stainless steel tank
LEU-COMP-THERM-042-001 through LEU-COMP-THERM-042-007	"Water-Moderated Rectangular Clusters of $U(2.35)O_2$ Fuel Rods (1.684 cm Pitch) Separated by Steel, Boral, Boroflex, Cadmium, or Copper Plates, with Steel Reflecting Walls"	Steel reflecting walls and steel absorber plates
MIX-COMP-FAST-001-001	"ZPR-6 Assembly 7: A Cylindrical Assembly with Mixed (Pu,U)-Oxide Fuel and Sodium with a Thick Depleted-Uranium Reflector"	Pu-U-Mo fuel plates
U233-SOL-THERM-003-002 through U233-SOL-THERM-003-010	"Paraffin-Reflected 5-, 5.4-, 6-, 6.6-, 7.5-, 8-, 8.5-, 9-, and 12-Inch Diameter Cylinders of ^{233}U Uranyl Fluoride Solutions"	Impurities in solution
U233-SOL-THERM-009-001 through U233-SOL-THERM-009-004	"Unreflected Large-Diameter Cylinders of ^{233}U Uranyl Nitrate Solutions"	Stainless steel tank

[a]N/A = not applicable.

fastest possible spectrum, no reflector was added. Therefore, the design consists of layers of uranium-molybdenum foils sandwiched between two layers of HEU.

A second critical experiment was designed as an additional fast spectrum application for TSURFER. It sacrifices some spectrum hardness in order to reduce the required HEU for criticality by including a graphite reflector surrounding the fuel regions. Figure 3 shows a simplified geometry for the Fast Reflected critical experiment and compares the spectra, normalized by peak channel, of both the bare and reflected fast critical experiments. The proposed reflected fast critical experiment, shown in red, has substantially increased the neutron population in the resonance and thermal energy regions.

III.B. Thermal Spectrum Critical Experiment Designs

The uranium-molybdenum fuel foils are designed for thermal spectrum reactors. However, to date, there are no thermal spectrum critical experiments containing uranium-molybdenum–alloy fuels. The following details two proposed thermal spectrum critical experiments featuring the uranium-molybdenum fuel foils: the Thermal critical experiment, comprising layers of uranium-molybdenum foils interleaved with Lucite moderator and surrounded by a graphite reflector, and an experiment composed similarly to the Thermal experiment but with additional molybdenum metal–only layers between the fuel foils and moderator, called the Thermal Maximum critical experiment. The purpose of the latter design is to achieve the maximum sensitivity possible to the molybdenum cross section in a thermal neutron spectrum.

Both thermal systems were designed as layers of fuel interlaced with layers of moderator. The minimum critical system in this configuration had 15 fuel layers of 13 foils each, with an $\sim$25-cm-thick graphite reflector for the Thermal design and an $\sim$50-cm-thick graphite reflector for the Thermal Maximum design. Figure 4 shows a simplified experiment geometry for the Thermal Maximum design, as well as calculated spectra for the Thermal and Thermal Maximum designs. Figure 4 is not drawn to scale in order to clearly show geometry details.[27–29]

As expected, dips in the neutron spectra due to resonance effects from molybdenum isotopes are more pronounced in the design with maximum molybdenum content. Additionally, the spectrum is more thermalized for the Thermal Maximum design as compared to the Thermal design, which is to be expected as additional hydrogenous moderating material was required to achieve criticality.

TSUNAMI was used to calculate the sensitivity of the system multiplication factor to changes in the molybdenum isotope cross section for all of the proposed critical experiments. As an example, Fig. 5 gives the sensitivity per unit lethargy for ^{97}Mo for both fast spectrum critical experiment designs as well as one of the fastest spectrum ORNL FBR critical experiments.

Since the designs feature a fast spectrum critical system using low-density fuel intended for a thermal spectrum, the molybdenum sensitivity is markedly different (and generally smaller) than that of the ORNL

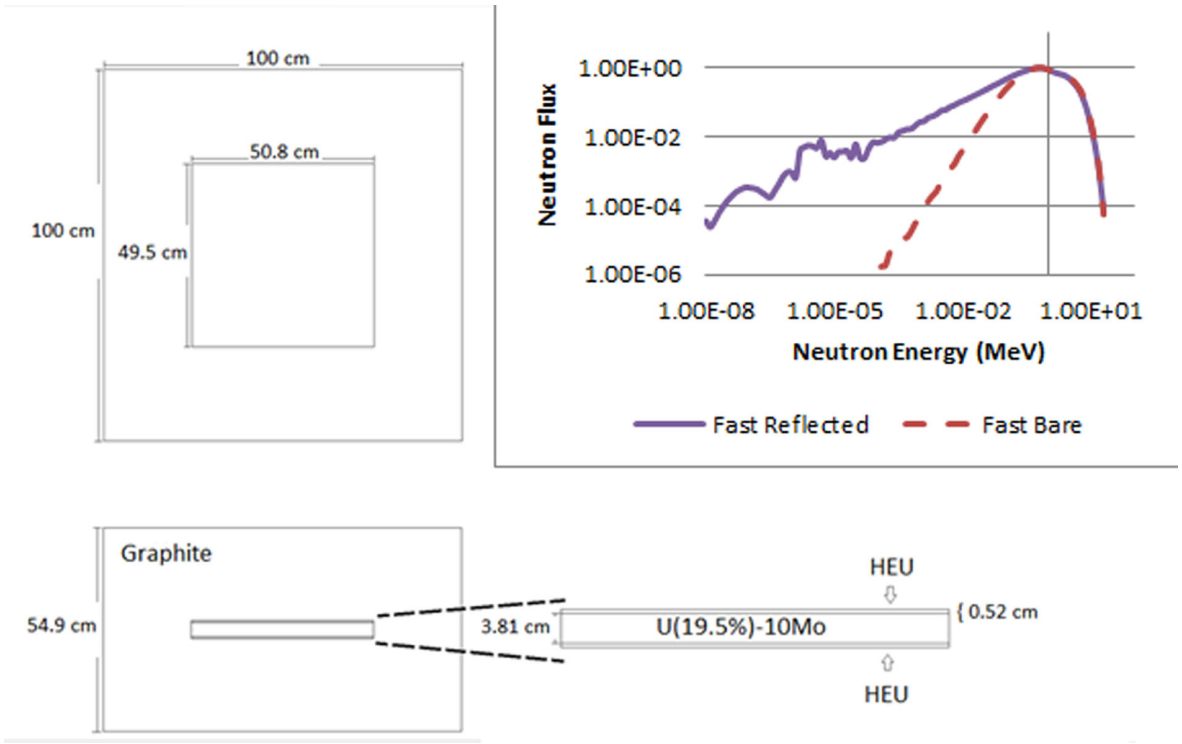

Fig. 3. Fast Reflected critical experiment design geometry and fast critical experiment spectra.

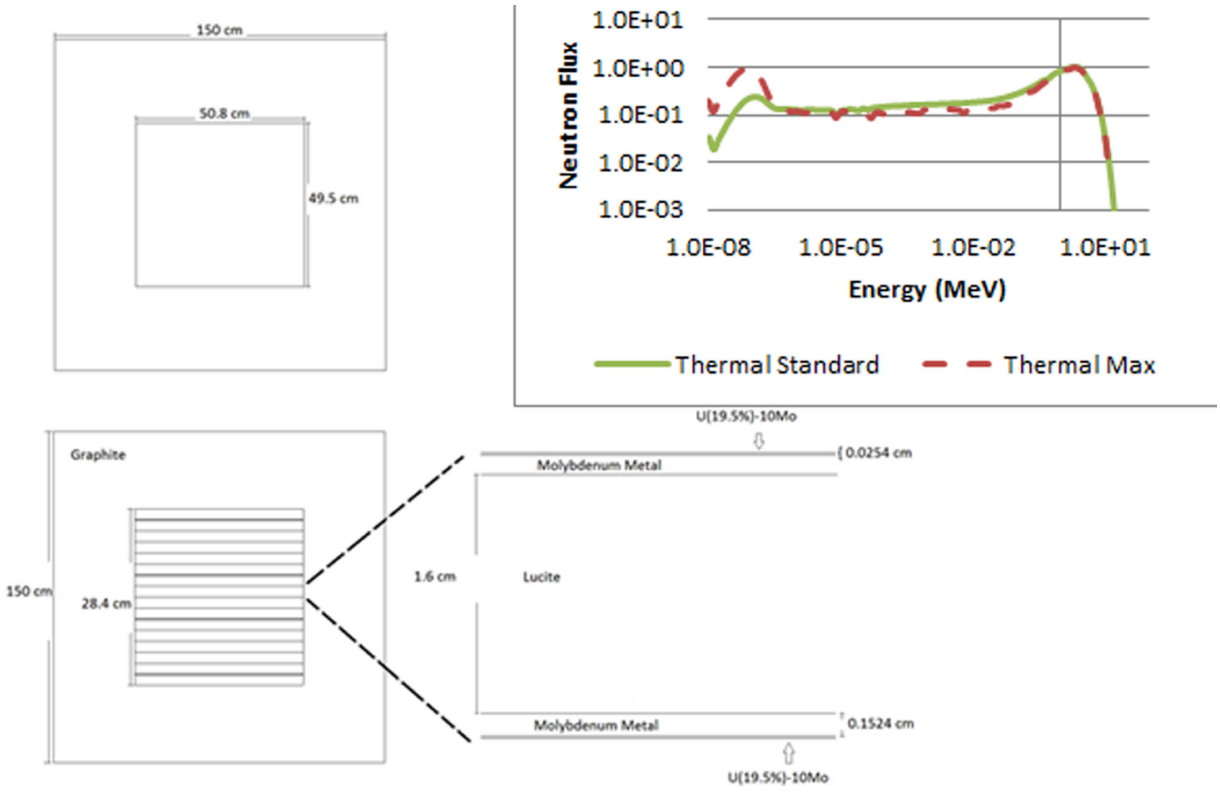

Fig. 4. Thermal Maximum critical experiment design geometry and thermal critical experiment spectra.

FBR critical experiment. However, given the low ^{235}U density of the uranium-molybdenum fuel as compared to the molybdenum-free HEU driver, the two proposed critical experiment designs offer adequate molybdenum sensitivity.

As with the fast spectrum designs, the thermal critical experiment systems were modeled in SCALE to take advantage of its TSUNAMI sensitivity and uncertainty package. Figure 6 gives the sensitivity per unit lethargy for ^{97}Mo for both thermal spectrum critical experiment designs as well as the most thermalized ORNL FBR critical experiment.

Both thermal critical experiment designs demonstrate low sensitivity to the molybdenum isotopes at high energies and significant sensitivity at thermal and resonance energies. The Thermal critical experiment design overall demonstrates lower sensitivity to the molybdenum isotopes, as there are simply few molybdenum atoms in the system as compared to the two other thermal critical experiments. However, the Thermal Maximum critical experiment demonstrates high levels of sensitivity to the molybdenum isotopes, especially throughout the resonance region.

IV. COVARIANCE DATA GENERATION

The ENDF data format includes two means of recording energy-wise cross-section covariance data: parameter-wise covariance data in File 32 and groupwise covariance data in File 33 (Refs. 3 and 4). Both of these file formats have advantages, and they must generally be used in tandem to fully describe an isotope's cross-section uncertainty data.

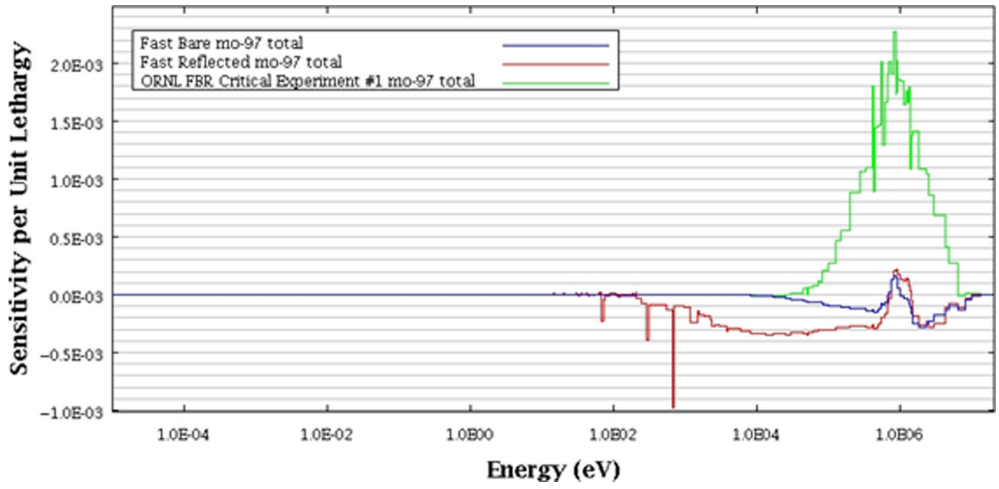

Fig. 5. Molybdenum-97 total cross-section sensitivity (%/%) for fast spectra critical experiment designs.

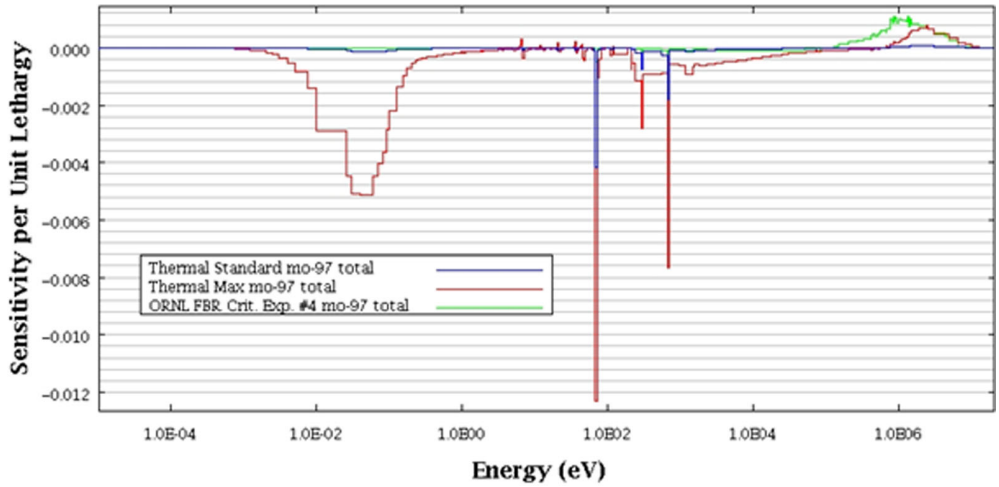

Fig. 6. Molybdenum-97 total cross-section sensitivity (%/%) for thermal spectra critical experiment designs.

In this section, a method is demonstrated for generating complete covariance data sets, including both File 32 and File 33 formatted data, for the natural isotopes of molybdenum. The retroactive covariance method of the SAMMY R-matrix analysis code is used to generate the resonance parameter-wise uncertainty and correlations in File 32 from experimental data. A combination of integral measurement uncertainty, a dispersion method, and high-energy covariances produced with the Empire-KALMAN code is used to generate the groupwise File 33 covariance data.[30]

IV.A. Resonance Parameter-Wise Covariance Data

The primary purpose of the molybdenum measurements at the RPI Linac was to generate an improved set of resonance parameters for the molybdenum isotopes. Many current experimental cross-section evaluations, including those based on the RPI measurements, do not retain their resonance parameter covariance matrix. However, the functionality exists in SAMMY to retroactively generate these missing covariance matrices. The first step in generating covariances for experimental data is to generate a fit to the experimental data using SAMMY. This process can be lengthy, as an initial "guess" of resonance parameters must be obtained, either through a parameter estimation code or from a parameter set from a prior evaluation. Manual adjustment of parameters and addition of parameters for resonances that were not included in the initial set must be undertaken over the course of many SAMMY runs to generate the final best-fit set of resonance parameters. For this work, however, a set of resonance parameters derived from the experimental data is already available.[31]

Therefore, to obtain a starting point for the covariance analyses, the SAMMY results of Ref. 31 were reproduced. To include effects of experimental resolution and Doppler broadening, self-shielding, and multiple-scattering events required knowledge of the experimental conditions, detailed in Ref. 31.

IV.A.1. Analysis with SAMMY

The RPI experimental results included data for neutron transmission from 0 to 2000 eV and for neutron capture from 0 to 600 eV. Resonance-wise covariance data generated from this evaluation will therefore be limited to resonances within the energy region covered by both transmission and capture experimental data, i.e., 0 to 600 eV.

Once this SAMMY fit was optimized to match the RPI resonance parameter set, subsequent SAMMY runs were completed for each isotope. In these runs the resonance parameters for only the selected isotope in the 0- to 600-eV energy region covered by both transmission and capture data are allowed to vary. This simulates variations in the experimental data covariance matrix V. Additionally, other sources of uncertainty, such as normalization, background, and experimental setup resolution function were propagated using SAMMY's Propagated Uncertainty Parameter (PUP) feature. Finally, the experimental covariance matrix and PUP-treated uncertainty information were saved as the Y and W matrices introduced in Eqs. (3) and (4).

Using the generated Y and W matrices, a final SAMMY run was completed with the option of generating ENDF-formatted File 32 covariance data. These are resonance parameter-wise covariance data for the resonances varied in the 0- to 600-eV energy range. This energy range does not cover the entire resolved resonance region for any of the natural molybdenum isotopes. However, for most isotopes, it does capture the effects of the large, low-lying resonances. While this does not result in a perfect representation of the resonance-to-resonance covariance data, it does produce the best possible set of covariance data given the experimental data available.

In order to visualize the resonance parameter covariance data produced by the retroactive method of SAMMY, it is helpful to convert it to groupwise covariance data. A groupwise covariance matrix for the total cross section in the resonance region of ^{97}Mo is plotted in Fig. 7 in the SCALE 44-group structure. Current covariance data assume complete correlation within energy regions, whereas the retroactively generated covariance data exhibit a finely resolved correlation structure. This is seen in the central images of Figs. 2 and 8. The uncertainty in each energy group is plotted above the correlation matrix in Fig. 8. The vector product of the uncertainty values and the correlation matrix yields the covariance matrix. On average, the resonance parameter-wise covariance data were 200 kbytes in size.

IV.B. Group Cross-Section–Wise Covariance Data

Retroactively generated resonance parameter covariance matrices show significant improvement in correlation data resolution as compared to current libraries that assume total correlation across all energy ranges. However, these covariance data often have cross-section variances that are too low to be considered physical by end users and are in fact below the minimum reasonable uncertainty values defined by the Cross Section Evaluation Working Group[32] (CSEWG). This low uncertainty can result from missing or unknown sources of uncertainty in the retroactive covariance generation process and model calculations. Without invalidating the normalized correlation coefficients obtained as described above, it can lead to unrealistically low variance magnitudes if the experimental data set alone is considered.

Additionally, by definition the resonance parameter covariance matrix applies only to the resolved resonance region as defined by its parameters. Other covariance data

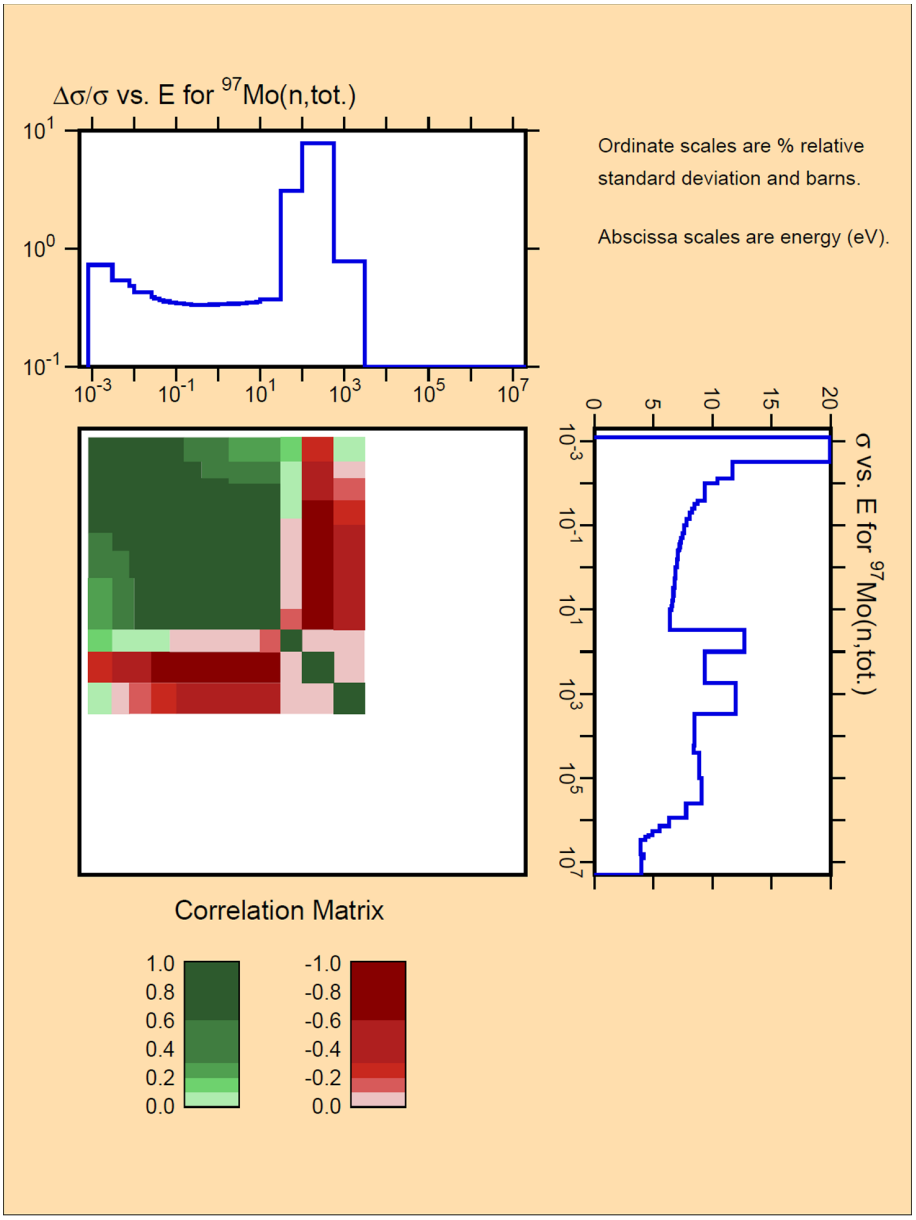

Fig. 7. Molybdenum-97 total retroactive resolved resonance covariance.

will be needed in the unresolved resonance region and high-energy region. The end goal then is to couple the improved fidelity correlations of the retroactive resonance parameter covariance matrix with reasonable uncertainty values from independent sources and to provide covariance data throughout all energy regions of interest.

To accomplish this, we incorporated uncertainty data from three additional sources: integral measurements at thermal and resonance energies; a dispersion analysis of select general-use nuclear data libraries in the resonance region; and currently used high-energy, low-fidelity covariances generated at BNL using the Empire-KALMAN code. These uncertainty data were tabulated in ENDF File 33 format, which provides a means of recording energy groupwise covariance data.

IV.B.1. Integral Measurement Uncertainty

Integral measurement uncertainties are tabulated in the *Atlas of Neutron Resonances* (the Atlas) and provide an additional connection with uncertainty data from experimental sources.[33] The most important quantities included in the Atlas for this work are

1. thermal cross sections (total, capture) with uncertainties

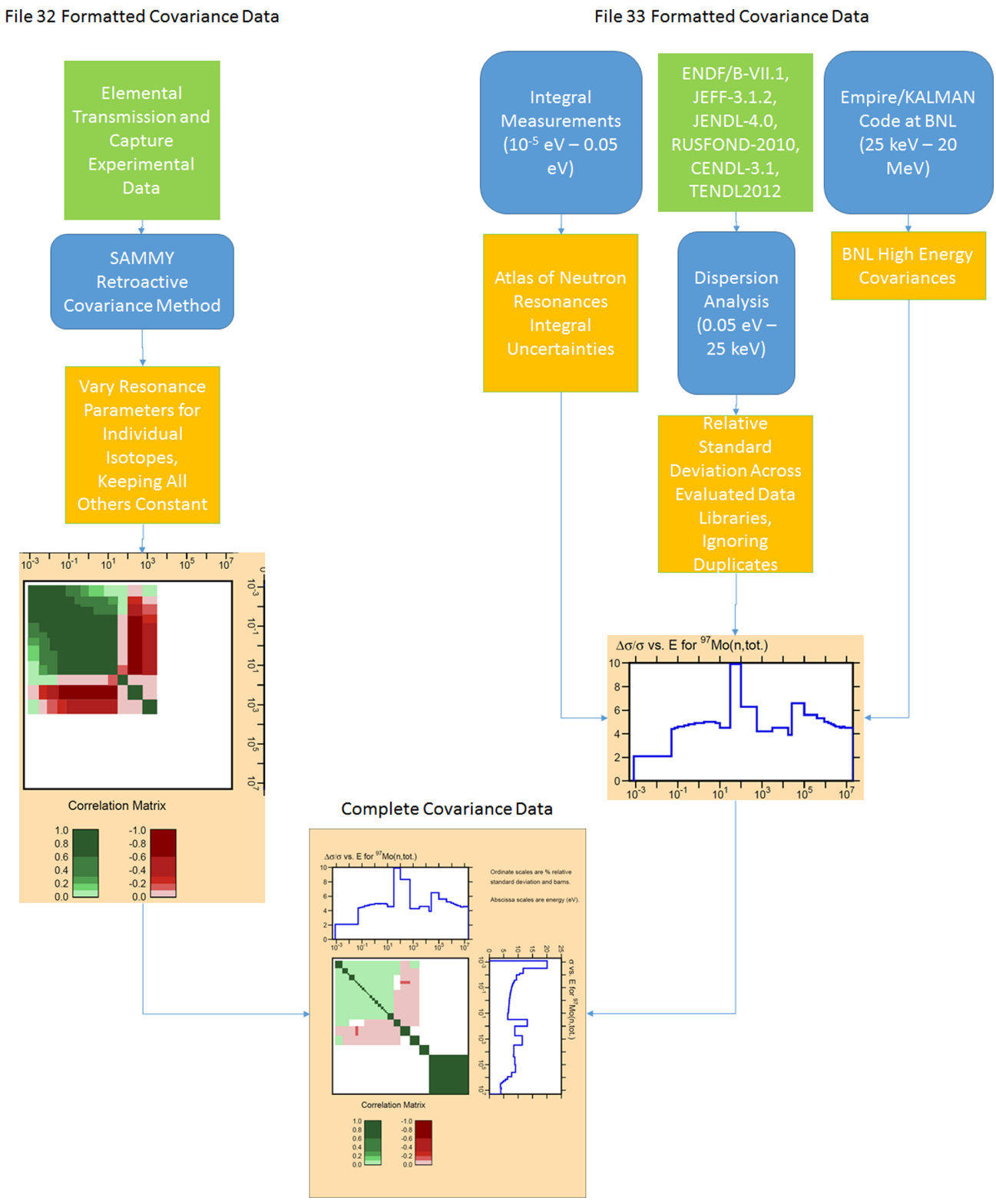

Fig. 8. Covariance data generation work flow.

2. scattering radii, with uncertainties
3. resonance integrals (capture), with uncertainties.

These values can serve as a check of the reasonableness of calculated uncertainty data, as well as provide direct cross-section uncertainty data in the

thermal energy region for evaluations with missing sources of uncertainty.

Table III summarizes key integral uncertainty values for the natural molybdenum isotopes.

In constructing File 33, the first three columns of Table II were used to determine the diagonal values of the covariance matrix in the thermal energy region, from 10^{-5} to 0.05 eV, for total, capture, and scattering interaction cross sections respectively, for energy groups where the File 32 covariance data reported an uncertainty below the acceptable limits as defined by the CSEWG.

IV.B.2. Dispersion Method

To provide an independent source of uncertainty data, the National Nuclear Data Center has taken to considering the dispersion between evaluations when generating covariance libraries. Dispersion methods consider the dispersion between evaluations as a further basis for uncertainty estimation. The concept is that the spread between independently evaluated cross sections from the major data libraries reflects the true opinion of the international community of evaluators with respect to the cross-section precision.[17,34,35] Advantages of this process include relative simplicity and ease of use, as well as transparency. The dispersion method of estimating cross-section uncertainty data has come under criticism because it does not derive directly from experimental data but rather from evaluated data that themselves are an amalgamation of adjusted experimental measurements and interaction model predictions. But, the dispersion method is used here only to supplement the resonance-wise covariances generated from experimental data, not as a stand-alone source of uncertainty data.

In order to complete a dispersion method analysis for natural molybdenum isotopes, six modern general-use cross-section libraries available through the Nuclear Energy Agency's online data bank were selected. Those libraries were ENDF/B-VII.1, JEFF-3.1.2, JENDL-4.0, RUSFOND-2010, CENDL-3.1, and TENDL2012 (Refs. 36, 37, and 38).

Total, capture, and elastic scattering cross sections for all natural isotopes of molybdenum from each of the above libraries were collapsed to the SCALE 44-group structure. The groupwise relative standard deviation across the independent evaluations was then calculated. The diagonal values of the covariance matrix in the resonance energy region, from 0.05 eV to 25 keV, were then matched to these calculated values using a combination of File 33 and File 32 formatted covariance data for their respective interactions where the File 32 covariance data alone reported an uncertainty below the acceptable limits as defined by the CSEWG.

IV.B.3. Empire-KALMAN High-Energy Covariances

In the high-energy region, model-based covariances have been generated using the coupled Empire-KALMAN code at BNL. This code operates similarly to SAMMY and generates covariance data based on parameters of high-energy region interaction models.[39] KALMAN is a Bayesian code based on the theory of the Kalman filter, which can estimate covariances by combining experimental uncertainties and correlations with theoretical predictions.

These are the highest-fidelity uncertainty and covariance data available for the high-energy region of the molybdenum isotopes and is currently included in ENDF/B-VII.1. The uncertainty values reported by BNL were assigned as the diagonal values of the covariance matrix in the high-energy region, from 25 keV to 20 MeV. On average, the group cross-section–wise covariance data required $\sim$15 kbytes of space.

Through this combination of integral measurement uncertainty, dispersion method analysis, and the high-energy covariances of the Empire-KALMAN code, a complete set of covariance data of reasonable variance magnitude spanning 10^{-5} eV to 20 MeV was generated for the natural molybdenum isotopes. Figure 8 provides a work-flow overview for the various sources of uncertainty information and how they were combined. Figure 9 provides an example of the results generated through this

TABLE III

Integral Uncertainties for Natural Molybdenum Isotopes from Ref. 33

	Thermal Total Cross Section	Thermal Capture	Scattering Radius	Resonance Integral
^{92}Mo	2.33%	25.00%	2.86%	N/A[a]
^{94}Mo	2.06%	17.65%	2.90%	N/A
^{95}Mo	5.70%	2.24%	2.86%	5.93%
^{96}Mo	1.86%	40.00%	2.88%	17.65%
^{97}Mo	2.12%	9.09%	2.90%	20.83%
^{98}Mo	2.20%	4.62%	2.90%	4.48%
^{100}Mo	2.11%	1.51%	2.90%	3.99%

[a]N/A = not available.

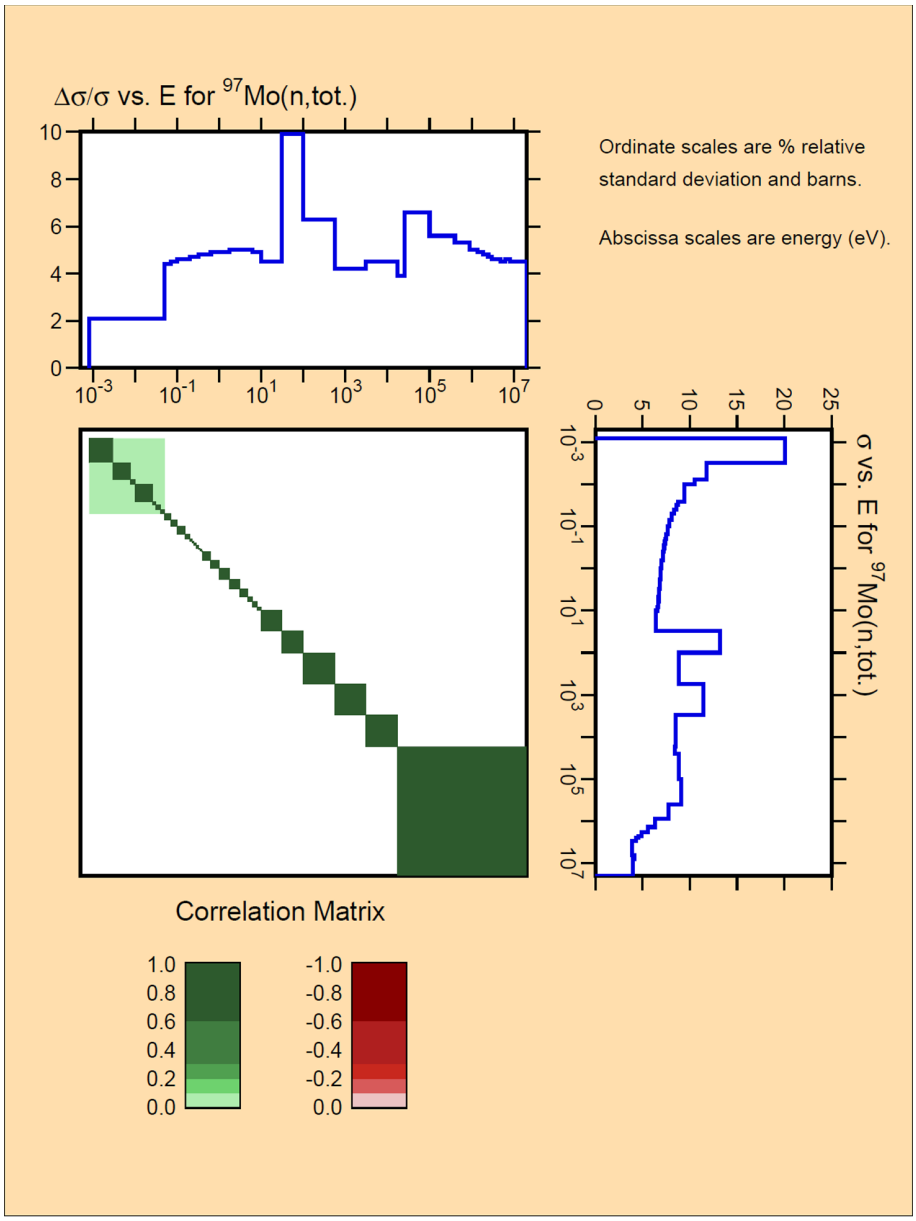

Fig. 9. Molybdenum-97 total File 33 variance.

work flow. Off-diagonal correlation will be regained by combining the retroactively generated File 32 data with the diagonal File 33 data. Apparent correlation at thermal energies is due to round-off error from NJOY processing.

Figure 10 shows the complete improved covariance library (File 32 and File 33 combined) for ^{97}Mo. Groupwise covariance data are utilized in the high-energy and unresolved resonance regions, while a combination of groupwise and parameter-wise covariance data is utilized in the resolved resonance region. The combination of parameter-wise and groupwise covariance data in the resonance region was done on the basis of a comparison to the CSEWG guidelines on acceptable minimum uncertainty from Ref. 32. When the parameter-wise uncertainty (collapsed to the same group structure as used for the File 33 data) for a given energy group was greater than or equal to the minimum uncertainty as dictated by Ref. 32, the File 32 data were used. When the parameter-wise uncertainty data for a given energy group was less than the CSEWG guidelines, the groupwise covariance data were modified so that the combination of parameter-wise and groupwise uncertainty data matched the integral measurement uncertainty or dispersion method uncertainty for that energy group. The combined File 32 and File 33 formatted covariance library for the molybdenum isotopes can now be used in sensitivity and

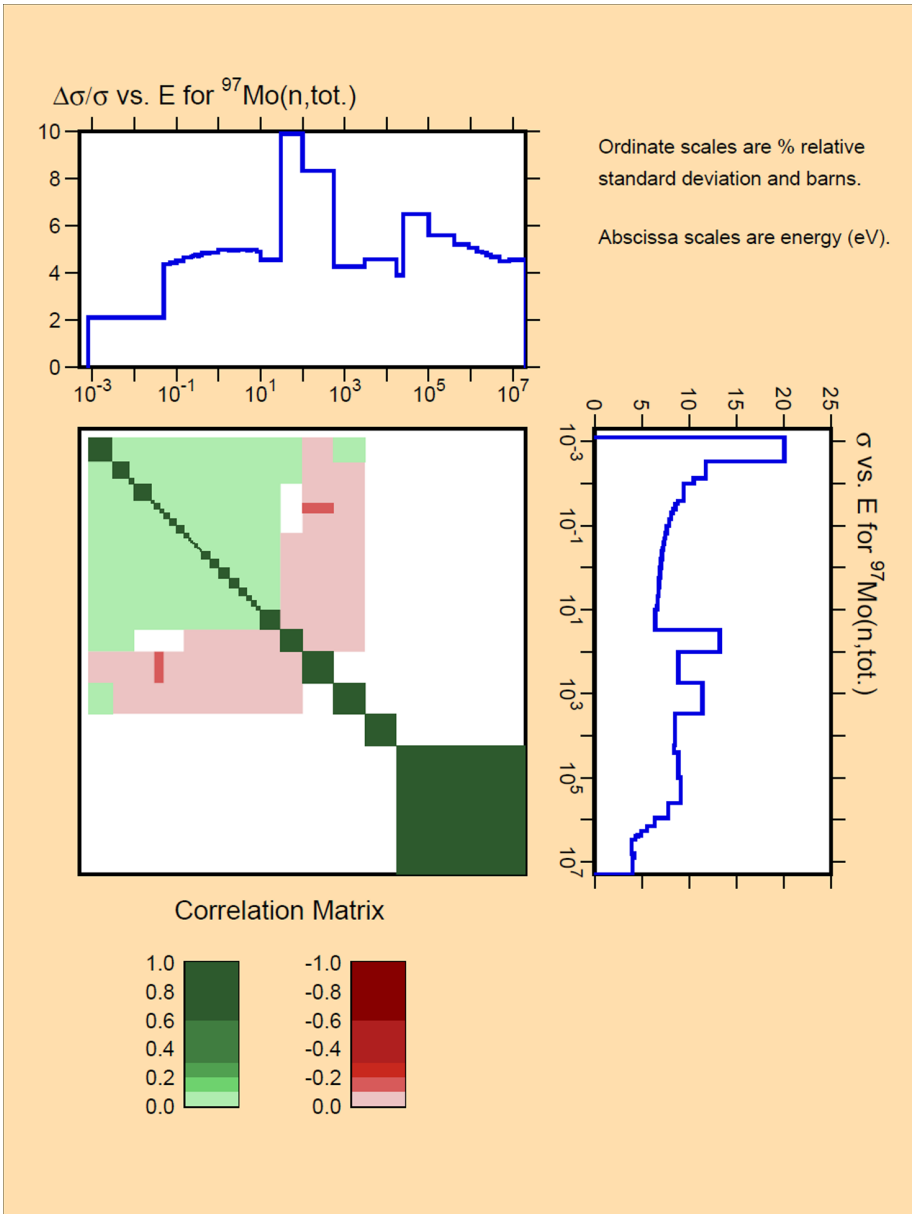

Fig. 10. Molybdenum-97 total cross-section improved covariance data.

uncertainty studies of the designed uranium-molybdenum foil fuel form critical experiments.

IV.C. Analytical Comparison of Low-Fidelity and Improved Molybdenum Covariance Data

The improved fidelity molybdenum covariance library generated is tied to the set of resonance parameters reported by RPI through the File 32 covariances. The first step toward comparing the new molybdenum covariance data against the existing library was then to incorporate those resonance parameters and covariance information into an ENDF/B formatted file.

As before, ENDF/B-VII.1, JEFF 3.1.1, and JENDL 4.0 evaluated nuclear data files were selected as the basis for the molybdenum nuclear data. The RPI experimental resonance parameters and File 32 and File 33 covariance data for total, elastic scattering, and capture reactions were inserted into the appropriate data files. Additionally, the current low-fidelity covariance data for the inelastic scattering and (*n*,2*n*) reactions was inserted into the JEFF 3.1.1 and JENDL 4.0 nuclear data files in order to ensure a one-to-one comparison with the ENDF/B-VII.1 nuclear data files, which already included these covariance data.

After combining the nuclear data files with the RPI resonance parameters and improved covariance data, the

SCALE module TSUNAMI regenerated the sensitivity profiles for the molybdenum sensitive critical experiments from the ICSBEP Handbook and the ORNL FBR program for each of the evaluated nuclear data libraries. The SCALE module TSURFER was then used with the regenerated sensitivity profiles and ENDF-, JEFF-, and JENDL-based covariance libraries to calculate the goodness of fit between the calculated results using the cross-section data and the reported experimental results.

TSURFER reports its goodness-of-fit metric in terms of the value of chi squared (χ^2) per degree of freedom. In order to maintain consistency across the set of experimental data, the SCALE manual recommends a maximum $\chi 2$ value per degree of freedom of 1.2. This sets the bounds of possible cross-section adjustment in terms of the cross-section covariance data. In order to achieve this maximum $\chi 2$ value, TSURFER eliminates experimental responses until $\chi 2$ per degree of freedom is less than 1.2. The individual experimental responses make up the degrees of freedom. Table IV compiles the goodness-of-fit results of the described TSURFER runs.

Based on its closest fit to the experimental data, JENDL 4.0 was selected as the basis for the cross-section and covariance data moving forward.

IV.C.1. Goodness-of-Fit and Bias Comparison

Care must be taken when comparing covariance data sets when differences in cross-section data are also present. In the case at hand, cross-section differences play a role in the form of the RPI resonance parameters. Further details of these cross-section differences can be found in Ref. 30. If the RPI parameters are assumed to be superior to the current set of resonance parameters in ENDF/B-VII.1 (unchanged from ENDF/B-VII.0 and used in the default SCALE 238-group library), then calculated multiplication factors should better match reported experimental values, and TSURFER should report a reduced bias, regardless of covariance data used. Similarly, if the high-fidelity covariance data are a more accurate reflection of the general uncertainty associated with molybdenum cross-section data, then TSURFER should report a reduced bias when the high-fidelity covariance data are used, regardless of cross-section data. However, this assumption may be complicated by the fact that the high-fidelity covariance data are tied to the RPI resonance parameters through the File 32 covariance data. Finally, when both the superior cross-section data (RPI resonance parameters) and improved covariance data are used, the lowest bias should be obtained. Tables V through VIII summarize the TSURFER bias results for the combinations discussed above.

Tables V through VIII list effective and absolute bias values for each proposed critical experiment design. The effective bias is the sum of all the biases from the individual (isotope, reaction) pairs possible in the experiment. The signs for these biases can be positive or negative and can therefore cancel each other out in the effective bias. The absolute bias is the sum of the absolute values of the individual biases. For ease of comparison, Fig. 11 compiles the last column of Tables V through VIII.

As can be seen in Fig. 11, there is generally a reduction in bias when the JENDL-based cross-section data are used, indicating that the combination of RPI resonance parameters and JENDL cross-section data is an

TABLE IV

χ^2 for ENDF, JEFF, and JENDL

	ENDF	JEFF	JENDL
χ^2 per degree of freedom	2.336E + 00[a]	2.707E + 00	1.195E + 00

[a]Read as 2.336×10^{00}.

TABLE V

TSURFER Bias: ENDF/B-VII.1 Cross Sections and Low-Fidelity Covariance Data

Name	Calculated k_{eff} Value	Initial Standard Deviation	Adjusted k_{eff} Value	Adjusted Standard Deviation	Effective Bias	Absolute Bias
Fast Bare	9.9779E-01[a]	1.07E-02	9.9953E-01	2.77E-03	−1.74E-03	1.20E-02
Fast Reflected	9.9870E-01	2.04E-02	1.0121E+00	5.09E-03	−1.34E-02	1.75E-02
Thermal Standard	9.9871E-01	4.89E-03	9.9874E-01	2.12E-03	−3.48E-05	8.03E-03
Thermal Maximum	9.9687E-01	5.96E-03	9.9632E-01	4.17E-03	5.50E-04	5.65E-03

[a]Read as 9.9779×10^{-01}.

TABLE VI

TSURFER Bias: ENDF/B-VII.1 Cross Sections and High-Fidelity Covariance Data

Name	Calculated k_{eff} Value	Initial Standard Deviation	Adjusted k_{eff} Value	Adjusted Standard Deviation	Effective Bias	Absolute Bias
Fast Bare	9.9779E-01[a]	1.07E-02	9.9967E-01	2.77E-03	−1.88E-03	1.28E-02
Fast Reflected	9.9870E-01	2.04E-02	1.0133E+00	4.98E-03	−1.46E-02	1.89E-02
Thermal Standard	9.9871E-01	4.89E-03	9.9878E-01	2.12E-03	−7.00E-05	7.94E-03
Thermal Maximum	9.9687E-01	5.96E-03	9.9654E-01	2.75E-03	3.36E-04	5.32E-03

[a]Read as 9.9779×10^{-01}.

TABLE VII

TSURFER Bias: RPI Resonance Parameters and Low-Fidelity Covariance Data

Name	Calculated k_{eff} Value	Initial Standard Deviation	Adjusted k_{eff} Value	Adjusted Standard Deviation	Effective Bias	Absolute Bias
Fast Bare	9.9795E-01[a]	1.07E-02	1.0001E+00	2.80E-03	−2.13E-03	3.64E-03
Fast Reflected	9.9860E-01	2.03E-02	9.9805E-01	4.88E-03	5.57E-04	3.72E-03
Thermal Standard	9.9828E-01	4.91E-03	1.0029E+00	2.13E-03	−4.66E-03	4.07E-03
Thermal Maximum	9.9765E-01	5.11E-03	1.0014E+00	4.22E-03	−3.76E-03	4.63E-03

[a]Read as 9.9795×10^{-01}.

TABLE VIII

TSURFER Bias: RPI Resonance Parameters and High-Fidelity Covariance Data

Name	Calculated k_{eff} Value	Initial Standard Deviation	Adjusted k_{eff} Value	Adjusted Standard Deviation	Effective Bias	Absolute Bias
Fast Bare	9.9795E-01[a]	1.07E-02	1.0001E+00	2.80E-03	−2.17E-03	3.71E-03
Fast Reflected	9.9860E-01	2.03E-02	9.9803E-01	4.75E-03	5.77E-04	3.74E-03
Thermal Standard	9.9828E-01	4.91E-03	1.0029E+00	2.13E-03	−4.65E-03	3.98E-03
Thermal Maximum	9.9765E-01	5.11E-03	1.0015E+00	2.78E-03	−3.82E-03	4.59E-03

[a]Read as 9.9795×10^{-01}.

improvement on the ENDF/B-VII.1 data. The comparison of covariance libraries is less clear-cut: For the fast spectrum results, the bias is slightly reduced for the low-fidelity covariance data set, while for the thermal spectrum cases, the bias is reduced for the improved covariance case. To reiterate, only the molybdenum isotope cross-section data and covariance data vary among the above cases; all other cross-section and covariance data are constant.

Isolating the bias associated specifically with molybdenum can lead to a clearer understanding of the impact of the improved covariance data. Figures 12 through 15 compile the total absolute bias for each molybdenum isotope for each combination of cross-section and covariance data for each proposed critical experiment design. It should be noted that even the current low-fidelity covariance data perform reasonably well. However, in all cases and for all the molybdenum isotopes, using the improved covariance data in conjunction with the RPI resonance parameters reduces the absolute bias as compared to the current cross-section data and covariance data. Additionally, for a clear majority of the molybdenum isotopes across the four experiment designs, the absolute bias is reduced when compared against the case where the RPI parameters and current low-fidelity data are used.

Finally, Fig. 16 displays the total absolute bias for elemental molybdenum across the four proposed critical

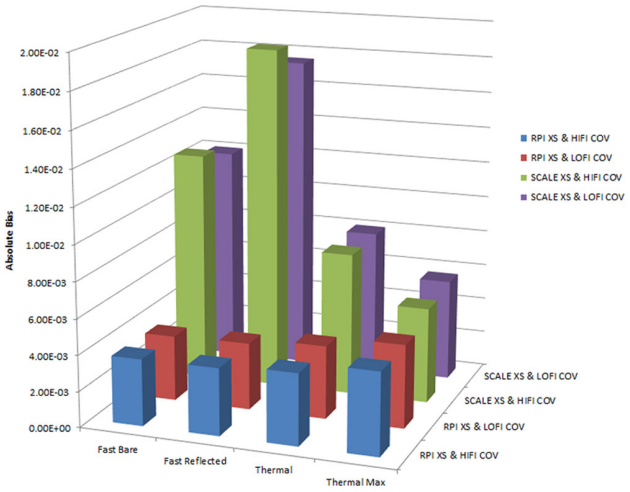

Fig. 11. Absolute bias comparison across experiment designs and nuclear data sets.

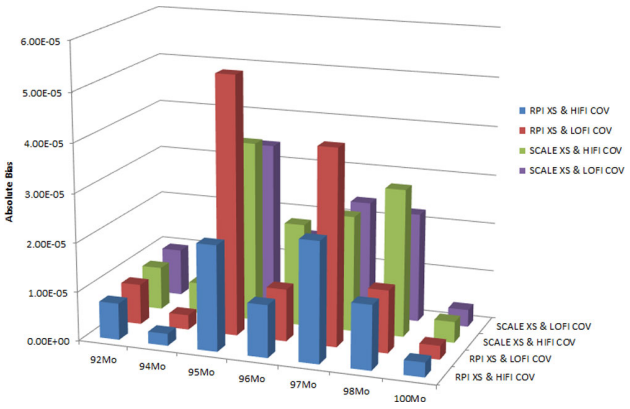

Fig. 12. Molybdenum isotope bias comparison across nuclear data sets for Fast Bare critical experiment design.

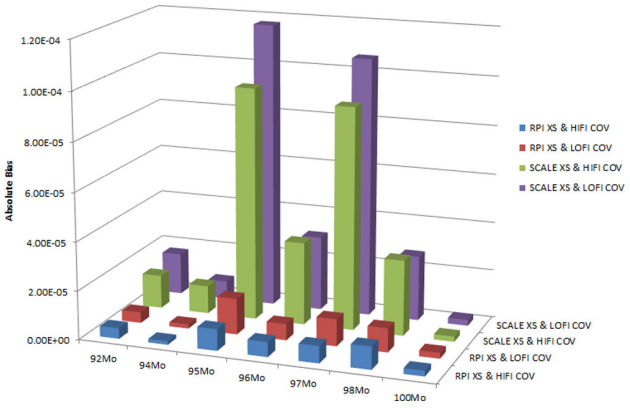

Fig. 13. Molybdenum isotope bias comparison across nuclear data sets for Fast Reflected critical experiment design.

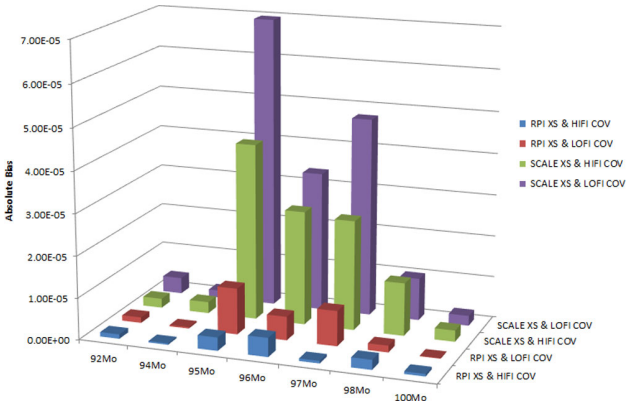

Fig. 14. Molybdenum isotope bias comparison across nuclear data sets for Thermal critical experiment design.

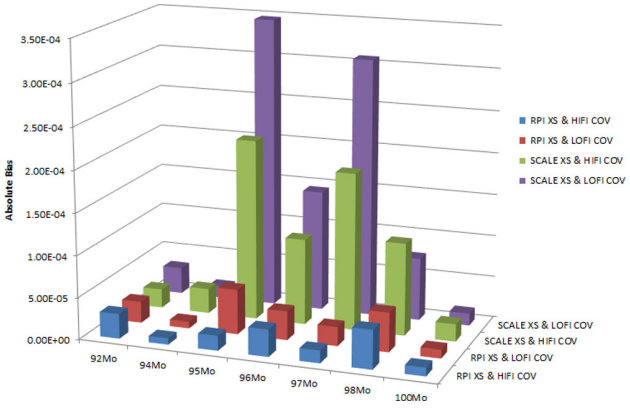

Fig. 15. Molybdenum isotope bias comparison across nuclear data sets for Thermal Maximum critical experiment design.

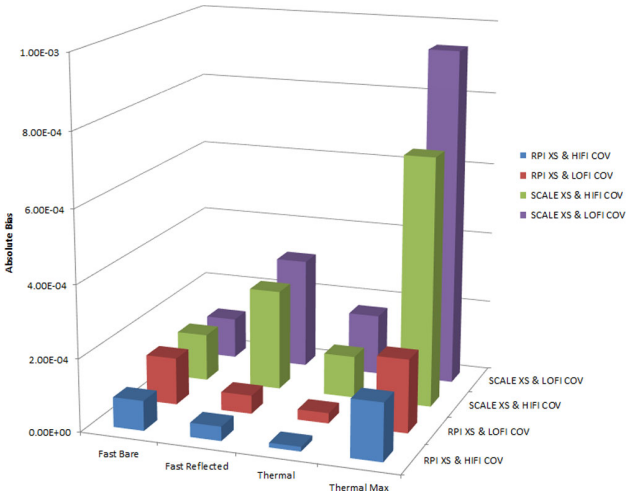

Fig. 16. Total molybdenum bias.

TABLE IX

Goodness of Fit for Combinations of Cross-Section and Covariance Data

	JENDL/RPI XS & HIFI COV	JENDL/RPI XS & LOFI COV	ENDF/B-VII.1 & HIFI COV	ENDF/B-VII.1 & LOFI COV
χ^2 per degree of freedom	1.195E+00[a]	1.197E+00	1.428E+00	1.379E+00

[a]Read as 1.195×10^{00}.

experiment designs and four combinations of cross-section and covariance data. The clear trend is a reduction in bias associated with molybdenum due to the use of improved cross-section and covariance data. Even the Fast Bare critical experiment, which has the lowest neutron population in the thermal and resonance regions, demonstrates a significant reduction in molybdenum isotope–related bias.

While the above discussion of absolute biases strongly indicates a qualitative improvement in the covariance data, it would still be possible for reduced absolute biases to appear with poorer covariance data if the goodness of fit of the calculated to experimental results due to the cross-section changes generated by TSURFER was also degraded. Table IX gives the χ^2 per degree of freedom measure of goodness of fit as reported by TSURFER for the four possible combinations of cross-section data and covariance data. JENDL/RPI XS refers to the cross-section data generated by inserting the resonance parameters from Ref. 31 in JENDL4.0 evaluated data files, while ENDF/B-VII.1 refers to the cross-section library currently used in the SCALE code package. Similarly, HIFI COV refers to the improved set of molybdenum covariance data generated as detailed previously, while LOFI COV refers to the existing low-fidelity molybdenum covariance data currently used in the SCALE code package. As seen with the absolute bias data, a significant improvement in goodness of fit is achieved through the improved cross-section data, and another slight improvement to the goodness of fit is observed when both the improved cross-section data and improved covariance data are used in conjunction.

An additional challenge to ascertaining the impact of the new molybdenum covariance data arose due to the high uncertainty in the ^{235}U high-energy capture cross section, combined with the high sensitivity to this cross section that all ^{235}U-fueled systems exhibit. The TSURFER adjustments to this cross section often dwarfed those of the molybdenum isotopes. Improvement in the high-energy ^{235}U capture cross section would be beneficial for all sensitivity and uncertainty studies similar to those demonstrated here.

V. CONCLUSIONS

The primary objective of this paper was to demonstrate a novel means to generate a new improved fidelity set of cross-section covariance data for the natural molybdenum isotopes utilizing an elemental cross-section evaluation. A key intended application of these covariance data was the modeling of systems using a new uranium-molybdenum–alloy fuel form for use in research and test reactors.

The Bayesian analysis code SAMMY was used to generate uncertainty correlation data throughout the resolved resonance region for each of the molybdenum isotopes. These data were stored using the ENDF File 32 covariance data format. Additionally, integral uncertainty measurements, a dispersion method analysis, and high-energy covariances generated at BNL were incorporated to ensure the new covariance data satisfied the requirements set forth by the CSEWG. These data were stored using the ENDF File 33 covariance data format.

A series of critical experiments was proposed as a means to compare the performance of the new molybdenum covariance data to the existing low-fidelity molybdenum covariance data. These critical experiments feature the new intermediate enrichment uranium-molybdenum–alloy fuel form.

The newly generated improved molybdenum covariance data library was used in a sensitivity and uncertainty study of existing molybdenum sensitive critical experiments and the proposed critical experiment series. When coupled with JENDL 4.0 cross-section data, the improved covariance data provided the best fit to the existing critical experiment data while simultaneously reducing the computational bias associated with the molybdenum isotopes as compared to the existing low-fidelity covariance data.

REFERENCES

1. P. SCHILLEBEECKX et al., "Determination of Resonance Parameters and Their Covariances from Neutron Induced Reaction Cross Section Data," *Nucl. Data Sheets*, **113**, 3054 (2012); http://dx.doi.org/10.1016/j.nds.2012.11.005.

2. D. NEUDECKER et al., "Impact of Model Defect and Experimental Uncertainties on Evaluated Output," *Nucl. Instrum. Methods Phys. Res. A*, **723**, 163 (May 2013); http://dx.doi.org/10.1016/j.nima.2013.05.005.

3. V. MCLANE et al., "ENDF-102 Data Formats and Procedures for the Evaluated Nuclear Data File ENDF-6," Brookhaven National Laboratory, National Nuclear Data Center (Apr. 2001).

4. M. HERMAN et al., "ENDF-6 Formats Manual," Brookhaven National Laboratory, National Nuclear Data Center (July 2010).

5. O. IWAMOTO et al., "Covariance Evaluation for Actinide Nuclear Data in JENDL-4," *J. Korean Phys. Soc.*, **59**, 1224 (Aug. 2011); http://dx.doi.org/10.3938/jkps.59.1224.

6. G. M. HALE, "Covariances from Light-Element R-Matrix Analyses," *Nucl. Data Sheets*, **109**, 2812 (2008); http://dx.doi.org/10.1016/j.nds.2008.11.015.

7. R. LITTLE et al., "Low-Fidelity Covariance Project," *Nucl. Data Sheets*, **109**, 2828 (2008); http://dx.doi.org/10.1016/j.nds.2008.11.018.

8. R. DUNAVANT et al., "Uranium-Molybdenum Fuel Foil Fabrication Development Activities at the Y-12 National Security Complex," *Proc. Int. Mtg. Reduced Enrichment for Research and Test Reactors (RERTR-2006)*, Cape Town, South Africa, October 29–November 2, 2006, Y-12 National Security Complex (2006).

9. N. M. LARSON, "Updated Users' Guide for SAMMY: Multilevel R-Matrix Fits to Neutron Data Using Bayes' Equations," ORNL/TM-9179/R6, Oak Ridge National Laboratory (July 2003).

10. A. M. LANE et al., "R-Matrix Theory of Nuclear Reactions," *Rev. Mod. Phys.*, **30**, *2, Part I* (Apr. 1958); http://dx.doi.org/10.1103/RevModPhys.30.257.

11. R. E. MacFARLANE, "RSICC Peripheral Shielding Routine Collection NJOY99.0," PSR-480 NJOY99.0, Oak Ridge National Laboratory (Mar. 2000).

12. D. WIARDA, "RSICC Peripheral Science Routine Collection AMPX-6," PSR-562, Oak Ridge National Laboratory (Oct. 2010).

13. G. ARBANAS et al., "Retroactive Covariance Matrix for ^{235}U in the Resolved-Resonance Region," Oak Ridge National Laboratory, *Proc. PHYSOR 2006*, Vancouver, Canada, September 10–14, 2006, American Nuclear Society (2006).

14. M. B. CHADWICK et al., "ENDF/B-VII.1: Nuclear Data for Science and Technology: Cross Sections, Covariances, Fission Product Yields and Decay Data," *Nucl. Data Sheets*, **112**, 2887 (2011); http://dx.doi.org/10.1016/j.nds.2011.11.002.

15. "The JEFF-3.1.1 Nuclear Data Library," JEFF Report 22, Organisation for Economic Co-operation and Development/Nuclear Energy Agency Data Bank (2009).

16. K. SHIBATA et al., "JENDL-4.0: A New Library for Nuclear Science and Engineering," *J. Nucl. Sci. Technol.*, **48**, 1 (2011); http://dx.doi.org/10.1080/18811248.2011.9711675.

17. C. M. MATTOON and P. OBLOZINSKY, "Issues in Neutron Cross Section Covariances," Brookhaven National Laboratory, National Nuclear Data Center; see also *J. Korean Phys. Soc.*, **59**, 1242 (Aug. 2011); http://dx.doi.org/10.3938/jkps.59.1242.

18. "SCALE: A Modular Code System for Performing Standardized Computer Analyses for Licensing Evaluations," ORNL/TM-2005/39, Version 6, Vols. I–III (Jan. 2009); see also CCC-750, Oak Ridge National Laboratory Radiation Safety Information Computational Center.

19. B. REARDEN et al., "TSUNAMI Primer: A Primer for Sensitivity/Uncertainty Calculations with SCALE," ORNL/TM-2009/027, Oak Ridge National Laboratory (Jan. 2009).

20. M. WILLIAMS et al., "An Adjustment Code to Determine Biases and Uncertainties in Nuclear System Reponses by Consolidating Differential Data and Benchmark Integral Experiments," Office of Nuclear Material Safety and Safeguards (Dec. 2006).

21. N. DOS SANTO et al., "Impact of Mock-Up Experimental Correlations and Uncertainties in the Transposition Process," *Proc. 3rd Int. Conf. Advancements in Nuclear Instrumentation Measurement Methods and Their Applications (ANIMMA)*, Marseille, France, June 23–27, 2013, IEEE (2013).

22. A. SANTAMARINA et al., "Re-Estimation of Nuclear Data and JEFF3.1.1 Uncertainty Calculations," *Proc. PHYSOR 2012*, Knoxville, Tennessee, April 15–20, 2012, American Nuclear Society (2012).

23. *International Handbook of Evaluated Criticality Safety Benchmark Experiments*, Organisation for Economic Co-operation and Development/Nuclear Energy Agency (Sep. 2010).

24. "Operating Manual for the Health Physics Research Reactor," ORNL/TM-9870, Oak Ridge National Laboratory (Nov. 1985).

25. W. E. KINNEY, "Oak Ridge National Laboratory Fast Burst Reactor: Critical Experiments and Calculations," ORNL 61-8-71, Oak Ridge National Laboratory (Aug. 1961).

26. S. BRAGG-SITTON et al., "Reactor Testing and Qualification: Prioritized High-Level Criticality Testing Needs," INL/EXT-11-22725, Idaho National Laboratory (Sep. 2011).

27. R. MOSTELLER et al., "The Initial Set of Zeus Experiments: Intermediate-Spectrum Critical Assemblies with a Graphite-HEU Core Surrounded by a Copper Reflector," *International Handbook of Evaluated Criticality Safety Benchmark Experiments*, HEU-MET-INTER-006.

28. D. LOAIZA et al., "Polyethylene Reflected and Moderated Highly Enriched Uranium System with Aluminum," *International Handbook of Evaluated Criticality Safety Benchmark Experiments*, HEU-MET-THERM-008.

29. R. BREWER et al., "Polyethylene Reflected and Moderated Highly Enriched Uranium System with Silicon," *International Handbook of Evaluated Criticality Safety Benchmark Experiments*, HEU-MET-THERM-001.

30. M. HERMAN et al., "EMPIRE: Nuclear Reaction Model Code System for Data Evaluation," *Nucl. Data Sheets*, **108**, 2655 (2007); http://dx.doi.org/10.1016/j.nds.2007.11.003.

31. G. LEINWEBER et al., "Resonance Parameters and Uncertainties Derived from Epithermal Neutron Capture and Transmission Measurements of Natural Molybdenum," *Nucl. Sci. Eng.*, **164**, 287 (2010); http://dx.doi.org/10.13182/NSE08-76.

32. D. SMITH, "Quality Assurance for ENDF/B-VII.1 Covariances," Argonne National Laboratory, *Proc. 2010 Cross Section Evaluation Working Group Mtg.*, Santa Fe, New Mexico, November 1–5, 2010.

33. S. F. MUGHABGHAB, *Atlas of Neutron Resonances*, 5th ed., Elsevier Press (2006).

34. M. HERMAN et al., "COMMARA-2.0 Neutron Cross Section Covariance Library," BNL-94830-2011, Brookhaven National Laboratory (Mar. 2011).

35. M. HERMAN, "Covariance Evaluation Methodology for Neutron Cross Sections," BNL-81623-2008, Brookhaven National Laboratory (Sep. 2008).

36. ROSFOND-2010 Library, Institute of Physics and Power Engineering, Obninsk, Russia (2010); http://www.ippe.ru/podr/abbn/libr/rosfond.php (current as of Oct. 30, 2014).

37. Z. G. GE et al., "The Updated Version of Chinese Evaluated Nuclear Data Library (CENDL-3.1)," *J. Korean Phys. Soc.*, **59**, 1052 (Aug. 2011); http://dx.doi.org/10.3938/jkps.59.1052.

38. A. J. KONING and D. ROCHMAN, "Modern Nuclear Data Evaluation with the TALYS Code System," *Nucl. Data Sheets*, **113**, 2841 (2012); http://dx.doi.org/10.1016/j.nds.2012.11.002.

39. T. KAWANO, "How Does KALMAN Work?," *Proc. Cross Section Evaluation Working Group Mtg.*, Upton, New York, November 6–9, 2007.

Reconstructing Double-differential and Energy-Differential Resonance Cross Sections Using the R-Matrix Limited Formalism in the AMPX Code

Andrew Holcomb[1, a], Luiz Leal[2], Farzad Rahnema[1], Dorothea Wiarda[2], and Goran Arbanas[2]

[1]*Georgia Institute of Technology, Atlanta, GA, 30332*

[2]*Oak Ridge National Laboratory, Bldg. 5700, Oak Ridge, TN, 37831*

INTRODUCTION

AMPX[1] is a cross-section processing code capable of generating multigroup and continuous energy cross-section libraries for use with a wide variety of modern transport codes. For example, AMPX can use ENDF/B files to generate cross-section libraries formatted for use with the Standardized Computer Analyses for Licensing Evaluations (SCALE) system.

The AMPX module POLIDENT is used to generate continuous energy cross-section libraries from ENDF/B file data. The module is capable of generating energy-differential cross-section libraries from resonance parameters using one of several available R-matrix approximations, including Single- and Multi-level Breit-Wigner, Reich-Moore, Adler-Adler, and R-Matrix Limited (RML) formalisms. If the double-differential cross section is needed, the AMPX module Y12 is responsible for performing the reconstruction, but does not currently utilize the RML formalism.

Approximations like Single and Multi-level Breit-Wigner do not allow inclusion of threshold reactions like inelastic scattering or (n,α) production, therefore new evaluations use the more rigorous RML formalism.

These newer evaluations also allow for the use of resonance parameters to calculate a more precise double-differential cross section than can otherwise be given by older ENDF/B evaluations. A new AMPX library module has been created that will allow calculation of the double-differential cross section from resonance parameters in the resolved resonance region using the RML formalism.

R-MATRIX ANGULAR DISTRIBUTION FORMULATION

R-matrix theory is most easily expressed in terms of channels, where we have defined a channel to include a complete description of the particle pair as well as the other information pertaining to interaction between the two particles. In accordance with the SAMMY notation [2], a channel is completely defined as $c = (\alpha, l, s, J)$, where α defines the particle-pair for the channel (including masses, charges, spins, parities, Q-value, etc.), l is the associated parity of the particle pair defined by α, s represents the channel spin, and J is the total angular momentum.

In the work by Blatt and Biedenharn [3], it was shown that the angular distribution cross section in the center-of-mass system can be expressed in terms of the product of Legendre polynomials and their associated collision-matrix dependent coefficients.

$$\frac{d\sigma_{\alpha\alpha'}(E)}{d\Omega_{CM}} = \sum_L B_{L\alpha\alpha'}(E) P_L(cos\beta) \quad (1)$$

In Eq. (1), we have again used notation consistent with the SAMMY manual [2]. Here, $\alpha\alpha'$ identifies the cross section under consideration, P_L is the Legendre polynomial of degree L, β is the angle of the outgoing particle relative to the incident particle in the center-of-mass system. The associated coefficients $B_{L\alpha\alpha'}$ are defined by an expression which is dependent on the collision matrix, the intrinsic spins of the projectile and target under consideration, the wave number associated with particle-pair α, and a geometric factor that is a function of several quantum numbers and the chosen Legendre degree:

$$B_{L\alpha\alpha'}(E) = \frac{1}{4k_a^2} \sum_{\substack{J_1,l_1,s_1,l_1',s_1' \\ J_2,l_2,s_2,l_2',s_2'}} \frac{G\{l_1 s_1 l_1' s_1' J_1\}\{l_2 s_2 l_2' s_2' J_2\} L}{(2i+1)(2I+1)} Re\left[\left(\delta_{c_1 c_1'} - U_{c_1 c_1'}(E)\right)\left(\delta_{c_2 c_2'} - U_{c_2 c_2'}(E)\right)\right] \quad (2)$$

The collision matrix, U, seen in Eq. (2) can be written as

$$U = \Omega W \Omega \quad (3)$$

[a] e-mail: andrewholcomb@gatech.edu

The matrix W, as given in Eq. (3), contains the R-matrix, and may be written as

$$W = P^{\frac{1}{2}}(I - RL)^{-1}(I - RL^{*})P^{\frac{-1}{2}} \quad (4)$$

We now see that the collision matrix defined in Eq. (3) is defined by the R-matrix, the potential scattering phase shifts (accounted for in Ω), the penetrability P, and L, a matrix defined in terms of the penetrability, shift factor, and arbitrary boundary constant at the channel radius. However, in practice, the presented formulation is computationally unstable. A more computationally stable formulation consists of substituting another matrix, X, for the matrix W such that

$$W = I + 2iX \quad (5)$$

Making the substitution in Eq. (5), we find that X is given by

$$X = P^{\frac{1}{2}}L^{-1}(L^{-1} - R)^{-1}RP^{\frac{1}{2}} \quad (6)$$

COMPARISON TO SAMMY RESULTS

In order to verify that the new AMPX library module was functioning as intended, test cases were run with SAMMY and the module extension, and the results were compared. For testing, two different isotopes and energy ranges were used in the comparison, namely ^{19}Fand ^{16}O. The energy grid was generated by SAMMY; in the future, the library module will be connected to the AMPX code that generates the grid. For these two isotopes, a variety of reaction channels is open; the neutron interaction with ^{19}F has two inelastic channels starting at 110 keV and 197 keV, respectively. For ^{16}O there is an (n, α) reaction starting near 2.4 MeV. The energy-differential and double-differential cross-section values for these reactions were compared between the two codes for both ^{19}F and ^{16}O.

Energy-Differential Cross-Section Comparison

^{19}F Results

Using SAMMY and the new library module, the neutron capture, elastic, and inelastic cross sections of ^{19}F were generated from the ENDF/B File 2 resonance parameters. The capture, elastic scattering, and inelastic scattering cross sections are shown in Figures 1, 2, and 3, respectively. The energy range was chosen to prominently display the resonant behavior of the cross section.

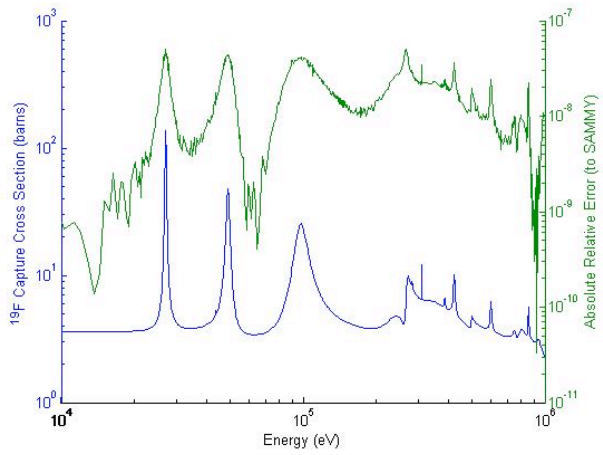

Fig. 1. ^{19}F capture cross section at T = 0K, as calculated by the new AMPX library module.

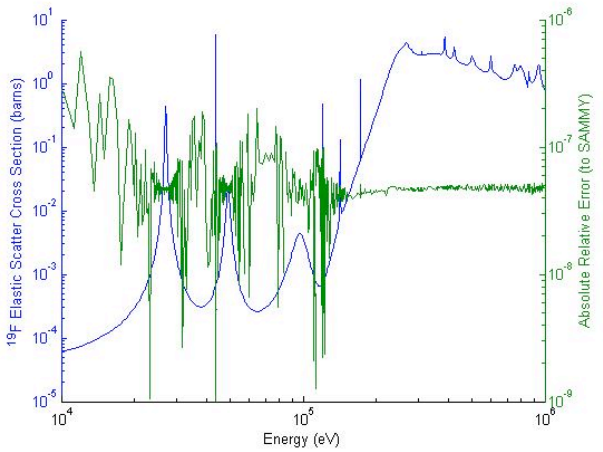

Fig. 2. ^{19}F elastic scattering cross section at T = 0K, as calculated by the new AMPX library module.

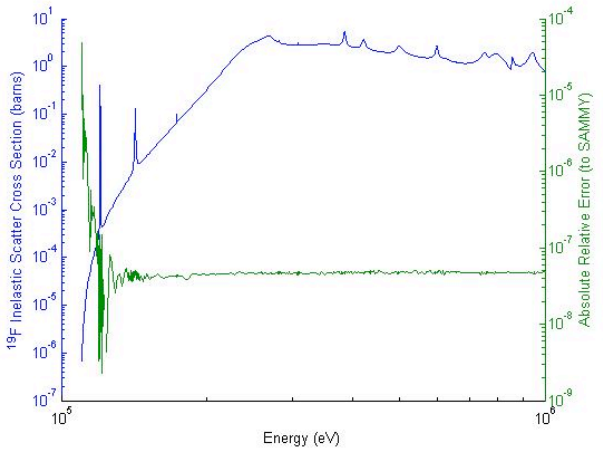

Fig. 3. ^{19}F inelastic scattering cross section at T = 0K, as calculated by the new AMPX library module.

The new AMPX library module produced cross-section values that were in excellent agreement with the SAMMY reconstruction. The maximum absolute relative difference was on the order of 10^{-5}, and the average absolute relative difference was on the order of 10^{-7}.

^{16}O Results

As before, the energy-differential neutron capture, elastic, and alpha production cross sections of ^{16}O were generated from the ENDF/B File 2 resonance parameters. The capture, elastic scattering, and alpha production cross sections are shown in Figures 4, 5, and 6, respectively. As before, the energy range was chosen to prominently display the resonant behavior of the cross section.

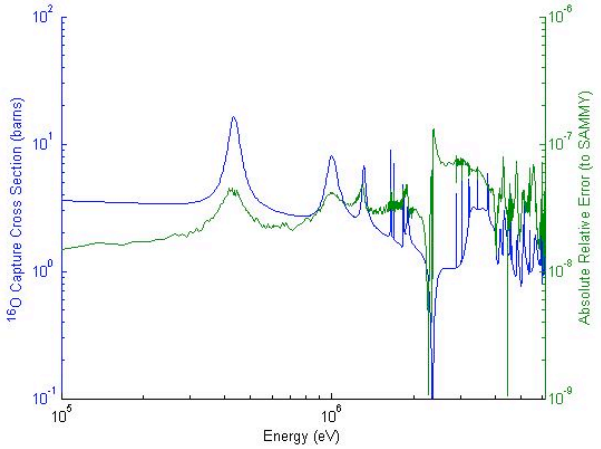

Fig. 4. ^{16}O capture cross section at T = 0K, as calculated by the new AMPX library module.

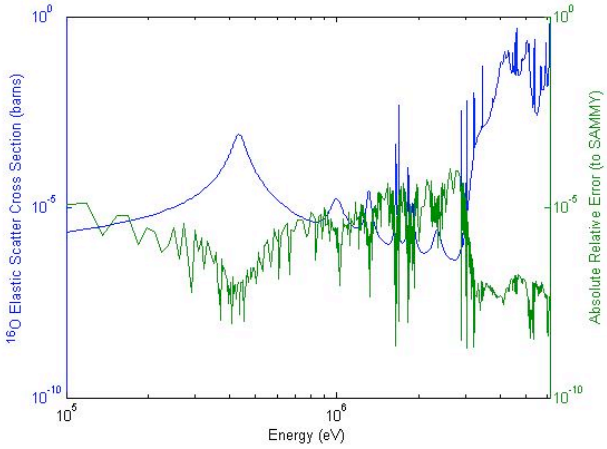

Fig. 5. ^{16}O elastic scattering cross section at T = 0K, as calculated by the new AMPX library module.

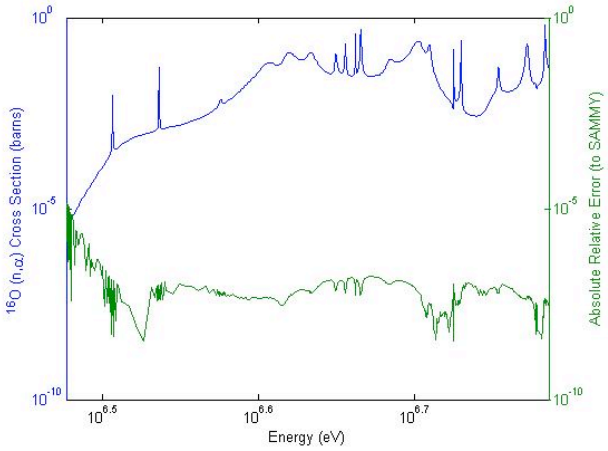

Fig. 6. ^{16}O alpha production cross section at T = 0K, as calculated by the new AMPX library module.

As expected, the new AMPX library module produced results consistent with the SAMMY cross-section values. The maximum absolute relative difference was on the order of 10^{-4}, and the average absolute maximum relative difference was on the order of 10^{-6}. The cross section near the threshold is on the order of 10^{-7} barns; once the cross section reaches the order of 10^{-5} barns, the maximum absolute relative difference is again on the order of 10^{-7}.

Double-Differential Cross-Section Comparison

^{19}F Results

The new AMPX library module and SAMMY code were used to generate the neutron elastic and inelastic double-differential cross section for ^{19}F. The elastic and inelastic double-differential cross sections are is shown in Fig. 7 and Fig. 8, respectively. The double-differential cross-section values were computed at 850 keV.

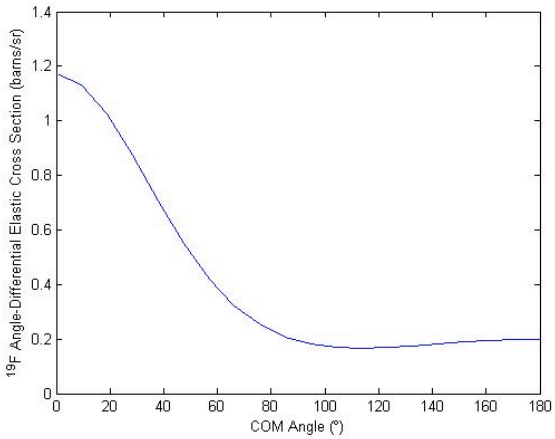

Fig. 7. ^{19}F double-differential elastic cross section at T = 0K and E=850 keV, as calculated by the new AMPX library module.

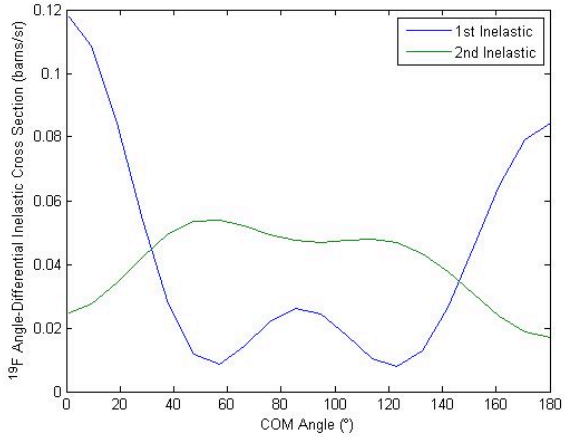

Fig. 8. ^{19}F double-differential inelastic cross sections at T = 0K and E=850 keV, as calculated by the new AMPX library module.

As with the ^{19}F energy-differential cross sections, the double-differential cross sections computed by the AMPX extension were found to be in excellent agreement with the SAMMY values. The values from each program were identical to within file output precision of four decimal digits.

^{16}O Results

In addition to ^{19}F, SAMMY and the new AMPX library module were used to calculate the neutron elastic and alpha production double-differential cross section for ^{16}O. The elastic double-differential cross section is shown in Fig. 9, and the double-differential cross section for alpha production is shown in Fig. 10. The double-differential cross-section values were computed at 5 MeV.

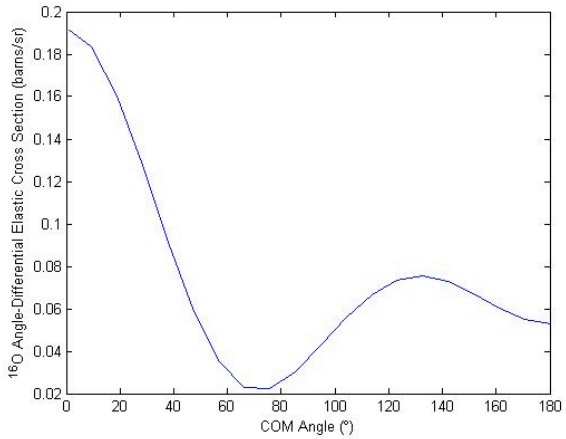

Fig. 9. ^{16}O double-differential elastic cross section at T = 0K and E=5 MeV, as calculated by the new AMPX library module.

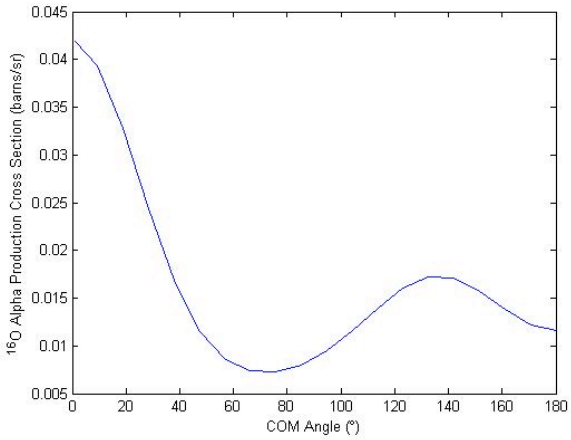

Fig. 10. ^{16}O double-differential alpha production cross section at T = 0K and E=5 MeV, as calculated by the new AMPX library module.

CONCLUSIONS

In this paper, a new AMPX library module capable of generating energy-differential and double-differential cross sections from resonance parameters using the RML formalism has been presented. The library module has been fully implemented into the AMPX run-time environment, and is in the process of being approved for inclusion in future AMPX releases. The new library module was shown to produce results consistent with those of the SAMMY code package.

ACKNOWLEDGEMENTS

This work is supported by the Nuclear Criticality Safety Program.

REFERENCES

1. M. E. Dunn and N.M. Greene, AMPX-2000: "A Cross-Section Processing System for Generating Nuclear Data for Criticality Safety Applications", Trans. Am. Nucl. Soc. (2002).
2. N. M. Larson, "Updated Users' Guide for SAMMY: Multilevel R-Matrix Fits to Neutron Data Using Bayes' Equations," ORNL/TM-9179/R8, Oak Ridge National Laboratory, Oak Ridge, TN, USA (2008).
3. J. M. Blatt and L. C. Biedenharn, "The Angular Distribution of Scattering and Reaction Cross Sections," *Rev. Mod. Phy.* **24**, 258 (1952).

NUCLEAR SCIENCE AND ENGINEERING · VOLUME 183 · 000–000 · JULY 2016

Resonance Parameter Adjustment Based on Integral Experiments

Vladimir Sobes,[a]* Luiz Leal,[a] Goran Arbanas,[a] and Benoit Forget[b]

[a]*Oak Ridge National Laboratory, P.O. Box 2008, MS-6170, Oak Ridge, Tennessee 37831*
[b]*Massachusetts Institute of Technology, 77 Massachusetts Avenue, Cambridge, Massachusetts 02139*

Received May 7, 2015
Accepted for Publication January 12, 2016
http://dx.doi.org/10.13182/NSE15-50

Abstract — *This project seeks to allow coupling of differential and integral data evaluation in a continuous-energy framework and to use the generalized linear least-squares (GLLS) methodology in the TSURFER module of the SCALE code package to update the parameters of a resolved resonance region evaluation. Recognizing that the GLLS methodology in TSURFER is identical to the mathematical description of a Bayesian update in SAMMY, the SAMINT code was created to use the mathematical machinery of SAMMY to update resolved resonance parameters based on integral data. Traditionally, SAMMY used differential experimental data to adjust nuclear data parameters. Integral experimental data, such as in the International Criticality Safety Benchmark Experiments Project, remain a tool for validation of completed nuclear data evaluations. SAMINT extracts information from integral benchmarks to aid the nuclear data evaluation process. Later, integral data can be used to resolve any remaining ambiguity between differential data sets, highlight troublesome energy regions, determine key nuclear data parameters for integral benchmark calculations, and improve the nuclear data covariance matrix evaluation. SAMINT is not intended to bias nuclear data toward specific integral experiments but should be used to supplement the evaluation of differential experimental data. Using GLLS ensures proper weight is given to the differential data.*

Keywords — *Nuclear data evaluation, differential and integral experimental data, continuous-energy coupled.*

Note — *Some figures may be in color only in the electronic version.*

I. INTRODUCTION

The objective of this work is to couple differential and integral data evaluation in a continuous-energy framework. More specifically, the goal is to use the same methodology as the generalized linear least-squares (GLLS) multigroup cross-section adjustment code TSURFER, a module of the standardized computer analyses for licensing applications (SCALE) code package,[1] to update the parameters of an evaluation of a resolved resonance region directly. Recognizing that the GLLS methodology in TSURFER is identical to the mathematical description of the simple Bayesian updating carried out in resonance evaluation code SAMMY (Ref. 2), the computer code SAMINT was created to help use the mathematical machinery of SAMMY to update resolved resonance parameters based on integral data.

The name SAMINT follows the tradition of naming add-on codes that supplement SAMMY by using the three-letter prefix "SAM" and a descriptive three-letter suffix; therefore, "SAM-" for *SAMMY* and "-INT" for *integral*.

Traditionally, SAMMY has used differential experimental data (i.e., σ versus E_i) to adjust nuclear data parameters, such as resonance energies, resonance widths, number of prompt neutrons per fission, etc. Integral experimental data, such as in the International Criticality Safety Benchmark Experiments Project[3] (ICSBEP), have

*E-mail: sobesv@ornl.gov

remained a tool only for validation of completed nuclear data evaluations. SAMINT can be used to extract information from integral benchmarks to aid the nuclear data evaluation process. Near the end of the evaluation based on differential experimental data, integral data can be used to resolve any remaining ambiguity between differential data sets, guide the evaluator to troublesome energy regions, inform the evaluator of the nuclear data parameters most important for integral benchmark calculations, and improve the nuclear data covariance matrix evaluation.

SAMINT is not intended to bias nuclear data toward fitting a certain set of integral experiments. Rather, it should be used to supplement the evaluation of differential experimental data. Using the GLLS methodology ensures that proper weight is given to the original differential data.

Section II gives an overview of the background information necessary to discuss the topic of nuclear data adjustments based on integral experiments. Building on the background information, Sec. III presents the mathematical arguments for the methodology developed in this research. Section IV provides a concrete application for the developed methodology. The conclusions and future work are discussed in Sec. V.

II. BACKGROUND

Accurate evaluated nuclear cross-section data are needed for radiation transport calculations for nuclear applications. In the cross-section evaluation procedure, data evaluators combine measured differential data with nuclear physics models to obtain the best representation of the measured data with covariance information. The evaluated differential data are tested and validated using radiation transport codes to compute measured integral parameters (i.e., neutron multiplication factor) in well-characterized benchmark experiments. Typically, the benchmark testing results are communicated to the nuclear data evaluator with limited or qualitative information that can be difficult to use to improve the differential evaluation.

The process of differential evaluation of the resolved resonance region is a mathematically overdetermined problem with no exact solution. Therefore, there is much choice left to the evaluator in seeking parameters that minimize a certain metric. Even once an evaluation is considered complete based on differential experimental data, it is not unique, and other possibilities exist that may satisfy the metrics used to determine the accuracy of the evaluation. A complete evaluation is not unique because the experimental data being analyzed have an associated uncertainty. Simply put, the experimentally measured cross-section value at every energy point is reported only as a mean value and a standard deviation. Therefore, it is statistically equivalent for the cross section reconstructed from the resonance parameters to pass above or below the mean experimental value by the same amount. This ambiguous choice previously has been left to the evaluator's expertise.

Much of the systematic uncertainty on differential cross-section data comes from the normalization of capture and inelastic cross-section measurements. These measurements demand that the experimenter has a high degree of knowledge of the experimental flux; unfortunately, this is not always the case. In the best case, this results in larger uncertainties over certain energy regions of the experimental data. In the worst case, the experimental cross-section data are misreported. This can be manifested in systematically larger or smaller mean values for the measured cross section or small uncertainty that does not reflect the actual state of knowledge. Unlike statistical uncertainty, systematic uncertainty can result in resolved resonance evaluations that produce a cross section that is too high over a large energy region. Therefore, the uncertainty on the normalization of experimental data is one of the biggest concerns in completing a new evaluation of a resolved resonance region based on differential experimental data.

Utilizing the nuclear data information from integral experiments can assist in resolving the ambiguity between equivalent data evaluations. Valuable information can be extracted from well-known integral experiments and used as a guide in the differential analysis. If the choice of having the cross section pass above rather than below an experimental point by the same amount results in an overall better performance in integral benchmark calculations, it must be the correct choice in the previously ambiguous decision.

The idea of using sensitivity and uncertainty (S/U) analysis tools to direct differential data evaluation based on integral parameter results is not new. The first published record of these ideas appeared at the third Geneva conference on the Peaceful Uses of Atomic Energy in 1964 (Refs. 4 and 5). Gandini et al.[6] in 1973 gave an example of how multigroup cross-section adjustments based on integral experiment feedback were used for fast reactor applications. In fact, in 1974, Pazy et al.[7] suggested methods for handling energy-dependent cross sections rather than multigroup data but limited to the fast energy region.

The recent push for more comprehensive uncertainty quantification in nuclear applications has made the idea of integral data feedback more popular than ever. However,

some of the current methods look to identify the areas where an improvement in differential data uncertainty is needed to improve integral results. For example, Aliberti et al.[8] discuss how to identify the needed uncertainties on input nuclear data to achieve the desired uncertainty in calculations for future nuclear system applications. More recently, Hoblit et al.[9] made progress in coupling differential and integral data analysis by suggesting a methodology for systematically adjusting multigroup cross sections based on feedback from a sensitivity analysis of integral experiments. This technique is proposed for unifying reaction cross-section libraries. Palmiotti et al.[10] also proposed a similar method for systematically adjusting multigroup cross sections based on integral experiments. However, both of these methods go back only as far as multigroup cross sections and limit their focus to energies above the resolved resonance region. Moreover, only single-dimensional cross-section data (i.e., cross section versus energy, not differential cross section with respect to angle or double differential cross section with respect to angle and energy) can be adjusted based on existing techniques.

For ease of discussion, we will contrast our proposed methodology in Sec. III to a traditional multigroup cross-section adjustment methodology using the SCALE6 codes TSUNAMI and TSURFER. The traditional analyses have been carried out in two parts: first, the sensitivity of each material is evaluated in every integral benchmark experiment using the TSUNAMI module of SCALE6. TSUNAMI is a module of SCALE6 that is capable of calculating the sensitivity of the k_{eff} of a system to every isotope in the problem using perturbation theory. Second, the TSURFER module of SCALE6 is used. The TSURFER code package is a GLLS code that can perform global differential data adjustments simultaneously to identify the data deficiencies for integral benchmark calculations. TSURFER provides the requisite quantitative information, thereby identifying specific differential data changes that improve agreement with integral calculations. Specifically, TSURFER performs GLLS computations for a selected set of integral experiments. In this approach, the k_{eff} or other integral responses are calculated using neutron transport codes with multigroup nuclear data processed from evaluated differential data. TSURFER uses sensitivity coefficients, within the accuracy of first-order sensitivity theory, to solve for a set of nuclear data adjustments that cause the calculated integral parameters to agree with their experimental values.

In the proposed methodology, systematic adjustment of the resonance parameters and covariance data is possible. Admittedly, the mathematical framework used for implementation of the methodology proposed here is not as advanced as has been published recently for model adjustment based on integral experiments.[11–14] However, in this work, a specific focus is made on preserving the fit to the original differential experimental data. The reconstructed continuous-energy cross section only changes within the experimental uncertainties in such a way as to improve both the differential and integral data fits. Furthermore, because it is the resonance parameters that are systematically changed because of the integral data feedback, the multidimensional cross-section data (i.e., differential and double-differential cross sections) are implicitly adjusted to reflect the identified inconsistencies between the differential and integral data. In this research, the unprecedented resonance analysis capability (SAMMY) is coupled with the S/U analysis tool (CE TSUNAMI-3D), thereby enabling the data evaluator to address specific advanced fuel cycle application needs.

III. METHODOLOGY

The CE TSUNAMI-3D module of the SCALE6 code package is vastly different from its predecessor, TSUNAMI-3D. CE TSUNAMI-3D computes the neutron transport calculation using continuous-energy Monte Carlo simulations and calculates the sensitivity coefficients using either the iterated fission probability methodology or the CLUTCH methodology.[15] In the end, CE TSUNAMI-3D is able to produce binned sensitivity coefficients of the integral system eigenvalue to the different reaction cross sections. We define the relative sensitivity coefficient S_{ijn} of the eigenvalue k_i of system i with respect to partial cross section $\sigma_j(E)$ for reaction j in energy bin n as

$$S_{ijn} = \frac{\partial k_i/k_i}{\partial\langle\sigma_j(E)\rangle_n/\langle\sigma_j(E)\rangle_n} . \quad (1)$$

In the SAMMY Bayesian updating process, the derivative of the continuous-energy reaction cross section $\sigma_j(E)$ with respect to resonance parameter P_t is needed and therefore, is calculated by SAMMY. We define this derivative as

$$G_{jt}(E) = \frac{\partial\sigma_j(E)}{\partial P_t} . \quad (2)$$

A very fine energy mesh can be used for the calculations, allowing the following two approximations:

$$\sigma_j(E_n) \approx \langle\sigma_j(E)\rangle_n \quad (3)$$

and

$$G_{jt}(E_n) = \frac{\partial \sigma_j(E)}{\partial P_t} \approx \frac{\partial \langle \sigma_j(E) \rangle_n}{\partial P_t} , \quad (4)$$

where the variable E_n corresponds to the average energy of the energy bin n. The sensitivity of the integral system eigenvalue k_i to the resonance parameter P_t is then

$$\frac{\partial k_i}{\partial P_t} = \sum_j \sum_n \frac{k_i}{\sigma_j(E_n)} S_{ijn} G_{jt}(E_n) . \quad (5)$$

We have already pointed out in Sec. I that TSURFER and SAMMY use the same mathematical model—the GLLS methodology—to make their updates. The GLLS methodology is independent of the physics of the problem. All one needs is a set of a priori parameters, an a priori covariance matrix, a vector of derivatives of the *theory* with respect to the parameters and a set of experimental data, and an associated covariance matrix.

We will use the SAMMY nomenclature to introduce the mathematical GLLS equations, and then we will describe what each of the mathematical variables corresponds to for SAMMY and TSURFER. Finally, we will present the basic linear algebra that went into SAMINT to use the SAMMY mathematical machinery to update resonance parameters based on integral data without any changes to the underlying SAMMY machinery.

The GLLS equations in SAMMY are written and calculated as follows:

$$M' = (M^{-1} + W)^{-1} , \quad (6)$$

$$W = G^t V^{-1} G , \quad (7)$$

$$P' = P + M' Y , \quad (8)$$

and

$$Y = G^t V^{-1} (D - T) , \quad (9)$$

where

P = parameters (1 × number of parameters)

D = data (1 × number of energy points)

T = *theory,* theoretical data evaluation (1 × number of energy points)

G = derivative of the *theory*, T, with respect to the parameters, P (number of parameters × number of energy points)

M = parameter covariance matrix (number of parameters × number of parameters)

V = data covariance matrix (number of energy points × number of energy points).

The variables are defined in the mathematical context as above, and primes indicate posterior values (the size of each variable is indicated in parentheses).

The variables W and Y are simply intermediate values in the GLLS equations. Note that this is not the only possible representation of the GLLS equations. TSURFER presents the GLLS equations in its own nomenclature. However, all of the variants can be analytically shown to give the same results.

TSURFER, in its current state, operates in the multigroup formalism and applies changes to multigroup one-dimensional reaction cross sections. Let us imagine that we had a continuous-energy TSURFER code (let us call it *CE TSURFER* in italicized font to remind ourselves that it is only a hypothetical code) that changed resonance parameters instead of multigroup cross sections. The variable P above would then be the resonance parameters, and the variable M would be the resonance parameter covariance matrix. The definitions of these two variables are then exactly the same as in SAMMY. Therefore, only three differences for the above variables would remain between the definitions of SAMMY and the hypothetical code *CE TSURFER* (Table I).

Notice that redefining the three variables described in Table I only affects the calculation of the intermediate variables W and Y from the GLLS equations. The code SAMMY has an option to read in previously generated W and Y matrices and perform the resonance parameter update based on Eqs. (6) and (8). Therefore, SAMINT functions by reading in G_{jt} and $\sigma(E_i)$ from SAMMY, combining them with S_{ijn} and k_i from CE TSUNAMI-3D and combining them as described above to calculate

TABLE I

Differences Between SAMMY and the Hypothetical Code *CE TSURFER* in the Definition of the GLLS Variables

GLLS	SAMMY	*CE TSURFER*
G	G_{jt}	$\partial k_i/\partial P_t$
V	Differential data covariance matrix	Integral data covariance matrix
$(D - T)$	Disagreement in partial cross sections	Disagreement in eigenvalues

$\partial k_i/\partial P_t$. Additionally, SAMINT reads $k_e \pm \Delta k_e$ and an integral data correlation matrix and calculates the W and Y matrices as

$$W = \left(\frac{\partial k_i}{\partial P_t}\right)^t (\Delta k_e C_{kk} \Delta k_e)^{-1} \left(\frac{\partial k_i}{\partial P_t}\right) \quad (10)$$

and

$$Y = \left(\frac{\partial k_i}{\partial P_t}\right)^t (\Delta k_e C_{kk} \Delta k_e)^{-1} (k_e - k_c) , \quad (11)$$

where

C_{kk} = integral experiment correlation matrix

k_e = experimentally measured eigenvalues with their associated one-standard-deviation uncertainty

Δk_e, k_c = calculated eigenvalues.

III.A. Iterative Procedure

The GLLS procedure involves a linearity assumption, which greatly restricts its area of application. In other words, if the initial guess is not *close* to the correct answer, the GLLS procedure may diverge. In SAMMY, an iterative procedure is described to help alleviate some of the restrictiveness of the linearity assumption. This is necessary because in our problem, we are faced with two nonlinearities:

1. The cross sections are not linearly dependent on the resonance parameters.

2. The calculated eigenvalues generally are not strictly linearly dependent on the cross sections.

In this section, we reformulate the iterative procedure described in Sec. IV.A.3 of the SAMMY user's manual in terms of our choice of variables. Note that this iterative capability takes SAMMY and SAMINT beyond the mathematical realm of TSURFER, which only implements the noniterative form of the GLLS equations with the previously described convergence problems.

In the linearity assumption, the Taylor series expansion around the prior value P is made. However, if instead the Taylor expansion is taken not around the prior value but rather around the new value P', an iterative scheme can be developed with $P = P^{(0)}$ and $P' = P^{(n)}$, that can alleviate the restrictions of the linearity assumption. The iterative procedure for resonance parameter adjustment for iteration n, can be shown to be

$$M^{(n+1)} = (M^{(0)-1} + W^{(n)})^{-1} , \quad (12)$$

$$W^{(n)} = \left(\frac{\partial k}{\partial P^{(n)}}\right)^t (\Delta k_e C_{kk} \Delta k_e)^{-1} \left(\frac{\partial k}{\partial P^{(n)}}\right) , \quad (13)$$

$$P^{(n+1)} = P^{(0)} + M^{(n+1)} Y^{(n)} , \quad (14)$$

and

$$Y^{(n)} = \left(\frac{\partial k}{\partial P^{(n)}}\right)^t (\Delta k_e C_{kk} \Delta k_e)^{-1} \times \left[k_e - k_c^{(n)} - \left(\frac{\partial k}{\partial P^{(n)}}\right)(P^{(0)} - P^{(n)})\right] . \quad (15)$$

Therefore, to iterate, we need to perform the following changes:

1. Evaluate the derivative of the eigenvalue of each integral experiment at the intermediate resonance parameter values $P^{(n)}$.

2. Include the additional term in the last equation in the square braces.

3. Remember to provide the initial resonance parameters and covariance matrix even though the derivatives are evaluated at the intermediate resonance parameter values.

To be correct, one must regenerate the cross-section libraries and all of the sensitivity data files for each iteration of the resonance parameters, such that the term $\partial k/\partial P^{(n)}$ is properly represented.

III.B. Predicted Posterior Eigenvalue

It is possible to predict the posterior eigenvalue if the behavior of the integral benchmarks is exactly linear with respect to the affected resonance parameters. As we have discussed above, the linearity assumption is valid only for small changes in resonance parameters. If any significant changes occur, the linearity assumption will most likely be violated, and the subsequent neutronics calculations will not reproduce the predicted posterior eigenvalue. For this reason, we term the posterior eigenvalue as the *predicted* eigenvalue. The predicted eigenvalue $k_p^{(0)}$ for the noniterative case is given by

$$k_p = k_c + \left(\frac{\partial k}{\partial P}\right)(P' - P) . \quad (16)$$

By visual inspection, we see that the same equation is true for the $k_p^{(n+1)}$ eigenvalue from the iterative case with the exception that we must add a correction to k_c:

$$k_p^{(n+1)} = \left[k_c^{(n)} + \left(\frac{\partial k}{\partial P^{(n)}}\right)(P^{(0)} - P^{(n)})\right] + \left(\frac{\partial k}{\partial P^{(n)}}\right)(P^{(n+1)} - P^{(0)}) . \quad (17)$$

Equation (17) can be simplified to

$$k_p^{(n+1)} = k_c^{(n)} + \left(\frac{\partial k}{\partial P^{(n)}}\right)(P^{(n+1)} - P^{(n)}) . \quad (18)$$

IV. RESULTS

In this section, we present an exercise calculation for the methodology introduced above. It is important to note that this demonstration calculation was not used to influence the ^{56}Fe resonance evaluation in any way. On the other hand, this problem is quite suitable for a code-to-code comparison.

The SAMINT code was used to adjust the evaluation of the resolved resonance region of ^{56}Fe, which previously had given discrepant results when used in integral benchmark calculations. Four integral experiments from ICSBEP were selected for the task. Table II gives the descriptive name of the four experiments as well as their titles in ICSBEP nomenclature.

In the analysis based on the integral data, all of the gamma widths in the evaluated resolved resonance region of ^{56}Fe above 450 keV were varied. Also, both of the widths associated with the inelastic channels were varied. A total of 1190 resonance widths were varied. These were the only resonance parameters that were deemed to be of importance by the evaluator. The entire evaluated resolved resonance region, 10^{-5} eV to 2 MeV, was considered, and an initial relative uncertainty of 0.1 was set for all varied resonance parameters.

Table III presents the computed k-eigenvalue divided by the experimental k-eigenvalue (C/E) before and after the resonance parameters were adjusted using SAMINT as well as the posterior k-eigenvalue predicted by SAMINT based on the linearity assumption. For this demonstration calculation, the desired k-eigenvalue for all four experiments was set to unity with 1 mk (100 pcm) uncertainty. The k_{eff} values of the four integral experiments were modeled as uncorrelated in this example. In the practical application of the SAMINT code, the known experimental correlations and uncertainties should be entered.

TABLE II

Four Integral Experiments Used in the ^{56}Fe Evaluation

ICSBEP Name	Experiment Title
HEU-MET-FAST-013	Sphere of highly enriched uranium reflected by steel
HEU-MET-FAST-021	Steel-reflected spherical assembly of ^{235}U (90%)
PU-MET-FAST-025	Spherical assembly of ^{239}Pu (δ, 98%) with 1.55-cm steel reflector
PU-MET-FAST-032	Steel-reflected spherical assembly of ^{239}Pu (α, 88%)

TABLE III

C/E Values for Iron Benchmarks Before and After Adjustment with SAMINT

ICSBEP Name	C/E Before Adjustment	C/E After Adjustment	C/E Predicted
HMF013	0.99850	1.00035	0.99933
HMF021	0.99633	1.00005	0.99950
PMF025	0.99892	1.00001	0.99994
PMF032	0.99792	1.00017	0.99968

The updating procedure produced the desired results of satisfying the integral benchmark calculations while maintaining a good fit of the differential data. Figures 1 and 2 present the reconstructed cross section, before and after the adjustment, on top of the differential experimental data used to come up with the evaluation before the integral data adjustment. These figures show how the information from the integral experiments can be used to make minor adjustments in the continuous-energy cross section that are beyond the resolution of the differential experimental data. Figure 1 shows a segment of the inelastic cross section plotted on top of differential experimental data of Negret et al.[16] Figure 2 shows a different segment of the inelastic cross section plotted on top of differential experimental data of Perey et al.[17] Only these two energy segments are shown because these are the only energy regions where observable changes in the inelastic cross section occurred. For all other energy regions, the posterior evaluation looks almost identical to the initial evaluation on a cross-section plot.

Judging by Figs. 1 and 2, it is difficult to argue whether the initial or posterior evaluation is a better fit for the experimental data. The least-squares chi-squared values for both differential experimental data sets evaluated over the entire energy region of validity are presented in Table IV. In this situation, the changes made based on the integral experimental data are on a finer scale than the differential experimental

TABLE IV

Least-Squares Chi-Squared Value for Differential Experimental Data

Experimental Data	Before Adjustment	After Adjustment
Negret et al.[16]	73.3382	73.6877
Perey et al.[17]	23.6023	22.9036

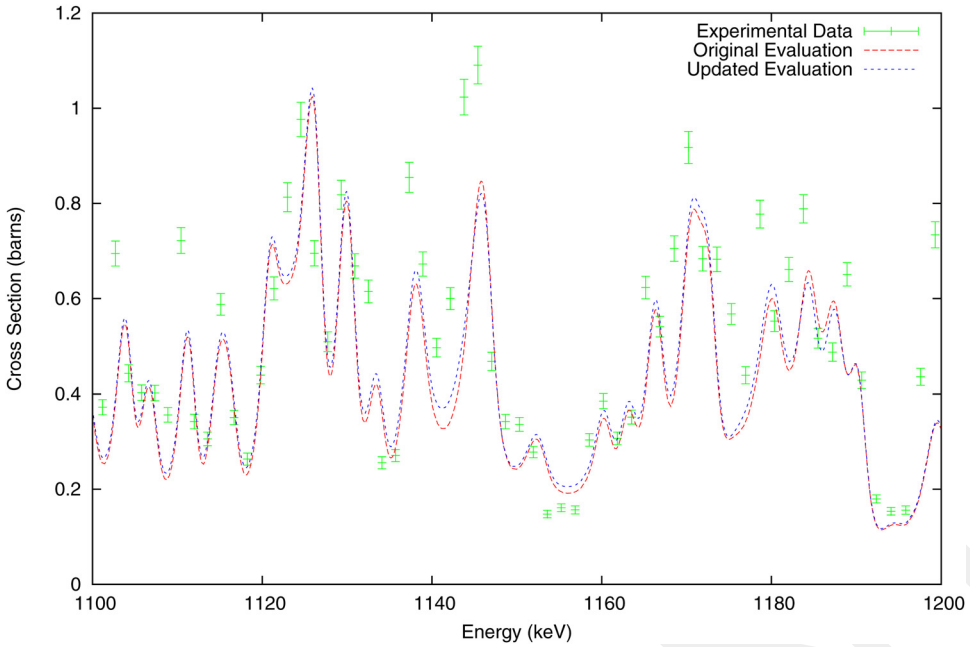

Fig. 1. Inelastic cross section of ^{56}Fe before and after the adjustment based on integral experimental data plotted on top of differential experimental data of Negret et al.,[16] presented with one-standard-deviation error bars.

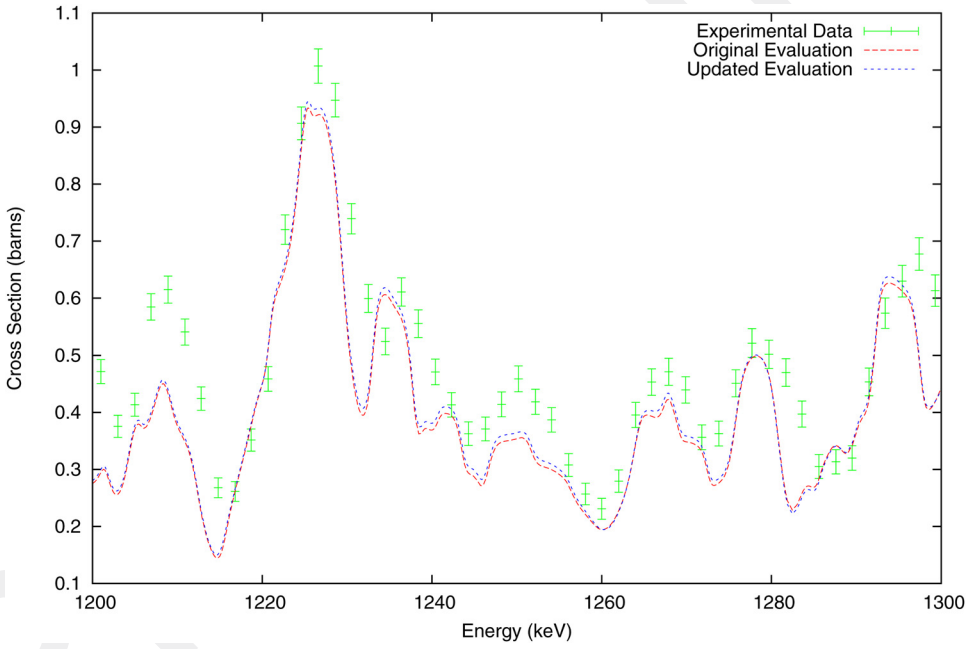

Fig. 2. Inelastic cross section of ^{56}Fe before and after the adjustment based on integral experimental data plotted on top of differential experimental data of Perey et al.[17] presented with one-standard-deviation error bars.

data. Using the integral experimental data to complement the differential experimental data is much of the goal of the SAMINT project.

V. CONCLUSIONS

This paper presents a new methodology for extracting valuable nuclear data information that is available in the integral benchmarks. The new methodology proposes a way of integrating the additional available information in the integral data into the evaluation of the resolved resonance region and interpreting that information in such a way as to change consistently the resonance parameters and update the covariance data. The key to this research was to show that it is possible to couple the information output from CE TSUNAMI-3D not just to multigroup

cross sections but also all the way back to the fundamental resonance parameters. Coupling back to the resonance parameters allows all of the reaction cross sections to be updated simultaneously, including the multidimensional cross sections and covariance data.

In Sec. IV, the proposed approach was demonstrated on the evaluation of the resolved resonance region of ^{56}Fe. In this practical example, 1190 resonance parameters were simultaneously and consistently varied based on information from four integral experiments. The evaluator previously would not have been able to use this valuable information to update the resonance evaluation systematically. The results presented in Sec. IV show that the adjustments made to the ^{56}Fe resonance parameters are completely consistent with the differential experimental data while they eliminate most of the observed discrepancy between the experimentally measured and calculated integral result.

The newly developed coupling methodology is proposed for use as another tool in the evaluator's toolbox. The development of the systematic procedure means that less emphasis will be put on the evaluator's expertise and judgment of how to interpret the limited nonquantitative feedback traditionally received from evaluation benchmarking on integral experiment computer models.

This new methodology can now be applied to new and existing evaluations to use more data than previously were available only in differential cross-section measurements. In particular, this new methodology can be applied to many of the isotopes that have questionable covariance data to evaluate the true state of knowledge based on the immense nuclear data information contained in integral benchmarks.

The authors hope to extend the new coupling methodology to treat the unresolved resonance region in a manner similar to the way SAMINT now treats the resolved resonance region. Further, extension of the same methodology should be possible to the high-energy region, where the fundamental cross-section model parameters will be adjusted based on information from integral experiments. Extending the methodology to both the unresolved and high-energy regions will be of great benefit because it will create a link across three different physics models for cross-section evaluation. Such a capability also will present the opportunity to calculate covariance matrices that will couple the three energy regions. Lastly, the authors hope to extend the SAMINT methodology to calculate resonance parameter changes based on eigenvalue sensitivity to angular distributions[18] and to incorporate the sensitivity coefficients that will be calculated by the developing TSUNAMI-3D generalized response sensitivity theory.[19]

Acknowledgments

This manuscript has been authored by UT-Battelle, LLC, under contract DE-AC05-00OR22725 with the U.S. Department of Energy. Support for this work has been provided by the U.S. Nuclear Criticality Safety Program as part of the Oak Ridge National Laboratory Nuclear Data Succession Planning Task. The authors would like to thank D. Wiarda for her continuous computer help and advice.

References

1. S. M. BOWMAN, "SCALE 6: Comprehensive Nuclear Safety Analysis Code System," *Nucl. Technol.*, **174**, *2*, 126 (2011); http://dx.doi.org/10.13182/NT10-163.
2. N. M. LARSON, "Updated Users' Guide for SAMMY: Multi-Level R-Matrix Fits to Neutron Data Using Bayes' Equations," ORNL/TM-9179/R8, ENDF-364/R2, United States Department of Energy (2003).
3. B. BRIGGS et al., "International Handbook of Evaluated Criticality Safety Benchmark Experiments," NEA No. 7166, Nuclear Energy Agency (2013).
4. G. CECCHINI et al., "Analysis of Integral Data for Few-Group Parameter Evaluation of Fast Reactors," *Proc. 3rd Int. Conf. Peaceful Uses of Atomic Energy*, Geneva, Switzerland, August 31–September 9, 1964, Vol. 2, p. 388 (1964).
5. M. HUMI et al., "Multi-Group Constants from Integral Data," *Proc. 3rd Int. Conf. Peaceful Uses of Atomic Energy*, Geneva, Switzerland, August 31–September 9, 1964, Vol. 2, p. 398 (1964).
6. A. GANDINI, M. PETILLI, and M. SALVATORES, "Nuclear Data and Integral Measurement Correlation for Fast Reactors," RT/FI(73)22, Comitato Nazionale Energia Nucleare (1973).
7. A. PAZY et al., "The Role of Integral Data in Neutron Cross Section Evaluation," *Nucl. Sci. Eng.*, **55**, 280 (1974); http://dx.doi.org/10.13182/NSE55-280.
8. G. ALIBERTI et al., "Nuclear Data Sensitivity, Uncertainty and Target Accuracy Assessment for Future Nuclear Systems," *Ann. Nucl. Energy*, **33**, *8*, 700 (2006); http://dx.doi.org/10.1016/j.anucene.2006.02.003.
9. S. HOBLIT et al., "Towards Unified Reaction Cross Sections Through Assimilation of Integral and Differential Experiments," *Proc. Int. Conf. Nuclear Data for Science and Technology (ND2013)*, New York, March 4–8, 2013.
10. G. PALMIOTTI et al., "Multigroup Cross-Section Adjustment Based on ENDF/B-VII.0 Data," *Proc. Int. Conf. Nuclear Data for Science and Technology (ND2013)*, New York, March 4–8, 2013.
11. D. G. CACUCI and M. IONESCU-BUJOR, "Best-Estimate Model Calibration and Prediction Through Experimental Data

Assimilation—I: Mathematical Framework," *Nucl. Sci. Eng.*, **165**, 18 (2010); http://dx.doi.org/10.13182/NSE09-37B.

12. M. C. BADEA, D. G. CACUCI, and A. F. BADEA, "Best-Estimate Predictions and Model Calibration for Reactor Thermal-Hydraulics," *Nucl. Sci. Eng.*, **172**, 1 (2012); http://dx.doi.org/10.13182/NSE11-10.
13. D. G. CACUCI, "Predictive Modeling of Coupled Multi-Physics Systems: I. Theory," *Ann. Nucl. Energy*, **70**, 266 (2014); http://dx.doi.org/10.1016/j.anucene.2013.11.027.
14. C. LATTEN and D. G. CACUCI, "Predictive Modeling of Coupled Systems: Uncertainty Reduction Using Multiple Reactor Physics Benchmarks," *Nucl. Sci. Eng.*, **178**, 156 (2014); http://dx.doi.org/10.13182/NSE13-110.
15. C. M. PERFETTI, "Advanced Monte Carlo Methods for Eigenvalue Sensitivity Coefficient Calculations," Dissertation, University of Michigan (2012).
16. A. NEGRET, C. BORCEA, and A. J. M. PLOMPEN, "Cross Section for Neutron Inelastic Scattering on ^{28}Si," *J. Korean Phys. Soc.*, **59**, *2*, 1765 (2011); http://dx.doi.org/10.3938/jkps.59.1765.
17. F. G. PEREY, W. E. KINNEY, and R. L. MACKLIN, "High Resolution Inelastic Cross-Section Measurements for Na, Si, and Fe," *Proc. Third Conf. Neutron Cross Section Technology*, Knoxville, Tennessee, March 13–15, 1971, Vol. 1, p. 191 (1971).
18. B. KIEDROWSKI et al., "MCNP Sensitivity/Uncertainty Accomplishments for the Nuclear Criticality Safety Program," LA-UR-14-24458, *Trans. Am. Nucl. Soc.*, **111**, 791 (2014).
19. C. M. PERFETTI and B. T. REARDEN, "Continuous-Energy Monte Carlo Methods for Calculating Generalized Response Sensitivities Using TSUNAMI-3D," *Proc. 2014 Int. Conf. Physics of Reactors (PHYSOR 2014)*, Kyoto, Japan, September 28–October 3, 2014.

Appendix B: Example of a Complete Evaluation

OAK RIDGE
NATIONAL LABORATORY
MANAGED BY UT-BATTELLE
FOR THE DEPARTMENT OF ENERGY

ORNL/TM-2007/115

^{233}U Cross-Section and Covariance Data Update for SCALE 5.1 Libraries

February 2008

Prepared by
L. C. Leal
D. Wiarda
B. T. Rearden
H. Derrien

UT-BATTELLE
ORNL-27 (4-00)

ORNL/TM-2007/115

Nuclear Science and Technology Division

^{233}U CROSS-SECTION AND COVARIANCE DATA UPDATE FOR SCALE 5.1 LIBRARIES

L. C. Leal
D. Wiarda
B. T. Rearden
and
H. Derrien

Date Published: February 2008

Prepared by
OAK RIDGE NATIONAL LABORATORY
Oak Ridge, Tennessee 37831-6283
managed by
UT-BATTELLE, LLC
for the
U.S. DEPARTMENT OF ENERGY
under contract DE-AC05-00PR22725

CONTENTS

Page

LIST OF FIGURES

Figure **Page**

LIST OF TABLES

Table **Page**

ACRONYMS

EALF	Energy of Average Lethargy Causing Fission
ENDF	Evaluated Nuclear Data Library
IAEA	International Atomic Energy Agency
ORELA	Oak Ridge Electron Linear Accelerator
ORNL	Oak Ridge National Laboratory
rel. s. d.	relative standard deviation
RPCM	Resonance Parameter Covariance Matrix

ACKNOWLEDGMENTS

The authors acknowledge two offices of the U.S. Department of Energy for sponsoring this work. These are DOE/NA-171 (Nuclear Criticality Safety Program) and DOE/EM-60 (EM Safety Management and Operations. Also it is acknowledged that K. R. Elam, formerly of the Oak Ridge National Laboratory performed the TSUNAMI calculations for this work.

ABSTRACT

Resonance parameter covariance data have been generated for ^{233}U in the resolved and unresolved resonance region using the computer code SAMMY. High-energy covariance uncertainties were generated at the International Atomic Energy Agency using the computer code EMPIRE. The covariance data were added to the ENDF/B-VII.0 evaluation of the ^{233}U cross sections. The covariance data were processed with the PUFF module in AMPX. Eighty-two benchmark calculations for systems including ^{233}U were done with the TSUNAMI sensitivity analysis sequence of the SCALE system. The work is in support of criticality safety evaluation of future operations at the Oak Ridge National Laboratory Building 3019.

1. INTRODUCTION

Resonance-parameter covariance matrix (RPCM) evaluation in the resolved and unresolved resonance regions were done for ^{233}U using the computer code SAMMY.[1] The RPCMs were obtained as a result of the resolved[2] and unresolved[3] resonance regions evaluation. The evaluations were done separately; that is, the resolved resonance evaluation was performed from 0 to 600 eV, and the unresolved evaluation was performed from 600 eV to 40 keV.

In the resonance region, pointwise cross sections are reconstructed using the R-matrix cross-section formalism with evaluated resonance parameters. Uncertainties in the reconstructed cross section are obtained by propagating the uncertainties from the resonance parameters. For reactor applications, group cross sections are produced by weighting the pointwise cross sections with a neutron flux spectrum and integrating over energies within a group. Consequently, uncertainties in the group cross sections are also derived from uncertainties in the resonance parameters.

To understand how uncertainties in the resonance parameters are calculated, we must consider the process by which the parameters are determined: resonance parameters are obtained by fitting experimental data using generalized least-squares techniques in conjunction with R-matrix theory. In SAMMY, both systematic and statistical uncertainties in the experimental data are incorporated directly into the fitting procedure, which then determines the long-range correlations in the RPCM. The experimental uncertainties come from a variety of sources, such as normalization, background, neutron time-of-flight (TOF), and sample thickness. It is important that the evaluator understand and include the uncertainties associated with the experimental data to assess the impact of these uncertainties in the evaluation process.

High-energy covariance evaluation was performed at the International Atomic Energy Agency (IAEA) by Roberto Capote[4] in coordination with Andrej Trkov and Mihaela Sin using the computer code EMPIRE.[5] Estimation was based on a Monte Carlo sampling of the model parameters,[5] taking such uncertainty of these parameters as to approximately cover the spread of the experimental data. Average uncertainties and the correlation matrices have been obtained following Donald Smith's formulation.[6] A more rigorous approach would utilize the Generalized Least Squares method, in which the calculated model covariance is taken as a prior for the least squares fitting based on the GANDR system.[7] However such an approach would require additional time and support. In addition to the RPCM and high-energy cross section uncertainty evaluations, covariance evaluation of the ^{233}U average number of neutrons released per fission was also performed.[8] The approach used to evaluate the resonance covariance for ^{233}U will be presented here. The resulting covariance evaluations were converted into the ENDF format and processed with the computer codes PUFF-IV[9] and ERRORJ.[10]

2. RESOLVED RESONANCE COVARIANCE EVALUATION

A Reich-Moore resolved resonance evaluation for ^{233}U was carried out with the code SAMMY in the energy region from 0 to 600 eV.[2] A total of 769 resonances, including the external levels,

was used. Each resonance of ^{233}U in the Reich-Moore formalism is described by five parameters (i.e., the resonance energy E_r, the gamma width Γ_γ, the neutron width Γ_n, and the two fission widths Γ_{f1}, and Γ_{f2}), for a total of 3845 parameters. The large number of resonance parameters leads to two major issues when generating a resonance covariance: (1) the large computer memory required to process the data and (2) the data storage for the resulting covariance file. The former has been addressed by using a DEC Alpha workstation with 32 GB of memory. The latter issue was not of a concern because the resulting ^{233}U covariance matrix in the ENDF format[11] is a manageable file of 100 MB.[12]

Several experimental data were used in the ^{233}U evaluation. To enable a SAMMY analysis of the ^{233}U cross sections at energies above 150 eV, two high-resolution measurements were performed at the Oak Ridge Electron Linear Accelerator (ORELA). Neutron transmission measurements with samples cooled to 11 K to reduce the Doppler effect, at a flight path of 79.8 m, were done by Guber et al.[13] The transmission measurements done with the sample cooled to 11 K have led to a reduction of the width of the resonances by a factor of 2 compared to the experiments at room temperature. Two sets of measurements were done with different sample thicknesses: (1) a set of measurements with a sample of 0.00298 at/b in the energy region 0.5 to 80 eV and (2) a set of measurements of 0.0119 at/b in the energy range 6 eV to 300 keV. In addition to the transmission measurements, two sets of fission cross-section measurements at a flight path of 80 m were also carried out by Guber et al.[14] in the energy ranges of 0.5 to 80 eV with a cadmium filter and another in the energy range from 10 eV to 700 keV with a ^{10}B filter, respectively. The fission cross-section measurements at the 80-m flight path have much better resolution that any of the previous fission measurements. These ORELA transmission and fission measurements were the primary data used in the ^{233}U evaluation in the energy range from 0.5 to 600 eV. Twelve measurements were included in the evaluation as shown in Table 1. Four of these measurements are the Oak Ridge National Laboratory (ORNL) transmission and fission cross section done by Guber et al. as explained above. The transmission measurements were done by Harvey et al.[15] in 1979, transmission measurements done by Moore et al.[16] in 1960, and transmission measurements done by Pattenden and Harvey[17] in 1963. Two sets of simultaneous measurements of capture and fission data were performed by Weston et al.[18] in 1970. Fission cross-section measurements were performed by Blons[19] in 1973, and fission measurements were performed by Deruytter and Wagemans[20] in 1974.

In addition to the microscopic data (from TOF measurements), a variety of integral quantities are available within SAMMY. These integral quantities are calculated by integrating over the microscopic absorption, fission, and capture cross sections. The integral quantities used in the ^{233}U evaluation are the Westcott factor, the K_1 value, the resonance integral I_x, and the capture-to-fission ratio (the α-ratio). These quantities are defined as follows:

1. Westcott factor:

$$g_w = \frac{2}{\sqrt{\pi}} \frac{\sigma_x}{\sigma_{0x}} \quad ,$$

where σ_x and σ_{0x} are the Maxwellian-averaged cross sections and the cross sections at 0.0253 eV.

2. K_1 factor:

$$K_1 = \nu\sigma_{0f} g_f - \sigma_{0a} g_a \ .$$

3. Resonance integral:

$$I_x = \int_{0.5eV}^{20MeV} \frac{\sigma_x}{E} dE \ .$$

4. α Ratio:

$$\alpha = \frac{I_c}{I_f} \ .$$

Some of the evaluated integral values for ^{233}U are shown in Table 2.

Table 1. Selected measurements for ^{233}U evaluation of RRR

Author	Energy region analyzed (eV)	Main features
Moore et al., 1960	0.020 – 15.0	Transmission; chopper, TOF 15.7-m sample 0.0037 and 0.0213 at/b
Pattenden and Harvey, 1963	0.080 – 15.0	Transmission; chopper, TOF 45-m sample 0.00057, 0.00308, 0.01219 at/b
Weston et al., 1968	1.0 – 600.0	Simultaneous measurements of capture and fission, Linac TOF 25.2 m
Weston et al., 1968	0.020 – 1.0	Simultaneous measurements of capture and fission, Linac TOF 25.6 m
Blons, 1973	4.0 – 600.0	Fission, Linac, TOF 50.1 m, sample at liquid nitrogen temperature
Deruyter and Wagemans, 1974	0.020 – 15.0	Fission, Linac, TOF 8.1 m
Harvey et al., 1979	0.020 – 1.2	Transmission, Linac, TOF 17.9-m sample 0.00605 and 0.0031 at/b
Wagemans et al., 1988	0.002 – 1.0	Fission, Linac, TOF 8.1 m
Guber et al., 1998	1.0 – 80.0	Transmission, Linac, TOF 80 m
		Cd filter, sample temperature 11 K
		Sample thickness 0.00298 at/b
Guber et al., 1998	7.0 – 600.0	Transmission, Linac, TOF 80 m
		^{10}B filter, sample temperature 11 K
		Sample thickness 0.0119 at/b
Guber et al., 1998	1.0 – 80.0	Fission, Linac, TOF 80 m
		Cd filter
Guber et al., 1998	7.0 – 600.0	Fission, Linac, TOF 80 m
		^{10}B filter

Table 2. Evaluated integral quantities

Quantity	ENDF/B-VI standard	Axton standard	BNL	Present work
g_a	0.9996 ± 0.0011	0.9995 ± 0.0011	0.9996 ± 0.0015	1.0003 ± 0.0009
g_f	0.9955 ± 0.0014	0.9955 ± 0.0014	0.9955 ± 0.0011	1.0004 ± 0.0012
I_a			897 ± 20	917.45 ± 8.0
I_f			760 ± 17	777.82 ± 5.0
K_1	742.60 ± 2.40	742.25 ± 2.37		746.77 ± 1.98

In the resonance parameter evaluation performed with SAMMY, the various cross sections were fitted using the R-matrix theory with the Reich-Moore approximation, including corrections for experimental conditions such as Doppler and resolution broadening, multiple scattering corrections, and backgrounds. The best fit to the experimental data is determined by means of a generalized least-squares fitting procedure. Experimental uncertainties are incorporated directly into the evaluation process to propagate those uncertainties into the resonance parameter results. Uncertainties treated in the evaluation process included statistical and systematic uncertainties for each different data set plus the quoted uncertainties for the integral data and thermal cross sections. The result of the evaluation is a complete RPCM associated with the resonance parameters. Average fission and capture cross sections and uncertainties calculated with the PUFF-IV code for a constant flux in energy intervals of 50 eV are shown in Table 3. The percentage cross section uncertainties relative standard deviation (rel. s. d.) are also shown. One can see that the average fission cross section uncertainties are from 0.9 to 2.2%, whereas the uncertainties for the average capture cross section are in between 2.4 to 3.7%.

Table 3. Uncertainty in the average fission and capture cross section calculated with PUFF-IV code using the RPCM

E_{min} (eV)	E_{max} (eV)	σ_f (barns)	Relative standard deviation (%)	σ_γ (barns)	Relative standard deviation (%)
10-5	50.0	84.905	0.9	13.857	2.4
50.0	100.0	39.053	1.0	7.313	2.6
100.0	150.0	29.719	1.0	4.876	2.7
150.0	200.0	20.973	1.1	3.062	2.7
200.0	250.0	23.080	1.1	3.758	2.8
250.0	300.0	23.139	1.1	3.263	2.9
300.0	350.0	17.400	1.3	2.369	2.8
350.0	400.0	19.148	1.3	2.525	3.1
400.0	450.0	9.712	1.8	1.143	3.9
450.0	500.0	12.395	1.7	1.623	3.1
500.0	550.0	14.604	1.8	1.781	3.2
550.0	600.0	12.433	2.2	2.228	3.7

3. UNRESOLVED RESONANCE COVARIANCE EVALUATION

An unresolved resonance evaluation for ^{233}U was done in the energy region from 600 eV to 40 keV. Above 600 eV the fluctuations in the measured cross sections are smaller than those in the resolved range but are still important for calculating the energy self-shielding of the cross section. These fluctuations are due to unresolved multiplets of resonances for which it is not possible to determine parameters of the individual resonances as is done in the resolved region. The mechanism utilized for the cross section treatment in the unresolved region is based on average values of physical quantities obtained in the resolved range. Knowledge of the average values for level spacings, strength functions, widths, and other relevant parameters is used to infer their behavior in the unresolved energy region.

Four sets of experimental data were used in the evaluation:

1. Effective average total cross sections of Guber et al.[13] obtained from experimental transmission measurements. These transmission measurements were performed at a 79.8-m flight path with sample thicknesses of 0.0119 at/b and with the sample cooled to 11 K. The average cross sections were derived by Derrien et al.[21] and corrected for self-shielding; the data were used from 600 eV to 40 keV.

2 Fission cross sections of Guber et al.[14] taken on the 80-m flight path. These data were used from 600 eV to 40 keV.

3. Fission and capture data of Weston et al.[18] obtained from the capture-to-fission ratio measurements done at a 25.2-m flight path from 600 eV to 2 keV.

4. Capture data of Hopkins extracted from capture-to-fission ratio measurements done with a collimated neutron beam incident in a target placed in a cadmium-loaded liquid scintillator.[22]

The computer code SAMMY was used to fit the data in the energy region from 600 eV to 40 keV. The average parameters obtained in the resolved resonance region and used in the SAMMY unresolved fit are shown in Table 4. The parameters are total angular momentum J, average level spacing $\langle D \rangle$, strength function S_n, fission width $\langle \Gamma_f \rangle$, effective fission degrees of freedom N_{eff}, and capture width $\langle \Gamma_\gamma \rangle$.

Table 4. Average values of the resonance parameters input used in the SAMMY unresolved resonance calculations for orbital angular momentum $l = 0$

J	$\langle D \rangle$ (eV)	$S_n \times 10^4$	$\langle \Gamma_f \rangle$ (meV)	N_{eff}	$\langle \Gamma_\gamma \rangle$ (meV)
Mixed levels	0.52 ± 0.08	0.895± 0.047	496		39.0 ± 3.0
2+	1.19 ± 0.12		760 ± 60	4.0	
3+	0.92 ± 0.10		296 ± 30	2.0	

The resulting unresolved parameters obtained from the SAMMY fit were reported to ENDF at 29 reference energies. The reference energies were determined based on the observed fluctuations

in the experimental data, which result from unresolved multiplets of resonances. These reference energies are 600, 682.5, 765, 872.5, 990, 1125, 1250, 1340, 1410, 1470, 1585, 1735, 1880, 2107.5, 2522.5, 3120, 447.5, 6250, 7275, 7775, 8350, 9350, 11000, 13500, 17500, 22500, 27500, 32500, and 40000 eV.

The results of the fit of the experimental data are given in Fig. 1. The experimental cross-section data shown in Fig. 1 are the total cross section of Guber et al.,[13] the fission cross section of Guber et al.,[14] the capture cross section of Weston et al.,[18] and the capture cross section of Hopkins et al.[22] The solid line represents the SAMMY fit to the data showing good agreement with the experimental data.

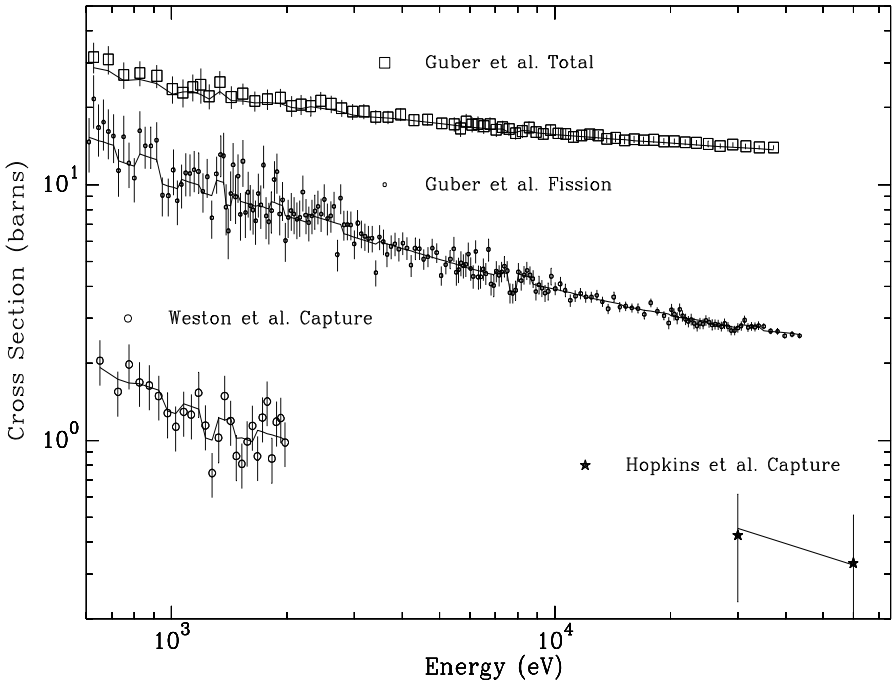

Fig. 1. Comparison of average cross sections calculated with SAMMY with the experimental data.

The RPCM matrix associated with the unresolved resonance parameters was obtained with SAMMY by fitting the experimental data, including the statistical and systematic uncertainties of the experimental data. Note that the data normalization is the most important issue in determining the average parameter covariance data. Because of limitation in the ENDF format, covariance data for the average resonance parameters can only be provided for the entire energy region, that is, from 600 eV to 40 keV. The uncertainties for average *s*-wave ($l = 0$) resonance parameters calculated with the covariance data are given in Table 5.

Table 5. Average values of the resonance parameters and uncertainties calculated with the covariance data generated with SAMMY for orbital angular momentum $l = 0$

J	$S_n \times 10^4$	$\langle \Gamma_f \rangle$ (meV)	$\langle \Gamma_\gamma \rangle$ (meV)
Mixed levels	0.939 ± 0.036	496	39.0 ± 2.0
2+		775.3 ± 17.0	
3+		317.4 ± 42.6	

Average fission, capture cross sections, and uncertainties calculated with a constant flux from 600 eV to 40 keV are shown in Table 6. The calculations were done with the PUFF-IV code. The uncertainties in the average cross sections in the unresolved energy region are larger than the uncertainties in the resolved energy region. This is explained because the cross section in the resolved energy region is known much better. In addition, the resolved resonance formalism (Reich-Moore formalism), together with the Bayes' method, provides an accurate representation of the cross section and a better estimate of the RPCM and cross-section uncertainties. The methodology used in the unresolved resonance region is based on the Single-Level Breit-Wigner formalism and the fitting of the average cross sections, which results in larger errors in the average cross sections.

Table 6. Uncertainty in the average fission and capture cross section calculated with PUFF-IV in the unresolved energy region

E_{min} (eV)	E_{max} (eV)	σ_f (barns)	Relative standard deviation (%)	σ_γ (barns)	Relative standard deviation (%)
600.0	1000.0	12.476	3.7	2.435	7.7
1000.0	1500.0	9.223	4.0	1.792	8.2
1500.0	2000.0	7.959	4.0	1.537	8.0
2000.0	3000.0	6.676	4.1	1.293	7.8
3000.0	4000.0	5.836	4.1	1.075	7.8
4000.0	6000.0	4.907	4.5	0.887	7.8
6000.0	10000.0	4.146	5.2	0.638	7.9
10000.0	15000.0	3.561	6.4	0.535	8.2
15000.0	20000.0	3.203	7.8	0.477	8.1
20000.0	25000.0	2.971	9.0	0.451	8.0
25000.0	30000.0	2.816	8.0	0.423	8.8
30000.0	40000.0	2.672	9.0	0.383	8.8

4. PROCESSING OF THE ^{233}U COVARIANCE DATA

The resolved and unresolved resonance region covariance data generated with SAMMY were converted into the ENDF format specified for FILE 32. The ENDF covariance format for the

resolved resonance region allows two options: LCOMP = 1 for which the full covariance data and correlations are entered explicitly, and LCOMP = 2 (compact formalism) that was developed to alleviate the use of computer storage. The LCOMP = 1 option lead to a file of 100 MB. The ENDF unresolved resonance format is very restricted, permitting only representation of the average unresolved resonance parameter uncertainties and covariance for the entire energy region. This format was used because there is no other alternative to represent the unresolved resonance covariance in ENDF. For the energies above 40 keV to 20 MeV, the ENDF format given in FILE 33 was used.

The evaluated covariance data were added to the existing ^{233}U ENDF/B-VII cross-section evaluation[23] and processed with the computer codes PUFF-IV and ERRORJ. In the resolved resonance region, the uncertainty in the average cross section obtained with SAMMY, PUFF-IV, and ERRORJ are in good agreement. SAMMY and PUFF-IV uncertainties are identical. It appears that the slight difference found in the ERRORJ results could result from the different procedure used for performing derivatives in these codes. Derivatives in the ERRORJ code are done numerically, whereas in SAMMY and PUFF-IV they are performed analytically. In the unresolved and high-energy regions, PUFF-IV and ERRORJ calculated uncertainties are identical. Data averaged, including cross sections and the number of neutrons per fission, $\bar{\nu}$, (prompt and total) and their respective uncertainties were generated in the 44-neutron group structure of the SCALE system.[24] The results are displayed in Figs. 2–6. Figure 2 shows the average total $\bar{\nu}$ and the uncertainties. The prompt $\bar{\nu}$ and the uncertainties are shown in Fig. 3.

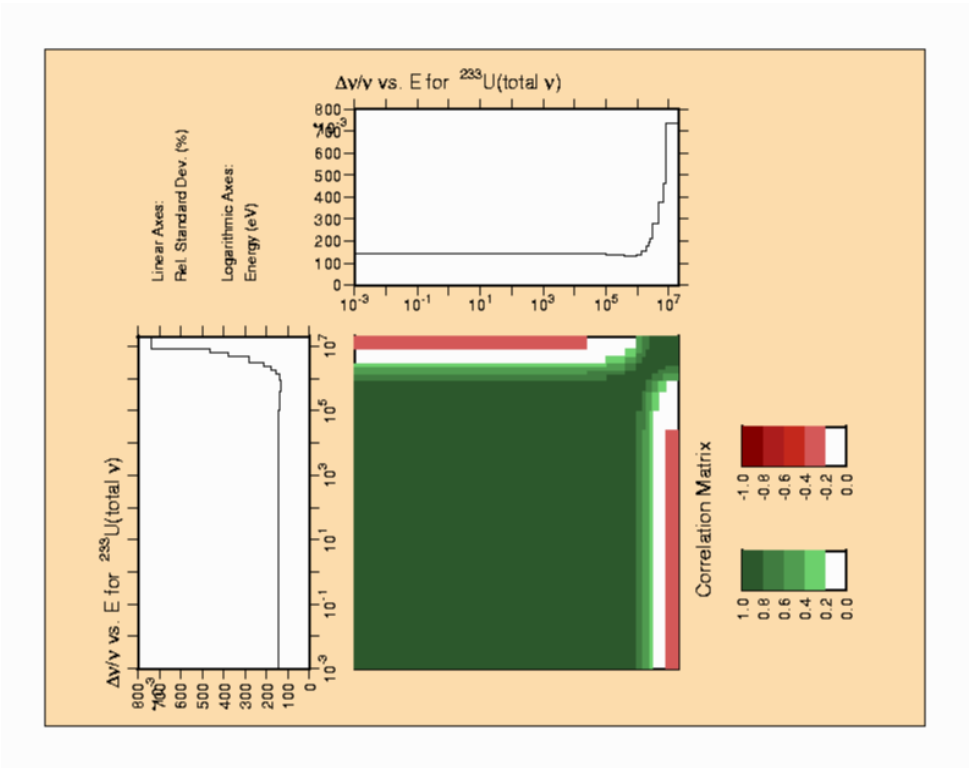

Fig. 2. Total $\bar{\nu}$ and uncertainties calculated in the 44-neutron groups of the SCALE system.

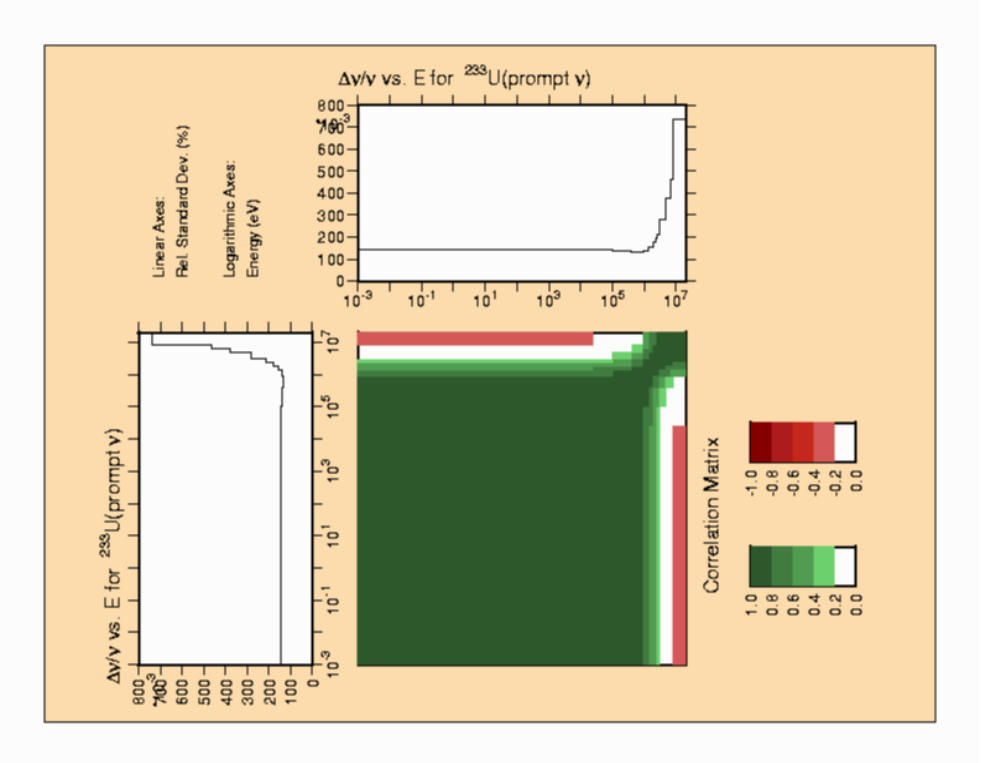

Fig. 3. Prompt $\bar{\nu}$ and uncertainties calculated in the 44-neutron groups of the SCALE system.

The 44-neutron group cross sections and uncertainties are shown in Figs. 4–6. The total cross sections are shown in Fig. 4. Uncertainties in the total cross sections range from 1 to 3.5%. Fission cross sections and uncertainties are displayed in Fig. 5. The maximum uncertainties in the fission cross sections in the resonance region (resolved and unresolved) are 4.5%. In the energy region above 40 keV to 20 MeV (high-energy region), the uncertainties in the fission cross sections can be as high as 9%. Capture cross section and uncertainties are shown in Fig. 6. As one would expect, high uncertainties in the capture cross sections are observed in the energy range above 40 keV. These results are consistent with the error in experimental data (systematic and statistical).

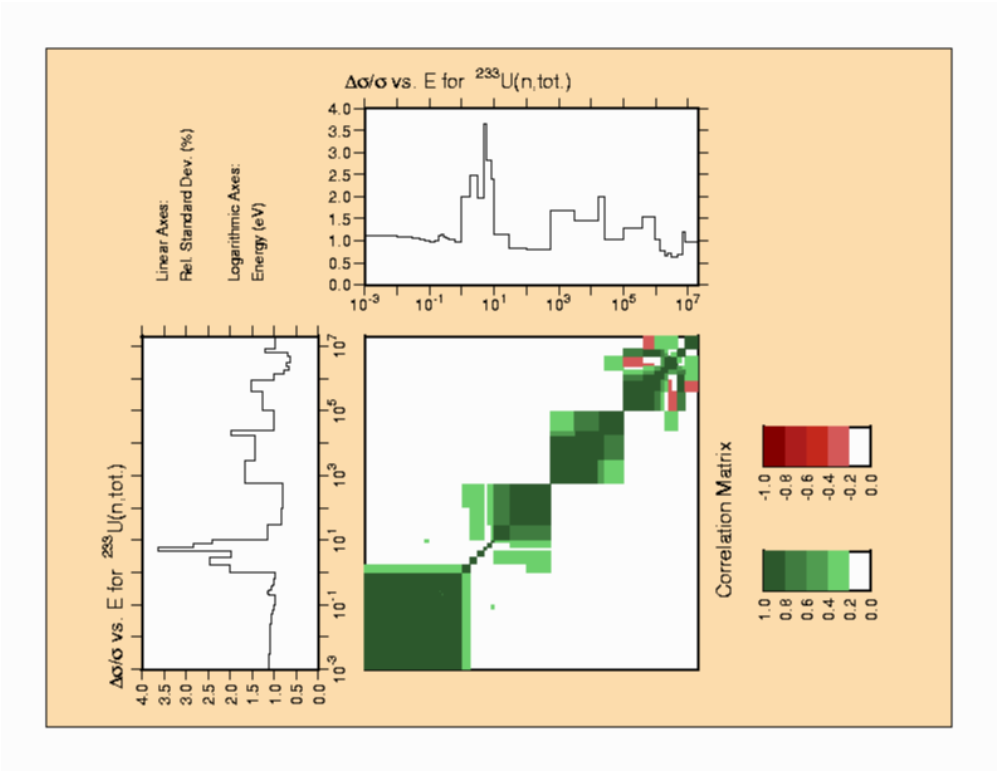

Fig. 4. ^{233}U total cross section calculated in the 44-neutron group structure of the SCALE system.

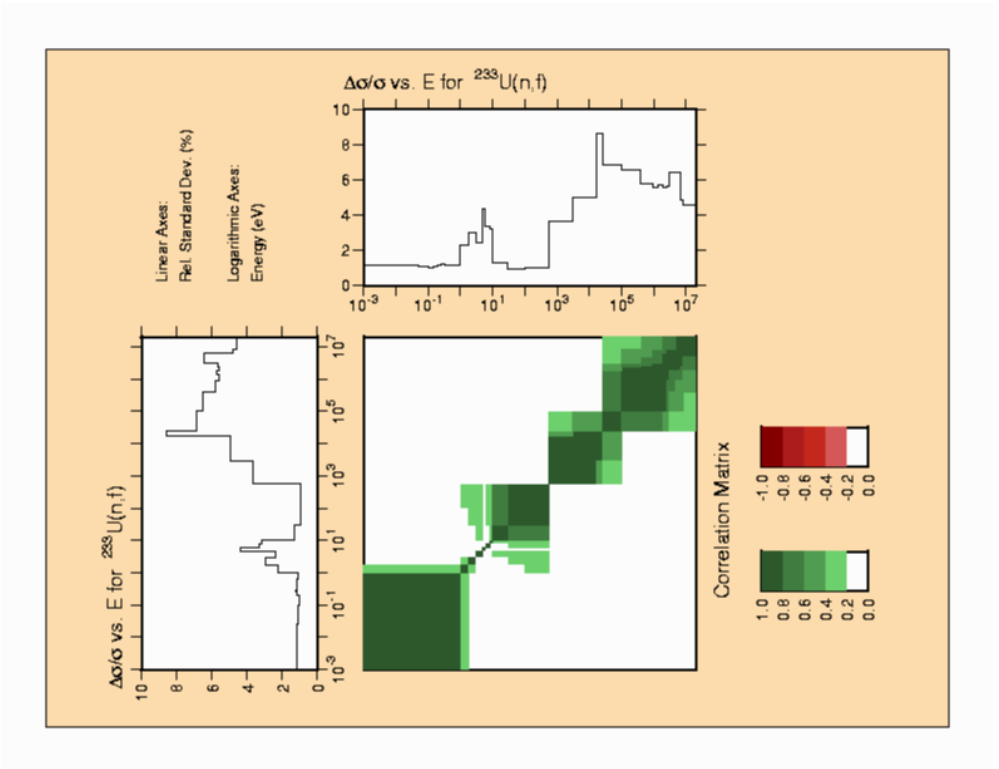

Fig. 5. ^{233}U fission cross section calculated in the 44-neutron group structure of the SCALE system.

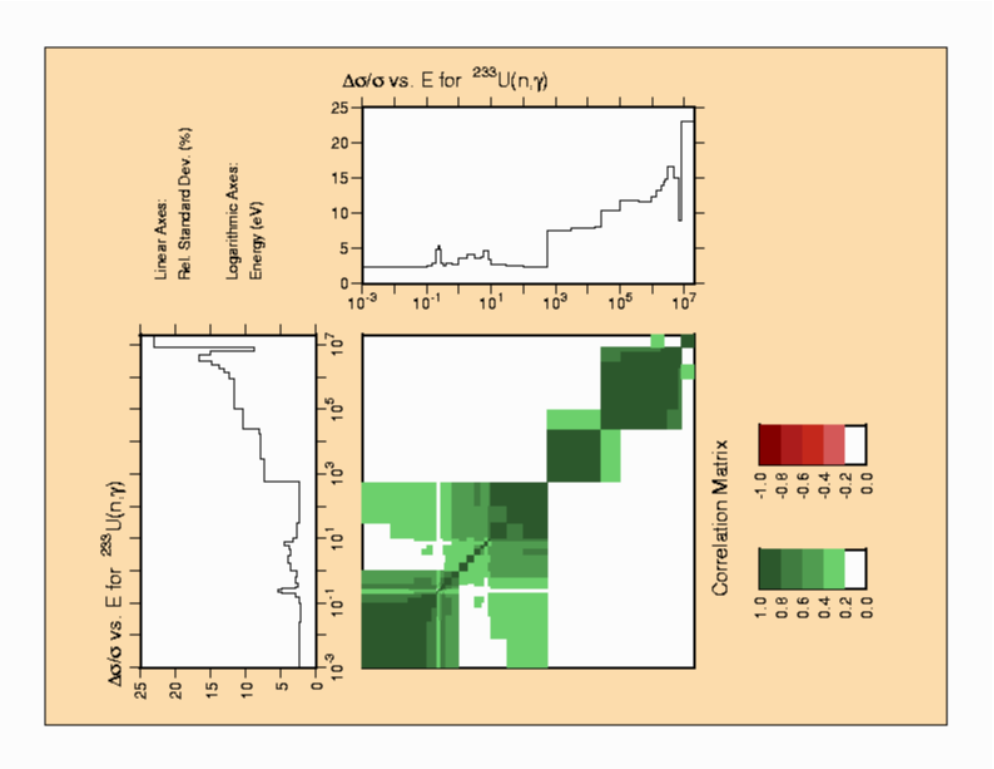

Fig. 6. ^{233}U capture cross section calculated in the 44-neutron group structure of the SCALE system.

5. PROCESSING OF ^{233}U ENDF FILE

The ^{233}U ENDF file was used to generate *centrm* formatted data and group-averaged cross section data along with the covariance information. The AMPX module *polident* was used to create point-wise cross section data at a temperature of T = 0 K. The energy mesh was generated to a precision of 0.001. The AMPX module *tgel* was used to calculate the total cross section as the sum of the relevant point-wise cross section data at T = 0 K. The AMPX module *broaden* was used to calculate the cross section data at temperatures T = 0 K, 300 K, 600 K, 900 K, 1200 K, and 2400 K. The resulting tab1 formatted file was converted to double precision using the module *charmin* so that the modules *bic* and *cajun* can be used to convert the data into a centrm formatted data file using the scale identifier 7009222.

The full AMPX input to generate the centrm library is

```
=shell
ln -fs /home/dw8/u233/U233.endf  ft11f001
end
=polident
-1$$ 5000000
0$$ 30 e
1$$ 1 t
2$$ 9222 11 2 6 e
4** a5 0.001 e
6$$ a3 0 15000 t
end
```

```
=shell
cp ft30f001 /home/dw8/u233/polident/u233
cp ft32f001 /home/dw8/u233/polident/u233.ft32
end
=tgel
-1$$ 5000000
0$$ 30 31 e t
end
=broaden
limit=5000000
logpt=31 logdp=34
t= 0 300 600 900 1200 2400
end
=shell
cp ft34f001 /home/dw8/u233/broaden/u233
end
=charmin
limit=5000000
in=34 out=35 single to double end
end
=bic
limit=5000000
lsu input=35 output=36 version=6
title=u233     9222 92233 ENDFB V7 REL0 REV0 MOD0 AMPX 06/29/05 n-ENDF-VIIb0.dat
end
=shell
cp ft36f001 /home/dw8/u233/centrmlib/u233
end
=shell
ln -fs /home/dw8/u233/centrmlib/u233 ft37f001
end
=cajun
-1$$ 5000000
0$$ 38
1$$ 1 e t
2$$ 37 1 t
3$$     9222
4$$  7009222
5$$ 0
t
end
=shell
cp ft38f001 /home/dw8/u233/centrmlib/92233-0
end
```

The AMPX modules *pickeze* and *jergens* are used to generate a weighting spectrum for the calculation of the group-averaged cross section data. The weighting spectrum is based on the point-wise cross section data at 300 K. The module *jergens* creates the following weighting spectra:

1. a Maxwellian-1/E-fission spectrum, 1/E above 10 MeV, identifier 1, and
2. the above Maxellian-1/E-fission spectrum, divided by the total cross section data, identifier 1099.

Use the AMPX module *y12* to produce point-wise kinematic data and the AMPX module *x10* to calculate multigroup constants for neutron interaction. It uses the standard 238-group structure with 90 thermal neutron groups and a neutron yield of 12.298. As a weighting function the Maxwellian-1/E-fission spectrum, 1/E above 10 MeV, normalized to the total cross section is

used. To calculate the cross section data in the unresolved resonance region, the AMPX module *prude* is used. The cross section data are generated for the background cross sections $\sigma_0 = 1.0 \times 10^{+8}$, $1.0 \times 10^{+6}$, $1.0 \times 10^{+5}$, and $1.0 \times 10^{+4}$ and temperatures of 1000 K, 100 K, 10 K, 1 K, and 1.0×10^{-6}K. These cross section data are converted to Bondarenko factors using the AMPX module *tabu*. Again the Maxwellian-1/E-fission spectrum, 1/E above 10 MeV, normalized to the total cross section is used as the weighting function. The AMPX module *unitab* is used to combine the group constants generated by *x10* and the Bondarenko factors generated by *tabu* into an AMPX master library. The thermal scattering matrix is calculated using the AMPX module *flange6* for temperatures 296 K, 600 K, 900 K, and 2000 K for the standard 238-group structure with 90 thermal neutron groups. The resulting master library is tested for validity using the AMPX module *rade*. The AMPX module *simonize* is used to assemble the AMPX master library containing all ^{233}U data.

The full AMPX input is

```
=shell
ln -fs  /scratch/e5a/u233dir/thefinalu233covevaluation.dat ft11f001
ln -fs /home/dw8/u233/broaden/u233 ft29f001
end
=pickeze
-1$$ 5000000
0$$ 29 31
1$$ 1 0 0 1 0 e t
2$$ 9222
5** 300.
t
end
=jergens
-1$$ a11 5000000 e
0$$ 31 30 18 1$$ 2 t
3$$ 1 0 4 t
3$$ 1099 4 0 t
2099 0 read 1.0   -1 0
2099 0 save 0 0 0
1099 2099 div  1.0 9222 1
1099 0 save   0    0 0
end
=y12
0$$ 32 11 e 1$$ 9222 2$$ 2 6 3$$ 32 8 8 8 8 5 t
t
end
=shell
cp ft32f001 /home/dw8/u233/fast.kinematics/u233
end
=x10
neutron
-1$$ 5000000
0$$ 1 30 31 32 1$$ 92233  238   90    0    5    0    0
2$$ 99 2099  9222 9222
3**  1.22989E+01
6$$ 99 2099
 t
 t
u233     9222 92233 ENDFB V7 REL0 REV0 MOD0 AMPX 08/04/05 n-ENDF-VIIb0.dat
end
=shell
cp ft01f001 /home/dw8/u233/238endf7.fast/u233
end
=prude
```

```
0$$ 34 1$$ 1 t
2$$ 9222 9 3 11 2 t
3** 1+8 1+6 1+5 1+4 1000 100 10 1 1-6
4** 300.0 900.0 2000.0 t
end
=tabu
-1$$ 500000 0$$ 2 34 30 1$$ 1   238  238 t
t   Use the Standard Group Structure
u233     9222 92233 ENDFB V7 REL0 REV0 MOD0 AMPX 08/04/05 n-ENDF-VIIb0.dat
10$$  9222 11$$ 99 3 2099 t
end
=shell
cp ft02f001 /home/dw8/u233/238endf7.BF/u233
cp ft34f001 /home/dw8/u233/unres.point/u233
end
=unitab
-1$$ 500000 0$$ 10 18 9 8   1  2  0  0  0  0  0  0  0  0  0  0
 1$$ 1   2 6$$ 2000 500 t
 2$$
    92233        1    92233     1111
    92233        2     9222     4444
t
end
=rade
-1$$ 5000000
1$$ 10 e t
end
=shell
cp ft10f001 /home/dw8/u233/238endf7.master/u233
end
=flange6
 t=296 t=600 t=900 t=2000   nl=3
 igm=238 neg=90 iftg=149 master=4
 za=92233 awr= 2.31043E+02 free= 1.22989E+01
 end
end
=rade
1$$  4 e t
end
=shell
cp ft04f001 /home/dw8/u233/238endf7.thermal/u233
end
=shell
ln -fs /home/dw8/u233/238endf7.master/u233 ft20f001
ln -fs /home/dw8/u233/238endf7.thermal/u233 ft21f001
end
=simonize
identifier=92233 master=1
id45= 7009222 source=endf
neutron=20       id19=92233
2dn=21           id19=92233 mt=   0
end
=rade
-1$$ 5000000
1$$ 1 e t
end
=shell
cp ft01f001 /home/dw8/u233/238endf7.masterfinal/u233
end
```

The new evaluation is included into the scale cross section library.

The covariance data are generated using the 44-group structure instead of the 238. The AMPX library containing the cross section data for the 238-group structure is therefore collapsed to the 44-group structure using a light-water reactor flux. The collapse is done using the AMPX module *malocs*. The 238-group ENDF/B-V SCALE library contains the flux used as identifier mat = 99 and mt = 9088. Because the resulting AMPX library uses the scale id 92233 and the ampx module *puff_iv* needs the endf material number, the module *ajax* is used to change the identifier prior to running *puff_iv*. A flux of Maxwellian - 1/E-Fission Spectrum is used over the whole range of covariances matrices generated.

The AMPX input is as follows

```
=shell
ln -sf /projects/scale/scale5/data/scale.rev14.xn238 ft88f001
ln -sf /home/dw8/u233/scale.rev14.xn238_withendf7_u233 ft89f001
end
=malocs
0$$ 89 20
1$$ 238 44 0 0 -88 0
3$$  99 9008 e
1t
4$$ 7r1 2 3 2r4 5 6 7 2r8 8r9 14r10 6r11 10r12 13
    7r14 11r15 12r16 30r17 16r18 2r19 6r20 3r21 6r22 14r23
    27r24 10r25 5r26 27 28 29 2r30 31 32 33 2r34 2r35 3r36
    2r37 38 39 40 41 42 3r43 9r44
2t
end
=ajax
0$$ 1  e
1$$ 1  t
2$$ 20 1  t
3$$
92233
4$$
9222 t
end
=shell
cp ft01f001 /home/dw8/u233/u233_puff_ampx
end
=shell
ln -fs /home/dw8/ampx/u233/U233.endf  ft32f001
ln -fs /home/dw8/ampx/u233/u233_puff_ampx  ft11f001
end
=jergens
0$$ 0 12 18
1$$ 1 t
3$$ 1099 0 4 t
=puff_iv
-1$$ 400000000 e
1$$ -1 0 0 11 32 9222 -12 -11 -12 1 2 2 a16 -1 e t
5## 59 1099 e t
coverx file for u233
end
=shell
cp ft01f001 /home/dw8/ampx/u233/coverx/u233
end
```

The new coverx file is incorporated into the scale covariance libraries.

6. BENCHMARK CALCULATIONS AND DATA UNCERTAINTY

The covariance data were verified though their use in 82 criticality safety benchmark experiments from the *International Handbook of Evaluated Criticality Safety Benchmark Experiments*.[25] Only experiments suitable for one-dimensional (1-D) modeling were selected for the verification. The TSUNAMI-1D sequence from SCALE 5.1 (Ref. 24) was used to generate k_{eff} sensitivities to each group-wise cross section data value used in the calculation of each benchmark. The calculations were performed using the SCALE 5.1 238-group ENDF/B-VI cross section data library, which was amended to include ENDF/B-VII data for ^{233}U (v6-238_u233) and the SCALE 5.1 recommended covariance data set for ENDF/B-VI, which was amended to include the ^{233}U covariance data described above. The results with the updated libraries were compared to baseline results for the same cases using the standard SCALE 5.1 238-group ENDF/B-VI library (v6-238) and the SCALE 5.1 recommended covariance data set for ENDF/B-VI.

The benchmark experiments are identified in Table 7, where some basic characteristics of the systems and the k_{eff} values with the two cross-section data libraries are shown. The uncertainties in the k_{eff} values for these systems are shown in Figs. 7–20. In these figures, results from two library sets are shown: (1) the standard 238-group ENDF/B-VI cross section library and 44groupv6rec covariance library (identified as v6-238 in the figures) and (2) the 238-group ENDF/B-VI cross section library with ENDF/B-VII data for ^{233}U and the 44group v6rec covariance library with ENDF/B-VII data for ^{233}U (identified as v6-238_u233 in the figures).

Figures 7 and 8 show the total uncertainty due to all covariance data. For fast systems, the total uncertainty is reduced from ~8% with ENDF/B-VI data to ~3% with ENDF/B-VII data. A small reduction in uncertainty is observed for intermediate energy systems, and values are nearly constant for thermal systems. Examining the uncertainty in k_{eff} generated by each process, much of the reduction in total uncertainty is due to ^{233}U fission uncertainties, as shown in Fig. 9. All other processes, shown in Figs. 10–20, show much smaller variations between the libraries. Some processes were not available in ENDF/B-VI, such as the covariance between ^{233}U fission and ^{233}U elastic, ^{233}U n,2n, and ^{233}U n,n′, shown in Figs. 14, 19, and 20, respectively.

Table 7. Benchmark experiments selected for verification of the ^{233}U covariance data

Case Number	Identifier	Description	EALF (eV)	Benchmark k-eff	Benchmark k-eff Uncertainty	k-eff v6-238	k-eff v6-238_u233
1	umf001t00x	^{233}U Metal, Fast Spectrum	1.11E+06	1.0000	0.0010	0.99380	1.00082
2	umf002t01x	^{233}U Metal, Fast Spectrum	1.02E+06	1.0000	0.0010	0.99854	1.00004
3	umf002t02x	^{233}U Metal, Fast Spectrum	1.06E+06	1.0000	0.0011	0.99626	0.99928
4	umf003t01x	^{233}U Metal, Fast Spectrum	1.08E+06	1.0000	0.0010	0.99722	0.99995
5	umf003t02x	^{233}U Metal, Fast Spectrum	1.06E+06	1.0000	0.0010	0.99935	1.00023
6	umf004t01x	^{233}U Metal, Fast Spectrum	9.60E+05	1.0000	0.0007	1.00497	1.00784
7	umf004t02x	^{233}U Metal, Fast Spectrum	8.58E+05	1.0000	0.0008	1.00827	1.00949
8	umf005t01x	^{233}U Metal, Fast Spectrum	9.45E+05	1.0000	0.0030	0.99536	0.99849
9	umf005t02x	^{233}U Metal, Fast Spectrum	7.67E+05	1.0000	0.0030	0.99765	0.99896
10	umf006t00x	^{233}U Metal, Fast Spectrum	9.96E+05	1.0000	0.0014	1.00191	1.00127
11	usi001t01x	^{233}U Solution, Intermediate Spectrum	6.78E+00	1.0000	0.0083	0.98960	0.99102
12	usi001t02x	^{233}U Solution, Intermediate Spectrum	7.92E+00	1.0000	0.0085	0.98455	0.98589
13	usi001t03x	^{233}U Solution, Intermediate Spectrum	8.52E+00	1.0000	0.0066	0.98518	0.98649
14	usi001t04x	^{233}U Solution, Intermediate Spectrum	3.71E+00	1.0000	0.0061	0.99399	0.99560
15	usi001t05x	^{233}U Solution, Intermediate Spectrum	9.12E+00	1.0000	0.0082	0.98823	0.98954
16	usi001t06x	^{233}U Solution, Intermediate Spectrum	4.27E+00	1.0000	0.0061	0.98729	0.98888
17	usi001t07x	^{233}U Solution, Intermediate Spectrum	9.55E+00	1.0000	0.0059	0.98531	0.98665
18	usi001t08x	^{233}U Solution, Intermediate Spectrum	4.52E+00	1.0000	0.0056	0.98217	0.98380
19	usi001t09x	^{233}U Solution, Intermediate Spectrum	7.31E+00	1.0000	0.0068	0.98207	0.98346
20	usi001t10x	^{233}U Solution, Intermediate Spectrum	1.00E+01	1.0000	0.0053	0.98187	0.98327
21	usi001t11x	^{233}U Solution, Intermediate Spectrum	7.72E+00	1.0000	0.0057	0.98255	0.98400
22	usi001t12x	^{233}U Solution, Intermediate Spectrum	4.41E+00	1.0000	0.0091	0.98559	0.98750
23	usi001t13x	^{233}U Solution, Intermediate Spectrum	5.03E+00	1.0000	0.0071	0.98586	0.98768
24	usi001t14x	^{233}U Solution, Intermediate Spectrum	2.29E+00	1.0000	0.0052	0.99150	0.99355
25	usi001t15x	^{233}U Solution, Intermediate Spectrum	5.40E+00	1.0000	0.0075	0.98353	0.98532
26	usi001t16x	^{233}U Solution, Intermediate Spectrum	1.79E+00	1.0000	0.0028	0.97659	0.97879
27	usi001t17x	^{233}U Solution, Intermediate Spectrum	2.53E+00	1.0000	0.0055	0.98996	0.99198

Table 7. Benchmark experiments selected for verification of the ^{233U} covariance data (continued)

Case Number	Identifier	Description	EALF (eV)	Benchmark k-eff	Benchmark k-eff Uncertainty	k-eff v6-238	k-eff v6-238_u233
28	usi001t18x	^{233}U Solution, Intermediate Spectrum	5.79E+00	1.0000	0.0057	0.98159	0.98338
29	usi001t19x	^{233}U Solution, Intermediate Spectrum	6.03E+00	1.0000	0.0083	0.97828	0.98010
30	usi001t20x	^{233}U Solution, Intermediate Spectrum	2.99E+00	1.0000	0.0056	0.98105	0.98308
31	usi001t21x	^{233}U Solution, Intermediate Spectrum	6.28E+00	1.0000	0.0050	0.97579	0.97766
32	usi001t22x	^{233}U Solution, Intermediate Spectrum	6.43E+00	1.0000	0.0049	0.98077	0.98270
33	usi001t23x	^{233}U Solution, Intermediate Spectrum	4.70E+00	1.0000	0.0047	0.99177	0.99373
34	usi001t24x	^{233}U Solution, Intermediate Spectrum	1.97E+00	1.0000	0.0081	0.99618	0.99891
35	usi001t25x	^{233}U Solution, Intermediate Spectrum	2.25E+00	1.0000	0.0081	0.98842	0.99106
36	usi001t26x	^{233}U Solution, Intermediate Spectrum	2.37E+00	1.0000	0.0065	0.99192	0.99452
37	usi001t27x	^{233}U Solution, Intermediate Spectrum	1.24E+00	1.0000	0.0051	0.99104	0.99375
38	usi001t28x	^{233}U Solution, Intermediate Spectrum	2.53E+00	1.0000	0.0061	0.98609	0.98866
39	usi001t29x	^{233}U Solution, Intermediate Spectrum	2.62E+00	1.0000	0.0098	0.97980	0.98237
40	usi001t30x	^{233}U Solution, Intermediate Spectrum	1.45E+00	1.0000	0.0053	0.97849	0.98117
41	usi001t31x	^{233}U Solution, Intermediate Spectrum	2.67E+00	1.0000	0.0071	0.99334	0.99594
42	usi001t32x	^{233}U Solution, Intermediate Spectrum	2.77E+00	1.0000	0.0053	0.97788	0.98051
43	usi001t33x	^{233}U Solution, Intermediate Spectrum	2.07E+00	1.0000	0.0046	0.99497	0.99760
44	ust001t01x	^{233}U Solution, Thermal Specturm	3.90E–02	1.0000	0.0031	0.99867	1.00555
45	ust001t02x	^{233}U Solution, Thermal Specturm	3.96E–02	1.0005	0.0033	0.99862	1.00550
46	ust001t03x	^{233}U Solution, Thermal Specturm	4.02E–02	1.0006	0.0033	0.99812	1.00501
47	ust001t04x	^{233}U Solution, Thermal Specturm	4.08E–02	0.9998	0.0033	0.99810	1.00499
48	ust001t05x	^{233}U Solution, Thermal Specturm	4.14E–02	0.9999	0.0033	0.99740	1.00431
49	ust005t01x	^{233}U Solution, Thermal Specturm	6.06E–02	1.0060	0.0020	1.00122	1.00684
50	ust008t01x	^{233}U Solution, Thermal Specturm	3.68E–02	1.0006	0.0029	0.99722	1.00424
51	ust012t06x	^{233}U Solution, Thermal Specturm	7.89E–02	0.9987	0.0011	1.00339	1.00861
52	ust015t01x	^{233}U Solution, Thermal Specturm	1.09E+00	1.0000	0.0075	0.99372	0.99701
53	ust015t02x	^{233}U Solution, Thermal Specturm	1.22E+00	1.0000	0.0070	0.98840	0.99159
54	ust015t03x	^{233}U Solution, Thermal Specturm	1.29E+00	1.0000	0.0068	0.98912	0.99227
55	ust015t04x	^{233}U Solution, Thermal Specturm	7.10E–01	1.0000	0.0041	0.98996	0.99313
56	ust015t05x	^{233}U Solution, Thermal Specturm	1.35E+00	1.0000	0.0055	0.98848	0.99158

Table 7. Benchmark experiments selected for verification of the ^{233U} covariance data (continued)

Case Number	Identifier	Description	EALF (eV)	Benchmark k-eff	Benchmark k-eff Uncertainty	k-eff v6-238	k-eff v6-238_u233
57	ust015t06x	^{233}U Solution, Thermal Specturm	1.40E+00	1.0000	0.0099	0.97890	0.98199
58	ust015t07x	^{233}U Solution, Thermal Specturm	7.81E–01	1.0000	0.0070	0.98754	0.99070
59	ust015t08x	^{233}U Solution, Thermal Specturm	1.45E+00	1.0000	0.0067	0.97519	0.97824
60	ust015t09x	^{233}U Solution, Thermal Specturm	1.48E+00	1.0000	0.0050	0.97050	0.97361
61	ust015t10x	^{233}U Solution, Thermal Specturm	1.12E+00	1.0000	0.0051	0.99011	0.99322
62	ust015t11x	^{233}U Solution, Thermal Specturm	6.83E–01	1.0000	0.0075	0.99664	1.00035
63	ust015t12x	^{233}U Solution, Thermal Specturm	7.56E–01	1.0000	0.0069	0.99654	1.00017
64	ust015t13x	^{233}U Solution, Thermal Specturm	7.96E–01	1.0000	0.0069	0.99420	0.99777
65	ust015t14x	^{233}U Solution, Thermal Specturm	4.58E–01	1.0000	0.0036	0.99800	1.00155
66	ust015t15x	^{233}U Solution, Thermal Specturm	8.35E–01	1.0000	0.0060	0.99171	0.99523
67	ust015t16x	^{233}U Solution, Thermal Specturm	8.56E–01	1.0000	0.0043	0.99045	0.99395
68	ust015t17x	^{233}U Solution, Thermal Specturm	4.95E–01	1.0000	0.0029	0.99735	1.00089
69	ust015t18x	^{233}U Solution, Thermal Specturm	8.86E–01	1.0000	0.0056	0.97627	0.97974
70	ust015t19x	^{233}U Solution, Thermal Specturm	9.00E–01	1.0000	0.0052	0.97642	0.97990
71	ust015t20x	^{233}U Solution, Thermal Specturm	2.84E–01	1.0000	0.0079	0.99869	1.00318
72	ust015t21x	^{233}U Solution, Thermal Specturm	3.11E–01	1.0000	0.0070	1.00064	1.00505
73	ust015t22x	^{233}U Solution, Thermal Specturm	3.25E–01	1.0000	0.0062	0.99836	1.00270
74	ust015t23x	^{233}U Solution, Thermal Specturm	3.38E–01	1.0000	0.0055	0.99598	1.00027
75	ust015t24x	^{233}U Solution, Thermal Specturm	3.46E–01	1.0000	0.0051	0.99231	0.99656
76	ust015t25x	^{233}U Solution, Thermal Specturm	2.20E–01	1.0000	0.0023	0.99705	1.00123
77	ust015t26x	^{233}U Solution, Thermal Specturm	1.25E–01	1.0000	0.0066	0.99673	1.00196
78	ust015t27x	^{233}U Solution, Thermal Specturm	1.29E–01	1.0000	0.0063	1.00068	1.00587
79	ust015t28x	^{233}U Solution, Thermal Specturm	1.31E–01	1.0000	0.0058	0.99850	1.00364
80	ust015t29x	^{233}U Solution, Thermal Specturm	1.33E–01	1.0000	0.0051	0.99682	1.00191
81	ust015t30x	^{233}U Solution, Thermal Specturm	1.35E–01	1.0000	0.0048	0.99598	1.00103
82	ust015t31x	^{233}U Solution, Thermal Specturm	1.36E–01	1.0000	0.0055	0.99506	1.00007

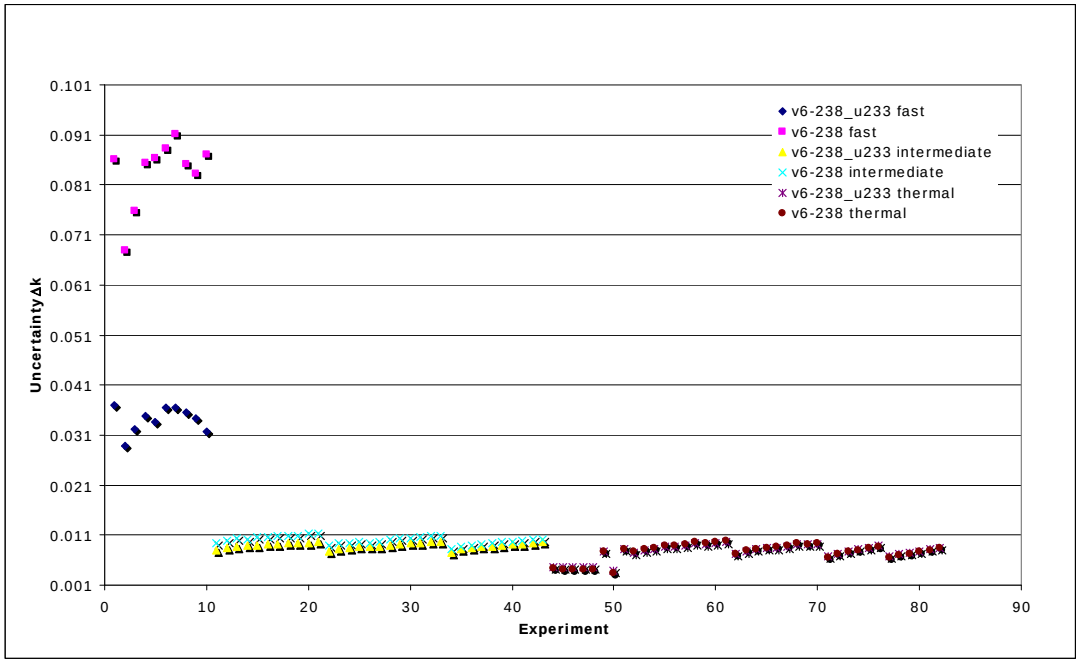

Fig. 7. Absolute k_{eff} uncertainties due to covariance data as a function of experiment number.

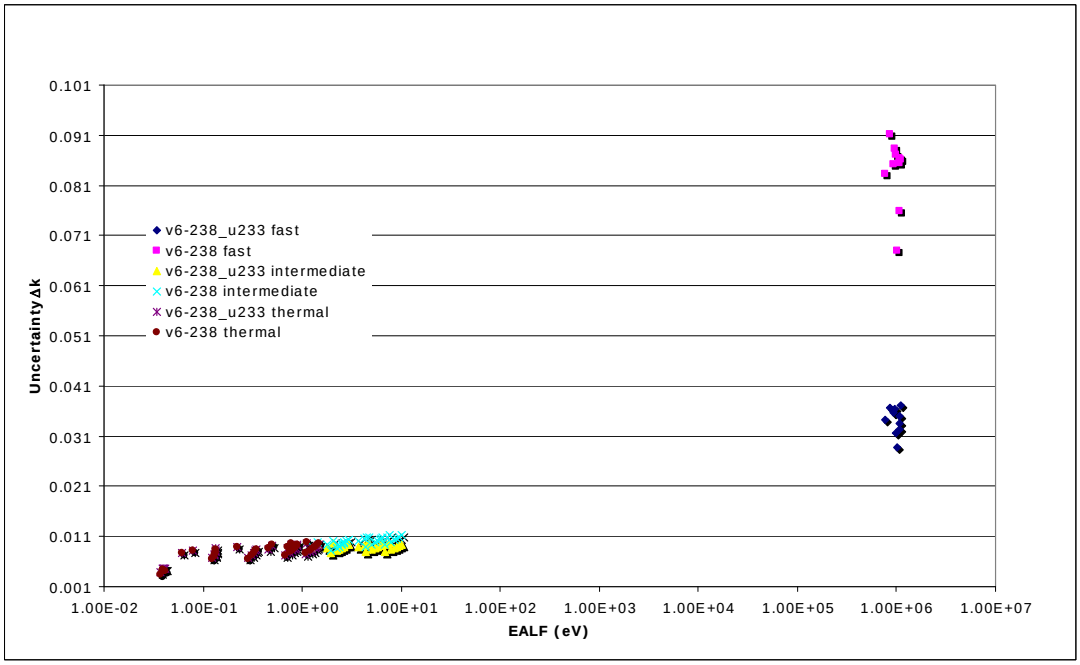

Fig. 8. Absolute k_{eff} uncertainties due to covariance data as a function of EALF.

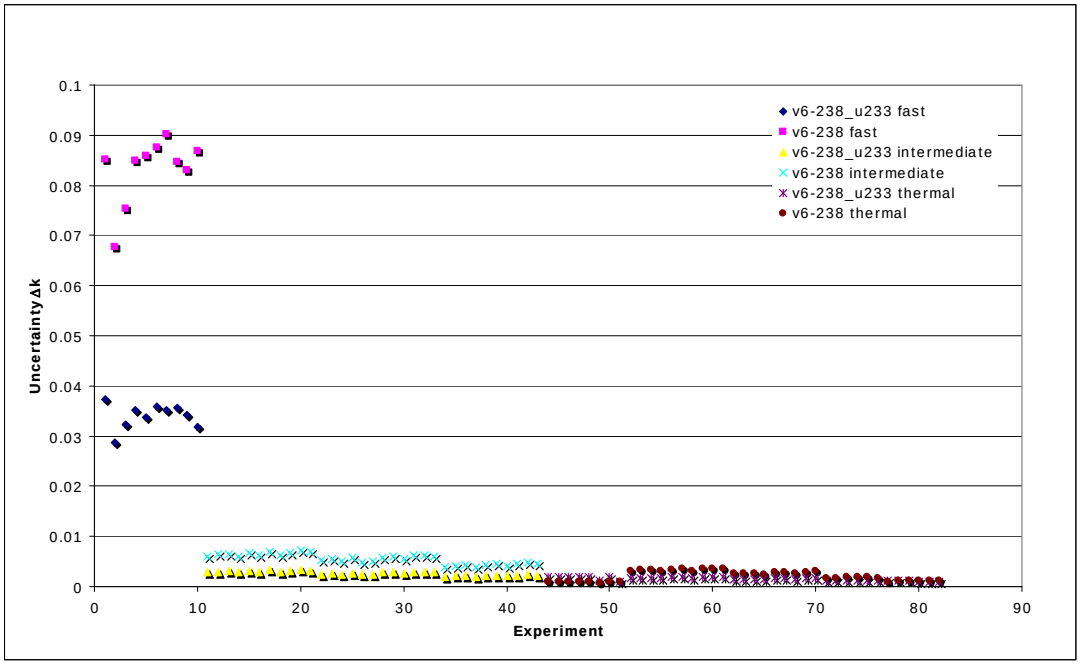

Fig. 9. Absolute k_{eff} uncertainties due to covariance data for ^{233}U fission.

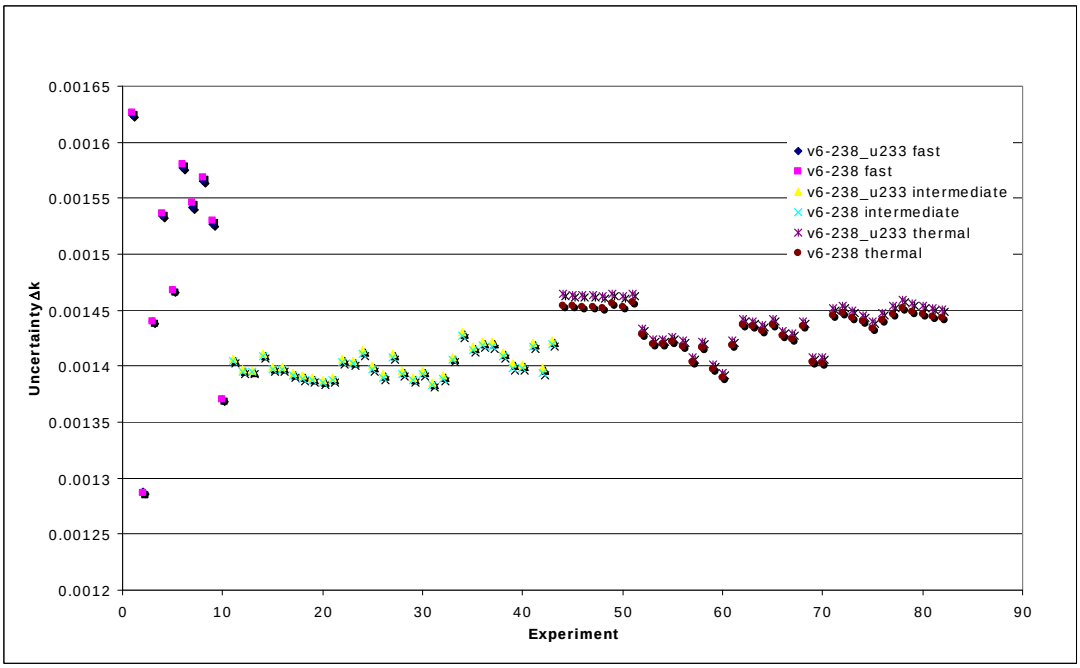

Fig. 10. Absolute k_{eff} uncertainties due to covariance data for ^{233}U $\bar{\nu}$.

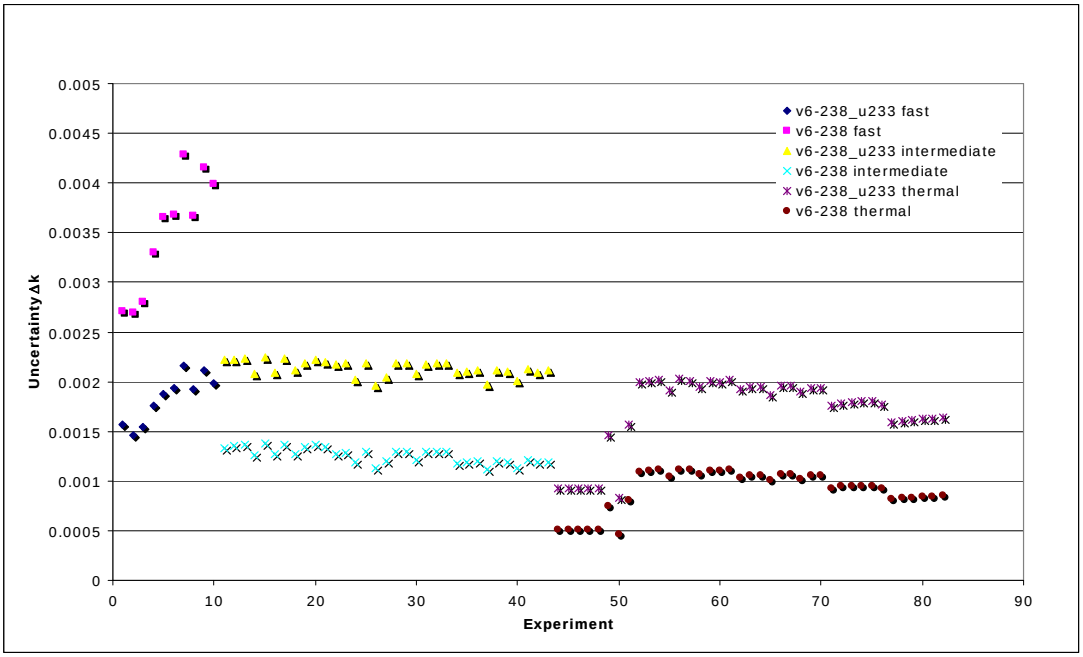

Fig. 11. Absolute k_{eff} uncertainties due to covariance data for ^{233}U n,gamma.

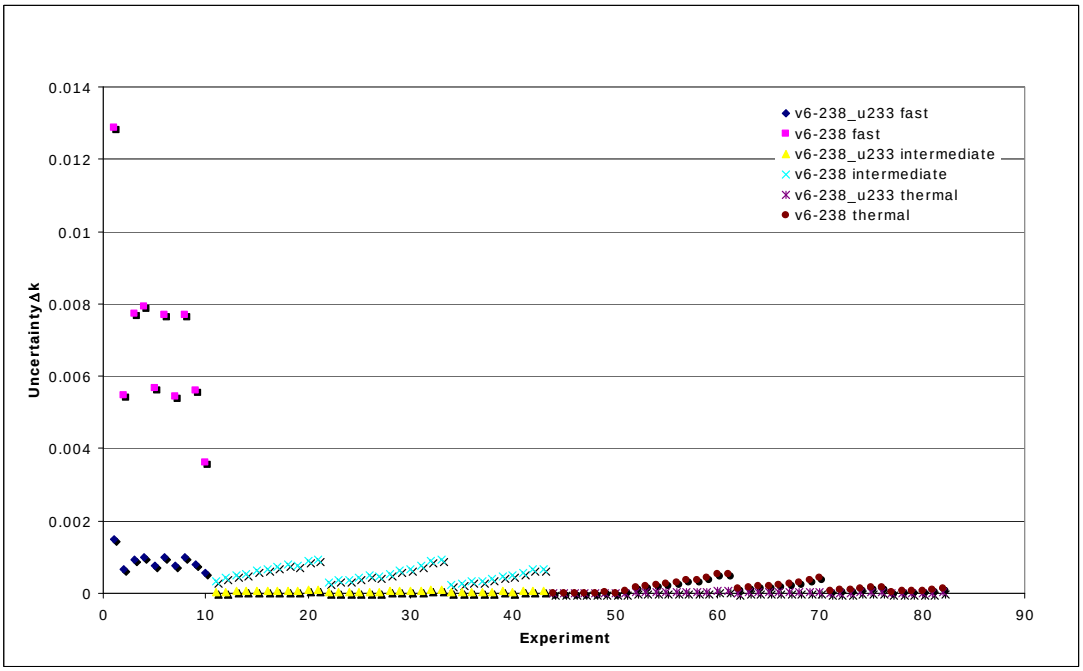

Fig. 12. Absolute k_{eff} uncertainties due to covariance data for ^{233}U elastic.

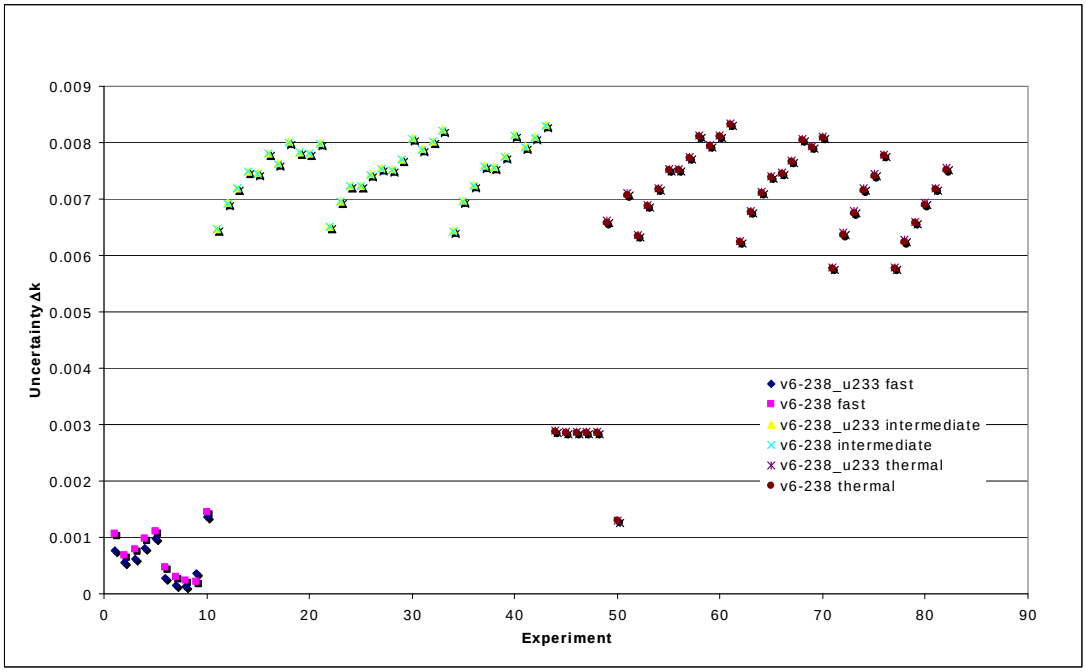

Fig. 13. Absolute k_{eff} uncertainties due to covariance data for ^{233}U chi.

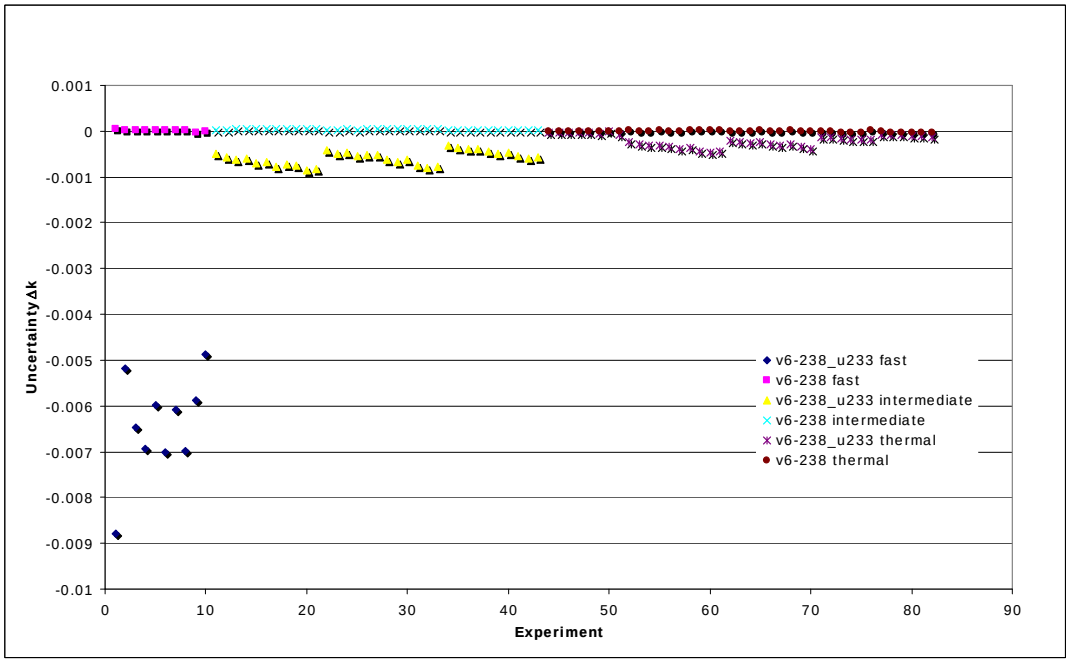

Fig. 14. Absolute k_{eff} uncertainties due to covariance data for ^{233}U fission to ^{233}U elastic.

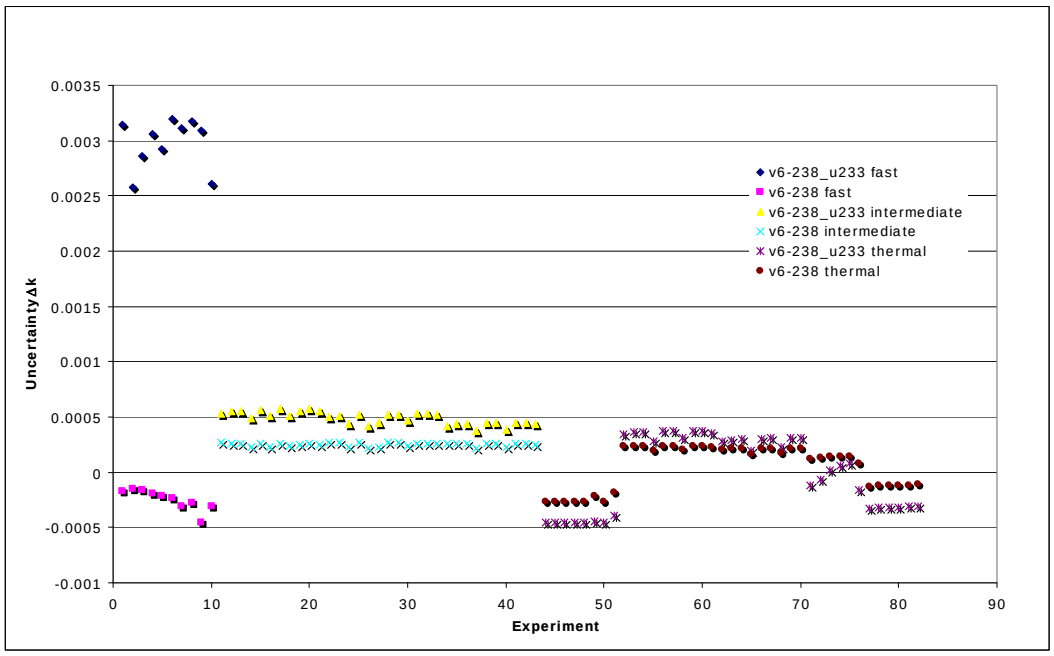

Fig. 15. Absolute k_{eff} uncertainties due to covariance data for ^{233}U fission to ^{233}U n,gamma.

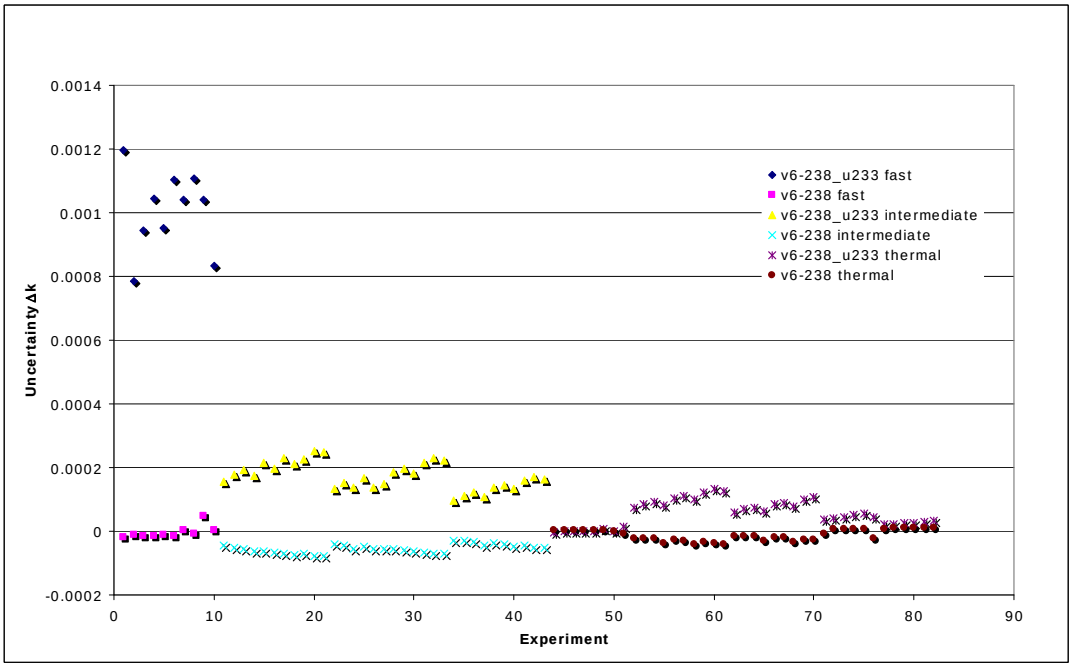

Fig. 16. Absolute k_{eff} uncertainties due to covariance data for ^{233}U n,gamma to ^{233}U elastic.

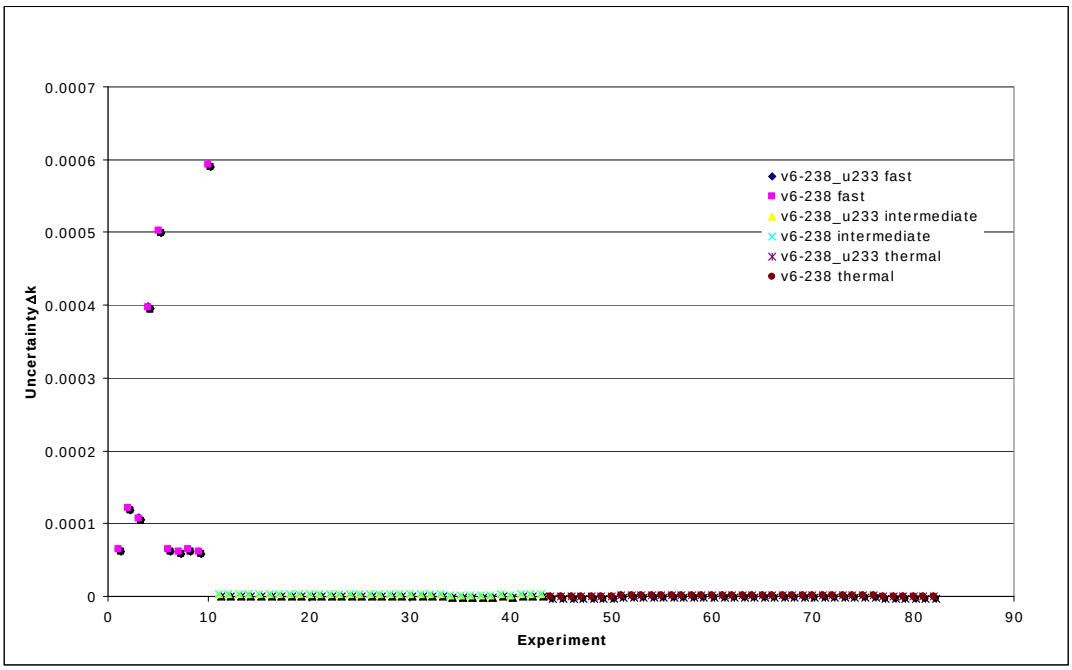

Fig. 17. Absolute k_{eff} uncertainties due to covariance data for ^{238}U fission to ^{233}U fission.

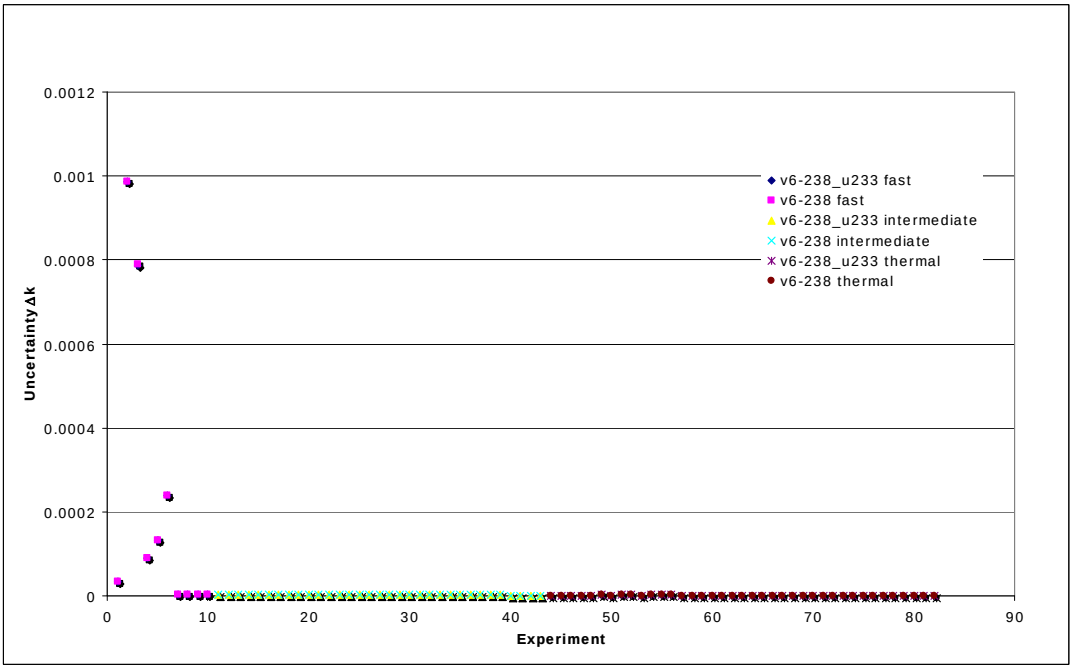

Fig. 18. Absolute k_{eff} uncertainties due to covariance data for ^{235}U fission to ^{233}U fission.

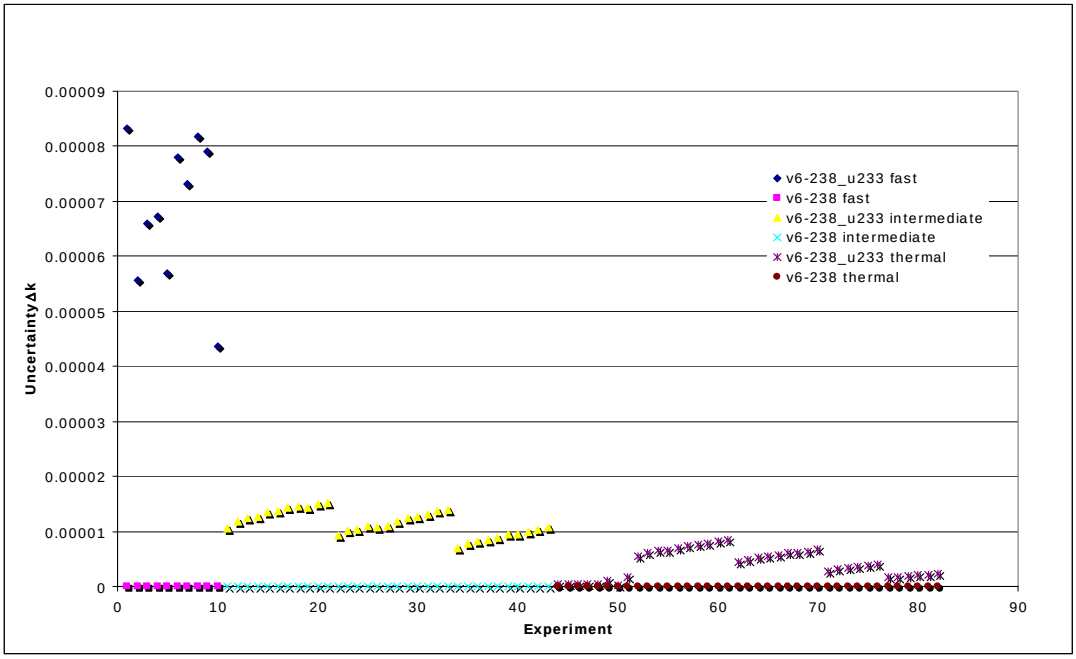

Fig. 19. Absolute k_{eff} uncertainties due to covariance data for ^{233}U n,2n.

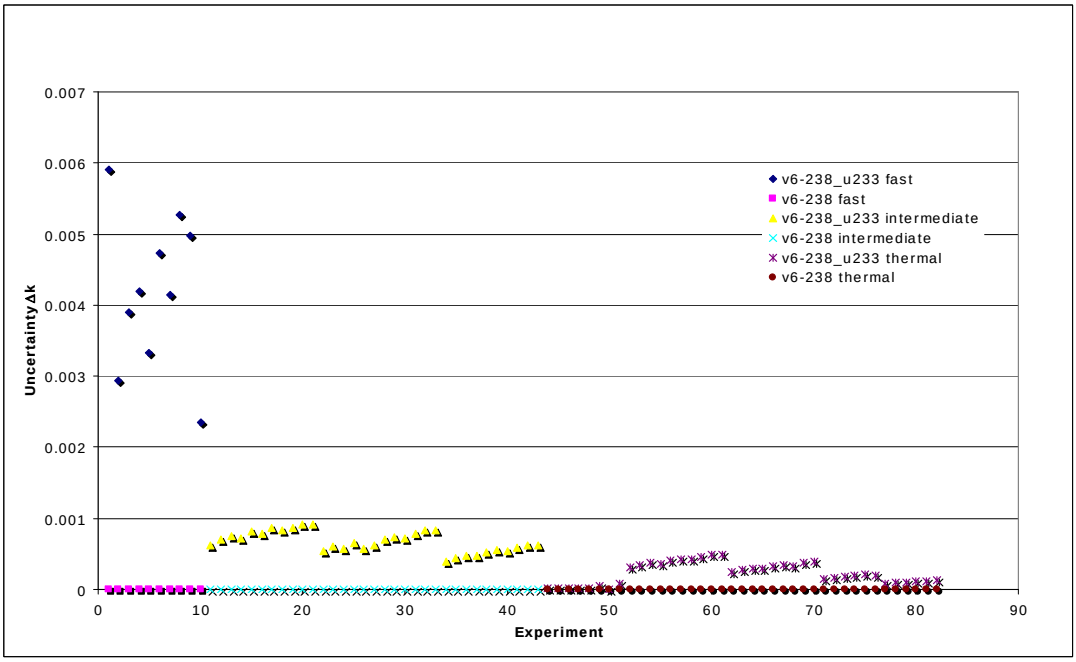

Fig. 20. Absolute k_{eff} uncertainties due to covariance data for ^{233}U n,n′.

7. CONCLUSIONS

Resonance-parameter covariance evaluations were performed in the resolved and unresolved resonance regions with the computer code SAMMY. The resolved resonance covariance evaluation was done in the energy range 0–600 eV, whereas the unresolved evaluation was performed in the energy region 600 eV to 40 keV. Above 40 keV to 20 MeV, the covariance data work was done at the IAEA. The covariance data were added to the ^{233}U ENDF/B/VII.0 evaluation and processed with the AMPX and PUFF-IV codes. Sensitivity analysis of 82 benchmark experiments with ^{233}U were done with the TSUNAMI code. The majority of the benchmark experiments used to verify the ^{233}U covariance data were taken from the *International Handbook of Evaluated Criticality Safety Benchmark Experiments*. For the fast systems the total uncertainty of the system multiplication factors was reduced from ~8% with ENDF/B-VI uncertainty to ~3% using the covariance evaluation done in this work. Small decreases in the uncertainty for thermal and intermediate energy systems are also observed. It appears that the reduction in the multiplication factor uncertainty is due to a decrease in the ^{233}U fission cross sections uncertainty. This is the result of a better resonance analysis and better differential fission cross section experiments used in the evaluation. The work presented here will support criticality safety calculations for the Oak Ridge National Laboratory Building 3019.

8. REFERENCES

1. N. M. Larson, *Updated Users' Guide for SAMMY: Multilevel R-Matrix Fits to Neutron Data Using Bayes' Equations*, ORNL/TM-9179/R7, Oak Ridge National Laboratory (2007).
2. L. C. Leal, H. Derrien, J. A. Harvey, K. H. Guber, N. M. Larson, and R. R. Spencer, *R-Matrix Resonance Analysis and Statistical Properties of the Resonance Parameters of ^{233}U in the Neutron Energy Range from Thermal to 600 eV*, ORNL/TM-2000/372, Oak Ridge National Laboratory and ENDF-365 (March 2001).
3. L. C. Leal, H. Derrien, N. M. Larson, and A. Courcelle, "An Unresolved Resonance Evaluation for ^{233}U from 600 eV to 40 keV," *2005 ANS Annual Meeting "The Next 50 Years: Creating Opportunities,* June 5–9, 2005, San Diego, California. *Trans. Am. Nucl. Soc*., **92**, 665–666 (June 2005).
4. R. Capote, M. Sin, A. Trkov, et al., "Extension of the Nuclear Reaction Model Code EMPIRE to Actinides' Nuclear Data Evaluation," *Nuclear Data Conference*, Nice, France, April 22–27, 2007.
5. M. Herman, R. Capote, B. Carlson, P. Oblozinsky, M. Sin, A. Trkov, and V. Zerkin, "EMPIRE, nuclear reaction model code, version 2.19 (Lodi)," www.nndc.bnl.gov /empire219, March 2005.
6. D. L. Smith, *Covariance Matrices for Nuclear Cross Sections Derived from Nuclear Model Calculations*, ANL/NDM-159, Argonne National Laboratory, November 2004.
7. D. W. Muir, A. Trkov, I. Kodeli, et al., "The Global Assessment of Nuclear Data, GANDR," *Nuclear Data Conference*, Nice, France, April 22–27, 2007.
8. K. Raskach, Oak Ridge National Laboratory, personal communication (March 2006).
9. D. Wiarda and M. E. Dunn, *PUFF-IV: A Code for Processing ENDF Uncertainty Data into Multigroup Covariance Matrices*, ORNL/TM-2006/147, Oak Ridge National Laboratory (October 2006).
10. K. Kosako and N. Yanano, "Preparation of a Covariance Processing System for the Evaluated Nuclear Data File, JENDL," JNC TJ 9440 99-003, 1999 [in Japanese]; K. Kosako, "Covariance Data Processing Code: ERRORJ," in *Proceedings of the Specialists' Meeting of Reactor Group Constants, February 22–23, 2001*, JAERI-Conf 2001-009, ed. J. Katakura, JAERI, Tokai, Japan (2001).
11. *ENDF*-102*, Data Formats and Procedures for the Evaluated Nuclear Data File, ENDF*-6, written by Members of the Cross Section Evaluation Working Group, ed. V. McLane, C. L. Dunford, and P. F. Rose, BNL-NCS-4495, Brookhaven National Laboratory (April 2001). Updated BNL-NCS-449504-Rev, ed. M. Herman (June 2005).
12. L. C. Leal, G. Arbanas, H. Derrien, N. M. Larson, and B. Rearden, "Covariance Generation for ^{233}U in the Resolved Resonance Region for Criticality Safety Applications," *Mathematics and Computation, Supercomputing, Reactor Physics and Nuclear and Biological Applications*, Palais des Papes, Avignon, France, September 12–15, 2005.
13. K. H. Guber, R. R. Spencer, L. C. Leal, P. E. Koehler, J. A. Harvey, R. O. Sayer, H. Derrien, T. E. Valentine, D. E. Pierce, V. M. Cauley, and T. A. Lewis, "High-Resolution Transmission Measurements of U-233 Using a Cooled Sample At the Temperature T=11 K," *Nucl. Sci. Eng.*, **139(2)**, 111–117 (2001).

14. K. H. Guber, R. R. Spencer, L. C. Leal, J. A. Harvey, N. W. Hill, G. Dos Santos, R. O. Sayer, and D. C. Larson, "New High-Resolution Fission Cross-Section Measurements of U-233 in the 0.4-eV to 700-keV Energy Range," *Nuc. Sci. Eng*. **135(2)**, 141-149 (2000).
15. J. A. Harvey, C. L. Moore, and N. W. Hill, *Proc. Int. Conf. on Neutron Cross Section for Technology, Knoxville, Oct. 22–26, 1979,* NBS Special Publication 594, p. 690 (1980).
16. M. S. Moore, M. G. Miller, and O. D. Simpson, "Slow Neutron Total and Fission Cross Sections of U-233," *Phys. Rev.,* **118,** 714 (1960).
17. N. J. Pattenden and J. A. Harvey, "Measurement of the Neutron Total Cross Section of U^{233} from 0.07 to 10,000 ev," *Nuc. Sci. Eng.,* **17**, 404-410 (1963).
18. L. W. Weston, R. Gwin, G. De Saussure, R. W. Ingle, J. H. Todd, C. W. Craven, R. W. Hockenbury, and R. C. Block, "Neutron Fission and Capture Cross-Section Measurements for Uranium-233 in Energy Region 0.02 to 1 eV," *Nuc. Sci. Eng.* **42(2)**, 143 (1970).
19. J. Blons, "High-Resolution Measurements of Neutron-Induced Fission Cross-Sections for U-233, U-235, Pu-239 and Pu-241 Below 30 keV," *Nucl. Sci. Eng.,* **51(2)**, 130–147 (1973).
20. A. J. Deruytter and C. Wagemans, "Measurement and Normalization of Relative Uranium-233 Fission Cross-Section In Low Resonance Region," *Nucl. Sci. Eng.,* **54(4)**, 423–431 (1974).
21. H. Derrien, J. A. Harvey, K. H. Guber, L. C. Leal, and N. M. Larson, *Average Neutron Total Cross Sections in the Unresolved Energy Region from ORELA High Resolution Transmission Measurements*, ORNL/TM-2003/291 (2004).
22. J. C. Hopkins and B. C. Diven, "Neutron Capture To Fission Ratios In U^{233}, U^{235}, Pu^{233}," *Nucl. Sci. Eng.*, **12**, 169–177 (1962).
23. M. B. Chadwick et al., "ENDF/B-VII.0: Next Generation Evaluated Nuclear Data Library for Nuclear Science and Technology," *Nuclear Data Sheet*, Vol. 107, December 2006.
24. *SCALE: A Modular Code System for Performing Standardized Computer Analyses for Licensing Evaluation*, ORNL/TM-2005/39, Version 5.1, Vols. I–III, "TSUNAMI-3D: Control Module for Three-Dimensional Cross-Section Sensitivity and Uncertainty Analysis for Criticality," Vol. I, Sect. C9, Oak Ridge National Laboratory (November 2006).
25. *International Handbook of Evaluated Criticality Safety Benchmark Experiments*, NEA/NSC/DOC(95)03, NEA Nuclear Science Committee, September 2006.

INTERNAL DISTRIBUTION

1. S. M. Bowman
2. B. L. Broadhead
3. M. D. DeHart
4. H. Derrien
5. M. E. Dunn
6. I. C. Gauld
7. J. C. Gehin
8. C. M. Hopper
9. J. O. Johnson
10. B. L. Kirk
11. N. M. Larson
12. L. C. Leal
13. D. E. Mueller
14. C. V. Parks
15. J. E. Rushton
16. J. C. Wagner
17. R. M. Westfall
18. D. A. Wiarda
19. M. L. Williams
20. Central Research Library
21. OTIC—RC, OSTI, CR

EXTERNAL DISTRIBUTION

22. J. Blair Briggs, Idaho National Laboratory, 2525 N. Fremont, P.O. Box 1625, Idaho Falls, ID 83415-3860
23. D. E. Carlson, U.S. Nuclear Regulatory Commission, RES/DSARE/REAHFB, MS T10-F13A, Washington, DC 20555-0001
24. J. M. Conde López, Consejo de Seguridad Nuclear, Jefe de Area de Ingeniería Nuclear, Subdirección General de Technologia Nuclear, Justo Dorado, 11, 28040 Madrid, SPAIN
25. P. Cousinou, Institut de Protection et de Sûreté Nucleaire, Département de Recherches en Sécurité, CECI B.P. 6 - 92265 Fontenzy-Aux-Roses, Cedex, France
26. D. Erickson, Fluor Government Group, P.O. Box 1050, MSIN T5-54, Richland, WA 99352
27. A. Garcia, U.S. Department of Energy, Idaho Operations Office, Idaho Falls, ID 83401-1226
28. J. N. Gulliford, BNFL, R101, Rutherford House, Risley, Warrington, Cheshire WA3 6AS
29. D. Hayes, Los Alamos National Laboratory, P.O. Box 1663, MS J562, Los Alamos, New Mexico 87545
30. D. Heinrichs, Lawrence Livermore National Laboratory, MS L-128, 7000 East Ave., Livermore, CA 94550-9234
31. R. Y. Lee, U.S. Nuclear Regulatory Commission, RES/DSARE/SMSAB, MS T10-K8, Washington, DC 20555-0001
32. R. Little, Los Alamos National Laboratory, P.O. Box 1663, Los Alamos, New Mexico 87545
33. J. McKamy, U.S. Department of Energy, National Security Administration, NA-171, 19901 Germantown Road, Germantown, MD 20874
34. R. McKnight, Argonne National Laboratory, 9700 S. Cass Ave., Argonne, IL 60439
35. J. Morman, Argonne National Laboratory, 9700 S. Cass Ave., Argonne, IL 60439
36. J. C. Neuber, AREVA NP GmbH Mechanical Analyses NEEA-G, Kaiserleistrasse 29, 63005 Offenbach am Main Germany

37. P. Oblozinsky, Brookhaven National Laboratory, National Nuclear Data Center, Bldg. 197D, P.O. Box 5000, Upton, NY 11973-5000
38. H. Okuno, Japan Atomic Energy Research Institute, Department of Fuel Cycle, Safety Research, 2-4 Shirakata-Shirane, 319-1195 Tokai-mura, Naka-Gun, Ibaraki-ken, JAPAN
39. E. Sartori, OECD/NEA Data Bank, Le Seine-Saint Germain, 12 Boulevard des Iles, F-92130 Issy-les-Moulineaux, FRANCE
40. D. E. Dei, Naval Reactors, 1240 Isaac Hull Avenue SE, Stop 8011, Washington Navy Yard, D.C. 20376-8011
41. Dae Y. Chung, U.S. Department of Energy, EM-60, 0B050, 1000 Independence Ave., SW, Washington, D.C. 20585
42. R. E. Wilson, U.S. Department of Energy, Rocky Flats Project Office, Federal Building 55, P.O. Box 25547, Denver, CO 80025-0547

Appendix C: Doppler Broadening Methodology (Application)

Creation of problem-dependent Doppler-broadened cross sections in the KENO Monte Carlo code

Article *in* Annals of Nuclear Energy · February 2016

Impact Factor: 0.96 · DOI: 10.1016/j.anucene.2015.10.011

4 authors, including:

Cihangir Celik

Oak Ridge National Laboratory

9 PUBLICATIONS **2** CITATIONS

SEE PROFILE

G. Ivan Maldonado

University of Tennessee

81 PUBLICATIONS **169** CITATIONS

SEE PROFILE

Luiz C Leal

Oak Ridge National Laboratory

212 PUBLICATIONS **1,809** CITATIONS

SEE PROFILE

Creation of problem-dependent Doppler-broadened cross sections in the KENO Monte Carlo code

Shane W.D. Hart[a,*], Cihangir Celik[a], G. Ivan Maldonado[b], Luiz Leal[a]

[a] *Oak Ridge National Laboratory*
[b] *The University of Tennessee*

Abstract

This paper introduces a quick method for improving the accuracy of Monte Carlo simulations by generating one- and two-dimensional cross sections at a user-defined temperature before performing transport calculations. A finite difference method is used to Doppler-broaden cross sections to the desired temperature, and unit-base interpolation is done to generate the probability distributions for double differential two-dimensional thermal moderator cross sections at any arbitrarily user-defined temperature. The accuracy of these methods is tested using a variety of contrived problems. In addition, various benchmarks at elevated temperatures are modeled, and results are compared with benchmark results. The problem-dependent cross sections are observed to produce eigenvalue estimates that are closer to the benchmark results than those without the problem-dependent cross sections.

Keywords: Monte Carlo, Doppler broadening, thermal scattering, KENO, SCALE

1. Introduction

Cross-section files are generally provided in Evaluated Nuclear Data Format (ENDF) formatted data files [1] that contain all of the necessary data to create continuous energy (CE) data libraries for use in a Monte Carlo calculation. To be useful, these ENDF data files are generally processed by a cross-section processing code such as AMPX [2] or NJOY [3] for use in a radiation transport code such as CE-KENO [4]. For one-dimensional cross sections, the data are usually provided at one temperature (designated as 0 K), and need to be Doppler-broadened to various temperatures before they can be used at reactor-level temperatures.

Exact Doppler-broadened cross sections can be done by the nuclear data-processing codes using Doppler broadening equations [5]; however, producing exact cross sections at a large number of temperatures would consume a significant amount of time and space, both in memory and on a hard disk. Therefore, cross-section libraries are generally only created at several different temperatures; for KENO, part of the SCALE code suite [6], there are generally six temperatures created. For KENO in CE mode, if the temperature desired is not one of the pregenerated temperatures, then the closest temperature is used. A case containing materials that are 50 K away from a library temperature can produce significantly different results when compared with a case that is using the temperature-corrected cross sections.

Two-dimensional cross sections are generally provided for thermal moderators in order to account for crystalline effects encounted when neutrons are traveling at thermal speeds. Unlike the one-dimensional cross sections, the ENDF files are usually provided at a variety of temperatures. However, no Doppler broadening is done on these temperatures, so the end result is the same: If a temperature desired by the user is sufficiently far from the library temperatures, errors in the eigenvalue estimates can occur. Some previous work has been done to provide for on-the-fly (OTF) Doppler broadening of one-dimensional neutron cross sections [7, 8, 9, 10, 11] in other Monte Carlo codes. For example, MCNP6 [12] ships with a utility to generate fits to cross-section data so that cross sections can be calculated on-the-fly for any temperature as desired. KENO previously had no such capability to Doppler broaden cross sections.

In this paper two methods are discussed to temperature-correct the provided cross sections. A finite difference method is employed for the one-dimensional cross sections. This method is much faster than the exact Doppler-broadening method developed by Cullen and can use the

*Corresponding author
Email addresses: hartsw@ornl.gov (Shane W.D. Hart), celikc@ornl.gov (Cihangir Celik), imaldona@utk.edu (G. Ivan Maldonado), leall@ornl.gov (Luiz Leal)

data libraries that have already been created. For two-dimensional thermal moderator data, a simple unit-base interpolation scheme is used on the probability distributions of the double differential cross sections. By combining the aforementioned methods with temperature interpolation on the probability tables covering the unresolved resonance range (such as in [13]), KENO will have temperature-corrected neutron cross sections for all energy regions of interest [14].

2. One-Dimensional Method

For one-dimensional cross sections the approach to be implemented into KENO utilizes a finite-difference method similar to that used by SAMMY [15], which is well suited for resonance analysis and light water reactor (LWR) applications. This approach is based on the Leal-Hwang scattering method [16], in which the Doppler broadened cross sections satisfy a heat equation of the form

$$\frac{\partial^2 F}{\partial u^2} = \frac{\partial F}{\partial \zeta}, \tag{1}$$

where F is the function of interest (in this case the cross section), u is the energy range, and ζ is the temperature. Then, because of the initial condition $F(u,0)$ for $-\infty < u < \infty$ and the boundary conditions $F(\infty,\zeta) = F(\infty,0)$ and $F(-\infty,\zeta) = F(-\infty,0)$, the function F can be calculated using the finite-difference method.

The application of the finite-difference method solves Eq. (1) by applying an explicit finite-difference formalism assuming constant meshes with $\delta u \equiv h$ and $\delta\zeta \equiv \gamma$. The first and second derivatives can then be expanded in a Taylor's series. Thus the explicit finite-difference equation for the function F at any u_i and ζ_{j+1} is

$$F_i^{j+1} = s(F_{i+1}^j + aF_i^j + F_{i-1}^j), \tag{2}$$

where $s \equiv \frac{\gamma}{h^2}$ and $a \equiv \frac{1-2s}{s}$. The finite-difference equation in Eq. (2) can be modified for nonuniform meshes as

$$F_i^{j+1} = s\left(aF_i^j + \frac{2(F_{i-1}^j \delta v_r + F_{i+1}^j \delta v_l)}{\delta v_r + \delta v_l}\right), \tag{3}$$

where $s \equiv \frac{\gamma}{\delta v_l \delta v_r}$, $a \equiv \frac{1-2s}{s}$, $\delta v_l = v_i - v_{i-1}$, $\delta v_r = v_{i+1} - v_i$, and v_i is the momentum at the i^{th} grid point.

Selecting a ΔT that is small (such as 1 K) allows for agreement within 0.1% to reference cross sections across all energies except for very low and very high energies. The increase in error at the edges of the energy range is due to limitations in the finite-difference method. Because each element in the energy grid uses the surrounding elements to calculate the new value, the finite-difference method produces poor cross-section estimates when surrounding elements are inaccurate or do not exist. In an attempt to alleviate these errors, extra points can be added past the known energy range. This reduces the error for cross sections at very high and very low energies by extrapolating the known cross-section data but does not eliminate it completely.

Doppler broadening is controlled by the dbx parameter in KENO. By setting dbx to 1, the finite difference approach is enabled. Fig. 1 show the results of using the finite-difference method to obtain cross sections for the ^{238}U scattering reaction at 900 K near the low-energy tail. As previously discussed, the error in the tail region quickly disappears as one moves away from the energy boundary.

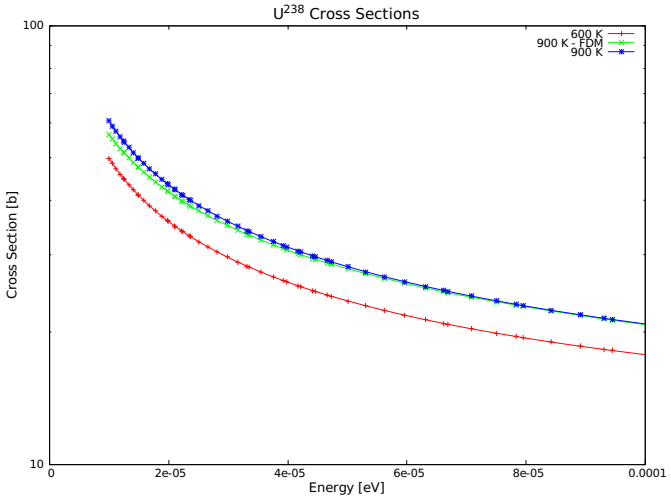

(a) Cross Sections

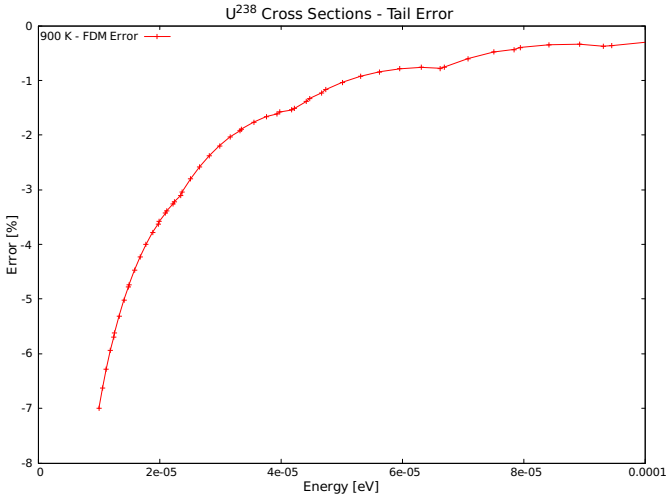

(b) Error

Figure 1: ^{238}U scattering cross sections showing a tail.

As seen in Fig. 1, the error at the low-energy tail can approach 10%. Although the error probably has little effect on the results, it would be beneficial to try and minimize it. One solution is to use linear interpolation for the first five momentum points on the energy grid. Since there are no resonances in this extremely small energy range, doing so would not introduce any errors into the broadened cross sections. By using interpolation for the first ten points, the results from Fig. 1 using the FDM con-

verge onto 900 K reference results.

An example of this approach is shown in Fig. 2 for ^{16}O. In Fig. 2a there is a large error (approaching 10%) in the lower tail region. This contrasts sharply with the lack of error in the rest of the energy space, although there is a small error when the finite difference method is used in the resonances. In Fig. 2b the error has mostly disappeared and is less than 0.2% in the tail region. The rest of the energy range is mostly unaffected by the change.

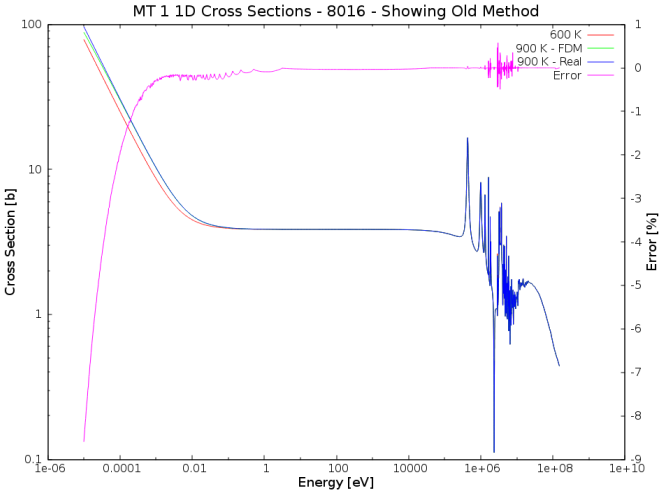

(a) No interpolation on first five points.

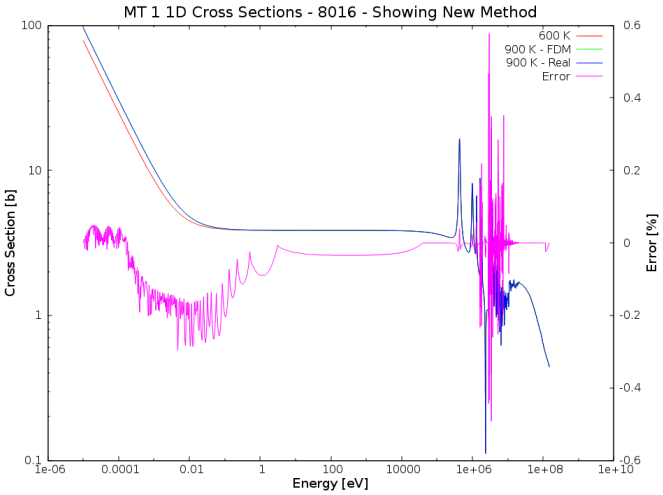

(b) Interpolation on first five points.

Figure 2: Differences in ^{16}O cross sections.

Another problem may arise when dealing with isotopes that do not have a large resonance structure, are light, or have some other small irregularites. One example is ^{1}H in water, which contains no resonances and also isn't smoothly decreasing around 0.01 eV. This slight bump causes an instability in the finite difference method as it propagates to the lower energies. This can be seen in Fig. 3a, where the Doppler-broadened cross sections actually exceed the higher-temperature cross sections for the low-energy range.

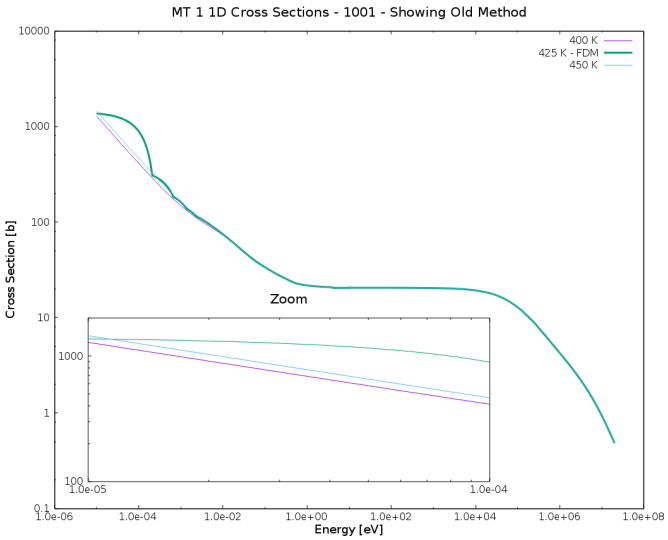

(a) Finite-difference method.

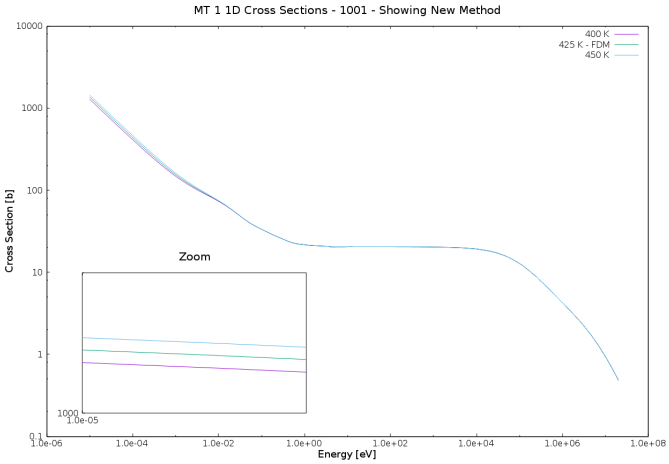

(b) Interpolation method.

Figure 3: Differences in ^{1}H cross sections.

Linear interpolation in the square root of temperature over the entire energy range can be used to remedy this problem. This should not introduce error due to the lack of resonances. Results from this interpolation are shown in Fig. 3b. Since this approach corrects the problem, interpolation should be used instead of the finite difference method for Doppler-broadening the one-dimensional cross sections for isotopes that have no resonance structure. If the cross sections are obtained from the ENDF thermal scattering sublibrary only interpolation is used.

3. One-Dimensional Results

A variety of test cases were run to test the impact of the one-dimensional problem-dependent Doppler broadening.

3.1. Pin Cell

The first case used a slightly enriched (3.5%) ^{235}U pin cell. Before problem-dependent Doppler broadening was

implemented, KENO would simply use cross sections at the closest temperature that was present in the libraries with no interpolation. If the user specified 760 K, KENO would use 900 K. As shown in Fig. 4, this leads to non-physical "steps" in the eigenvalue as the library changes to another temperature. KENO was run with the problem-dependent Doppler broadening enabled (titled CE-OTF), which shows a much smoother and more accurate eigenvalue curve as the temperature of the fuel increases.

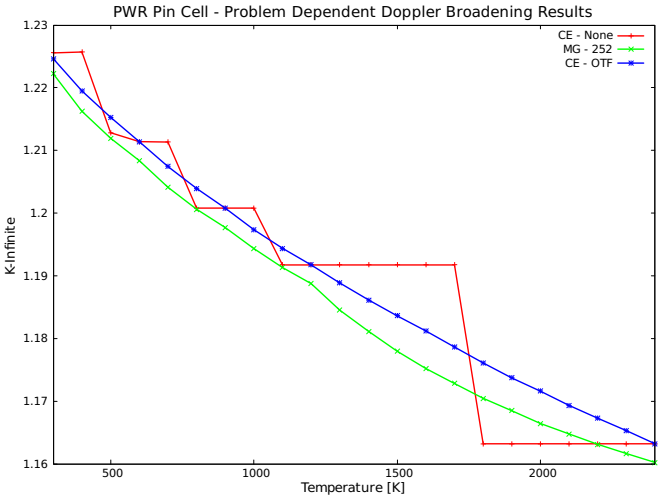

Figure 4: Results for a PWR pin cell showing impact of problem-dependent Doppler broadening.

The multigroup 252 group library results are also shown in Fig. 4. Currently multigroup KENO uses linear interpolation to temperature-adjust multigroup libraries, which explains why it produces non-step-like eigenvalue estimates that show good agreement with the CE results when Doppler broadening is enabled. Current reference libraries that ship with KENO include the temperatures 293 K, 565 K, 600 K, 900 K, 1200 K, and 2400 K. KENO broadens from the closest, lower, cross section data file available. When the user requests a temperature that already exists on the provided library, KENO will not perform Doppler broadening. In Fig. 4 this manifests as the Doppler broadening results converging with the reference results at library temperatures.

3.2. Radial and Axial Temperature Effects

In order to better understand the effect of radial and axial temperature profiles in a fuel pin, two additional pin cell models were created. These pin cells were very similar to the one described previously, but one had nine radial temperature regions and the other had nine radial temperature regions and nine axial temperature regions (a total of 81 different temperature regions). These pin cells were designed to more closely mimic the temperature profile found in an operating reactor.

Fig. 5 shows the radial temperature used in the first case along with the temperatures used in KENO without problem-dependent Doppler broadening.

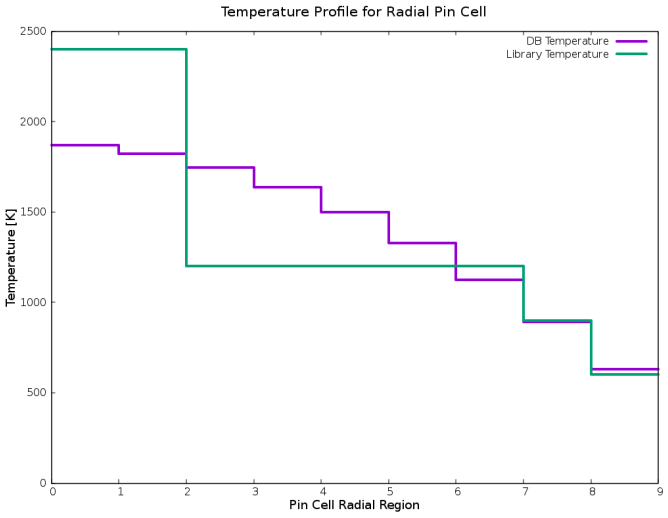

Figure 5: Radial temperature for the fuel pin model.

The impact of Doppler broadening on the eigenvalue is shown in Table 1, where σ is the statistical uncertainty of k-effective from the Monte Carlo run.

Table 1: Eigenvalue results for pin cell with different radial temperatures.

	No DB	DB	Difference [pcm]
Eigenvalue (σ)	1.31489 (0.00015)	1.31260 (0.00014)	-174

For the case where both the axial and radial temperatures vary, the temperature profiles in both the axial and radial directions are shown in Fig. 6. Axial region 1 is the center axial region of the fuel pin, with axial region 2 being the region directly above and below it. Eigenvalue results are shown in Table 2.

For both cases, the overall impact is to lower the eigenvalue. Fig. 4 shows that this is the expected behavior. As the temperature in the pin cell increases, the eigenvalue decreases. Since the net effect of the radial and axial profiles is to increase the average pin cell temperature, the eigenvalue should be lower than that of the non-Doppler-broadened case.

Table 2: Eigenvalue results for a pin cell with different axial and radial temperatures.

	No DB	DB	Difference [pcm]
Eigenvalue (σ)	1.31623 (0.00014)	1.31387 (0.00015)	-179

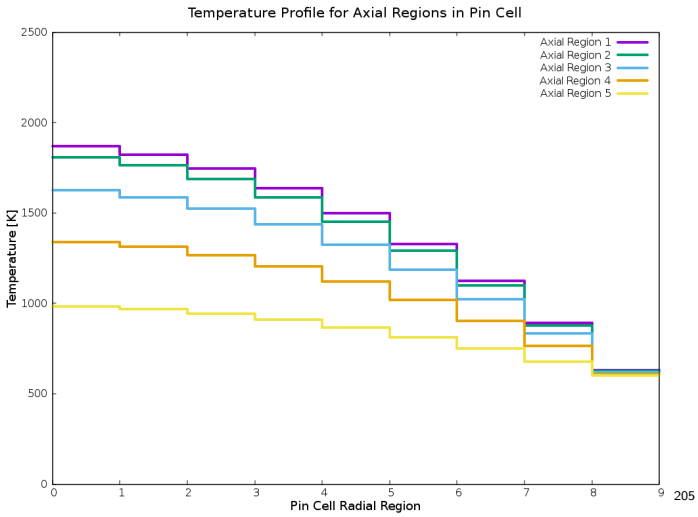

Figure 6: Radial temperature for each axial region of a pin cell.

3.3. 3D Assembly

The next test case used is that of the full 3D assembly shown in Fig. 7 [17]. The fuel assembly used low-enriched uranium and had 18 different temperatures along the length of the fuel rods. The large number of fuel regions with different temperatures will highlight the effects of Doppler broadening on the cross sections. Traditional KENO calculations would use the same cross sections for all 18 temperatures because all temperatures are near the same reference library, which, in this case, results in a 193 pcm difference in reactivity.

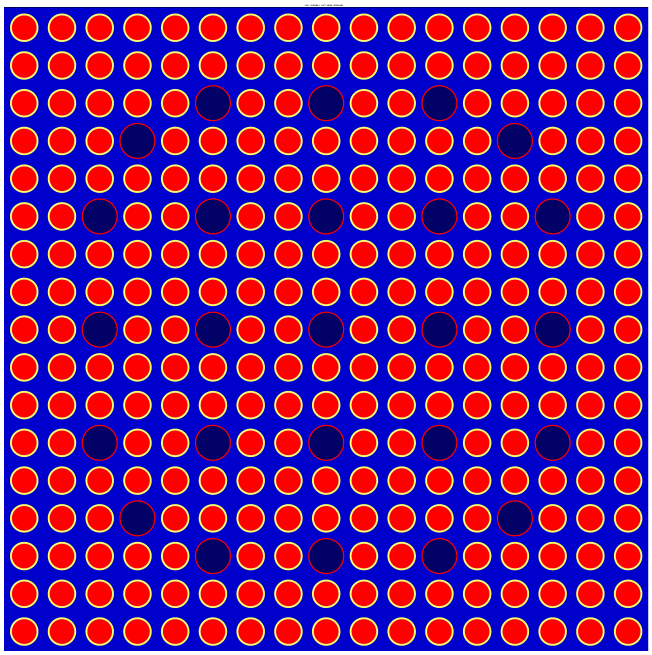

Figure 7: Radial view of a 3D assembly model generated by KENO.

Table 3: 3D assembly-problem-dependent Doppler-broadening results.

Case	Eigenvalue (σ)	Difference vs. Multi-Group
MG	1.04323 (0.00003)	-
CE No DB	1.04617 (0.00005)	282
CE w/ DB	1.04424 (0.00005)	97

As seen in Table 3, using Doppler-broadened cross sections induces a difference of several hundred pcm. The impact on the run time is minimal because all cross sections are Doppler-broadened before any transport calculations are done. Cross sections would have to be recalculated any time the temperature changed, making thermohydraulic coupling inefficient. Most isotopes can be Doppler-broadened in a few seconds, and the worst-case scenario of ^{238}U takes less than 1 min.

4. Two-Dimensional Method

After the one-dimensional cross sections have been Doppler-broaded, the next step is to Doppler-broaden the two-dimensional cross sections (or kinematics data) used for the thermal moderators.

4.1. Interpolation Method on Double Differential Probability Data

KENO uses cumulative probability distribution functions (CDFs) and probability distribution functions (PDFs) of the double differential scattering cross sections. The PDFs and CDFs are stored on an AMPX Continuous Energy (CE) library for use by KENO. During problem setup, KENO will open the CE library with the closest temperature to the model temperature and will use the data for all neutron interactions with the thermal moderator.

The method implemented in KENO uses linear interpolation on the cosine (μ) and energy (E) probabilities. This is different than previous methods done using on-the-fly sampling of the thermal neutron scattering data.[18] For interpolation on cosines, no extra manipulation needs to be done, and the interpolated probability can be determined by

$$p(\mu|E_{in},T) = p(\mu|E_{in},T_i) + \frac{T-T_i}{T_{i+1}-T_i}\left[p(\mu|E_{in},T_{i+1}) - p(\mu|E_{in},T_i)\right], \quad (4)$$

where E_{in} is the incident energy of the neutron. For the outgoing energy (E) probabilities, a traditional unit-base

normalization [19] is applied before linear interpolation is done. The equation is then the same as Eq. (4):

$$p(\hat{E}|\mu, E_{in}, T) = p(\hat{E}|\mu, E_{in}, T_i) + \frac{T - T_i}{T_{i+1} - T_i}\left[p(\hat{E}|\mu, E_{in}, T_{i+1}) - p(\hat{E}|\mu, E_{in}, T_i)\right] . \quad (5)$$

Typically the interpolation is done on one of the CDF or PDF, and then the other value is recalculated.

The unit-base normalization is required when the energy range of a probability distribution varies at different temperatures or incoming energies. Looking at Fig. 8, we can observe the major problem with Cartesian interpolation; the panel at E will have features from the lower panel at the low end and from the upper panel at the high end. This will cause the resulting function to have artificial peaks when the distributions shift as a function of energy, as is usually the case.

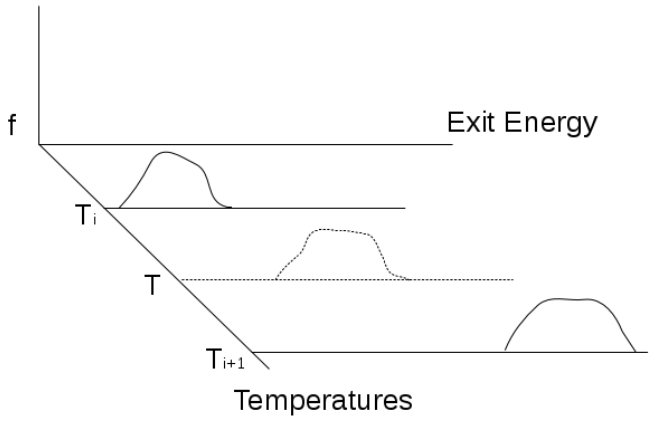

Figure 8: Interpolation between two-dimensional panels.

Eqs. (4) and (5) are relatively simple; however, a lot of effort has to go into ensuring that the interpolation is done on the same E_{in} and μ grid. Much of the coding is involved in dealing with this "bookkeeping." Generally, this is more difficult for the exit energy probabilities, as there the μ and E_{in} grids have to be the same. For those cases, the μ and E_{in} grid from the closest temperature is used as a reference, and a "dummy" panel is created at the desired angles and energies for the far temperature using (unit-base) linear interpolation. Eq. (5) can then be used to calculate the probabilities at the intermediate temperature.

For the case where the cosine probabilities are equiprobable (generally the case for incoherent inelastic scattering), it is beneficial to do linear interpolation on the cosines instead of on the cosine CDFs and PDFs. This is done by using linear interpolation in temperature:

$$\mu = \mu_i + \frac{T - T_i}{T_{i+1} - T_i}\left(\mu_{i+1} - \mu_i\right) . \quad (6)$$

4.2. Two-Dimensional Results

In order to test the Doppler broadening of the kinematic two-dimensional data, a variety of moderators have to be used. Some moderators will only have incoherent inelastic scattering, but some moderators will also have either incoherent or coherent elastic scattering. The Doppler-broadening routines need to be able to handle all such cases successfully.

4.2.1. Incoherent Inelastic Scattering

Incoherent inelastic scattering (stored exclusively in MT 1007) is present in all thermal moderators and is arguably the most important scattering method present in the cross-section libraries. While any isotope would test this successfully, hydrogen in water was chosen as the main testing material. Hydrogen in water is the thermal moderator for the vast majority of operating nuclear reactors. As such, it is important to see if the interpolation scheme is producing reasonable results.

For hydrogen in water, data exist in the SCALE/ENDF cross-section libraries at the temperatures 293 K, 350 K, 400 K, 450 K, 500 K, 550 K, 600 K, 650 K, and 800 K. Interpolation is controlled by the dbx parameter in KENO. By setting dbx to 2, two-dimensional interpolation is enabled. Results from these cases are shown in Fig. 9. As

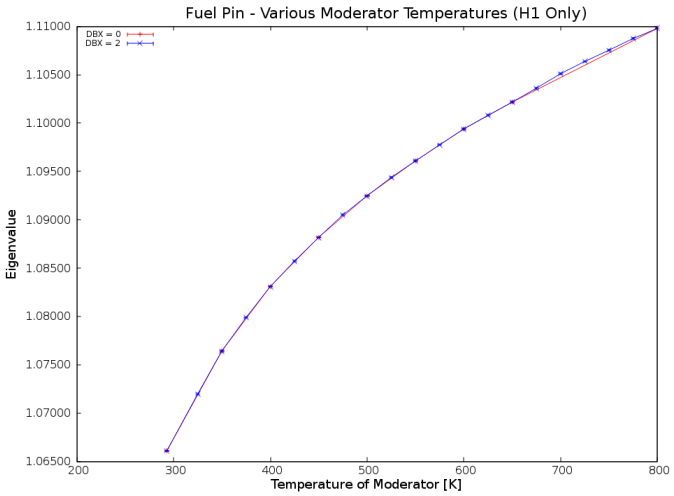

Figure 9: 2D interpolation results from pin cell (hydrogen in water).

can be seen from Fig. 9, results from the interpolated runs fall into the expected range of k-effective. There is some disagreement between 650 K and 800 K eigenvalues, but this is expected due to the large difference in temperature between the two reference libraries.

4.2.2. Coherent Elastic Scattering

Coherent elastic scattering is present in many crystalline materials and is characterized by the presence of Bragg edges. Bragg edges result in a histogram style of PDF (see Fig. 10), where neutrons will scatter at discrete angles. Elastic scattering is stored in MT 1008, and this

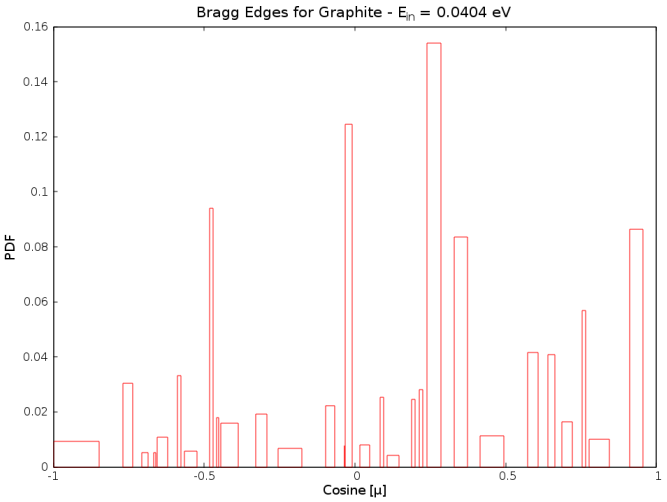

Figure 10: Bragg edges in graphite.

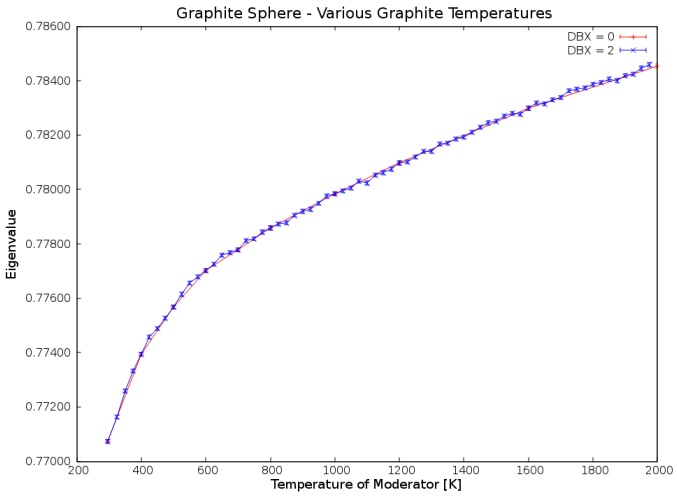

Figure 11: 2D interpolation results from graphite sphere.

histogram nature is one easy way to test whether or not the scattering stored in MT 1008 is coherent or incoherent.

Interpolating the Bragg edge-scattering data is relatively easy. If a specific scattering cosine exists at both temperatures, the new PDF can be interpolated between the two temperatures. If the specific scattering cosine only exists on one of the two temperatures, then the PDF is obtained by interpolating between the temperature where it exists and zero. In this way, the final results will contain the aggregate of the PDFs from both temperatures. The CDFs are then recalculated from the PDF data.

To test interpolation on this type of scattering, graphite is used as a moderator. The case tested involved a sphere of uranium surrounded by a larger sphere of the graphite moderator. The fuel was slightly enriched uranium oxide (UO_2) at 900 K. The graphite temperature was varied to obtain the results. Results from the current reference temperatures and from using interpolation are shown in Fig. 11. The eigenvalues resulting from the interpolation runs are consistent with what is expected by interpolating the eigenvalues from the reference library runs.

4.2.3. Incoherent Elastic Scattering

Incoherent elastic scattering is stored much like incoherent inelastic scattering, except that it is stored in MT 1008 and does not generally use equiprobable cosine bins. Therefore it can be treated much the same as inelastic scattering, except allowances have to be made to allow for cosines to exist on some temperatures and not others. An isotope will not have both incoherent and coherent elastic scattering. Therefore, MT 1008 can be used for both types of scattering.

The test case used for incoherent elastic scattering was hydrogen in polyethylene. Like all thermal moderators, hydrogen in polyethylene contains incoherent inelastic scattering in MT 1007; however it also contains incoherent elastic scattering in MT 1008. Unlike the other cases presented thus far, there are only two reference temperatures available for polyethylene: 293 K and 300 K. Results from the current reference temperatures and from using interpolation are shown in Fig. 12. Again, the eigenvalues resulting from these interpolation runs are consistent with what is expected by interpolating the eigenvalues from the reference library runs.

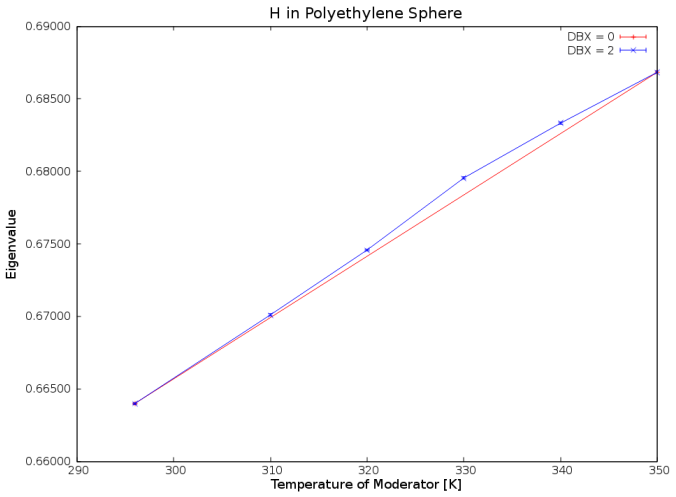

Figure 12: 2D interpolation results from polyethylene sphere.

5. Benchmarks

The *International Handbook of Evaluated Reactor Physics Benchmark Experiments (IHERPhBE)* [20] was prepared by a working group of experienced reactor physics personnel. It contains reactor physics benchmark specifications that have been derived from experiments performed at various nuclear experimental facilities around the world. The benchmark specifications are intended for use to validate calculation techniques. The most recent edition of

the handbook contains data from 53 different experimental series that were performed at 31 different reactor facilities.

Many of the benchmarks in the handbooks were conducted at room temperature. Therefore one goal was to find several elevated-temperature benchmarks that could be used to test the effectiveness of the problem-dependent Doppler-broadening methods. Several benchmarks were identified, all at elevated temperatures of around 500 K. Since the closest cross-section libraries provided with SCALE are at 565 K, it should provide a good check for the accuracy of the Doppler-broadening methods.

5.1. KRITZ-2:19

The first evaluation, known as KRITZ-2:19, was an experiment with mixed-oxide rods at an 18.00 mm pitch. Criticality was obtained by controlling the boron content in the water and by adjusting the water level. The square inner tank was filled with water up to the level needed to achieve criticality. The space between the inner tank and the cylindrical outer tank served as a dump area and was effectively filled with steam.

The experimental, measured, and benchmark-model k_{effs} are given in Table 4. As a critical reactor, it was expected that the measured and experimental k_{eff} will be unity. Due to simplifications made in the model, it was determined that the benchmark k_{eff} will actually be slightly above unity. The benchmark k_{eff} was the value expected to be calculated with the Monte Carlo codes. Tables 5 and 6 show the benchmark results from MCNP (obtained from the evaluation report) and from KENO, respectively. MCNP used a weighted mixture of cross sections from the two closest temperature libraries to obtain cross sections that are accurate at the desired temperatures. KENO was fairly close to the MCNP results for the cold case when they are both using the ENDF 7.0 library. When the 7.1 library was used, the eigenvalue fell slightly but was still within two standard deviations of the benchmark. For the hot case, KENO was extremely close to the MCNP JEFF result only when Doppler broadening was enabled. This was expected since the temperature of the hot case is 510 K, which is sufficiently far from the closest library (565 K) to introduce error.

5.2. KRITZ-2:1

The second KRITZ evaluation, known as KRITZ-2:1, was a rectangular array of low enriched uranium Zircalloy-2 fuel rods in light water [21]. Again, criticality was achieved by regulating the concentration of boron in water and by adjusting the water level.

The experimental, measured, and benchmark-model k_{effs} are given in Table 7. The statements regarding the k_{eff} values made in regard to KRITZ-2:19 (Section 5.1) also apply for this KRITZ case. Tables 8 and 9 show the benchmark results from MCNP (obtained from the evaluation report) and from KENO for the cold and hot

Table 4: Experimental, measured, and benchmark-model k_{eff} for KRITZ-2:19.

	Cold	Hot
Measured	1.0000 ± 0.0001	1.0000 ± 0.0001
Experimental	1.0000 ± 0.0015	1.0000 ± 0.0019
Benchmark	1.0077 ± 0.0030	1.0055 ± 0.0027

Table 5: Benchmark results for KRITZ-2:19 cold case.

	k_{eff}	$\frac{C}{E} - 1$ (%)
MCNP JEFF 3.1	1.0023 ± 0.0001	-0.54
MCNP ENDF/B-VII.0	1.0031 ± 0.0001	-0.44
KENO ENDF/B-VII.0 DBX = 0	1.0027 ± 0.0001	-0.50
KENO ENDF/B-VII.1 DBX = 0	1.0019 ± 0.0001	-0.58

Table 6: Benchmark results for KRITZ-2:19 hot case.

	k_{eff}	$\frac{C}{E} - 1$ (%)
MCNP JEFF 3.1	1.0011 ± 0.0001	-0.44
KENO ENDF/B-VII.0 DBX = 0	0.9991 ± 0.0001	-0.64
KENO ENDF/B-VII.0 DBX = 2	1.0010 ± 0.0001	-0.45
KENO ENDF/B-VII.1 DBX = 0	0.9986 ± 0.0001	-0.69
KENO ENDF/B-VII.1 DBX = 2	1.0005 ± 0.0001	-0.50

cases, respectively. Again, MCNP used a weighted mixture of cross sections from the two closest libraries to obtain cross sections that are accurate at the desired temperatures. For the cold case, KENO was actually slightly closer to the benchmark values than MCNP. For the hot case, KENO was slightly further away from the benchmark than MCNP. Without Doppler broadening, the KENO results are particularly off the benchmark. Enabling Doppler broadening increased the k_{eff} by ∼150 pcm and made the results closer to the benchmark. Like previous cases, enabling direct $S(\alpha, \beta)$ lowered the k_{eff} by ∼10 pcm, which was generally within one standard deviation of the original KENO result.

6. Conclusions

Typically, reactor analysis tools ship with only a subset of temperatures that a reactor physics analyst needs in order to accurately model a problem. A one-dimensional method to Doppler-broaden cross secions was expanded and coded into the Monte Carlo code KENO. By using this method, cross sections can be Doppler-broadened to any temperature that the user selects. Doppler broadening is done before neutron transport begins. Therefore the method has been christened as "problem-dependent Doppler pre-broadening." Using the temperature-corrected data shows an immediate impact when a temperature that is not in a library is used. Having correct temperatures for each fuel and moderator region will become increasingly important as Monte Carlo is used to model full reactors. It is also a paramount ability if accurate coupling to thermal-hydraulic codes is desired.

In addition to Doppler broadening the one-dimensional cross sections, correcting the temperature of the two-dimensional kinematics data was also examined. A unit-base interpolation sheme was devised and implemented for the energy and scattering cosine cumulative distribution functions. It was shown that, by using this method, more accurate results could be obtained at temperatures between those provided by the libraries.

A variety of benchmarks taken from reactor physics and criticality safety benchmark evaluations were used to verify the accuracy of the new methods. Efforts were made to find evaluations that contained cases that were run at an elevated temperature in order to test the effectiveness of the Doppler-broadening mechanisms. Overall, the results became more accurate when the Doppler-broadening methods were used. In the future, as model complexity and multiphysics couplings increase, it will become more and more important to have an accurate cross-section and scattering methodology.

Acknowledgements

The work documented in this paper was performed with support from the U.S. Department of Energy Nuclear Criticality Safety Program.

Table 7: Experimental, measured, and benchmark-model k_{eff} for KRITZ-2:1.

	Cold	Hot
Measured	1.0000 ± 0.0001	1.0000 ± 0.0001
Experimental	1.0000 ± 0.0018	1.0000 ± 0.0026
Benchmark	1.0025 ± 0.0020	1.0024 ± 0.0028

Table 8: Benchmark results for KRITZ-2:1 cold case.

	k_{eff}	$\frac{C}{E} - 1$ (%)
MCNP JEFF 3.1	0.9975 ± 0.0001	-0.50
MCNP ENDF/B-VII.0	0.9981 ± 0.0001	-0.43
KENO ENDF/B-VII.0 DBX = 0	0.9990 ± 0.0001	-0.35

Table 9: Benchmark results for KRITZ-2:1 hot case.

	k_{eff}	$\frac{C}{E} - 1$ (%)
MCNP JEFF 3.1	0.9992 ± 0.0001	-0.33
KENO ENDF/B-VII.0 DBX = 0	0.9958 ± 0.0001	-0.66
KENO ENDF/B-VII.0 DBX = 2	0.9973 ± 0.0001	-0.51

References

[1] A. Trkov, M. Herman, D. Brown, ENDF-6 Formats Manual: Data Formats and Procedures for the Evaluated Nuclear Data Files ENDF/B-VI and ENDF/B-VII, Tech. rep., CSEWG Document ENDF-102, Report BNL-90365-2009 Rev. 2, Brookhaven National Laboratory, Upton, New York (2011).

[2] M. Dunn, N. Greene, AMPX-2000: A cross-section processing system for generating nuclear data for criticality safety applications, Trans. Am. Nucl. Soc 86 (2002) 118–119.

[3] R. E. MacFarlane, D. W. Muir, NJOY99.0 - Code System for Producing Pointwise and Multigroup Neutron and Photon Cross Sections from ENDF/B Data, Los Alamos, New Mexico, pSR-480/NJOY99.00 (2000).

[4] D. Hollenbach, L. Petrie, S. Goluoglu, N. Landers, M. Dunn, KENO-VI: A general quadratic version of the keno program, Tech. rep., Oak Ridge National Laboratory, Oak Ridge, TN (2011).

[5] D. E. Cullen, O. Ozer, C. R. Weisbin, Exact Doppler broadening of evaluated neutron cross sections, in: Trans. Am. Nuc. Soc., Vol. 16, ANS, 1973, p. 320.

[6] ORNL, Scale: A Comphrehensive Modeling and Simulation Suite for Nuclear Safety Analysis and Design, Oak Ridge National Laboratory, Oak Ridge, Tennessee, oRNL/TM-2005/39 (2011).

[7] G. Yesilyurt, W. R. Martin, F. Brown, On-The-Fly Doppler Broadening for Monte Carlo Codes, in: International Conference on Mathematics, Computational Methods & Reactor Physics, ANS, Saratoga Springs, New York, 2009, may 3–7.

[8] G. Yesilyurt, W. R. Martin, F. B. Brown, On-the-Fly Doppler Broadening for Monte Carlo Codes, Nuclear Science and Engineering 171 (3) (2012) 239–257.

[9] F. B. Brown, W. R. Martin, G. Yesilyurt, S. Wilderman, Progress with On-The-Fly Neutron Doppler Broadening in MCNP, in: Transactions of the American Nuclear Society, ANS, Chicago, Illinois, 2012, june 24–28.

[10] W. R. Martin, S. Wilderman, F. B. Brown, G. Yesilyurt, Implementation of On-the-Fly Doppler Broadening in MCNP, in: International Conference on Mathematics and Computational Methods Applied to Nuclear Science & Engineering, ANS, Sun Valley, Idaho, 2013, may 5–9.

[11] T. H. Trumbull, Treatment of Nuclear Data for Transport Problems Containing Detailed Temperature Distributions, Nuclear Technology 156 (1) (2006) 75–86.

[12] X-5 Monte Carlo Team, MCNP–a general purpose monte carlo n-particle transport code, Tech. Rep. LA-UR-03-1987, Los Alamos National Laboratory, version 5 (April 2003).

[13] J. Walsh, B. Forget, K. Smith, B. Kiedrowski, F. Brown, Direct, on-the-fly calculation of unresolved resonance region cross sections in monte carlo simulations, in: Proc. ANS MC2015, 2015.

[14] S. Hart, G. I. Maldonado, C. Celik, L. C. Leal, Problem-dependent doppler broadening of continuous-energy cross section in the KENO Monte Carlo code, in: PHYSOR 2014, American Nuclear Society, Kyoto, Japan, 2014.

[15] N. M. Larson, Updated Users' Guide for SAMMY: Multilevel R-Matrix Fits to Neutron Data Using Bayes' Equations, Oak Ridge National Laboratory, oRNL/TM-9179/R8 (2008).

[16] L. C. Leal, R. Hwang, A Finite Difference Method for Treating the Doppler Broadening of Neutron Cross Sections, in: American Nuclear Society, Los Angles, CA, 1987.

[17] B. T. Rearden, W. J. Marshall, C. M. Perfetti, J. Miss, Y. Richet, Quantifying the effect of undersampling biases in Monte Carlo reaction rate tallies, Tech. rep., Organisation for Economic Cooperation and Development Nuclear Energy Agency Expert Group on Advanced Monte Carlo Techniques Benchmark Proposal (2013).

[18] A. T. Pavlou, W. Ji, On-the-fly sampling of temperature-dependent thermal neutron scattering data for monte carlo simulations, Annals of Nuclear Energy 71 (2014) 411–426.

[19] R. J. Doyas, S. T. Perkins, Interpolation of tabular secondary neutron and photon energy distributions, Nucl. Sci. Eng 50 (1973) 390–392.
URL `http://www.ans.org/pubs/journals/nse/a_26575`

[20] N. N. S. Committee, et al., International handbook of evaluated reactor physics benchmark experiments, Tech. rep., NEA/NSC/DOC (2006).

[21] L. Snoj, J. C. Gehin, KRITZ-2:1 Experiment on Regular H_2O/Fuel Pin Lattices with Low Enriched Uranium Fuel at Temperatures 248.5 °C, Tech. Rep. KRITZ-LWR-RESR-002, Jozef Sefan Institute and Oak Ridge National Laboratory (March 2009).

Appendix D: Lecture at University

Brief Review of the R-Matrix Theory

L. C. Leal

Introduction

Resonance theory deals with the description of the nucleon-nucleus interaction and aims at the prediction of the experimental structure of cross sections. Resonance theory is basically an interaction model which treats the nucleus as a black box, whereas nuclear models are concerned with the description of the nuclear properties based on models of the nuclear forces (nuclear potential). Any theoretical method of calculating the neutron-nucleus interactions or nuclear properties cannot fully describe the nuclear effects inside the nucleus because of the complexity of the nucleus and because the nuclear forces, acting within the nucleus, are not known in detail. Quantities related to internal properties of the nucleus are taken, in this theory, as parameters which can be determined by examining the experimental results.

The general R-matrix theory, introduced by Wigner and Eisenbud in 1947, is a powerful nuclear interaction model. Despite the generality of the theory, it does not require information about the internal structure of the nucleus; instead, the unknown internal properties, appearing as elements in the R-matrix, are treated as parameters and can be determined by examining the measured cross sections.

A brief review of the R-matrix theory will be given here and the interaction models which are specializations of the general R-matrix will be described. The practical aspects of the general R-matrix theory, as well as the relationship between the collision matrix U and the level matrix A with the R-matrix, will be presented.

Overview of the R-Matrix Theory

The general R-matrix theory has been extensively described by Lane and Thomas. An overview is presented here as introduction for the resonance formalisms which will be described later.

To understand the basic points of the general R-matrix theory, we will consider a simple case of neutron collision in which the spin dependence of the constituents of the interactions is neglected. Although the mathematics involved in this special case is over-simplified, it nevertheless contains the essential elements of the general theory.

As mentioned before, the nuclear potential inside the nucleus is not known; therefore, the behavior of the wave function in the internal region of the nucleus cannot be calculated directly from the Schrödinger equation. In the R-matrix analysis the inner wave function of the angular momentum l is expanded in a linear combination of the eigenfunctions of the energy levels in the compound nucleus. Mathematically speaking, if $\phi_l(E,r)$ is the inner wave function at any energy E and $\phi_l(E_\lambda,r)$ is the eigenfunction at the energy eigenvalue $E_{\lambda,}$ the relation becomes

$$\phi_l(E,r) = \sum_\lambda A_{l\lambda}\,\phi_l(E_\lambda,r) \ . \qquad \textbf{(1)}$$

Both $\phi_l(E,r)$ and $\phi_l(E_\lambda,r)$ are solutions of the radial Schrödinger equations in the internal region given by

$$\left\{\frac{d^2}{dr^2} + \frac{2m}{\hbar^2}\left[E - V(r) - \frac{l(l+1)\hbar^2}{2mr^2}\right]\right\}\phi_l(E,r) = 0 \qquad \textbf{(2)}$$

and

$$\left\{\frac{d^2}{dr^2} + \frac{2m}{\hbar^2}\left[E_\lambda - V(r) - \frac{l(l+1)\hbar^2}{2mr^2}\right]\right\}\phi_l(E_\lambda,r) = 0 \ . \qquad \textbf{(3)}$$

Since all terms in this expression must be finite at $r = 0$, both functions vanish at that point. In addition, the logarithmic derivative of the eigenfunction at the nuclear surface, say at $r = a$, is taken to be constant so that

$$\left[\frac{d\phi_l(E_\lambda,r)}{dr}\right]_{r=a} = a^{-1} B_l \phi_l(E_\lambda,a) \ , \qquad \textbf{(4)}$$

where B_l is an arbitrary boundary constant.

Since we are dealing with eigenfunctions of a real Hamiltonian, $\phi_l(E_\lambda,r)$ are orthogonal. Assuming that $\phi_l(E_\lambda,r)$ are also normalized, we have

$$\int_0^a \phi_l(E_\lambda,r)\,\phi_l(E_{\lambda'},r)\,dr = \delta_{\lambda\lambda'} \ . \qquad \textbf{(5)}$$

From Eq. (xx-1) and the orthogonality condition, we find the coefficients $A_{l\lambda}$,

$$A_{l\lambda} = \int_0^a \phi_l(E_\lambda,r)\,\phi_l(E,r)\,dr \ . \qquad \textbf{(6)}$$

To proceed to the construction of the R-matrix, Eq. (xx-2) is multiplied by $\phi_l(E_\lambda,r)$ and Eq. (xx-3) is multiplied by $\phi(E_\lambda,r)$. Subtracting and integrating the result over the range 0 to a (as in Eq. (xx-6)) produces the expression for the coefficients $A_{l\lambda}$:

$$A_{l\lambda} = \frac{\hbar^2}{2m}(E_\lambda - E)^{-1}\left[\phi_l(E_\lambda,r)\frac{d\phi_l(E,r)}{dr} - \phi_l(E,r)\frac{d\phi_l(E_\lambda,r)}{dr}\right]_{r=a} . \qquad \textbf{(7)}$$

Inserting $A_{l\lambda}$ into Eq. (xx-1) for r=a at the surface of the nucleus and using Eq. (xx-4), gives the following expression for the wave function:

$$\phi_l(E,a) = \frac{\hbar^2}{2ma}\sum_\lambda \left[\frac{\phi_l(E_\lambda,a)\phi_l(E_\lambda,a)}{E_\lambda - E}\right]\left[r\frac{d\phi_l(E,a)}{dr} - B_l\phi_l(E,r)\right]_{r=a} . \qquad \textbf{(8)}$$

Equation (xx-8) relates the value of the inner wave function to its derivative at the surface of the nucleus. The R matrix is defined as

$$R_l = \frac{\hbar^2}{2ma}\sum_\lambda \left[\frac{\phi_l(E_\lambda,a)\phi_l(E_\lambda,a)}{E_\lambda - E}\right] \qquad \textbf{(9)}$$

or

$$R_l = \sum_\lambda \frac{\gamma_{\lambda l}\gamma_{\lambda l}}{E_\lambda - E} , \qquad \textbf{(10)}$$

where $\gamma_{\lambda l}$, the reduced width amplitude for the level λ and angular momentum *l*, is defined as

$$\gamma_{\lambda l} = \sqrt{\frac{\hbar^2}{2ma}}\,\phi_l(E_\lambda,a) . \qquad \textbf{(11)}$$

The reduced width amplitude depends on the value of the inner wave function at the nuclear surface. Both E_λ and $\gamma_{\lambda l}$ are the unknown parameters of the R matrix which can be evaluated by examining the measured cross sections.

The generalization of Eq. (xx-10) is obtained by including the neutron-nucleus spin dependence and several possibilities in which the reaction process can occur. The concept of channel is introduced to designate a possible pair of nucleus and particle and the spin of the pair. The channel containing the initial state is called the entrance channel (channel c), whereas, the channel

containing the final state is the exit channel (channel c'). The elements of the R matrix in the general case are given by

$$R_{cc'} = \sum_{\lambda} \frac{\gamma_{\lambda c}\,\gamma_{\lambda c'}}{E_{\lambda} - E} \ , \qquad \textbf{(12)}$$

where the reduced width amplitude becomes

$$\gamma_{\lambda c} = \sqrt{\frac{\hbar^2}{2 m_c a_c}}\ \phi_c(E_{\lambda}, a_c) \ . \qquad \textbf{(13)}$$

The next objective is to relate the R-matrix to the cross-section formalism so that cross sections can be computed once the elements of the R-matrix are known.

Relation between the R-matrix and the Collision Matrix U

The general expressions for the neutron-nucleus cross sections are based on the collision matrix, also known as U-matrix, whose elements can be expressed in terms of the elements of the R-matrix. From basic quantum mechanics theory the cross sections for the neutron-nucleus interaction can be given as a function of the matrix U as follows:

(1) Elastic Cross Section

$$\sigma_n = \pi \lambda\!\!\!^{-2} \sum_{l} (2l+1) |\, 1 - U_l|^2 \ , \qquad \textbf{(14)}$$

(2) Reaction Cross Section which includes everything which is not elastic scattering (i.e., reaction=fission, capture, inelastic, ...)

$$\sigma_r = \pi \lambda\!\!\!^{-2} \sum_{l} (2l+1)(\, 1 - |\, U_l|^2) \ , \qquad \textbf{(15)}$$

3) Total Cross Section

$$\sigma_t = 2\pi \lambda\!\!\!^{-2} \sum_{l} (2l+1)(\, 1 - Re|\, U_l|\,) \ , \qquad \textbf{(16)}$$

where $\lambda\!\!\!^{-}$ is the neutron reduced wavelength given by

$$\lambda\!\!\!^{-} = \frac{\hbar}{\sqrt{2mE}} \ . \qquad \textbf{(17)}$$

We first derive the relationship between the U and R matrices, for a simple case of spinless neutral particles. The total wave function in the region outside the nuclear potential can be expressed as a linear combination of the incoming and outgoing wave functions. If $\phi_l^{inc}(r)$ and $\phi_l^{out}(r)$ are the incoming and outgoing wave functions for a free particle, respectively, the solution of the radial Schrödinger equation can be written as

$$\phi_l(r) = C_l\left[\phi_l^{inc}(r) - U_l\phi_l^{out}(r)\right] \qquad \text{for } r \geq a\ , \qquad \textbf{(18)}$$

where C_l is a normalization constant.

The presence of the U-matrix in Eq. (xx-18) (in this case a matrix of one element) indicates that the amplitudes of the incoming and outgoing wave functions are, in general, different. The case of $|U_l| = 1$ corresponds to pure elastic scattering which means that no reaction has occurred.

The Schrödinger equation for $\phi_l^{inc}(r)$ and $\phi_l^{out}(r)$ is the same as Eq. (xx-2) with $V(r) = 0$ since the potential outside the nucleus is zero. The solution is a combination of the spherical Bessel (j_l) and Neumann (n_l) functions

$$\phi_l^{inc}(r) = kr\left[n_l(kr) + i\,j_l(kr)\right]\ , \qquad \textbf{(19)}$$

and

$$\phi_l^{out}(r) = kr\left[n_l(kr) - i\,j_l(kr)\right]\ , \qquad \textbf{(20)}$$

where $i = \sqrt{-1}$.

The relation between the U and the R-matrices is obtained by first noting that Eq. (xx-8) can be written as

$$\phi_l(E,a) = \left[r\frac{d\phi_l(E_\lambda,a)}{dr} - B_l\phi_l(E,r)\right]_{r=a} R_l\ , \qquad \textbf{(21)}$$

where R_l is given in Eq. (xx-9).

Equation (xx-21), when combined with Eq. (xx-18), provides the relation between R and U-matrices as

$$U_l = \left(\frac{\phi_l^{inc}}{\phi_l^{out}} \right)_{r=a} \frac{1 - \left[\left(\frac{r}{\phi_l^{inc}} \frac{d\phi_l^{inc}}{dr} - B_l \right)_{r=a} \right] R_l}{1 - \left[\left(\frac{r}{\phi_l^{out}} \frac{d\phi_l^{out}}{dr} - B_l \right)_{r=a} \right] R_l} \quad . \tag{22}$$

We define the logarithmic derivative as

$$L_l^* = \left(\frac{r}{\phi_l^{out}} \frac{d\phi_l^{out}}{dr} \right)_{r=a} \quad . \tag{23}$$

Since from Eqs. (xx-19) and (xx-20), ϕ_l^{inc} and ϕ_l^{out} are complex conjugates,

$$L_l = \left(\frac{r}{\phi_l^{inc}} \frac{d\phi_l^{inc}}{dr} \right)_{r=a} \quad . \tag{24}$$

Equation (xx-22) becomes

$$U_l = \left(\frac{\phi_l^{inc}}{\phi_l^{out}} \right)_{r=a} \frac{1 - (L_l^* - B_l)_{r=a} R_l}{1 - (L_l - B_l)_{r=a} R_l} \quad . \tag{25}$$

Equation (xx-25) represents the desired relationship between the collision matrix U and the matrix R.

The representation of the neutron cross sections will depend on the reduced width amplitudes $\gamma_{\lambda c}$ and E_λ which are unknown parameters of Eq. (xx-25). Those parameters are obtained by fitting the experimental cross section.

The general relation between the matrices U and R is similar to Eq. (xx-25) with each term converted to matrix form:

$$\boldsymbol{U} = \boldsymbol{\rho}^{1/2} \boldsymbol{\phi}_{out}^{-1} [\boldsymbol{I} - \boldsymbol{R}(\boldsymbol{L} - \boldsymbol{B})]^{-1} [\boldsymbol{I} - \boldsymbol{R}(\bar{\boldsymbol{L}} - \boldsymbol{B})] \boldsymbol{\phi}_{inc} \boldsymbol{\rho}^{-1/2} \quad . \tag{26}$$

All matrices in Eq. (xx-26) are diagonal except the **R** matrix. The matrix elements of $\boldsymbol{\rho^{1/2}}$ are given by $(k_c a_c)^{1/2}$.

It should be noted that no approximation was used in deriving Eq. (xx-26). That equation represents an exact expression relating **U** and **R**, and leads to the determination of the cross section according to Eqs. (xx-14, xx-15, and xx-16).

To avoid dealing with matrices of large dimensions, several approximations of the R-matrix theory have been introduced. We will discuss various of these cross-section formalisms in the pages to come; we begin by introducing the level matrix A.

Relation between U, R, and A

Another presentation of Eq. (xx-26) may be obtained by introducing the following definitions

$$\boldsymbol{L_0 = S_0 + iP} \ , \tag{27}$$

$$\boldsymbol{L_0 = L - B} \ , \tag{28}$$

and

$$\boldsymbol{S_0 = S - B} \ , \tag{29}$$

where **S** and **P** are real matrices which contains the shift and the penetration factors, respectively and $\boldsymbol{L_0 = L - 2iP}$.

From Eqs. (xx-20, xx-23, and xx-27), the penetration factors can be written as $\boldsymbol{P = \rho(\phi_{inc}\phi_{out})^{-1}}$, and Eq. (xx-26) becomes

$$\boldsymbol{U = \Omega[I + 2iP^{1/2}(I - RL_0)^{-1}RP^{1/2}]\Omega} \ , \tag{30}$$

with $\boldsymbol{\Omega = \phi_{inc}^{1/2}\,\phi_{out}^{-1/2}}$.

It should be realized that the R-matrix is a channel matrix; i.e. it depends on the entrance and outgoing channels c and c'. The level matrix concept introduced by Wigner attempts to relate the U matrix to a matrix in which the indices are the energy levels of the compound nucleus, the level

matrix of elements $A_{\mu\lambda}$. In relating the channel matrix to the level matrix we recall that the **R** matrix is defined as

$$\boldsymbol{R} = \sum_{\lambda} \frac{\gamma_\lambda \times \gamma_\lambda}{E_\lambda - E} \ , \tag{31}$$

where $\gamma_\lambda \times \gamma_\lambda$ indicates the direct product between two vectors.

The expression $\boldsymbol{I} - \boldsymbol{R}\boldsymbol{L}_0 = \mathbf{1} - \sum_{\lambda} \frac{\gamma_\lambda \times \gamma_\lambda}{E_\lambda - E} \boldsymbol{L}_0$ can be written as

$$\boldsymbol{I} - \boldsymbol{R}\boldsymbol{L}_0 = \mathbf{1} - \sum_{\lambda} \frac{\gamma_\lambda \times \beta_\lambda}{E_\lambda - E} \ , \tag{32}$$

where we have defined $\beta_\lambda = \boldsymbol{L}_0 \gamma_\lambda$, and $\boldsymbol{L}_0$ is a symmetric matrix. The form of Eq. (xx-32) suggests the following relation

$$(\boldsymbol{I} - \boldsymbol{R}\boldsymbol{L}_0)^{-1} = \mathbf{1} + \sum_{\mu\lambda} (\gamma_\mu \times \gamma_\lambda) \boldsymbol{A}_{\mu\lambda} \ , \tag{33}$$

where the indices μ and λ refer to energy levels in the compound nucleus and $\boldsymbol{A}$ is determined as follows:

Multiplying Eqs. (xx-32) and (xx-33) and using the identity $(\boldsymbol{x}\times\boldsymbol{y})(\boldsymbol{z}\times\boldsymbol{w}) = (\boldsymbol{y}.\boldsymbol{z})(\boldsymbol{x}\times\boldsymbol{w})$, we obtain the following expression,

$$\sum_{\lambda\nu} (\gamma_\mu \times \beta_\nu) \boldsymbol{A}_{\mu\nu} - \sum_{\lambda} \frac{\gamma_\lambda \times \beta_\lambda}{E_\lambda - E} - \sum_{\lambda\mu\nu} \frac{\gamma_\lambda \times \beta_\nu}{E_\lambda - E} (\beta_\lambda . \gamma_\mu) \boldsymbol{A}_{\mu\nu} = 0 \ . \tag{34}$$

Factoring the term $\gamma_\lambda \times \beta_\nu$ in the above equation, we find that the level matrix $\boldsymbol{A}_{\mu\lambda}$ satisfies the equation

$$\boldsymbol{A}_{\lambda\nu}(E_\lambda - E) - \sum_{\mu} (L_0 \gamma_\lambda . \gamma_\mu) \boldsymbol{A}_{\mu\nu} = \delta_{\lambda\nu} \ . \tag{35}$$

The evaluation of the matrix $(\boldsymbol{I} - \boldsymbol{R}\boldsymbol{L}_0)^{-1}\boldsymbol{R}$ which appears in Eq. (xx-30) is obtained by combining Eqs. (xx-31) and (xx-33) which gives

$$(\boldsymbol{I}-\boldsymbol{RL_0})^{-1}\boldsymbol{R}=\sum_{\lambda}\left[\frac{\gamma_\lambda\times\gamma_\lambda}{E_\lambda-E}+\frac{1}{E_\lambda-E}\sum_{\mu}(\gamma_\mu\times\gamma_\lambda)\sum_{\nu}(\beta_\nu\cdot\gamma_\lambda)\boldsymbol{A}_{\mu\nu}\right]. \qquad \textbf{(36)}$$

Using Eq. (xx-35) as $\sum_{\nu}(\beta_\nu\cdot\gamma_\lambda)\boldsymbol{A}_{\mu\nu}=-\delta_{\lambda\mu}+(E_\lambda-E)\boldsymbol{A}_{\lambda\mu}$ gives

$$(\boldsymbol{I}-\boldsymbol{RL_0})^{-1}\boldsymbol{R}=\sum_{\mu\lambda}(\gamma_\mu\times\gamma_\lambda)\boldsymbol{A}_{\mu\lambda}\ . \qquad \textbf{(37)}$$

Hence, the collision matrix is related to the level matrix as

$$\boldsymbol{U}=\Omega\left[\boldsymbol{I}+2i\,\boldsymbol{P}^{1/2}\left(\sum_{\mu\lambda}(\gamma_\mu\times\gamma_\lambda)A_{\mu\lambda}\right)\boldsymbol{P}^{1/2}\right]\Omega\ . \qquad \textbf{(38)}$$

The elements of the collision matrix for entrance and exit channels c and c', respectively, are given as

$$U_{cc'}=\Omega_c\left[\delta_{cc'}+i\sum_{\mu\lambda}(\Gamma^{1/2}_{\mu c}A_{\mu\lambda}\,\Gamma^{1/2}_{\lambda c'})\right]\Omega_{c'}\ , \qquad \textbf{(39)}$$

where

$$\Gamma^{1/2}_{\mu c}=\gamma_{\mu c}(2P_c)^{1/2} \qquad \textbf{(40)}$$

is the level width, and from Eq. (xx-35) the level matrix is

$$A^{-1}_{\mu\lambda}=(E_\lambda-E)\delta_{\mu\lambda}-\sum_{c}(\gamma_{\mu c}L_{0c}\gamma_{\lambda c})\ . \qquad \textbf{(41)}$$

It should be remembered that no approximation has been introduced in the formal derivation of the collision matrix up to this point.

Simplified Models Derived from the General R-Matrix Theory

In this session we will present the approximations introduced to the R-matrix and, likewise, to the level matrix A which leads to various simplified resonance formalisms. The cross section formalisms frequently used are the single-level Breit-Wigner (SLBW), the Multilevel Breit-Wigner (MLBW), the Adler-Adler (AA), and the Reich-Moore (RM) formalism (also known as the reduced R-matrix formalism). A new methodology, called multipole representation of the cross section, was developed at Argonne National Laboratory by R. N. Hwang; in this approach the cross section representation is done in the momentum space ($\sqrt{E}$). We will address the approximations needed to obtain these simplified R-matrix models.

The starting points in deriving these formalisms will be the level matrix A and its relation to the collision matrix U.

The collision matrix is given by

$$U_{cc'} = e^{-i(\phi_c+\phi_{c'})}\left[\delta_{cc'} + 2i\,P_c^{1/2}\Big(\sum_{\mu\lambda}\gamma_{\lambda c}\,A_{\lambda\mu}\,\gamma_{\mu c'}\Big)\,P_{c'}^{1/2}\right]. \qquad \textbf{(42)}$$

The level matrix is represented as

$$A^{-1}_{\lambda\mu} = (E_\lambda - E)\,\delta_{\lambda\mu} - \sum_c \gamma_{\lambda c}\,L_{0c}\,\gamma_{\mu c}\ . \qquad \textbf{(43)}$$

1. Multilevel Breit-Wigner (MLBW) Formalism

In the MLBW approximation the level matrix is assumed to be diagonal, which means that the off-diagonal elements of the second term in the matrix given in Eq. (xx-43) are neglected, i.e.,

$$\sum_c\ (\gamma_{\lambda c}\,L_{0c}\,\gamma_{\mu c}) \approx \delta_{\lambda\mu}\sum_c\ L_{0c}\,\gamma^2_{\mu c}\ . \qquad \textbf{(44)}$$

Hence Eq. (xx-43) becomes

$$A^{-1}_{\lambda\mu} = (E_\lambda - E - \sum_c\ L_{0c}\,\gamma^2_{\lambda c})\,\delta_{\lambda\mu}\ . \qquad \textbf{(45)}$$

From Eqs. (xx-27) and (xx-40) we have $L_{0c} = (S_c - B_c) + i\,P_c$ and $\gamma^2_{\lambda c} = \dfrac{\Gamma_{\lambda c}}{2P_c}$, which leads to

$$A^{-1}_{\lambda\mu} = (E_\lambda - E + \Delta_\lambda - \frac{i}{2}\Gamma_\lambda)\,\delta_{\lambda\mu}\ , \qquad \textbf{(46)}$$

where $\Delta_\lambda = -\sum_c \frac{S_c - B_c}{2P_c}\Gamma_{\lambda c}$ (energy shift factor for the MLBW) and $\Gamma_\lambda = \sum_c \Gamma_{\lambda c}$. Redefining $E_\lambda \rightarrow E_\lambda + \Delta_\lambda$, the level matrix becomes

$$A_{\lambda\mu} = \frac{\delta_{\lambda\mu}}{E_\lambda - E - \frac{i}{2}\Gamma_\lambda} \quad . \tag{47}$$

The collision matrix given by Eq. (xx-42) becomes

$$U_{cc'} = e^{-i(\phi_c + \phi_{c'})}\left[\delta_{cc'} + i\sum_\lambda \frac{\Gamma_{\lambda c}^{1/2}\Gamma_{\mu c'}^{1/2}}{E_\lambda - E - \frac{i}{2}\Gamma_\lambda}\right] . \tag{48}$$

From this point, we proceed to the derivation of the cross section formalism in the MLBW representation. For a reaction in which $c \neq c'$ (fission, capture, or inelastic scattering channels) the collision matrix and the reaction cross section are given respectively by

$$U_{cc'} = e^{-i(\phi_c + \phi_{c'} - \frac{\pi}{2})} \sum_\lambda \frac{\Gamma_{\lambda c}^{1/2}\Gamma_{\mu c'}^{1/2}}{E_\lambda - E - \frac{i}{2}\Gamma_\lambda} \quad , \tag{49}$$

and

$$\sigma_{cc'} = \pi\lambda\!\!\!^{-2} \mid U_{cc'}|^2 = \pi\lambda\!\!\!^{-2}\, U_{cc'}U_{cc'}^* \tag{50}$$

where we have used the identity $i = e^{i\pi/2}$ in Eq. (xx-49). Inserting Eq. (xx-49) into Eq. (xx-50) gives

$$\sigma_{cc'} = \pi\lambda\!\!\!^{-2}\sum_\lambda\sum_{\lambda'} \frac{\Gamma_{\lambda c}^{1/2}\Gamma_{\lambda c'}^{1/2}\,\Gamma_{\lambda' c}^{1/2}\Gamma_{\lambda' c'}^{1/2}}{(\epsilon_\lambda - E)(\epsilon_{\lambda'}^* - E)} \quad , \tag{51}$$

where we have made $\epsilon_\lambda = E_\lambda - \frac{i}{2}\Gamma_\lambda$ and $\epsilon_\lambda^* = E_\lambda + \frac{i}{2}\Gamma_\lambda$. This expression can be further modified by using the following identity

$$\frac{1}{(\epsilon_\lambda - E)(\epsilon_{\lambda'}^* - E)} = \frac{1}{(\epsilon_{\lambda'}^* - \epsilon_\lambda)}\left[\frac{1}{(\epsilon_\lambda - E)} - \frac{1}{(\epsilon_{\lambda'}^* - E)}\right], \tag{52}$$

which gives

$$\sigma_{cc'} = \pi \lambda\!\!\!^{-2}\left\{\sum_{\lambda\lambda'} \frac{M_{\lambda\lambda'}^{cc'}}{(\epsilon_{\lambda'}^* - \epsilon_\lambda)(\epsilon_\lambda - E)} - \sum_{\lambda\lambda'} \frac{M_{\lambda\lambda'}^{cc'}}{(\epsilon_{\lambda'}^* - \epsilon_\lambda)(\epsilon_{\lambda'}^* - E)}\right\}, \tag{53}$$

where $M_{\lambda\lambda'}^{cc'} = \Gamma_{\lambda c}^{1/2}\Gamma_{\lambda c'}^{1/2}\Gamma_{\lambda' c}^{1/2}\Gamma_{\lambda' c'}^{1/2}$. The second term in Eq. (xx-53) is the complex conjugate of the first term, hence

$$\sigma_{cc'} = 2\pi \lambda\!\!\!^{-2} Re\left\{\sum_\lambda \frac{1}{\epsilon_\lambda - E} \sum_{\lambda'} \frac{M_{\lambda\lambda'}^{cc'}}{\epsilon_{\lambda'}^* - \epsilon_\lambda}\right\}. \tag{54}$$

The term in the summation on λ' can be expanded to give

$$\sigma_{cc'} = 4\pi \lambda\!\!\!^{-2}\sum_\lambda \frac{\Gamma_{\lambda c}\Gamma_{\lambda c'}}{\Gamma_\lambda^2}\left[(Re\, C_\lambda^{cc'})\psi_\lambda + (Im\, C_\lambda^{cc'})\chi_\lambda\right], \tag{55}$$

where

$$C_\lambda^{cc'} = 1 + \sum_{\lambda \neq \lambda'} \frac{\gamma_{\lambda' c}}{\gamma_{\lambda c}} \frac{i\Gamma_{\lambda c}}{E_{\lambda'} - E + \frac{i}{2}(\Gamma_{\lambda'} + \Gamma_\lambda)} \frac{\gamma_{\lambda' c'}}{\gamma_{\lambda c'}}, \tag{56}$$

and the line shapes ψ_λ and χ_λ are defined as

$$\psi_\lambda = \frac{\Gamma_\lambda^2/4}{(E_\lambda - E)^2 + \Gamma_\lambda^2/4}, \tag{57}$$

and

$$\chi_\lambda = \frac{(E_\lambda - E)\Gamma_\lambda/2}{(E_\lambda - E)^2 + \Gamma_\lambda^2/4} \ . \qquad \textbf{(58)}$$

Equation (xx-55) is the MLBW cross section form for the reaction cross section. A similar procedure can be followed to derive the elastic cross section.

2. Single Level Breit-Wigner (SLBW) Formalism

The SLBW cross section formalism is a particular case of Eq. (xx-55) when the second term in Eq. (xx-56) is zero, that is, $C_\lambda^{cc'} = 1$.

3. Adler-Adler (AA) Formalism

The AA approximation consists of applying an orthogonal complex transformation which diagonalizes the level matrix as given in Eq. (xx-43). We are looking for a transformation such that

$$O A^{-1} O^{-1} = \underline{\epsilon} - E \ , \qquad \textbf{(59)}$$

or

$$A = O^{-1} (\underline{\epsilon} - E)^{-1} O \ , \qquad \textbf{(60)}$$

where $O O^{-1} = O^{-1} O = I$. Here O is a orthogonal complex matrix and $\underline{\epsilon}$ is a diagonal matrix of complex elements. The elements of the matrix in Eq. (xx-60) are given as

$$A_{\lambda\mu} = \sum_\nu \frac{O_{\lambda\nu} O_{\mu\nu}}{\epsilon_\nu - E}. \qquad \textbf{(61)}$$

The collision matrix of Eq. (xx-42) then becomes

$$U_{cc'} = e^{-i(\phi_c + \phi_{c'})} \left[\delta_{cc'} + i \sum_\nu \frac{g_{\nu c}^{1/2} g_{\nu c'}^{1/2}}{\epsilon_\nu - E} \right], \qquad \textbf{(62)}$$

where $g_{\nu c}^{1/2} = \sum_\lambda O_{\lambda\nu} \Gamma_{\lambda c}^{1/2}$ and $g_{\nu c'}^{1/2} = \sum_\mu O_{\mu\nu} \Gamma_{\mu c'}^{1/2}$. The elements of the O matrix are determined from

$$(E_\lambda - E)\,\delta_{\lambda\mu} - \sum_c \gamma_{\lambda c} L_{0c} \gamma_{\mu c} = \sum_\nu O_{\lambda\nu} \epsilon_\nu O_{\mu\nu} \ , \qquad \textbf{(63)}$$

where Eq. (xx-43) has been used.

Because of the energy dependence of L_{0c} through the penetration factor P_c, the elements $O_{\lambda\nu}$ will, in general, be energy-dependent. In the AA approach, the energy dependence of L_{0c} is neglected. This assumption works very well for fissile isotopes where the resonance region is predominantly described by s-wave resonances (angular momentum corresponding to l=0) for which the penetration factor is energy independent. However, the assumption breaks down when p-wave (l=1) or other neutron partial wave functions with angular momentum l greater than 1 are present.

The reaction cross section in the AA formalism can be obtained in a similar way to that developed for the MLBW. The result is

$$\sigma_{cc'} = 2\pi\lambda^2 \sum_\lambda \frac{\nu_\lambda G_\lambda^{cc'} + (\mu_\lambda - E) H_\lambda^{cc'}}{(\mu_\lambda - E)^2 + \nu_\lambda^2} \ , \qquad \textbf{(64)}$$

where the following definitions were made

$$H_\lambda^{cc'} - i G_\lambda^{cc'} = \sum_{\lambda'} \frac{g_{\lambda c} g_{\lambda c'} g_{\lambda' c} g_{\lambda' c'}}{\epsilon_{\lambda'}^* - \epsilon_\lambda} \ , \qquad \textbf{(65)}$$

and

$$\epsilon_\lambda = \mu_\lambda - i\nu_\lambda \ . \qquad \textbf{(66)}$$

4. Reich-Moore Formalism

The approach proposed by Reich and Moore for treating the neutron-nucleus cross sections consists of eliminating the off-diagonal contribution of the photon channels. The rationale for this assumption is this: systematic measurements of the resonance widths, mainly in the case of the neutron and fission widths, show strong fluctuations among resonances of the same total angular momentum and parity. It should be expected, from Eq. (xx-40), that these fluctuations are connected either to the reduced widths $\gamma_{\lambda c}$ or to the penetration factors P_c. However, it is improbable that such

fluctuations are due to the penetration factors because they are either constant or a smooth function of the energy. Hence, the fluctuations must be related to the reduced widths. Porter and Thomas noted that the reduced widths $\gamma_{\lambda c}$ of Eq. (xx-13) are functions of the channel functions $\phi_c(E_\lambda, a_c)$ which, in turn, are projections of the eigenfunctions of the compound nucleus onto the nuclear surface and exhibit random size variations. Consequently, the large number of gamma channels implies that $\sum_{c\in\gamma} \gamma_{\mu c}\,\gamma_{\lambda c}$ is very small for $\mu \neq \lambda$. The second term of the level matrix in Eq. (xx-43) is divided in two parts as

$$\sum_c \gamma_{\lambda c} L_{0c} \gamma_{\mu c} = \sum_{c\in\gamma} \gamma_{\lambda c} L_{0c} \gamma_{\mu c} + \sum_{c\notin\gamma} \gamma_{\lambda c} L_{0c} \gamma_{\mu c} \ , \qquad \textbf{(67)}$$

and in the RM approximation

$$\sum_{c\in\gamma} \gamma_{\lambda c} L_{0c} \gamma_{\mu c} \approx \delta_{\mu\lambda} \sum_{c\in\gamma} L_{0c} \gamma_{\lambda c}^2 \ . \qquad \textbf{(68)}$$

The level matrix becomes

$$A_{\lambda\mu}^{-1} = (E_\lambda - E + \Delta_{\lambda\gamma} - \frac{i}{2}\Gamma_{\lambda\gamma})\,\delta_{\lambda\mu} + \sum_{c\notin\gamma} \gamma_{\lambda c} L_{0c} \gamma_{\mu c} \ , \qquad \textbf{(69)}$$

where, similarly to the MLBW, the following definitions were made:

$\Delta_{\lambda\gamma} = -\sum_{c\in\gamma} \frac{S_c - B_c}{2P_c}\,\Gamma_{\lambda c}$ (Energy shift factor), and $\Gamma_{\lambda\gamma} = \sum_{c\in\gamma} \Gamma_{\lambda c}$. Note that these quantities are different from that in the MLBW formalism. Again, redefining $E_\lambda \to E_\lambda + \Delta_\lambda$ we have

$$A_{\lambda\mu}^{-1} = (E_\lambda - E - \frac{i}{2}\Gamma_{\lambda\gamma})\,\delta_{\lambda\mu} + \sum_{c\notin\gamma} \gamma_{\lambda c} L_{0c} \gamma_{\mu c} \ . \qquad \textbf{(70)}$$

From this point we are going to derive a relation between the collision and the level matrix in the RM representation. Multiplying Eq. (xx-70) by $A_{\alpha\lambda}$ and summing over λ gives

$$\frac{\delta_{\alpha\mu}}{(E_\mu - E - \frac{i}{2}\Gamma_{\mu\gamma})} = A_{\alpha\mu} - \sum_{c\notin\gamma} \sum_\lambda \frac{A_{\alpha\lambda} \gamma_{\lambda c} L_{0c} \gamma_{\mu c}}{(E_\mu - E - \frac{i}{2}\Gamma_{\mu\gamma})} \ . \qquad \textbf{(71)}$$

Multiplying Eq. (xx-71) on the left by $\gamma_{\alpha c'}$ and on the right by $\gamma_{\alpha c''}$ and summing over α and μ gives

$$\sum_{\mu} \frac{\delta_{\mu c'} \delta_{\mu c''}}{E_\mu - E - \frac{i}{2}\Gamma_{\mu\gamma}} = \sum_{\mu}\sum_{\alpha} \gamma_{\alpha c'} A_{\alpha\mu} \gamma_{\mu c''} - \sum_{c\notin\gamma}\sum_{\alpha}\sum_{\lambda} \gamma_{\lambda c'} A_{\alpha\lambda} \gamma_{\lambda_{\lambda c}} L_{0c} \sum_{\mu} \frac{\gamma_{\mu c} \gamma_{\mu c''}}{E_\mu - E - \frac{i}{2}\Gamma_{\mu\gamma}} \quad . \tag{72}$$

If we define

$$R_{c'c''} = \sum_{\mu} \frac{\delta_{\mu c'} \delta_{\mu c''}}{E_\mu - E - \frac{i}{2}\Gamma_{\mu\gamma}} \tag{73}$$

and

$$Q_{c'c} = \sum_{\mu}\sum_{\alpha} \gamma_{\alpha c'} A_{\alpha\mu} \gamma_{\mu c''} \ , \tag{74}$$

then Eq. (xx-72) becomes

$$R_{c'c''} = \sum_{c\notin\gamma} Q_{c'c} \left(\delta_{cc''} - L_{0c} R_{cc''}\right) \ . \tag{75}$$

Note that this R matrix is an approximation, not to be confused with the exact R-matrix defined earlier.

Rearranging Eq. (xx-75) gives

$$Q_{cc'} = \sum_{c''\notin\gamma} R_{cc''} \left(\delta_{c''c'} - L_{0c''} R_{c''c'}\right)^{-1} \ . \tag{76}$$

Hence, from Eq. (xx-42) the collision matrix in the RM approximation becomes

$$U_{cc'} = e^{-i(\phi_c + \phi_{c'})} \left\{ \delta_{cc'} + 2i P_c^{1/2} \left[\sum_{c''\notin\gamma} R_{cc''} \left(\delta_{c''c'} - L_{0c''} R_{c''c'}\right)^{-1} \right] P_{c'}^{1/2} \right\} . \tag{77}$$

Equation (xx-77) relates the collision matrix to the Reich-Moore R-matrix in a form similar to that in the case of the general R-matrix theory. In the general R-matrix, the elements are

$$R_{cc'} = \sum_{\lambda} \frac{\gamma_{\lambda c}\,\gamma_{\lambda c'}}{E_{\lambda} - E} \ , \tag{78}$$

whereas in the RM approximation they are

$$R_{cc'} = \sum_{\lambda} \frac{\delta_{\lambda c}\,\delta_{\lambda c'}}{E_{\lambda} - E - \frac{i}{2}\Gamma_{\lambda\gamma}} \ . \tag{79}$$

Equation (xx-79) is frequently referred to as the reduced R-matrix theory.

We now proceed to obtain a form for the cross section in the RM approximation, by writing Eq. (xx-77) as

$$U_{cc'} = e^{-i(\phi_c + \phi_{c'})}\Omega_{cc'} \ , \tag{80}$$

where

$$\Omega_{cc'} = \delta_{cc'} + 2i\,P_c^{1/2}\left[\sum_{c''\notin\gamma} R_{cc''}\left(\delta_{c''c'} - L_{0c''}R_{c''c'}\right)^{-1}\right]P_{c'}^{1/2} \ . \tag{81}$$

It is useful to write the reduced R-matrix as

$$R_{cc'} = \frac{1}{i}\,P_c^{-1/2}\,K_{cc'}\,P_{c'}^{-1/2} \ , \tag{82}$$

in which the elements of *K* are given by

$$K_{cc'} = i\,P_c^{1/2}\,R_{cc'}\,P_{c'}^{1/2} \ . \tag{83}$$

The explicit form of $K_{cc'}$ is

$$K_{cc'} = \frac{i}{2} \sum_{\lambda} \frac{\Gamma_{\lambda c}^{1/2} \, \Gamma_{\lambda c'}^{1/2}}{E_{\lambda} - E - \frac{i}{2} \Gamma_{\lambda \gamma}} \ . \qquad \textbf{(84)}$$

Therefore $\Omega_{cc'}$ becomes

$$\Omega_{cc'} = \delta_{cc'} + 2i \, P_c^{1/2} \sum_{c'' \notin \gamma} \frac{1}{i} P_c^{-1/2} K_{cc''} P_{c''}^{-1/2} \left(\delta_{c''c'} - L_{0c''} \frac{1}{i} P_{c''}^{-1/2} K_{c''c'} P_{c'}^{-1/2} \right)^{-1} P_{c'}^{1/2} \ . \qquad \textbf{(85)}$$

Recalling that $L_{0c} = (S_c - B_c) + iP_c$ and making $B_c = S_c$, the expression for $\Omega_{cc'}$ becomes

$$\Omega_{cc'} = \delta_{cc'} + 2 \sum_{c'' \notin \gamma} K_{cc''} P_{c''}^{-1/2} \left(\delta_{c''c'} - P_{c''}^{1/2} K_{c''c'} P_{c'}^{-1/2} \right)^{-1} P_{c'}^{1/2} \ . \qquad \textbf{(86)}$$

The matrix form of Eq. (xx-86) is

$$\boldsymbol{\Omega} = \boldsymbol{I} + 2 \boldsymbol{K} \boldsymbol{P}^{-1/2} (\boldsymbol{I} - \boldsymbol{P}^{1/2} \boldsymbol{K} \boldsymbol{P}^{-1/2})^{-1} \boldsymbol{P}^{1/2} \ . \qquad \textbf{(87)}$$

Equation (xx-87) can be further reduced by using the identity $(\boldsymbol{B} + \boldsymbol{C})^{-1} = \boldsymbol{v}(\boldsymbol{wBv} + \boldsymbol{wCv})^{-1} \boldsymbol{w}$. Letting $\boldsymbol{B} = \boldsymbol{I}$, $\boldsymbol{C} = -\boldsymbol{P}^{1/2} \boldsymbol{K} \boldsymbol{P}^{-1/2}$, $\boldsymbol{w} = \boldsymbol{P}^{-1/2}$ and $\boldsymbol{v} = \boldsymbol{P}^{1/2}$ we have

$$\boldsymbol{\Omega} = \boldsymbol{I} + 2 \boldsymbol{K} (\boldsymbol{I} - \boldsymbol{K})^{-1} \ . \qquad \textbf{(88)}$$

If we then add and subtract $2(\boldsymbol{I} - \boldsymbol{K})^{-1}$ the expression becomes,

$$\boldsymbol{\Omega} = 2 \, (\boldsymbol{I} - \boldsymbol{K})^{-1} - \boldsymbol{I} \ , \qquad \textbf{(89)}$$

for which the elements are, explicitly,

$$\Omega_{cc'} = 2 \, (I - K)^{-1}_{cc'} - \delta_{cc'} \ . \qquad \textbf{(90)}$$

The collision matrix of Eq. (xx-80) then takes the form

$$U_{cc'} = e^{-i(\phi_c + \phi_{c'})} [2(I - K)^{-1}_{cc'} - \delta_{cc'}] \ , \qquad \textbf{(91)}$$

where the elements of $(I-K)_{cc'}$ are given as

$$(I-K)_{cc'} = \delta_{cc'} - \frac{i}{2}\sum_{\lambda} \frac{\Gamma_{\lambda c}^{1/2}\,\Gamma_{\lambda c'}^{1/2}}{E_{\lambda} - E - \frac{i}{2}\Gamma_{\lambda\gamma}} \ . \qquad \textbf{(92)}$$

The RM cross sections are written in terms of the transmission probability, defined as

$$\rho_{cc'} = \delta_{cc'} - (I-K)^{-1}_{cc'} \ , \qquad \textbf{(93)}$$

for which the collision matrix can be written as

$$U_{cc'} = e^{-i(\phi_c + \phi_{c'})}[\delta_{cc'} - 2\rho_{cc'}] \ , \qquad \textbf{(94)}$$

The cross sections can then be obtained by using Eqs. (xx-14), (xx-15), and (xx-16) as,

$$\sigma_t = 2\pi\lambda\!\!\!^{-2}\sum_l (2l+1)\left[(1-\cos 2\phi_l) + 2Re(\rho_{nn}\, e^{-2i\phi_l})\right] \ , \qquad \textbf{(95)}$$

$$\sigma_{abs} = 4\pi\lambda\!\!\!^{-2}\sum_l (2l+1)\left[Re(\rho_{nn}) - |\rho_{nn}|^2)\right] \ , \qquad \textbf{(96)}$$

$$\sigma_f = 4\pi\lambda\!\!\!^{-2}\sum_l (2l+1)\sum_{c\in f} |\rho_{nc}|^2 \ , \qquad \textbf{(97)}$$

and

$$\sigma_\gamma = \sigma_{abs} - \sigma_f \ . \qquad \textbf{(98)}$$

5. Conversion of RM parameters into AA parameters

A procedure to convert RM parameters into an equivalent set of AA parameters was developed by DeSaussure and Perez. Their approach consisted of writing the RM transmission probabilities ρ_{nn} and ρ_{nc} as the ratio of polynomials in energy; these polynomials can then be expressed in terms of partial fraction expansions by matching the AA cross sections as:

$$\frac{1}{\sqrt{E}}\rho_{nn} = \frac{P_n^{N-1}(E)}{P^N(E)} = \sum_{\lambda=1}^{N} \frac{r_{\lambda n}}{d_\lambda - E} \ , \qquad \textbf{(99)}$$

and

$$\frac{1}{\sqrt{E}}|\rho_{nc}|^2 = \frac{|P_c^{N-1}(E)|^2}{|P^N(E)|^2} = \sum_{\lambda=1}^{N}\left[\frac{r_{\lambda c}}{d_\lambda - E} + \frac{r_{\lambda c}^*}{d_\lambda^* - E}\right] \qquad c \neq n \ , \qquad \textbf{(100)}$$

where

$$P^N = Q\,\Delta \ , \qquad \textbf{(101)}$$

$$P_n^{N-1} = Q\,\frac{\Delta - m_{nn}}{\sqrt{E}} \ , \qquad \textbf{(102)}$$

$$Q = \prod_\lambda (E_\lambda - E - \frac{i}{2}\Gamma_{\lambda\gamma}) \ , \qquad \textbf{(104)}$$

$$|P_c^{N-1}|^2 = \frac{|Q\,m_{nc}|^2}{\sqrt{E}} \ , \qquad \textbf{(103)}$$

and $\Delta = |I - K|$.

Equations (xx-99) and (xx-100) have poles $d_\lambda = \mu_\lambda - i\,\nu_\lambda$ which are roots of the equation

$$P^N(E) = Q\Delta = 0 \ , \qquad \textbf{(105)}$$

and are identifiable as the parameters of the Adler-Adler formalism. In deriving this methodology DeSaussure and Perez neglected the energy dependence of the neutron widths, i.e., $\Gamma_n \propto \sqrt{E}$. This assumption limits the application of this methods to s-wave cross section. Hwang has extended the application of the DeSaussure and Perez approach to the calculation of cross sections for any angular momentum. In his approach, instead of using energy space, Hwang noted that the dependence of Γ_n on $\sqrt{E}$ suggests that an expansion in terms of $\sqrt{E}$ would lead to a rigorous representation of the cross section. Since momentum is proportional to $\sqrt{E}$, Hwang calls his methodology a rigorous pole representation in the momentum space or, for short, a multipole representation of the cross sections (MP). The transformation of the RM parameters into the MP parameters is obtained as

$$\rho_{nn} = \frac{P_n^{2M-1}(E)}{P^{2M}(E)} = \sum_{\lambda=1}^{2M} \frac{r_{\lambda n}}{d_\lambda - \sqrt{E}} \ , \qquad \textbf{(106)}$$

and

$$|\rho_{nc}|^2 = \frac{|P_c^{2M-1}(E)|^2}{|P^{2M}(E)|^2} = \sum_{\lambda=1}^{2M} \left[\frac{r_{\lambda c}}{d_\lambda - \sqrt{E}} + \frac{r_{\lambda c}^*}{d_\lambda^* - \sqrt{E}} \right] \qquad c \neq n \ , \qquad \textbf{(107)}$$

where

$$M = (l+1)N \ , \qquad \textbf{(108)}$$

and N is the number of resonance parameters in the RM representation. The factor Q of Eq. (xx-104) becomes

$$Q = \prod_{\lambda=1}^{N} (E_\lambda - E - \frac{i}{2}\Gamma_{\lambda\gamma}) \ q_l(\sqrt{E}) \ , \qquad \textbf{(109)}$$

where

$$q_0(\sqrt{E}) = 1, \qquad \textbf{(110)}$$

$$q_1(\sqrt{E}) = 1 + (k\,a)^2 \ , \qquad \textbf{(111)}$$

and

$$q_2(\sqrt{E}) = 9 + 3\,(k\,a)^2 + (k\,a)^4 \ . \qquad \textbf{(112)}$$

Doppler Broadening and Effective Cross Sections

The Doppler broadening of cross sections is a well-known effect which is caused by the motion of the atoms of the target nuclei. Since the target nuclei are not at rest in the laboratory system, the neutron-nucleus cross section will depend on the relative speed of the neutron and the nucleus. The effective cross section for mono-energetic neutrons of mass *m* and energy *E* (laboratory velocity *v*) is given by the number of neutrons per unit volume, multiplied by the number of target nuclei per unit volume, times the probability that a reaction will occur per unit time at an energy equivalent to the relative velocity $|\,v - W\,|$, integrated over all values of *W*, the velocity of the nucleus. The relation between the cross section measured in the laboratory and the effective cross section is

$$v\,\bar{\sigma}(m v^2/2) = \int d^3W\; p(\vec{W})\;\; |\vec{v} - \vec{W}|\;\; \sigma(m|\vec{v} - \vec{W}|^2/2) \ , \qquad \textbf{(113)}$$

where $\bar{\sigma}(m v^2/2)$ is the effective or Doppler-broadened cross section for incident particles with speed *v* [laboratory energy $mv^2/2$]. The distribution of velocities of the target nuclei is described by $p(\vec{W})$. A major issue is the choice of the appropriate velocity distribution function of the target nuclei. Let us now assume that the target nuclei have the same velocity distribution as the atoms of an ideal gas; i.e. the Maxwell-Boltzmann distribution,

$$p(\vec{W})\, d^3W \;=\; \frac{1}{\pi^{3/2}}\;\exp\!\left(-\frac{W^2}{u^2}\right)\;\frac{d^3W}{u^3}\ , \qquad \frac{M}{2}\,u^2 \;=\; k\,T\,, \qquad \textbf{(114)}$$

where *M* is the nuclear mass and *kT* the gas temperature in energy units. Combining Eqs. (xx-113) and (xx-114) gives

$$v\bar{\sigma}(m v^2/2) \;=\; \frac{1}{\pi^{3/2}\,u^3}\;\int\limits_{\text{all } \vec{W}} d^3W\;\; \exp\!\left(-\frac{W^2}{u^2}\right)\;\; |\vec{v} - \vec{W}|\;\; \sigma(m|\vec{v} - \vec{W}|^2/2) \quad . \qquad \textbf{(115)}$$

Note that, from the above definitions, a *1/v* cross section remains unchanged.

Changing the integration variable from $\vec{W}$ to $\vec{w} \;=\; \vec{v} - \vec{W}$ and choosing spherical coordinates simplifies the integral to the following:

$$v\bar{\sigma}\left(\frac{mv^2}{2}\right) = \frac{1}{\pi^{3/2}u^3}\int_{\text{all }\vec{w}} d^3w\ \exp\left(-\frac{(v^2-2vw\cos\theta+w^2)}{u^2}\right)\ w\,\sigma\left(\frac{mw^2}{2}\right)$$

$$= \frac{1}{\pi^{3/2}u^3}\int_0^{\pi} d\phi \int_0^{\infty} w^2\,dw \int_0^{\pi} d(\cos(\theta)\ \exp\left(-\frac{(v^2-2vw\cos\theta+w^2)}{u^2}\right)\ w\,\sigma\left(\frac{mw^2}{2}\right)$$

$$= \frac{1}{\pi^{3/2}u^3}\int_0^{2\pi} d\phi \int_0^{\infty} dw\, w^3\,\sigma\left(\frac{mw^2}{2}\right)\exp\left(-\frac{(v^2+w^2)}{u^2}\right)\int_{-1}^{+1} d\mu\ \exp\left(-\frac{2vw\mu}{u^2}\right) \qquad \textbf{(116)}$$

$$= \frac{2\pi}{\pi^{3/2}u^3}\int_0^{\infty} dw\, w^3\,\sigma\left(\frac{mw^2}{2}\right)\exp\left(-\frac{(v^2+w^2)}{u^2}\right)\left(\frac{-u^2}{2vw}\right)\left[\exp\left(-\frac{2vw}{u^2}\right)-\exp\left(+\frac{2vw}{u^2}\right)\right]$$

$$= \frac{1}{v\sqrt{\pi}\,u}\int_0^{\infty} dw\, w^2\,\sigma\left(\frac{mw^2}{2}\right)\left[\exp\left(-\frac{(v-w)^2}{u^2}\right)-\exp\left(-\frac{(v+w)^2}{u^2}\right)\right] .$$

This equation, known as the Solbrig's kernel, may be more familiar when written as the sum of two integrals,

$$\bar{\sigma}\left(E=\frac{mv^2}{2}\right) = \frac{1}{v^2\sqrt{\pi}\,u}\int_0^{\infty} dw\, w^2\,\sigma\left(\frac{mw^2}{2}\right)\exp\left(-\frac{(v-w)^2}{u^2}\right)$$
$$-\frac{1}{v^2\sqrt{\pi}\,u}\int_0^{\infty} dw\, w^2\,\sigma\left(\frac{mw^2}{2}\right)\exp\left(-\frac{(v+w)^2}{u^2}\right) \quad . \qquad \textbf{(117)}$$

At sufficiently high energies, the contribution from the second integral may be omitted since the value of the exponential is vanishingly small.

To simplify Eq. (xx-117) further, we make the following definition:

$$\begin{aligned} s(w) &= \sigma(\ m(w)^2/2) \qquad \text{for } w>0 \\ &= -\sigma(m(-w)^2/2) \qquad \text{for } w<0\ . \end{aligned} \qquad \textbf{(118)}$$

Equation (xx-117) then becomes

$$\bar{\sigma}\left(\frac{mv^2}{2}\right) = \frac{1}{v^2\sqrt{\pi}\,u}\int_{-\infty}^{\infty} dw\, w^2 s(w)\exp\left(-\frac{(v-w)^2}{u^2}\right) \quad . \tag{119}$$

For programming convenience, we make a change of variable from velocity to square root of energy. Thus instead of *v* we use

$$V = \sqrt{E} = v\sqrt{m/2} \quad ; \tag{120}$$

we redefine *W* to be

$$W = w\sqrt{m/2} \quad , \tag{121}$$

and define *U* as

$$U = \sqrt{m/2}\,u = \sqrt{mkT/M} \quad . \tag{122}$$

In addition, *S*(*W*) is set equal to *s*(*w*), or

$$\begin{aligned} S(W) &= \sigma((W)^2) \qquad \text{for } W>0 \\ &= -\sigma((-W)^2) \qquad \text{for } W<0 \ . \end{aligned} \tag{123}$$

These changes give the formulation which is used in SAMMY for the exact monatomic free gas model (FGM):

$$\bar{\sigma}(V^2) = \frac{1}{V^2\sqrt{\pi}\,U}\int_{-\infty}^{\infty} dW\, W^2\, S(W)\exp\left(-\frac{(V-W)^2}{U^2}\right) \quad . \tag{124}$$

These equations hold for 1/*v* cross sections, for constant cross sections, and for cross sections with resonance structure.

To transform to the high-energy Gaussian approximation (hereafter referred to as HEGA) from the FGM, define *E* as V^2 and E' as W^2. Then Eq. (xx-124) takes the form

$$\bar{\sigma}(E) \cong \frac{1}{E\sqrt{\pi}\,U}\int_{E_{\min}>0}^{\infty} \frac{dE'}{2\sqrt{E'}}\, E'\,\sigma(E')\exp\left(-\frac{\left(\sqrt{E}-\sqrt{E'}\right)^2}{U^2}\right), \tag{125}$$

in which the lower limit has been changed from -∞ to E_{min}, a number above zero, since the next step involves approximations which are valid only for $E' >> 0$. If we expand the integrand of Eq. (xx-125) in powers of *(E-E')* for values of E'/E close to 1 and set $\delta = E' - E$, then

$$\begin{aligned}\sqrt{E} - \sqrt{E+\delta} &= \sqrt{E}\left(1 - \sqrt{1+\frac{\delta}{E}}\right) \\ &\approx \sqrt{E}\left[1 - \left(1 + \frac{1}{2}\frac{\delta}{E}\right)\right] \\ &\approx -\frac{1}{2}\frac{E-E'}{\sqrt{E}}\end{aligned} \quad . \qquad \textbf{(126)}$$

Defining Δ^2 (Doppler width) as

$$\begin{aligned}\Delta^2 &= 4EU^2 \\ &= \sqrt{\frac{4kTE}{M/m}}\end{aligned} \quad , \qquad \textbf{(127)}$$

(Note that this quantity is energy-dependent) then the HEGA becomes

$$\bar{\sigma}_{HEGA}(E) \cong \frac{1}{\sqrt{\pi}\,\Delta}\int_{-\infty}^{\infty} dE'\ \sigma(E')\exp\left(-\frac{(E-E')^2}{\Delta^2}\right) \quad , \qquad \textbf{(128)}$$

where the lower limit was extended to negative infinity since that portion of the integrand is essentially zero. This is the usual Gaussian formulation of the free gas model.

Other Energy-Dependent Cross Sections

No discussion of Doppler broadening would be complete without an analysis of the effects of Doppler broadening on particular types of cross sections. Here we examine some important types of energy dependencies.

Doppler Broadening of 1/*v* Cross Sections

Doppler broadening is expected to preserve (i.e., leave unchanged) a 1/*v*-cross section. To test whether this is the case with FGM and/or HEGA broadening, we note that a 1/*v*-cross section may be expressed as

$$\sigma(W^2) = \frac{\sigma_0 V_0}{W} \quad , \tag{129}$$

where the subscript "0" denotes constants. To evaluate the FGM with this type of cross section, note that our function *S* of Eq. (xx-123), combined with Eq. (xx-129), gives

$$\begin{aligned} S(W) &= \frac{\sigma_0 V_0}{W} \quad \text{for } W \geq 0 \\ &= -\frac{\sigma_0 V_0}{-W} = \frac{\sigma_0 V_0}{W} \quad \text{for } W < 0 \quad . \end{aligned} \tag{130}$$

From Eq. (xx-11) the FGM-broadened form of the 1/*v* cross section is therefore

$$\bar{\sigma}(V^2) = \frac{\sigma_0 V_0}{V^2 \sqrt{\pi}\, U} \int_{-\infty}^{+\infty} W \, dW \, e^{-(V-W)^2/U^2} = \frac{\sigma_0 V_0}{V} \quad , \tag{131}$$

i.e., in the exact same mathematical form as the original of Eq. (xx-129). In other words, a 1/*v* cross section is conserved under Doppler broadening with the free gas model.

That is not the case for HEGA broadening. With the HEGA from Eq. (xx-128), the Doppler-broadened 1/*v* cross section takes the form

$$\bar{\sigma}_{HEGA}(E) = \frac{1}{\sqrt{\pi}\,\Delta} \int_{-\infty}^{+\infty} dE' \, \frac{\sigma_0 V_0}{\sqrt{E'}} \, e^{-(E-E')^2/\Delta^2} = \frac{\sigma_0 V_0}{\sqrt{\pi}\,\Delta} \int_{-\infty}^{+\infty} \frac{dE'}{\sqrt{E'}} \, e^{-(E-E')^2/\Delta^2} \quad , \tag{132}$$

which is not readily integrable analytically. What *is* clear is that the result is *not* 1/*v*.

Doppler Broadening of a Constant Cross Section

In contrast to the 1/*v* cross section, a constant cross section is <u>not</u> conserved under Doppler broadening. That it is true experimentally can be seen by examining very low energy capture cross sections, for which the unbroadened cross section is constant (which can be shown

by taking the low-energy limit of the Reich-Moore equations, for example) but the experimental cross section rises with decreasing energy. See, for example, the S elastic cross section from 0.01 to 1.0 eV or the Cu elastic cross section below 2.0 eV (on pages 100 and 234, respectively, of [VM88]), which clearly rise with decreasing energy.

To calculate analytically what effect FGM and HEGA broadening have upon a constant cross section, we first note that a constant cross section can be expressed as

$$\sigma(E) = \sigma_0 \quad . \tag{133}$$

The function *S* needed for our formulation of FGM broadening (see Eq. (xx-123)) is found to be

$$\begin{aligned} S(W) &= \sigma_0 \quad \text{for } W \geq 0 \\ &= -\sigma_0 \quad \text{for } W < 0 \quad , \end{aligned} \tag{134}$$

so that Eq. (xx-124) gives, for the FGM-broadened constant cross section,

$$\bar{\sigma}(V^2) = \frac{\sigma_0}{V^2 \sqrt{\pi}\, U} \left[\int_0^\infty dW\, W^2\, e^{-(V-W)^2/U^2} - \int_{-\infty}^0 dW\, W^2\, e^{-(V-W)^2/U^2} \right] . \tag{135}$$

Replacing (*W*-*V*) / *U* by *x* gives

$$\bar{\sigma}(V^2) = \frac{\sigma_0 U^3}{V^2\sqrt{\pi}\,U}\left[\int_{-v}^{\infty} dx\ (x^2+2xv+v^2)\ e^{-x^2} - \int_{-\infty}^{-v} dx\ (x^2+2xv+v^2)\ e^{-x^2}\right]$$

$$= \frac{\sigma_0}{v^2\sqrt{\pi}}\left[\int_{0}^{\infty} + \int_{-v}^{0} - \int_{-\infty}^{0} + \int_{-v}^{0}\right] dx\ (x^2+2xv+v^2)\ e^{-x^2}$$

$$= \frac{\sigma_0}{v^2\sqrt{\pi}}\left[2\int_{0}^{\infty} dx\ (2xv)\ e^{-x^2} + 2\int_{-v}^{0} dx\ (x^2+2xv+v^2)\ e^{-x^2}\right]$$

$$= \frac{\sigma_0\, 4v}{v^2\sqrt{\pi}}\int_{0}^{\infty} x\,dx\ e^{-x^2} + \frac{2\sigma_0}{v^2\sqrt{\pi}}\int_{-v}^{0} x^2\,dx\ e^{-x^2} \qquad \textbf{(136)}$$

$$+ \frac{4v\,\sigma_0}{v^2\sqrt{\pi}}\int_{-v}^{0} x\,dx\ e^{-x^2} + \frac{2\sigma_0 v^2}{v^2\sqrt{\pi}}\int_{-v}^{0} dx\ e^{-x^2}$$

$$= \frac{\sigma_0 4}{v\sqrt{\pi}}\,\frac{1}{2} + \frac{2\sigma_0}{v^2\sqrt{\pi}}\left(-\frac{v}{2}e^{-v^2} + \frac{\sqrt{\pi}}{4}\left[\operatorname{erfc}(0) - \operatorname{erfc}(v)\right]\right)$$

$$+ \frac{4\sigma_0}{v\sqrt{\pi}}\left(-\frac{1}{2}\left[1-e^{-v^2}\right]\right) + \frac{2\sigma_0}{\sqrt{\pi}}\left[\operatorname{erfc}(0) - \operatorname{erfc}(v)\right]$$

$$= \frac{\sigma_0}{v\sqrt{\pi}}\,e^{-v^2} + \sigma_0\left(\frac{1}{2v^2}+1\right)\left(1 - \operatorname{erfc}(v)\right)$$

in which we have replaced *V/U* by *v*.

In the limit of small *v*, the quantity in Eq. (xx-6) becomes

$$\bar{\sigma}(V^2) \to \sigma_0\left[\frac{1}{\sqrt{\pi}\,v} + \frac{1}{2v^2}\,\frac{2}{\sqrt{\pi}}\,(v+v^3)\right] \to \frac{\sigma_0}{\sqrt{\pi}\,v}\quad , \qquad \textbf{(137)}$$

so that the leading term is 1/*v*; this is somewhat counterintuitive but is nevertheless observed in measured low-energy cross sections. For large values of *v*, the limiting case is

$$\bar{\sigma}(V^2) \to \sigma_0\left[0 + 1\times 1\right] \to \sigma_0\quad ; \qquad \textbf{(138)}$$

i.e., the broadened cross section is a constant, as expected.

In contrast, HEGA broadening preserves a constant cross section everywhere:

$$\bar{\sigma}_{HEGA}(E) = \frac{\sigma_0}{\sqrt{\pi}\,\Delta}\int_{-\infty}^{\infty} dE'\; e^{-(E-E')^2/\Delta^2} = \sigma_0 \quad ; \tag{139}$$

that is, the Gaussian kernel is normalized to unity, as expected. This result, which may intuitively appear to be correct, is nevertheless unphysical. As discussed above, It is well known that measured (and therefore Doppler-broadened) cross sections exhibit 1/*v* behavior at very low energies.

Doppler Broadening of the Line Shapes ψ and χ

Equations (xx-57) and (xx-58) can be written as

$$\psi(x) = \frac{1}{1+x^2} \ , \tag{140}$$

and

$$\chi = \frac{x}{1+x^2} \ , \tag{141}$$

where $x = \dfrac{2(E_\lambda - E)}{\Gamma_\lambda}$.

The HEGA of these functions are obtained by replacing $\sigma(E)$ in Eq. (xx-128) by ψ and χ, which gives

$$\psi(x,\theta) = \frac{\theta}{2\sqrt{\pi}}\int_{-\infty}^{+\infty} dy\; \frac{\exp[-\frac{1}{4}\theta^2(x-y)^2]}{1+y^2} \ , \tag{142}$$

and

$$\chi(x,\theta) = \frac{\theta}{2\sqrt{\pi}} \int_{-\infty}^{+\infty} dy \; 2y \, \frac{\exp[-\frac{1}{4}\theta^2 (x-y)^2]}{1+y^2} \;, \qquad \textbf{(143)}$$

where $\theta = \frac{\Gamma}{\Delta}$.

22.106 Neutron Interactions and Applications

Spring 2010

Appendix E: Curriculum Vitae

Luiz Carlos Leal

Business Address:

IRSN
31 Avenue de la Division Leclerc
92260 Fontenay-aux-Roses,
France

Phone: +33 01 58 35 93 83

EDUCATION

The University of Tennessee, Knoxville
Ph.D. in Nuclear Engineering, May 1990

Federal University of Rio de Janeiro, Brazil
M.Sc. in Nuclear Engineering, June 1980

Federal University of Rio de Janeiro, Brazil
B.Sc. in Physics, December 1977

WORK EXPERIENCE

2015–Present **Deputy Head of Reactor Physics Research and Safety Assessment Laboratory**
Laboratoire d'expertise et de recherche en neutronique des réacteurs (LNR), Institut de Radioprotection et de Sûreté Nucléaire (IRSN)

2004–2015 **Distinguished R&D Staff**
Nuclear Data and Criticality Safety Group, Reactor and Nuclear Systems Division, Oak Ridge National Laboratory, Oak Ridge, TN

2011–2014 **Research Affiliate**
Nuclear Engineering Department, Massachusetts Institute of Technology, Boston, MA

2001–2004 **Senior Research Development Staff Member**
Nuclear Science and Technology Division, Oak Ridge National Laboratory, Oak Ridge, TN
Acted as the technical director of the nuclear data activities in support of the DOE Nuclear Criticality Safety Program.

1996–2001 **Senior Nuclear Engineer**
Radiation Information Analysis Section and Leader, Nuclear Data Group, Oak Ridge National Laboratory, Oak Ridge, TN
In this capacity had the overall responsibility for nuclear data measurement and evaluation at the Oak Ridge Linear Accelerator (ORELA) and also responsible for nuclear data evaluations presently in the US Evaluated Nuclear Data Files.

1993–1996 **Nuclear Engineer**
Radiation Information Analysis Section, Nuclear Data Group, Oak Ridge National Laboratory, Oak Ridge, TN

Luiz Carlos Leal

Business Address:

IRSN
31 Avenue de la Division Leclerc
92260 Fontenay-aux-Roses,
France

Phone: +33 01 58 35 93 83

1990–
1993 **Nuclear Engineer**
Theory and Analyses Group of the Reactor Analysis Division, Argonne National Laboratory, Argonne, IL
Activities included processing of the newly released nuclear data file (ENDF/B version VI) for reactor analyses, development of new techniques for resonance treatment for the ENDF/B-VI neutron cross-section representation, processing of data for photon interaction for reactor calculations, reactor core analysis and design, cross section generation, and static and dynamic analysis utilizing deterministic and Monte Carlo codes.

1986–
1990 **Graduate Research Assistant**
Engineering Physics and Mathematics Division, Oak Ridge National Laboratory, Oak Ridge, TN
Performed the R-matrix analysis and evaluation of the ^{235}U neutron cross-sections in the resolved energy range. The ENDF/B-VI data files have subsequently adopted the resulting resolved resonance parameters. Developed a computer code for treating the neutron interaction cross section in the unresolved energy range.

1985–
1986 **Research Assistant**
Applied Physics Division, Argonne National Laboratory, Argonne, IL
Worked on processing of neutron cross sections. Work included the development of a finite difference algorithm applied to the Doppler broadening of cross sections.

1980–
1985 **Nuclear Engineer**
Brazilian Nuclear Energy Commission
Worked on the development, applications, and implementation of computer codes for nuclear reactor design and analysis.

1979–
1980 **Assistant Professor**
Physics Department, Federal University of Paraiba, Brazil

1977–
1979 **Research Assistant**
Nuclear Engineering Department, Federal University of Rio de Janeiro
Worked o the development of algorithms for calculating neutron scattering kernel in light and heavy water (H_20 and D_20) based on the Nelkin and Butler model.

PROFESSIONAL AFFILIATIONS

Fellow of the American Nuclear Society

(A) Reactor Physics Division

Session Organizer, International Conference on Mathematics and Computations, Reactor Physics, and Environmental Analyses, Portland, Oregon, April 1995

PROFESSIONAL AFFILIATIONS (continued)

Session Organizer, Physics of Nuclear Science and Technology, Long Island, New York, October 1998

International Program Committee on the International Conference on Nuclear Data for Science and Technology, Tsukuba, Ibaraki, Japan, October 2001

International Program Committee and Session organizer for PHYSOR 2002 Seoul, South Korea, October 2002
Session Organizer of several ANS Annual Meetings

(B) Mathematics and Computation Division

International Program Committee and Session Organizer, Mathematics and Computation Meeting, Gatlinburg, Tennessee, April 2003

(C) Criticality Safety Division

Session Organizer, International Conference on Criticality Safety, Palais des Congres, Versailles, France September 1999

OTHER PROFESSIONAL ACTIVITIES

Ph.D. Thesis Advisor at Georgia Institute of Technology. Ongoing PhD Thesis to be presented by Andrew Holcomb, November 2015.

Ph.D. Thesis Advisor at Georgia Institute of Technology. Ongoing PhD Thesis to be presented by Christopher Chapman, November 2017.

Ph.D. Thesis Advisor and Committee participant at The University of Texas, Austin. PhD Thesis presented by Christopher van der Hoeven, November 2013.

Ph.D. Thesis Advisor and Committee participant at The Massachusetts Institute of Technology. PhD Thesis presented by Vladimir Sobes, September 2013.

Ph.D. Thesis Advisor and Committee participant at Institut Polytechnique de Grenoble, France. Ph.D. Thesis presented by Benoit Habert, November 2009.

Committee member of the defense for "Habilitation a Diriger les Recherches," presented by Ivan Kodeli at the University of Orsay, Paris, France.

Ph.D. Thesis Advisor and Committee participant at The Pennsylvania State University. Ph.D. Thesis presented by F. Arzu Alpan, November 2003.

Lecturer at the International Centre for Theoretical Physics, lecture presented at the Workshop on Nuclear Data and Nuclear Reactors: Physics, Design and Safety, Trieste, Italy, March 2000.

Lecturer at the Massachusetts Institute of Technology (MIT). Subject: R-matrix theory and nuclear data application to reactor design and criticality safety.

Lecturer at the Korea Advanced Institute of Science and Technology, South Korea, August 2011

PROFESSIONAL AFFILIATIONS (continued)

Lecturer at the Soul National University, South Korea, August 2011

Lecturer at the Federal University of Rio de Janeiro, Brazil, June 2012

ANS Executive Committee Member of the Reactor Physics Division, 2001–2003.

AWARDS

2010 Technical Excellence Award winner in the Criticality Safety Division of the American Nuclear Society (http://ncsd.ans.org/site/awards.html).

Outstanding paper, "Finite Difference Method for Treating Doppler Broadening of Cross Sections," American Nuclear Society Eastern Regional Student Conference, Raleigh, NC, April 1987.

First place honors at the Student Design Contest Graduate Category, "Performance Analysis of the Browns Ferry Radwaste System," American Nuclear Society, Los Angeles, CA, November 1987.

Outstanding paper, "Statistical Properties of the ^{235}U Resonance Parameters Up to 300 eV," American Nuclear Society Eastern Regional Student Conference, Knoxville, TN, March 1989.

Fellowship of the International Atomic Energy Agency (IAEA), 1985–1986.

PUBLICATIONS

1. C. van der Hoeven, E. Schneider, and L. Leal, "Generation of Improved Isotopic Molybdenum Covariances from Elemental Cross-Section Data Using SAMMY," *Nucl. Sci. Eng.* **179**, 1-21, (2015).

2. L. Leal, A. Daskalakis, Y. Danon, A. Negret, and A. Plompen, "R-matrix Evaluation of ^{56}Fe Including Elastic, Inelastic, and Angular Dependent Cross Sections," WINS 2014 Workshop on Elastic and Inelastic Neutron Scattering, Dresden, Germany, December 3-5, 2014.

3. Andrew Holcomb, Luiz Leal, Farzad Rahnema, Dorothea Wiarda, and Goran Arbanas, "Reconstructing Double-Differential and Energy Energy-Differential Resonance Cross-Sections Using the R-Matrix Limited Formalism in the AMPX Code," *Trans. Am. Nucl. Soc*. **111**, 887–890 (2014).

4. Vladimir Sobes, Luiz Leal, and Goran Arbanas, "Nuclear Data Adjustment with SAMMY Based on Integral Experiments," *Trans. Am. Nucl. Soc*. **111**, 843–845 (2014).

5. L. Leal, V. Sobes, M. Pigni, K. Guber, G. Arbanas, D. Wiarda, M. Dunn, E. Ivanov, T. Ivanova, and E. Letang, "ORNL NuclearData Evaluation Accomplishments for FY 2014," *Trans. Am. Nucl. Soc*. **111**, 780–783 (2014).

6. Vladimir Sobes, Luiz Leal, and Goran Arbanas, "User's Guide to SAMINT: A Code for Nuclear Data Adjustment with SAMMY Based on Integral Experiments," ORNL/TM-2014/245, August 2014.

7. P. Pereslavtsev, U. Fischer, A. Konobeyev, V. Sobes, L. Leal, "New Evaluation of n+^{63,65}Cu Nuclear Cross Section Data up to 200 MeV Neutron Energy" Nuclear Data Sheets Volume 118, April 2014, Pages 158–160.

8. M. T. Pigni, L. C. Leal, M. E. Dunn, K. H. Guber, A. Trkov, G. Žerovnik, F. Emiliani, S. Kopecky, C. Lampoudis, P. Schillebeeckx, P. Siegler, "Evaluation of Tungsten Neutron Cross Sections in the Resolved Resonance Region," Nuclear Data Sheets Volume 118, April 2014, pages 118-147.

9. Gašper Žerovnik, Andrej Trkov, and Luiz C. Leal, "Challenges and solutions for random sampling of parameters with extremely large uncertainties and analysis of the 232Th resonance covariances," Nuclear Instruments and Methods in Physics Research Section A Accelerators Spectrometers Detectors and Associated Equipment April 2014, Volume 74, pages 339–343.

10. L. Leal, A. Kahler, G. Noguere, O. Bouland, and Y. Penneliau, "Resonance Evaluations of ^{235}U for the CIELO Project," *NEMEA-7/CIELO – International Collaboration on Nuclear Data*, Geel, Belgium, November 5-8, 2013.

11. L. Leal, R. Sayer, A. Kahler, R. MacFarlane, and T. Ivanova, "Resonance Evaluations for ^{56}Fe, and ^{16}O for the CIELO Project," *NEMEA-7/CIELO – International Collaboration on Nuclear Data*, Geel, Belgium, November 5-8, 2013.

12. L. Leal, A. Kahler, G. Noguere, and T. Iavanova, "Overview of the Resonance Evaluations for ^{16}O, ^{56}Fe, ^{235}U, and ^{239}Pu for the CIELO Project," *NEMEA-7/CIELO – International Collaboration on Nuclear Data*, Geel, Belgium, November 5-8, 2013.

13. B. A. Khuwaileh, G. Arbanas, M. L. Williams, L. C. Leal, H. Abdel-Khalik, and M. E. Dunn, "The Effect of Implicit Self-Shielding on the Inverse Sensitivity/Uncertainty Method for Thermal Reactors," *Trans. Am. Nucl. Soc.* **109**, 804-807 (2013).

14. G. Arbanas, B. A. Khuwaileh, M. Williams, L. C. Leal, M. E. Dunn, and H. S. Abdel-Khalik, "Integral Benchmark Experiments in the Inverse Sensitivity/Uncertainty Computations," *Trans. Am. Nucl. Soc*. **109**, 808-811 (2013).

15. V. Sobes, L. Leal, and B. Forget, "Coupled Differential and Integral Data Analysis for Improved Uncertainty Quantification," in *Proceedings of the 2013 ANS Winter Meeting and Nuclear Technology Expo*, Washington, D.C., November 10-14, 2013.

16. M. T. Pigni, L. C. Leal, M. E. Dunn, K. H. Guber, F. Emiliani, S. Kopecky, C. Lampoudis, P. Schillebeeckx, and P. Siegler, "Evaluation of Tungsten Neutron Cross Sections in the Resolved Resonance Region," *International Conference on Nuclear Data for Science and Technology (ND 2013)*, New York, New York, March 4-8, 2013.

17. V. Sobes, L. Leal, K. Guber, B. Forget, S. Kopecky, P. Schillebeeckx, and P. Siegler, "New Resolved Resonance Region Evaluation for ^{63,65}Cu for Nuclear Criticality Safety Program," *International Conference on Nuclear Data for Science and Technology (ND 2013)*, New York, New York, March 4-8, 2013.

18. L. C. Leal, G. Noguere, C. de Saint Jean, and A. C. Kahler, "^{239}Pu Resonance Evaluation for Thermal Benchmark System Calculations," *International Conference on Nuclear Data for Science and Technology (ND 2013)*, New York, New York, March 4-8, 2013.

19. L. C. Leal, Y. Danon, D. Williams, and M. Jandel, "^{235}U Resolved Resonance Evaluation for Benchmark Calculations in the Intermediate Energy Region," in *Proceedings of the 2013 ANS Annual Meeting*, Atlanta, Georgia, June 16-20, 2013.

20. L. Leal et al., "ORNL Resolved Resonance Covariance Generation for ENDF/B-VII.1," Nuclear Data Sheets, **113**, 3101-3119, November 2012.

21. L. Leal, R. MacFarlane, A. Plompen, A. Negret, and C. Borcea, "^{56}Fe Resonance Evaluation Up to 1.5 MeV," *WINS 2012*, Boston, Massachusetts, September 17-19, 2012.

22. M. E. Dunn, L. C. Leal, K. H. Guber, G. Arbanas, D. Wiarda, R. O. Sayer, H. Derrien, and J. Harvey, "Resonance Region Cross-Section Data Advancements for Nuclear Criticality Safety Applications," in *Proceedings of ICNC 2011*, Edinburgh, U.K., September 19-22, 2011.

23. K. H. Guber, L. C. Leal, C. Lampoudis, S. Kopecky, P. Schillebeeckx, F. Emiliani, R. Wynants, and P. Siegler, "New Improved Nuclear Data for Nuclear Criticality and Safety," in *Proceedings of ICNC 2011*, Edinburgh, U.K., September 19-22, 2011.

24. L. C. Leal, K. H. Guber, G. Arbanas, D. Wiarda, P. E. Koehler, and A. Kahler, "Resonance Evaluation of ^{48}Ti Including Covariance for Criticality Safety Applications," in *Proceedings of ICNC 2011*, Edinburgh, U.K., September 19-22, 2011.

25. G. Arbanas, M. E. Dunn, N. M. Larson, L. C. Leal, M. L. Williams, B. Becker, and R. Dagan, "Computation of Temperature-Dependent Legendre Moments of a Double-Differential Elastic Cross Section," in *Proceedings of the International Conference on Mathematics and Computational Methods Applied to Nuclear Science and Engineering (M&C 2011)*, Rio de Janeiro, Brazil, May 8-12, 2011.

26. L. Leal and K. Shibata, *Assessment of the Unresolved Resonance Treatment for Cross-section and Covariance Representation*, Nuclear Science/NEA/WPEC-32, NEA/NSC/WPEC/DOC(2011)430, a report by the working Party of International Evaluation Co-operation of the NEA Nuclear Science Committee, Nuclear Energy Agency, Organisation for Economic Co-operation and Development, April 2011.

27. L. C. Leal, C. De Saint Jean, and G. Noguere, "Comparison of Resonance Parameter Covariance Generation Using CONRAD and SAMMY Computer Codes," *Trans. Am. Nucl. Soc*. **102**, 506-508 (2010).

28. K. H. Guber, H. Derrien, L. C. Leal, G. Arbanas, D. Wiarda, P. Koehler, and J. A. Harvey, "Astrophysical Reaction Rates for ^{58,60}Ni(n,γ) from New Neutron Capture Cross Section Measurements," *Phys. Rev. C* **82**, 057601 (2010).

29. B. Habert, C. De Saint Jean, L. C. Leal, and Y. Rugama, "Retroactive Generation of Covariance Matrix of Nuclear Model Parameters Using Marginalization Techniques," *Nucl. Sci. Eng.* **166**(3), 276-287, November 2010.

30. L. C. Leal, H. Derrien, C. De Saint Jean, G. Noguere, and J. M. Ruggieri, "Covariance Generation using CONRAD and SAMMY Computer Codes," in *Proceedings of Wonder 2009–2nd International Workshop on Nuclear Data Evaluation for Reactor Applications*, Cadarache, France, September 29-October 2, 2009.

31. H. Derrien, L. C. Leal, K. H. Guber, D. Wiarda, and G. Arbanas, "Reevaluation of ^{58}Ni and ^{60}Ni Resonance Parameters in the Energy Range Thermal to 800 keV" in *Proceedings of Wonder 2009–2nd International Workshop on Nuclear Data Evaluation for Reactor Applications*, Cadarache, France, September 29-October 2, 2009.

32. H. Derrien, L. C. Leal, and N. M. Larson, "R-Matrix Analysis of ^{238}U High Resolution Neutron Transmissions and Capture Cross Sections in the Energy Range 0 keV to 20 keV," *Nucl. Sci. Eng.* **161**(2), 131-159, February 2009.

33. L. C. Leal, G. Arbanas, H. Derrien, and D. Wiarda, "Resonance Region Covariance Analysis Method and New Covariance Data for Th-232, U-233, U-235, U-238, and Pu-239, *Nuclear Data Sheets* **109**(12), 2868-2873, December 2008.

34. A. Trkov, R. Capote, I. Kodeli, and L. C. Leal, "Evaluation of Tungsten Nuclear Reaction Data with Covariances," *Nuclear Data Sheets* **109**(12), 2905-2909, December 2008.

35. D. Wiarda, G. Arbanas, L. C. Leal, and M. E. Dunn, "Recent Advances with the AMPX Covariance Processing Capabilities in PUFF-IV," *Nuclear Data Sheets* **109**(12), 2791-2795, December 2008.

36. H. Derrien, L. C. Leal, and N. M. Larson, "R-Matrix Analysis of ^{232}Th Neutron Transmissions and Capture Cross Sections in the Energy Range Thermal to 4 keV," *Nucl. Sci. Eng*. **160**(2), 149-167, October 2008.

37. H. Derrien, L. C. Leal, N. M. Larson, K. H. Guber, D. Wiarda, and G. Arbanas, "Neutron Resonance Parameters of ^{55}Mn from Reich-Moore Analysis of Recent Experimental Neutron Transmission and Capture Cross Sections," in *Proceedings of PHYSOR 2008 – International Conference on the Physics of Reactor*, Interlaken, Switzerland, September 14-19, 2008.

38. L. C. Leal, D. Mueller, G. Arbanas, D. Wiarda, H. Derrien, "Impact of the ^{235}U Covariance Data in Benchmark Calculations," in *Proceedings of PHYSOR 2008 – International Conference on the Physics of Reactor*, Interlaken, Switzerland, September 14-19, 2008.

39. H. Derrien, L. C. Leal, and N. M. Larson, *Neutron Resonance Parameters and Covariance Matrix of ^{239}Pu*, ORNL/TM-2008/123, Oak Ridge National Laboratory, Oak Ridge, Tenn., August 2008.

40. K. H. Guber, D. Wiarda, L. C. Leal, H. Derrien, C. Ausmus, D. Brashear, and J. A. White, "New Neutron-Induced Cross-Section Measurements for Weak s-process Studies," NIC X_214.pdf in *Proceedings of Science, 10th Symposium on Nuclei in the Cosmos*, Mackinac Island, Michigan, July 27–August 1, 2008.

41. L. C. Leal and C.-S. Gil, "Comparison of the Uncertainties of k_{eff} Using the Recently Developed Covariance Data," *Trans. Am. Nucl. Soc*. **98**, 207–208 (2008).

42. L. C. Leal, D. Wiarda, and G. Arbanas, "Covariance Representation in the Resonance Region: Application to ^{233}U," *Trans. Am. Nucl. Soc*. **98**, 651–653 (2008).

43. L. C. Leal, D. Wiarda, B. T. Rearden, and H. Derrien, *^{233}U Cross-Section and Covariance Data Update for SCALE 5.1 Libraries*, ORNL/TM-2007/115, Oak Ridge National Laboratory, Oak Ridge, Tenn., January 2008.

44. M. E. Dunn, G. Arbanas, L. C. Leal, and D. Wiarda, "Approximating large resonance parameter covariance matrices with group-wise covariance matrices for advanced nuclear fuel cycle applications," p. 139-142, NEMEA-4—Neutron Measurements, Evaluations and Applications, Nuclear Data Needs for Generation IV and Accelerator Driven Systems, in *Proceedings of the CANDIDE Workshop*, October 16–18, 2007, Prague, Czech Republic (January 2008).

45. L. C. Leal, H. Derrien, M. E. Dunn, and D. Mueller, *Assessment of Fission Product Cross-Section Data for Burnup Credit Applications*, ORNL/TM-2005/065, Oak Ridge National Laboratory, Oak Ridge, Tenn., December 2007.

46. C. Myers, B. L. Kirk, and L. C. Leal, "Comparative Analysis of Nuclear Cross Sections in Monte Carlo Methods for Medical Physics Applications," in *Proceedings of the Computational Medical Physics Working Group Workshop II*, Gainesville, FL, September 30-October 3, 2007.

47. L. Leal, R. Westfall, D. Eghbali, and F. Trumble, "Assessment of Titanium Cross Sections and Uncertainties for Application in Criticality Safety," p. 50–52 in *Proceedings of the 8th International Conference on Nuclear Criticality Safety (ICNC 2007)*, Vol. II, St. Petersburg, Russia, May 28–June 1, 2007.

48. L. Leal, H. Derrien, N. Larson, G. Arbanas, and R. Sayer, "ORNL Methodology for Covariance Generation for Sensitivity/Uncertainty Analysis," p. 25–29 in *Proceedings of the 8th International Conference on Nuclear Criticality Safety (ICNC 2007)*, Vol. II, St. Petersburg, Russia, May 28–June 1, 2007.

49. R. Capote, A. Trkov, I. Kodeli, E. Soukhovitskii, L. C. Leal, M. Herman, and D. Muir, "Evaluation of Cross Sections of Tungsten Isotopes Including Covariance Estimation," in *Proceedings of International Conference on Nuclear Data for Science and Technology (ND 2007)*, Nice, France, April 22–27, 2007.

50. H. Derrien, L. C. Leal, and N. M. Larson, "^{239}Pu Neutron Resonance Parameters Revisited and the Covariance Matrix in the Neutron Energy Range Thermal to 2.5 keV," in *Proceedings of International Conference on Nuclear Data for Science and Technology (ND-2007)*, Nice, France, April 22–27, 2007.

51. M. E. Dunn, N. M. Larson, H. Derrien, and L. C. Leal, "Perspective on Advances in Resonance-Region Nuclear Modeling and Opportunities for Future Research," invited paper in *Proceedings of International Conference on Nuclear Data for Science and Technology (ND 2007)*, Nice, France, April 22–27, 2007.

52. K. H. Guber, P. Koehler, D. Wiarda, J. A. Harvey, T. E. Valentine, R. O. Sayer, L. C. Leal, N. M. Larson, and T. S. Bigelow, "New Neutron Cross-Section Measurements from ORELA and New Resonance Parameter Evaluations," in *Proceedings of International Conference on Nuclear Data for Science and Technology (ND 2007)*, Nice, France, April 22–27, 2007.

53. N. M. Larson, L. C. Leal, R. O. Sayer, H. Derrien, D. Wiarda, and G. Arbanas, "Current Status of the R-Matrix Code SAMMY, with Emphasis on the Relationship to ENDF Formats," in *Proceedings of International Conference on Nuclear Data for Science and Technology (ND 2007)*, Nice, France, April 22–27, 2007.

54. L. C. Mihailescu, I. Sirakov, R. Capote, A. Borella, K. H. Guber, S. Kopecky, L. C. Leal, P. Schillebeeckx, P. Siegler, R. Wynants, and E. Soukhovitskii, "Evaluation of the ^{103}Rh Neutron Cross Section Data in the Unresolved Resonance Region for Improved Criticality Safety," in *Proceedings of International Conference on Nuclear Data for Science and Technology (ND 2007)*, Nice, France, April 22–27, 2007.

55. L. Leal and H. Derrien, "Evaluation of ^{231}Pa and ^{233}Pa Resonance Parameters and Covariance in the Resolved Resonance Region," *Trans. Am. Nucl. Soc*. **95**, 768–769 (2006).

56. D. Wiarda, M. E. Dunn, N. M. Larson, and L. C. Leal, "Processing of ENDF/B-VII Covariance Data for Use of Sensitivity/Uncertainty Analysis," *Trans. Am. Nucl. Soc*. **95**, 290–291 (2006).

57. H. Derrien, L. C. Leal, and N. M. Larson, *Evaluation of ^{232}Th Neutron Resonance Parameters in the Energy Range 0 keV to 4000 keV*, ORNL/TM-2006/53, Oak Ridge National Laboratory, Oak Ridge, Tenn., October 2006.

58. L. Leal, H. Derrien, G. Arbanas, N. Larson, and D. Wiarda, "Covariance Data for ^{232}Th in the Resolved Resonance Region 0 to 4 keV," in *Proceedings of PHYSOR 2006*, American Nuclear Society Topical Meeting on Reactor Physics: Advances in Nuclear Analysis and Simulation, Vancouver, British Columbia, Canada, September 10–14, 2006.

59. G. Arbanas, L. C. Leal, N. M. Larson, and H. Derrien, "Retroactive Covariance Matrix for 235U in the Resolved-Resonance Region," in *Proceedings of PHYSOR 2006*, American Nuclear Society Topical Meeting on Reactor Physics: Advances in Nuclear Analysis and Simulation, Vancouver, British Columbia, Canada, September 10–14, 2006.

60. H. Derrien, L. C. Leal, and N. M. Larson, "New Evaluation of the ^{232}Th Neutron Resonance Parameters in the Energy Range 0 to 4000 keV," in *Proceedings of PHYSOR 2006*, American Nuclear Society Topical Meeting on Reactor Physics: Advances in Nuclear Analysis and Simulation, Vancouver, British Columbia, Canada, September 10–14, 2006.

61. D. Wiarda, M. E. Dunn, N. M. Greene, N. M. Larson, and L. C. Leal, "New Capabilities for Processing Covariance Data in Resonance Region," in *Proceedings of PHYSOR 2006*, American Nuclear Society Topical Meeting on Reactor Physics: Advances in Nuclear Analysis and Simulation, Vancouver, British Columbia, Canada, September 10–14, 2006.

62. K. H. Guber, L. C. Leal, R. O. Sayer, P. E. Koehler, D. Wiarda, T. E. Valentine, H. Derrien, J. A. Harvey, S. Kopecky, P. Siegler, P. Schillebeeckx, R. Wynants, I. Ivanov, A. Borella, R. Nelson, M. Devlin, and N. Fotiadis, "New Neutron Cross-Section Measurements on ^{19}F, ^{39,41}K, ^{55}Mn, and ^{103}Rh for Improved Nuclear Criticality Safety," C033.pdf in *Proceedings of PHYSOR 2006*, American Nuclear Society Topical Meeting on Reactor Physics: Advances in Nuclear Analysis and Simulation, Vancouver, British Columbia, Canada, September 10–14, 2006.

63. M. Herman, P. Oblozinsky, D. Rochman, T. Kawano, and L. Leal, "Fast Neutron Covariances for Evaluated Data Files," in *Proceedings of PHYSOR 2006*, American Nuclear Society Topical Meeting on Reactor Physics: Advances in Nuclear Analysis and Simulation, Vancouver, British Columbia, Canada, September 10–14, 2006.

64. N. M. Larson, L. C. Leal, H. Derrien, G. Arbanas, R. O. Sayer, and D. Wiarda, "A Systematic Description of the Generation of Covariance Matrices," in *Proceedings of PHYSOR 2006*, American Nuclear Society Topical Meeting on Reactor Physics: Advances in Nuclear Analysis and Simulation,Vancouver, British Columbia, Canada, September 10–14, 2006.

65. R. O. Sayer, K. H. Guber, L. C. Leal, N. M. Larson, and T. Rauscher "R-Matrix Analysis of C1 Neutron Cross Sections up to 1.2 MeV," *Phys. Rev. C* **73**, 044603 (2006).

66. K. H. Guber, L. C. Leal, R. O. Sayer, P. E. Koehler, H. Derrien, D. Wiarda, and J. A. Harvey, "Neutron Cross-Section Measurements at ORELA," pp. 25–34 in *Proceedings of the Oak Ridge Electron Linear Accelerator (ORELA) Workshop*, held at Oak Ridge National Laboratory, Oak Ridge, Tennessee, July 14–15, 2005; ORNL/TM-2005/272, comp. Michael E. Dunn, Oak Ridge National Laboratory, Oak Ridge, Tenn., February 2006.

67. L. C. Leal, G. Arbanas, H. Derrien, N. M. Larson, and B. Rearden, "Covariance Data for ^{233}U in the Resolved Resonance Region for Criticality Safety Applications," 262.pdf in *Proceedings of M&C 2005 International Topical Meeting on Mathematics and Computation, Supercomputing, Reactor Physics and Nuclear and Biological Applications*, Palais Des Papes, Avignon, France, September 12–15, 2005, on CD-ROM, American Nuclear Society, LaGrange Park, Illinois (2005).

68. A. Courcelle, H. Derrien, L. Leal, and N. Larson, "Analysis of the ^{238}U Resonance Parameters Using Random-Matrix Theory," 167.pdf in *Proceedings of M&C 2005 International Topical Meeting on Mathematics and Computation, Supercomputing, Reactor Physics and Nuclear and Biological Applications*, Palais Des Papes, Avignon, France, September 12–15, 2005, on CD-ROM, American Nuclear Society, LaGrange Park, Illinois (2005).

69. L. C. Leal, H. Derrien, N. M. Larson , and A. Courcelle, "An Unresolved Resonance Evaluation for ^{233}U from 600 eV to 40 keV," *Trans. Am. Nucl. Soc*. **92**, 665–666 (June 2005).

70. G. Arbanas, L. C. Leal, and N. M. Larson, "Impact of Missing Resonances in Determining Group Cross Sections and Uncertainties," *Trans. Am. Nucl. Soc*. **92**, 672–673 (June 2005). C. S. Melhus, M. S. Rivard, B. L. Kirk, and L. C. Leal, "Clinical Brachytherapy Dosimetry Parameters and Mixed-Field Dosimetry for a High Rate CF-252 Brachytherapy Source," in *Proceedings of The Monte Carlo 2005 Topical Meeting, The Monte Carlo Method: Versatility Unbounded in a Dynamic Computing World*, Chattanooga, Tennessee, April 17–21, 2005; on CD-ROM, American Nuclear Society, LaGrange Park, Illinois (2005).

71. C. S. Melhus, M. S. Rivard, B. L. Kirk, and L. C. Leal, "Storage Safe Shielding Assessment for a HDR Californium-252 Brachytherapy Source," usr-cmelhus-1-paper.pdf in *Proceedings of The Monte Carlo 2005 Topical Meeting, The Monte Carlo Method: Versatility Unbounded in a Dynamic Computing World*, Chattanooga, Tennessee, April 17–21, 2005; on CD-ROM, American Nuclear Society, LaGrange Park, Illinois (2005).

72. L. C. Leal and H. Derrien, "Statistical Properties of the s- and p-Wave Resonances for ^{238}U," *Trans. Am. Nucl. Soc*. **91**, 566–567 (November 2004).

73. K. H. Guber, L. C. Leal, R. O. Sayer, P. E. Koehler, T. E. Valentine, H. Derrien, and J. A. Harvey, "New Neutron Cross-Section Measurements at ORELA and Their Application in Nuclear Criticality Calculations," presented at the 18th International Conference on the Application of Accelerators in Research and Industry (CAARI), October 10-15, 2004, Ft. Worth, Texas.

74. R. O. Sayer, K. H. Guber, L. C. Leal, and N. M. Larson, "New Resonance Parameter Evaluation of C1 Neutron Cross Sections" pp. 386–389, Vol. 769 in *Proceedings of the International Conference on Nuclear Data for Science and Technology*, Santa Fe, New Mexico, September 26–October 1, 2004.

75. K. Volev, N. Koyumdjieva, A. Brusegan, A. Borella, P. Siegler, N. Janeva, A. Lukyanov, L. Leal, and P. Schillebeechx, "Evaluation of the ^{232}Th Neutron Cross Sections between 4 keV and 140 keV," pp. 87–90, Vol. 769 in *Proceedings of the International Conference on Nuclear Data for Science and Technology*, Santa Fe, New Mexico, September 26–October 1, 2004.

76. L. C. Leal, H. Derrien, K. H. Guber, R. O. Sayer, and N. M. Larson, "Recent Cross-Section Evaluations in the Resonance Region at the Oak Ridge National Laboratory," pp. 332–337, Vol. 769 in *Proceedings of the International Conference on Nuclear Data for Science and Technology*, Santa Fe, New Mexico, September 26–October 1, 2004.

77. L. C. Leal, N. M. Larson, H. Derrien, T. Kawano, and M. B. Chadwick, "A New Approach for Nuclear Data Covariance and Sensitivity Generation," pp. 338–341, Vol. 769 in *Proceedings of the International Conference on Nuclear Data for Science and Technology*, Santa Fe, New Mexico, September 26–October 1, 2004.

78. K. H. Guber, L. C. Leal, R. O. Sayer, P. E. Koehler, T. E. Valentine, H. Derrien, and J. A. Harvey, "New Neutron Cross-Section Measurements at ORELA for Improved Nuclear Data Calculations," pp. 1706–1711, Vol. 769 in *Proceedings of the International Conference on Nuclear Data for Science and Technology*, Santa Fe, New Mexico, September 26–October 1, 2004.

79. H. Derrien, A. Courcelle, L. C. Leal, N. M. Larson, and A. Santamarina, "Evaluation of ^{238}U Resonance Parameters from 0 to 20 keV," pp. 276–281, Vol. 769 in *Proceedings of the International Conference on Nuclear Data for Science and Technology*, Santa Fe, New Mexico, September 26–October 1, 2004.

80. H. Derrien, J. A. Harvey, K. H. Guber, L. C. Leal, and N. M. Larson, *Average Neutron Total Cross Sections in the Unresolved Energy Range from ORELA High Resolution Transmission Measurements*, ORNL/TM-2003/291, Oak Ridge National Laboratory, Oak Ridge, Tenn., May 2004.

81. K. H. Guber, L. C. Leal, R. O. Sayer, P. E. Koehler, T. E. Valentine, H. Derrien and J. A. Harvey, "Neutron Cross-Sections Measurements at ORELA for Improved Nuclear Data and their Application," in *Proceedings of ICRS-10 RPS 2004: 21st Century Challenges in Radiation Protection and Shielding*, Funchal, Madeira Island, Portugal, May 9–14, 2004.

82. R. O. Sayer, K. H. Guber, L. C. Leal, N. M. Larson, and T. Rauscher, "R-Matrix Evaluation of Cl Neutron Cross Sections up to 1.2 MeV," in *Proceedings of ICRS-10 RPS 2004: 21st Century Challenges in Radiation Protection and Shielding*, Funchal, Madeira Island, Portugal, May 9–14, 2004.

83. L. C. Leal, H. Derrien, N. M. Larson, and F. A. Alpan, "Covariance and Sensitivity Data Generation at ORNL," in *Proceedings of ICRS-10 RPS 2004: 21st Century Challenges in Radiation Protection and Shielding*, Funchal, Madeira Island, Portugal, May 9–14, 2004.

84. F. A. Alpan, L. C. Leal, and A. Courcelle, "Effect of Energy Self-Shielding Methods on ^{238}U for Criticality Safety Problems," 95398.pdf in *Proceedings of PHYSOR 2004 - The Physics of Fuel Cycles and Advanced Nuclear Systems: Global Developments*, Chicago, Ill., April 25–29, 2004, on CD-ROM, American Nuclear Society, La Grange Park, Ill. (2004).

85. L. C. Leal, H. Derrien, and N. M. Larson, "An Unresolved Resonance Evaluation for ^{235}U," in *Proceedings of PHYSOR 2004 - The Physics of Fuel Cycles and Advanced Nuclear Systems: Global Developments*, Chicago, Ill., April 25–29, 2004, on CD-ROM, American Nuclear Society, La Grange Park, Ill. (2004).

86. K. H. Guber, L. C. Leal, R. O. Sayer, P. E. Koehler, T. E. Valentine, H. Derrien, and J. A. Harvey, "New Neutron Cross Section Measurements at ORELA for Improved Nuclear Data," in *Proceedings of PHYSOR 2004 - The Physics of Fuel Cycles and Advanced Nuclear Systems: Global Developments*, Chicago, Ill., April 25–29, 2004, on CD-ROM, American Nuclear Society, La Grange Park, Ill. (2004).

87. H. Derrien, L. C. Leal, and N. M. Larson, "Status of a New Evaluation of the Neutron Resonance Parameters of ^{238}U at ORNL," 94991.pdf in *Proceedings of PHYSOR 2004 - The Physics of Fuel Cycles and Advanced Nuclear Systems: Global Developments*, Chicago, Ill., April 25–29, 2004, on CD-ROM, American Nuclear Society, La Grange Park, Ill. (2004).

88. M. J. Rivard, K. E. Evans, L. C. Leal, and B. L. Kirk, "Selective Perturbation of in Vitro Linear Energy Transfer Using High-Z Vaginal Applicators for Cf-252 Brachytherapy," *Nuclear Instruments and Methods in Physics Research Section B: Beam Interaction with Materials and Atoms* **213**, 621-625, January 2004.

89. K. H. Guber, P. E. Koehler, H. Derrien, T. E. Valentine, L. C. Leal, R. O. Syer, and T. Rauscher, "Neutron Capture Reaction Rates for Silicon and Their Impact on the Origin of Presolar Mainstream SiC Grains," *Phys. Rev. C.* **57**(6), 062802, June 2003.

90. L. C. Leal and H. Derrien, "R-Matrix Evaluation of ^{19}F Neutron Cross Sections up to 1 MeV," American Nuclear Society, San Diego, California, June 2003.

91. L. C. Leal, "ORNL Tools for Cross Section Measurements and Evaluation," presented at the Workshop on Nuclear Data Needs for Generation IV Nuclear Energy Systems Brookhaven National Laboratory, Upton, New York April 24-25, 2003.

92. K. H. Guber, P. E. Koehler, H. Derrien, T. E. Valentine, L. C. Leal, R. O. Sayer, and T. Rauscher, "Maxwellian Average Neutron Capture Cross Sections for Silicon and their Impact on the Origin of Presolar Mainstream SiC Grains," *Phys. Rev. C.*

93. F. B. Guimaraes, C. Y. Fu, and L. C. Leal, "Nuclear Cross-Section Calculations in the 1 MeV to 5 GeV Range with Combined Semi-Classical and Quantum Mechanical Models," ORNL/TM-200/191 (ENDF-366), February 2002.

94. C. Y. Fu, F. B. Guimaraes, L. C. Leal, "Combining Intranuclear-Cascade and Preequilibrium Hauser-Feshbach Models for Nuclear Cross-Section Calculations Between 1 MeV and 5GeV," *Nucl. Sci. Eng.* 143, 164-176 (2003).

95. K. H. Guber, L. C. Leal, R. O. Sayer, P. E. Koehler, T. E. Valentine, H. Derrien, and J. A. Harvey, "Neutron Cross Sections Measurements at ORELA for Improved Nuclear Data and Their Applications," in *Proceedings of International Conference on the New Frontiers of Nuclear Technology: Reactor Physics, Safety and High-Performance Computing, PHYSOR 2002*, Seoul, South Korea, October 7-10, 2002.

96. S.-Y. Oh, J. Chang, and L. Leal, "Statistical Assignment of Neutron Orbital Angular Momentum to a Resonance," in *Proceedings of International Conference on the New Frontiers of Nuclear Technology: Reactor Physics, Safety and High-Performance Computing, PHYSOR 2002*, Seoul, South Korea, October 7-10, 2002.

97. M. E. Dunn and L. C. Leal, "Calculating Probability Tables for the Unresolved-Resonance Region Using Monte Carlo Methods," in *Proceedings of International Conference on the New Frontiers of Nuclear Technology: Reactor Physics, Safety and High-Performance Computing, PHYSOR 2002*, Seoul, South Korea, October 7-10, 2002.

98. L. C. Leal, H. Derrien, K. H. Guber, J. A. Harvey, and N. M. Larson, "Evaluation of the ^{233}U Neutron Cross Sections in the Resolved Resonance," in *Proceedings of Energy Range, International Conference on the New Frontiers of Nuclear Technology: Reactor Physics, Safety and High-Performance Computing, PHYSOR 2002*, Seoul, South Korea, October 7-10, 2002.

99. H. Derrien, L. C. Leal, K. H. Guber, T. Valentine, N. M. Larson, and T. Rauscher, *Evaluation of Silicon Neutron Resonance Parameters in the Energy Range Thermal to 1800 keV*, ORNL/TM-2001/271, Oak Ridge National Laboratory, Oak Ridge, Tenn., August 2002

100. K. H. Guber, R. O. Sayer, T. E. Valentine, L. C. Leal, R. R. Spencer, P. E. Koehler, J. A. Harvey, and T. Rauscher, "New Maxwellian Average Neutron Capture Cross Sections for ^{35,37}Cl," *Phys. Rev. C* **65**, April 2002.

101. L. C. Leal, K. H. Guber, R. R. Spencer, H. Derrien, and R. Q. Wright, "Aluminum Data Measurements and Evaluation for Criticality Safety Applications," SNS Workshop, Oak Ridge, TN, March 2002.

102. M. J. Rivard, K. E. Evans , L. C. Leal , B. L. Kirk, "Selective Perturbation of in vivo Linear Energy Transfer Using High-Z Vaginal Applicators for Cf-252 Brachytherapy," in *Proceedings 5th Industrial Radiation and Radioisotope Measurement Applications (IRRMA-V)*, Bologna, Italy, June 9-14, 2002, *Beam Interactions with Materials and Atoms Section B of Nuclear Instruments & Methods in Physics Research.*

103. H. Derrien, K. Guber, J. Harvey, N. Larson, and L. Leal, "Average Cross Section of ^{233}U, ^{235}U, and ^{239}Pu from ORELA Transmission Measurements and Statistical Model Analysis of the Data," Nuclear Science and Technology, in *Proceedings of the International Conference on Nuclear Data for Science and Technology*, Tsukuba, Ibaraki, Japan, October 7-12, 2001.

104. R. Sayer, L. Leal, N. Larson, R. Spencer, and R. Q. Wright, "R-Matrix Evaluation of ^{16}O Cross Sections up to 6.3 MeV," Nuclear Science and Technology, in *Proceedings of the International Conference on Nuclear Data for Science and Technology*, Tsukuba, Ibaraki, Japan, October 7-12, 2001.

105. K. Guber, L. Leal, R. Sayer, R. Spencer, P. Koehler, T. Valentine, H. Derrien, and J. Harvey, "Neutron Cross Sections Measurements for Light Elements at ORELA and their Application in Nuclear Criticality," Nuclear Science and Technology, in *Proceedings of the International Conference on Nuclear Data for Science and Technology*, Tsukuba, Ibaraki, Japan, October 7-12, 2001.

106. K. Guber, P. Koehler, T. Valentine, and L. Leal, "Neutron Cross Section Measurements at the Spallation Neutron Source," Nuclear Science and Technology, in *Proceedings of the International Conference on Nuclear Data for Science and Technology*, Tsukuba, Ibaraki, Japan, October 7-12, 2001.

107. C. Y. Fu, F. B. Guimaraes, and L. Leal, "Combining Semi-Classical and Quantum Mechanical Methodologies for Nuclear Cross-Sections Calculations between 1 MeV and 5 GeV," Nuclear Science and Technology, in *Proceedings of the International Conference on Nuclear Data for Science and Technology*, Tsukuba, Ibaraki, Japan, October 7-12, 2001.

108. L. Leal, H. Derrien, N. Larson, K. Guber, T. Valentine, and R. Sayer, "Nuclear Data Measurements, Analysis and Evaluation at the Oak Ridge National Laboratory in Support of Nuclear Criticality Safety," Nuclear Science and Technology, in *Proceedings of the International Conference on Nuclear Data for Science and Technology*, Tsukuba, Ibaraki, Japan, October 7-12, 2001.

109. L. C. Leal, "Data Analysis and Evaluation with SAMMY," in *Proceedings of the Workshop "Nuclear Reaction Data and Nuclear Reactors: Physics, Design and Safety,"* Vol. I and II, ICTP, Trieste, Italy, eds. N. Paver, M. Herman, A. Gandini (2001). Vol. I: Theory and Practice in Nuclear Data Evaluation.

110. C. Y. Fu, F. B. Guimaraes, and L. Leal, *Combining Semi-Classical and Quantum Mechanical Methodologies for Nuclear Cross-Sections Calculations between 1 MeV and 5 GeV*, ORNL/TM-2001/191 (ENDF-366), Oak Ridge National Laboratory, Oak Ridge, Tenn. (2001).

111. H. Derrien, J. A. Harvey, N. M. Larson, L. C. Leal, and R. Q. Wright, *Neutron Total Cross Sections of ^{235}U from Transmission Measurements in the Energy Range 2 kev to 300 kev and Statistical Model Analysis of the Data*, ORNL/TM-2000/129, Oak Ridge National Laboratory, Oak Ridge, Tenn. (2000).

112. K. H. Guber, L. C. Leal, R. O. Sayer, R. R. Spencer, P. E. Koehler, T. A. Valentine, H. Derrien, J. Andrzejewski, Y. M. Gledenov, and J. A. Harvey, "Neutron Cross Sections Measurements for Light Elements at ORELA and Their Application in Nuclear Criticality and Astrophysics," *World Scientific* (2000).

113. R. O. Sayer, L. C. Leal, N. M. Larson, R. R. Spencer, and R. Q. Wright, *R-Matrix Evaluation of ^{16}O Neutron Cross Sections up to 6.3 MeV*, ORNL/TM-2000/212, Oak Ridge National Laboratory, Oak Ridge, Tenn. (2000).

114. R. Q. Wright, L. C. Leal, H. Derrien, N. M. Larson, and W. C. Jordan, "Data Testing of the ORNL Aluminum Evaluation," ANS Annual Meeting (2000).

115. L. C. Leal, H. Derrien, and N. M. Larson, "Nuclear Data Evaluation for Reactor Applications," ANS Annual Meeting, Milwaukee, Wisconsin, June 2001.

116. L. C. Leal, O. W. Hermann, S. M. Bowman, and C. V. Parks, "Automatic Rapid Process for the Generation of Problem-Dependent SAS2H/ORIGEN-S Cross-Section Libraries," *Nucl. Technol.* **127**, 1, July 1999. Also as ORNL/TM 13584.

117. L. C. Leal, H. Derrien, N. M. Larson, and R. Q. Wright, "R-Matrix Analysis of ^{235}U Neutron Transmission and Cross-Section Measurements in the 0- to 2.25-keV Energy Range," *Nucl. Sci. Eng.* **131**, 230, February 1999. Also as ORNL/TM 13516.

118. L. C. Leal, N. M. Larson, D. C. Larson and D. M. Hetrick, "R-Matrix Evaluation of ^{28}Si, ^{29}Si, ^{30}Si up to 1.8 MeV," in *Proceedings of International Conference on Nuclear Data for Science and Technology*, Part I, p. 929, Trieste, Italy, May 19-24, 1997.

119. L. C. Leal, H. Derrien, and N. M. Larson, "Statistical Properties of the S-wave Resonances of ^{235}U," in *Proceedings of International Conference on Nuclear Data for Science and Technology*, Part I, p. 864, Trieste, Italy, May 19-24, 1997.

120. L. C. Leal, O. W. Hermann, J. C. Ryman, and B. L. Broadhead, "An Alternative to the SAS2H/ORIGEN-S Sequence to Account for Water-Density Effects in BWR Systems," American Nuclear Society/European Nuclear Society International Meeting, Washington, DC, November 10-14, 1997.

121. O. Bouland, H. Derrien, N. M. Larson, and L. C. Leal, "R-Matrix Analysis of the ^{240}Pu Neutron Cross Sections in the Thermal to 5700 eV Energy Range," *Nucl. Sci. Eng.* **127**, 105, October 1997.

122. H. Derrien, N. M. Larson, and L. C. Leal, *Covariance Matrices for Use in Criticality Safety Predictability Studies*, ORNL/TM-13492, Oak Ridge National Laboratory, Oak Ridge, Tenn., September 1997.

123. D. M. Hetrick, D. C. Larson, N. M. Larson, L. C. Leal, and S. J. Epperson, *Evaluation of ^{28,29,30}Si Neutron Induced Cross Sections for ENDF/B-VI*, ORNL/TM-11825, Oak Ridge National Laboratory, Oak Ridge, Tenn., April 1997.

124. L. C. Leal and R. Q. Wright, *Assessment of the Available ^{233}U Cross-Section Evaluation in the Calculation of Critical Benchmark Experiments*, ORNL/TM-13313, Oak Ridge National Laboratory, Oak Ridge, Tenn., October 1996.

125. L. C. Leal, R. R. Spencer, D. T. Ingersoll and T. A. Gabriel, "Assessment of the Neutron Cross-Section Database for Mercury for the ORNL Spallation Source," in *Proceedings of International Workshop on the Technology and Thermal Hydraulics of Heavy Liquid Metals, Schurns*, Montafon Valley, Austria, March 25-28, 1996.

126. R. Q. Wright, L. C. Leal and J. M. Rammsy, "Data Testing of ORNL ^{235}U Evaluation," American Nuclear Society Annual Meeting, Reno, Nevada, June 16-20, 1996.

127. L. C. Leal, R. Q. Wright and J. M. Rammsy, "Self-Shielded Reaction-Rate Calculations for ^{235}U from 0 to 2250 eV," American Nuclear Society Annual Meeting, Reno, Nevada, June 16-20, 1996.

128. L. C. Leal and N. M Larson, *SAMDIST: A Computer Code for Calculating Statistical Distributions for R-Matrix Resonance Parameters*, ORNL/TM-13092, Oak Ridge National Laboratory, Oak Ridge, Tenn., September 1995.

129. J. M. Rammsy, L. C. Leal, and N. M. Greene, "Resonance Integral Generated Using the Multipole Approach," American Nuclear Society Winter Meeting, San Francisco, CA, November 1995.

130. L. C. Leal, N. M. Larson, and H. Derrien, "Re-evaluation of the ^{235}U Cross Section for ENDF/B-VI," American Nuclear Society Winter Meeting, San Francisco, CA, November 1995.

131. O. Bouland, H. Derrien, N. M. Larson, and L. C. Leal, "Reich-Moore Evaluation of the ^{240}Pu Resonance Parameters," American Nuclear Society Winter Meeting, San Francisco, CA, November 1995.

132. L. C. Leal, J. R. Deen, and W. L. Woodruff, "Validation of the WIMSD4M Cross-Section Generation Code with Benchmark Results," in *Proceedings of International Conference on Mathematics and Computations, Reactor Physics, and Environment Analyses*, Portland, Oregon, May 1995.

133. J. Vujic, E. Greenspan, S. Slater, T. Postma, L. Leal, G. Casher, and I. Soares, "Development of Coupled SCALE4.2/GTRAN2 Computational Capability for Advanced MOX Fueled Assembly Designs," in *Proceedings of International Conference on Mathematics and Computations, Reactor Physics, and Environment Analyses*, Portland, Oregon, May 1995.

134. L. C. Leal, O. W. Hermann, and C. V. Parks, "Automatic Rapid Processing Cross-Section Libraries for the Prediction of PWR Spent Fuel Isotopic Composition," in *Proceedings of International Conference on Mathematics and Computations, Reactor Physics, and Environment Analyses*, Portland, Oregon, May 1995.

135. L. C. Leal, "Revision and Reevaluation of the ^{235}U Cross Sections for ENDF/B-VI to Address Integral Data Measurements," ENFIR/ENAN Joint Conferences, Aguas de Lindoia, Brazil, August 1995.

136. L. C. Leal, R. M. Westfall, W. C. Jordan, and R. Q. Wright, "Nuclear Data Needs for Application in Nuclear Criticality Safety Programs," in *Proceedings of the Fifth International Conference on Nuclear Criticality Safety*, Albuquerque, New Mexico, September 1995.

137. L. C. Leal, O. W. Hermann, and C. V. Parks, "ARP: A PC-Compatible Scheme for Generating ORIGEN-S Cross Section Library," in *Proceedings of Sixth Annual International Conference, High Level Radioactive Waste Management*, Las Vegas, Nevada, April 30-May 5, 1995.

138. L. C. Leal, O. W. Hermann, and C. V. Parks, "Automatic Rapid Processing SCALE/SAS2H Produced Parameter-Dependent Cross Sections for ORIGEN-S," American Nuclear Society, Annual Meeting, New Orleans June 1994.

139. L. C. Leal, R. N. Hill and H. S. Khalil, "An Evaluation of Neutron and Gamma Heating in Fission Product Isotopes," American Nuclear Society Annual Meeting, San Diego, CA, 1993.

140. L. C. Leal, T A. Daly, J. R. Liaw and E. K. Fujita, "Neutron Source From Spontaneous Fission and ($\boldsymbol{\alpha}$,n) Reactions in Mixture," American Nuclear Society Winter Meeting, San Francisco, CA, November 1991.

141. L. C. Leal, G. de Saussure and R. B. Perez, "An R-Matrix Analysis of the ^{235}U Neutron Induced Cross Sections up to 500 eV," *Nucl. Sci. Eng*. **103**, 1-17 (1991).

142. L. C. Leal, R. N. Hwang and C. G. Stenberg, "Computation of Multiple Parameters Using Preliminary ENDF/B-VI Data," American Nuclear Society Winter Meeting, Washington, DC, November 1990.

143. L. C. Leal, "Resonance Analysis and Evaluation of the ^{235}U Neutron Induced Cross Sections," Ph.D. Thesis, presented to the Nuclear Engineering Department of The University of Tennessee, Knoxville, TN; April 1990; also published as ORNL/TM-11547.

144. L. C. Leal, G. de Saussure and R. B. Perez, "Calculation of Resonance Self-shielding in ^{235}U," American Nuclear Society Annual Meeting, Nashville, Tenn. (1990).

145. G. de Saussure, L. C. Leal and R. B. Perez, Reich-Moore and Adler-Adler Representation of the ^{235}U Cross Sections in the Resolved Resonance Region," in *Proceedings of International Conference on Physics of Reactors: Operation, Design, and Computation*, Marseille-France, April 23-26, 1990.

146. L. C. Leal, G. de Saussure and R. B. Perez, *URR Computer Code: A Code to Calculate Resonance Neutron Cross-Section Probability Tables, Bondarenko Self- Shielding Factors, and Self-Shielding Ratios for Fissile and Fertile Nuclide*, ORNL/TM-11297/R1, Oak Ridge National Laboratory, Oak Ridge, Tenn.

147. L. C. Leal, G. de Saussure, R. B. Perez and R. Q. Wright, "Test of the ENDF/B Unresolved Resonance Formalism for ^{235}U," American Nuclear Society Winter Meeting, San Francisco, CA, 1989.

148. L. C. Leal, G. de Saussure, R. R. Winters and R. B. Perez, "Statistical Properties of the ^{235}U Resonance Parameters up to 300 eV," American Nuclear Society, Atlanta, GA, June 1989.

149. G. de Saussure, L. C. Leal, R. B. Perez, N. M. Larson and M. S. Moore, "A New Resonance-Region Evaluation of Neutron Cross Sections for ^{235}U," *Nucl. Sci. Eng.* **103**, 109-118 (1989).

150. M. S. Moore, L. C. Leal, G. de Saussure, R. B. Perez and N. M. Larson, "Resonance Structure in the Fission of (^{235}U+n)," in *Proceedings of the International Conference Fifty Years Research in Nuclear Fission*, Berlin, Germany, April 1989.

151. L. C. Leal, G. de Saussure, R. B. Perez, "Analysis of the ^{235}U Neutron Cross Sections in the Resolved Resonance Range," *Fifty Years with Nuclear Fission* **2**, 939-945, April 1989.

152. R. B. Perez, G. de Saussure, L. C. Leal and Roger L. Macklin, "On the Unresolved Resonance Region Representation of Neutron Induced Cross Sections," in *Proceedings of the International Reactor Physics Conference*, Jackson Hole, WY, Sept 1988.

153. G. de Saussure, L. C. Leal and R. B. Perez, "A New Resonance-Region Evaluation of Neutron Cross Sections for ^{235}U," in *Proceedings of the International Reactor Physics Conference*, Jackson Hole, WY, Sept 1988.

154. J. A. Harvey, N. W. Hill, F. G. Perey, G. L. Tweed and L. C. Leal, "High-Resolution Neutron Transmission Measurements on ^{235}U, ^{239}Pu, and ^{238}U," in *Proceedings of the International Conference on Nuclear Data for Science and Technology*, Mito, Japan, May 1988.

155. H. Derrien, G. de Saussure, N. M. Larson, L. C. Leal and R. B. Perez, "R-Matrix Analysis of the ^{235}U and ^{239}Pu Neutron Cross Sections," *Proceedings of the International Conference on Nuclear Data for Science and Technology*, Mito, Japan, May 1988.

156. L. C. Leal, G. de Saussure, R. B. Perez, "R-Matrix Analysis of the ^{235}U Neutron Cross Sections," American Nuclear Society, San Diego, CA, June 1988.

157. L. C. Leal and R. N. Hwang, "A Finite Difference Method for Treating the Doppler Broadening of Neutron Cross Sections," American Nuclear Society, Los Angeles, CA, Nov 1987.

158. L. C. Leal, KERNELBUT Computer Code, INIS-BR-028967/1983 (in Portuguese).

159. L.C. Leal, 1DX and Generator Computer Code, INIS-BR-028966/1983 (in Portuguese).

160. L. C. Leal and J. A. W. Nobrega, HAMMER, LITHE and HELP computer code, INIS-BR-028964/1983 (in Portuguese).

161. L. C. Leal and J. A. W. Nobrega, EXTERMINATOR-2 computer code, S-BR-028965/1983 (in Portuguese).

162. J. A. W. Nobrega, C. F. Silva, and L. C. Leal, "Conversion and Implementation of Nuclear Computer Code, INIS-BR- 1 19/1983 1 (in Portuguese).

163. L. C. Leal and J. T. Assis, "Scattering Kernel Computation for Thermal Neutron in H20 and D20," Second Meeting of Reactor Physics, Itaipava/Rio de Janeiro Brazil, April 1981.

164. L. C. Leal, "Utilization of The Nelkin Model in the HAMMER Code for Calculation of Reactor Parameters," M.Sc. Thesis, presented to the Nuclear Engineering Department/COPPE of The Federal University of Rio de Janeiro/Brazil, July 1980 (in Portuguese).

ARGONNE NATIONAL INTRA-LABORATORY MEMOS:

1. L. C. Leal, C. G. Stenberg and K. L. Derstine, "Conversion of Cross Section Processing Codes from IBM to SUN" (# 1), March 1993.

2. L. C. Leal, C. G. Stenberg and C. H. Adams, "Conversion of Binary ISOTXS and PMATRX Files from IBM to SUN," October 1992.

3. L. C. Leal, "Implementation of the MCNP Code Version 4.2 on the SUN Workstation," May 1992.

4. R. N. Hwang and L. C. Leal, "Summary of Recent Development of the MARIA-SHIELD Module for Treating Resonance Absorption in the Annular Cells," April 1992.

5. L. C. Leal, T. A. Daly and J. R. Liaw, "A Method for Computing Neutron Source from Spontaneous Fission and (**α**,n) Reaction in Mixtures," July 1991.

6. L. C. Leal, C. G. Stenberg and R. N. Hill, "Gamma Production Data for Natural Zirconium for SDX Library," February 1991.

7. L. C. Leal, "ENDF Utility Codes GETMAT, LISTEF and PLOTEF," January 1991.

8. L. C. Leal, "Investigation of the Procedure for Generating Neutron- Proton Production and Photon Interaction Data at ANL," January 1991.